Structural and functional studies of *Xv*Prx2, a type II peroxiredoxin protein from the Resurrection Plant *Xerophyta viscosa*

Ezenwa James Onyemata

A thesis submitted in fulfillment of the requirements for the award of Philosophiae Doctor (Biotechnology) in the Department of Biotechnology, Faculty of Natural Sciences, University of the Western Cape

Supervisor: A. Prof. D. J.R. Pugh

Co-supervisors: Dr. R. A. Atkinson and Dr. M. S. Rafudeen

December 2012

ABSTRACT

Structural and functional studies of *Xv*Prx2, a type II peroxiredoxin from the resurrection plant *Xerophyta viscosa*

E. J. Onyemata, Department of Biotechnology, Faculty of Natural Sciences, University of the Western Cape

*Xv*Prx2 is a 1-Cys-containing member of the Prx5 subfamily of peroxiredoxins isolated from the resurrection plant *Xerophyta viscosa*. It is reported to be up-regulated during periods of desiccation and to protect nucleic acids and cellular proteins from oxidative damage through scavenging of reactive oxygen species, suggesting that it may play a role the desiccation tolerance of *X. viscosa* (Govender, 2006). Members of the Prx5 subfamily have previously been reported to occur as non-covalent homodimers associating across an A-type interface. PrxD from *Populus tremula*, a close homologue of *Xv*Prx2, forms disulphide bonds with glutathione (glutathionylation) resulting in the unfolding of the Cp-loop and α_2-helix and disruption of the homodimer, on the basis of which glutathionylation has been proposed as a physiological mechanism for regeneration of all members of the Prx5 subfamily (Noguera-Mazon*, et al.*, 2006b).

Chapter 3 of this thesis describes the development of procedures for expression and purification of large quantities of unlabeled and ^{15}N- and ^{13}C-enriched samples of *Xv*Prx2 using a bacterial expression system. Protein crystals were grown for X-ray diffraction studies, but they diffracted to insufficient resolution for structure determination.

Chapter 4 describes the investigation of the oligomeric state of *Xv*Prx2 using size exclusion chromatography, non-denaturing mass spectrometry and nuclear magnetic resonance spectroscopy (NMR). Consistent with previous reports *Xv*Prx2 was found to form non-covalent homodimers; the oligomeric state was found to be highly pH-dependent, being monomeric below pH 6 and homodimeric above. Both states were present in the vicinity of pH 6, exchanging slowly on the NMR time scale but rapidly on the time scale of size exclusion chromatography. This is the first report of pH-dependent oligomerization in Prx5 subfamily members.

Over 90% of the backbone resonances of the homodimeric form were successfully assigned at pH 7.2, but attempts to use chemical shift perturbation analysis to map the dimerization interface were frustrated by the poor stability of the protein at pH 5 which did not allow for assignment of the monomeric form. Attempts to assign side-chain resonances of the homodimeric form at pH 7.2 were also unsuccessful, due to poor coherence transfer resulting from the large effective molecular weight of the complex (36 kDa), but a highly downshifted resonance at -0.53 ppm, which is a useful marker for the homodimeric state, was successfully assigned to Ile42. Structures of other Prx5 subfamily members have highlighted the presence of a network of hydrogen bonds stabilizing the α_2-helix, which are likely to also affect the stability of the homodimer; the pH-dependence of the homodimerisation was found to be consistent with a model in which a single ionisable group with a pK_a of 6.0 can accept a hydrogen bond when ionized, thereby stabilizing the homodimer, but cannot accept the hydrogen bond when protonated.

Chapter 5 reports on the effect of mutating two ionisable residues potentially playing a role in the stability of the α_2-helix. Replacing His55 by alanine extended the stability of the monomer up to pH 8, indicating that the hydrogen bond accepted by His55 from Arg129 is important in stabilizing the homodimer in the wild type protein above pH 6. At pH 6 the H55A mutant was found to be monomeric and stable at 25 °C for a number of weeks and may therefore provide a means of investigating the structure and function of the monomeric form of the protein. Contrary to expectation replacing Cys51 by serine stabilized the homodimer at lower pH values than the wild type.

Oxidation of *Xv*Prx2 with a range of concentrations of H_2O_2 yielded only the over-oxidized sulphinic acid (-SOOH) form. This is consistent with multiple reports that the sulphenic acid (-SOH) form is unstable and readily oxidized to higher oxidation states. Despite the disappearance of the downfield-shifted resonance at -0.52 ppm, which had been found to be diagnostic of the homodimer, analysis of the effect of oxidation on the ^{15}N-HSQC spectrum, combined with results from size exclusion chromatography, suggests that oxidation does not abolish the homodimer. A possible explanation is that the α_2-helix is disrupted by oxidation, but not sufficiently to destabilize the homodimer.

Consistent with reports of its effect on *Pt*PrxD, glutathionylation completely disrupted the *Xv*Prx2 homodimer. Glutathionylation was achieved both by incubation of oxidized glutathione (GSSG) with reduced *Xv*Prx2, and by incubation of reduced glutathione (GSH) with oxidized *Xv*Prx2. Complete glutathionylation was achieved despite the fact that the protein was over-oxidised to the sulphinic acid (-SOOH) form.

Following glutathionylation, *Xv*Prx2 could be completely regenerated by addition of DTT, yielding a ^{15}N-HSQC spectrum indistinguishable from that prior to oxidation. The implication of this result is that glutathionylation combined with DTT should provide an effective way of regenerating *Xv*Prx2 following oxidation by H_2O_2. Kinetics assays are proposed using both DTT and the physiologically appropriate electron donor glutaredoxin to investigate the activities of wild type *Xv*Prx2 and the H55A mutant reported in this thesis.

Key words: peroxiredoxin, structure, monomer, non-covalent dimer, NMR, electrospray ionization mass spectrometry (ESI-MS), size exclusion chromatography (SEC), oligomeric state, pH, X-ray crystallization

DECLARATION

I declare that *"**Structural and functional studies of XvPrx2, a type II peroxiredoxin protein from the Resurrection Plant Xerophyta viscosa**"* is my own work that has not been submitted for any degree or examination in any other university, and that all the sources I have used or quoted have been indicated or acknowledged by complete references.

Ezenwa James Onyemata

December 2012

Signed …….

ACKNOWLEDGEMENTS

I am grateful to the National Research Foundation of South Africa and the National Centre for Scientific Research of France for financial support.

I am highly indebted to my supervisor Prof David Pugh for his input, guidance, support, effort and time spent in the completion of this thesis. I wish to thank my co-supervisor Dr Andrew Atkinson for his supervision with the analysis of NMR relaxation data, acquisition of triple resonance NMR data and the assignment of backbone and side chain resonances. I am grateful to Dr Suhail Rafudeen for providing biological context to this work and for financial support. I would like to thank Dr Muhammed Sayed with whom this study was conceived. I would like to thank Dr Kershini Govender for providing the template used for the amplification of *Xv*Prx2. I thank Dr John Poole for his assistance with collection of some NMR data set and side chain resonance assignments. My sincere appreciation goes to Dr Mervin Meyer for all his financial and technical assistance through this process. I wish to thank Prof Jasper Rees for his mentorship and support.

I would also like to thank Dr Jahansha Ashkani, Dr Andrew Faro, Dr Kenechukwu Obikeze, Dr Abidemi Kappo, Dr Gerald-Chamkpu, Mrs Ronke Saibu, Mrs Cathrine Madueke, Mr Faqeer Hassiem, and to all my friends for their support and encouragement. Special thanks are due Mrs Melvine Pretorius and Francis Starkey.

I would also like to express my gratitude to my family for the patience, love and understanding during this phase of my life, especially to my dear wife Sandra Tochukwu Onyemata for all her support, sacrifice and understanding.

ABBREVIATIONS

Amp	ampicillin
APS	ammonium persulphate
Apxs	ascorbate peroxidases
BCP	bacterioferritin comigratory protein
BSA	bovine Serum Albumin
bp	base pairs
C-terminus	carboxyl terminus
C_P	active site cysteine
C_R	resolving cysteine
Da	dalton
DNA	deoxyribonucleic acid
DTT	dithio-threitol
EDTA	ethylene diamine tetra-acetic acid
EtBr	ethidium bromide
ESI	electrospray ionisation
FF	fully folded
Fig	figure
GPxs	glutathione peroxidases
GS	glutamine synthase
GSH	reduced glutathione
GSSG	oxidized glutathione
GST	glutathione-S-transferase
Hrs	hours
HSQC	heteronuclear single quantum coherence

IPTG	isopropyl *β-D*-thiolgalactopyranoside
kDa	kilo dalton
LB	luria broth
LU	locally unfolded
MWCO	molecular weight cut-off
MS	mass spectrometry
MW	molecular weight
m/z	mass to charge ratio
NMR	Nuclear Magnetic Resonance Spectroscopy
nm	nano meter
PAGE	polyacrylamide gel electrophoresis
PCR	polymerase chain reaction
PEG	polyethylene glycol
PDB	protein data bank
PMSF	phenylmethylsulphonyl fluoride
PPM	parts per million
*Pt*PrxD	D-type peroxiredoxin from *Populus tremula*
Prx	Peroxiredoxin
ROS	reactive oxygen species
RNS	reactive nitrogen species
SH	sulfhydryl
SOH	sulphenic
SO_2H	sulphinic
SO_3H	sulphonic
SDS	sodium dodecyl sulfate

TBE	Tris-Boric acid-EDTA
TE	Tris-EDTA
TEMED	*N, N, N', N'*-tetramethylethylenediamine
Tfb	transformation buffer
Tris	Tris (2-amino-2-hydroxymethyl) propane-1, 3-diol
Tpxs	thioredoxin
TSA	thiol-specific antioxidant
UV	ultraviolet
*Xv*Prx2	peroxiredoxin from *Xerophyta viscosa*

TABLE OF CONTENTS

LIST OF FIGURES

LIST OF TABLES

Chapter 1: literature review

1.1 Introduction

Plant water deficit occurs when the rate of transpiration exceeds the rate of water uptake, leading to desiccation (Bray, 1997). Response to desiccation by plants takes the form of stomata closure, a process that results in the transfer of high-energy electrons to oxygen and nitrogen species, leading to the formation of reactive oxygen and nitrogen radicals (ROS and RNS). Partially reduced or activated ROS and RNS, produced by photosynthetic organisms as by-products of normal cellular metabolism during steady state functioning at the levels of mitochondrial and chloroplastic electron transfer chains are highly reactive and toxic and can lead to cell destruction (Takahashi & Asada, 1988). *In vitro* studies conducted by several groups have demonstrated that ROS and RNS participate in many physiological processes such as signal transduction, modulation of transcription factors and cell differentiation (Finkel, 1998; Kang*, et al.*, 1998; Sundaresan*, et al.*, 1995). The dual roles of ROS and RNS in the regulation of important processes as well as in toxicity implies a tight regulation of the their concentrations. Cells have developed many enzymatic and non-enzymatic anti-oxidative systems for regulation of these molecules, including glutathione-dependent peroxidases (Apxs, GPxs), thioredoxin peroxidases (TPxs), and the recently characterized peroxiredoxins (Prxs) (Noguera-Mazon*, et al.*, 2006a), which are the subject of this review.

Peroxiredoxins (Prxs), previously named thiol-specific antioxidants (TSA), thioredoxin peroxidases (TPx) or Peroxidoxins, are multi-functional thiol-dependent anti-oxidant peroxidases, which are ubiquitously expressed in many organisms and in many cellular compartments (Dietz, 2003; Kim*, et al.*, 1988). They are heme-free abundant low

efficiency peroxidases, which achieve the reduction of various peroxides including alkyl-hydroperoxides, hydrogen peroxides and peroxinitrates, using a conserved catalytic cysteine residue and thiol-containing proteins as reductants (Rouhier & Jacquot, 2005). Peroxiredoxins were first identified through studies involving the regulation of glutamine synthase (GS) in yeast where it was found to confer protection against oxidative inactivation of the GS (Kim*, et al.*, 1985). Purified GS suffered a gradual loss in activity when stored in a thiol-containing buffer but retained activity when stored in the same buffer containing extracts from *Saccharomyces cereviseae*, which suggested the presence of an anti-oxidant molecule within the extract. A 25 kDa protein was subsequently isolated from the yeast extract and shown to protect GS from oxidative inactivation by ROS in the presence of a number of thiol-containing compounds including dithiothreitol (DTT), mercaptoethanol, thiolglycerol, gluthione and dyhroliporic acid (Kim*, et al.*, 1985).

The first cDNA clone encoding a plant peroxiredoxin (pBS128) was reported by Goldmark and co-workers (Goldmark*, et al.*, 1992). Northern hybridization methods using pBS128 revealed that Prx genes are expressed predominantly in parts of the plant which survive desiccation, such as the seed, suggesting a role for them in abiotic stress response (Rhee*, et al.*, 1994).

A number of functions have been proposed for Prxs including roles in the maintenance of seed dormancy, in growth and development, in ROS-and RNS-dependent signalling, in pathogen defence and in the protection of cellular organelles including the mitochondrial DNA against oxidative degradation (Banmeyer*, et al.*, 2005; Dietz*, et al.*, 2006; Rouhier*, et al.*, 2004).

A group of plants commonly known as resurrection plants posses a unique and effective mechanism of coping with drought stress by being desiccation tolerant (Scott, 2000). *Xerophyta viscosa* (*X. viscosa*), a desiccation-tolerant plant, survives dehydration to 5% relative water content and achieves complete rehydration reaching full physiological activity within 3 days following rehydration (Sherwin & Farrant, 1998). Resurrection plants can be used as model systems to gain insight into drought tolerance serving as potential source of genes that could provide tolerance to abiotic stress. An increased expression of a number of several antioxidant enzymes has been noted in response to drought in resurrection plants (Smirnoff, 1993). *Xv*Prx2, a novel antioxidant enzyme, was isolated and characterized from *X. viscosa* (Govender, 2006; Mowla, et al., 2002).

XvPrx2 is a 1-Cys containing peroxiredoxin shown to be present in multiple homologues in X. viscosa (Govender, 2006). *Xv*Prx2 was identified as one of the genes up-regulated during desiccation periods of *X. viscosa*. Previous studies have shown that XvPrx2 protects nucleic acids and other cellular proteins from oxidative damage through the scavenging of ROS suggesting a role for it in the tolerance of desiccation by X. viscosa (Govender, 2006).

*Xv*Prx2 is a potential candidate for the transformation of maize which experiences loss of about 70 % of maximum achievable crop yields in comparison to optimal crop yields (Neumann, 1995) as a result of dessication. Thus efforts to improve the drought tolerance of maize achievable by transforming it with stress response genes such as *Xv*Prx2 will require a full understanding of the structural properties and function of this gene and how this contributes to the regulation of ROS and RNS during desiccation.

This project is aimed at understanding the structural and functional properties of *Xv*Prx2 and in particular how its structural property is affected by ROS and other factors such as pH.

1.2 Catalytic cycle of peroxiredoxins

All Prxs have in common a catalytic cycle that uses a conserved active site cysteine (C_p) to reduce peroxides. The catalytic cycle of Prxs involves three chemical steps: (1) peroxidation, in which the peroxide is reduced (ROOH→ROH) with corresponding oxidation of the catalytic thiol (Prx-S_P^- → Prx-S_P-OH), (2) resolution, in which another thiol (S_R^-) attacks the sulphenic (SOH) group, forming a disulphide Prx-S_P-S_R-R', and (3) recycling, in which the disulphide is reduced by another thiol (R"-SH), regenerating both S_P and S_R (Prx-S_PH and R'-S_RH). The resolving thiol forms part of a cysteine which either forms part of the same Prx molecule, which is then called a 2-Cys Prx, or an independent molecule, in which case the Prx is known as a 1-Cys Prx. Resolution of 2-Cys Prx's may take place by the formation of head-to-tail homodimers (typical 2-Cys) or by conformational changes within a single molecule bringing the C_P and C_R into proximity (atypical 2-Cys). Step 1 occurs whilst the protein is in the fully folded (FF) conformation while steps 2 and 3 lead to a change in protein conformation from FF to locally unfolded (LU) and back to FF (FF→LU→FF) (Hall*, et al.*, 2011; Noguera-Mazon*, et al.*, 2006a). A schematic representation of the catalytic reaction of Prx is shown in Fig 1.1.

Step 1

Peroxidation is a nucleophilic bimolecular substitution reaction (S_N2 reaction) whereby

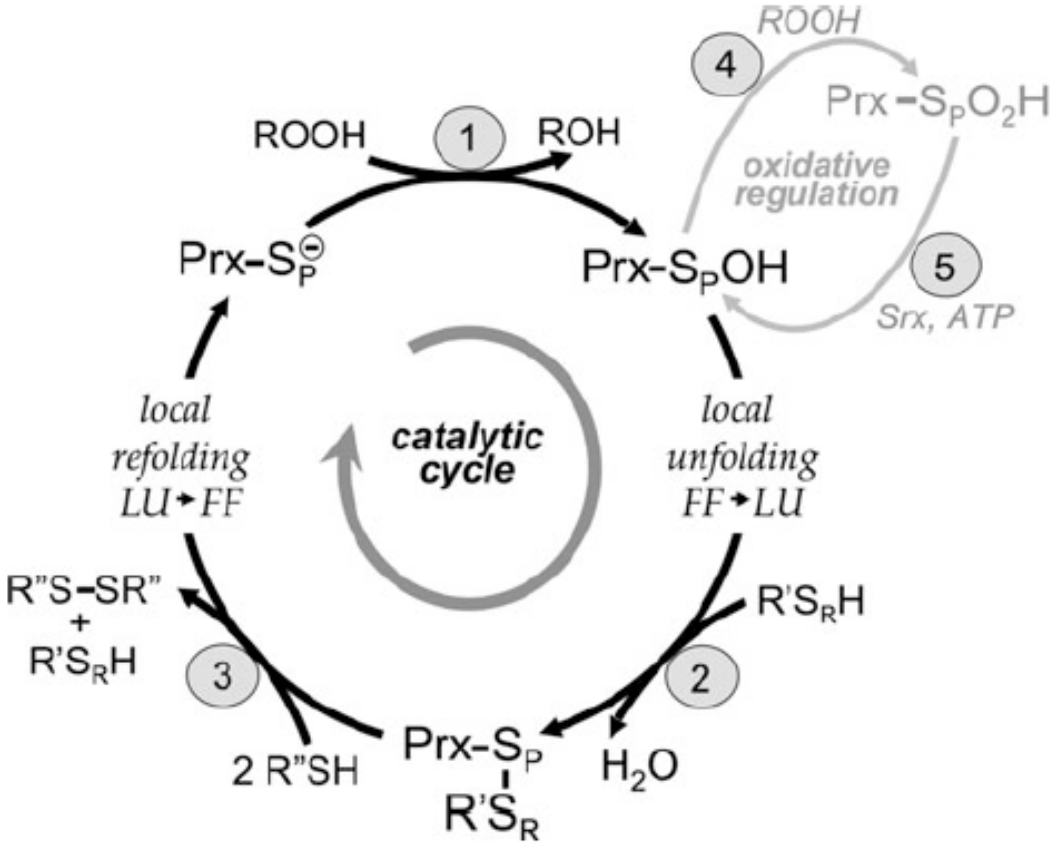

Fig 1.1: Prx catalytic cycle. The catalytic cycle of Prx involves three main chemical steps including **(1)** peroxidation, **(2)** resolution, and **(3)** recycling. Prx undergoes two distinct conformational changes during the catalytic cycle: FF (fully folded, active-site intact) and LU (locally unfolded, disulfide between the C_P and the C_R). The formation of disulphide bonds in step 2 requires that a local unfolding event occur following which a local refolding event needs to occur to reform the peroxide-binding active site following disulphide reduction in step 3. Inactivation of sensitive eukaryotic 2-Cys Prxs allows for temporary build up of H_2O_2, which plays signalling function. The inactivated form can be rescued through an ATP-dependent reaction catalyzed by sulfiredoxin (Srx) (step 5). Prxs have a 1-Cys or 2-Cys reaction mechanism. For the 1-Cys Prx, the resolving cysteine comes either from a small molecule or another protein while for the 2-Cys the resolving cysteine comes from within the protein (the same subunit or a different sub-unit). The generic Prx is represented as a monomer, with S_P designating the sulfur atom of the C_P while the C_R (from R" with S_R designates the sulfur atom). Different proteins, including Trx and AhpF, have been identified as R" in step 3. The figure was taken from (Hall*, et al.*, 2011).

a nucleophile (S_P-O^-) attacks an electrophile (RO_BO_AH) resulting in the formation of S_pO_AH (a nucleophile-electrophile bonded product) and displacement of one of the peroxide's oxygen atoms (O_B), following the breaking of the bond between O_A and O_B. The formation of a new bond between the nucleophile and one of the substrate's oxygen atoms (S_pO_AH) results in products such as alcohol (or water) and nitrate (Hall*, et al.*, 2010).

In addition to the conserved cysteine (C_P) the active site contains a trio of conserved residues: proline, threonine (occasionally serine) and arginine (Fig 1.2). Three of the four conserved residues are found close together in the sequence in the configuration $PXXXTXXC_P$, which is known as the C_P loop (Fig 1.3). The conserved arginine occurs later in the amino acid sequence but is in close proximity to the C_P loop in the folded structure (Fig 1.2). A fifth conserved residue, which is most frequently glutamic acid, glutamine or histidine, occurs 3 or 4 residues after C_P and is positioned close to the conserved arginine in the folded structure (Fig 1.2).

The active site environment of the C_P contributes to the lowering of the pK_a of the C_P, from 8.5 in solution thiols to somewhere in the range of 5 - 6 (Nelson*, et al.*, 2008; Ogusucu*, et al.*, 2007). However calculations have shown that lowering of the pK_a of C_P only accounts for 10^6-fold rate increase in the reactivity of Prxs (Hall*, et al.*, 2010). The rest of the activity comes from interactions within the active site of the protein, which enables the stabilization and activation of the transition state of substrates (see Section 1.5).

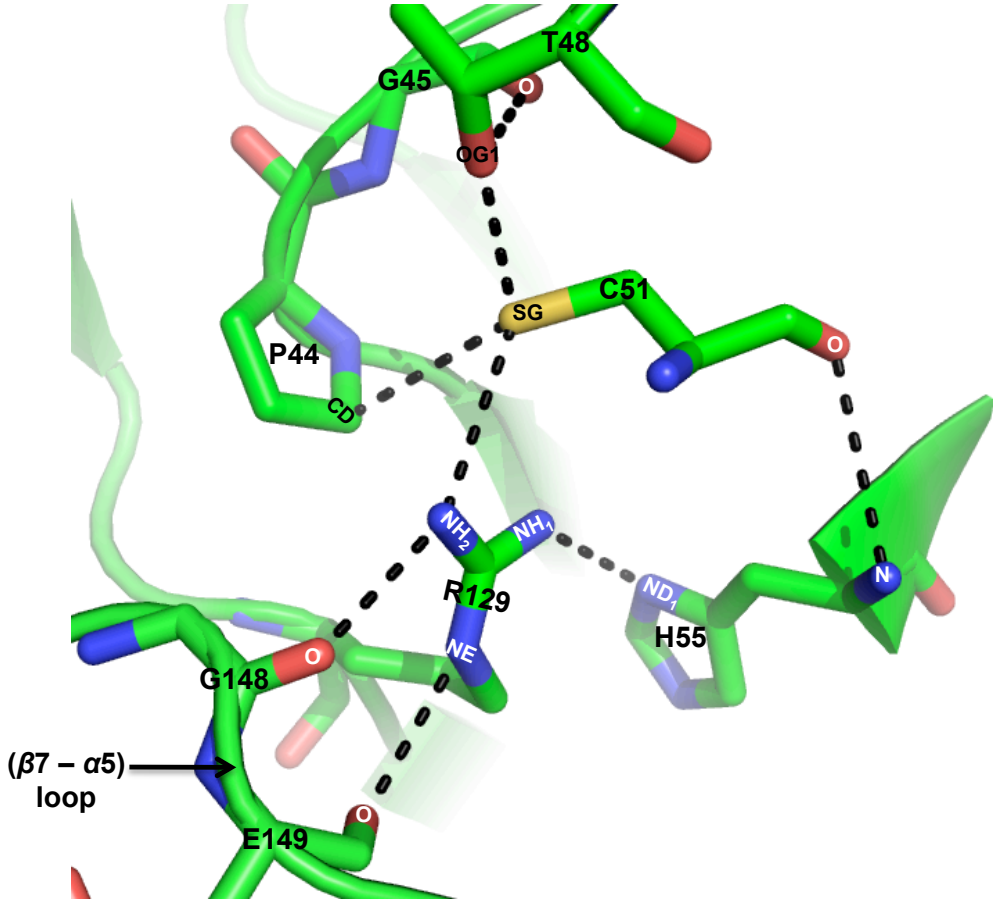

Fig 1.2: Prx active site hydrogen-bonding interactions. Thick broken lines represent the hydrogen-bonding interactions by active site residues of Prx. A number of hydrogen-bonding interactions stabilize the C_P, allowing it to activate and react with substrates. The image was generated from the structure of Peroxiredoxin from *Populus tremula* (PDB 1TP9) and has been visualized using the PYMOL Molecular Graphics System (2003) Delano Scientific, San Carlos, CA, USA.

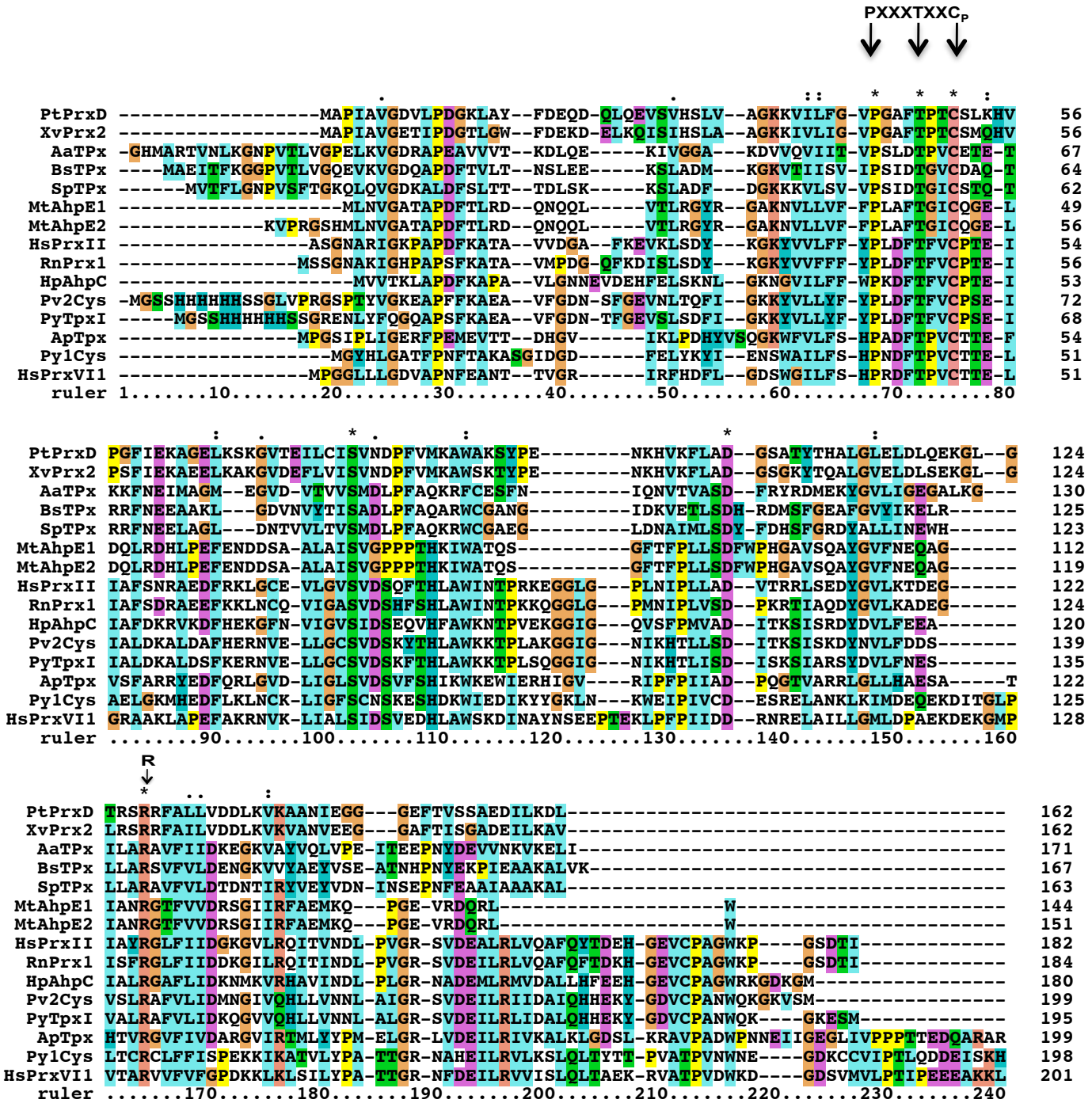

Fig 1.3: Sequence alignment of representative members of Prx subfamilies. N-terminal extensions can be seen for the Tpx subfamily while C-terminal extensions are seen for the Prx1 and Prx6 subfamilies. A number of insertions appear in a subfamily-specific manner at different locations within the alignment. These insertions have implication for the structural features of individual subfamilies (Section 1.5). Residues of the C_P-loop motif and the conserved arginine that are involved in extensive hydrogen-bonding interactions within the active site of Prxs (Fig 1.2) have been indicated. The alignment was created using MUSCLE (Edgar, 2004).

Step 2

Resolution occurs when the resolving thiol (S_RH), present within the protein (2-Cys mechanism) or from an external source (1-Cys mechanism), attacks the sulphenic acid group (S_pOH) to release a water molecule and form a disulphide (Prx-S_p-S_R-R'). Prior to the attack on the S_pOH group by the S_RH, the S_pOH group is in a FF protected active site with the result that there is a need to expose this group, a requirement that is met by conformational changes that involves unfolding of the active site to the locally unfolded (LU) conformation (FF→ LU) (see Fig 1.1) (Hall*, et al.*, 2011). Both states (the FF and LU) are thought to exist in a dynamic equilibrium following oxidation until the protein becomes locked in a LU state, following the formation of the disulphide bridge (Hall*, et al.*, 2011).

Step 3

Recycling occurs when the disulphide is reduced by a thiol-containing protein or small molecule regenerating the free thiols S_pH and S_RH. A number of thiol-containing proteins or small molecules including glutathione, thioredoxins, glutaredoxins, cyclophilins, NADPH-dependent thioredoxin reductase C and ascorbate have been found to fulfill this role (Rhee*, et al.*, 2005). The reduction of the disulphide allows the FF active site to refold preparing the Prx for another round of catalysis.

The resolving step is in competition with additional peroxide substrates which further oxidize the sulphenic acid intermediate to higher oxidation states sulfinic acid (S_pO_2H) and or sulphonic (S_pO_3H), often called "over-oxidation". Over-oxidation is widely reported to be resistant to resolution and recycling, leading to the inactivation of the enzyme. The structure of the C_P of *Plasmodium falciparium* Prx and two other Prxs

revealed that the geometry of the active site plays a role in determining the state of oxidation of the S_pH. Sarma and co-workers showed that once oxidized oxygen atoms attached to the C_p can occupy three possible sites ($O^{\delta1}$, $O^{\delta2}$ and $O^{\delta3}$) and that the state of oxidation is dependent on which of the positions is occupied by the attached oxygen (Sarma*, et al.*, 2005). The authors suggest that the S_pOH intermediate is formed when the peroxide substrate binds to the active site pocket in such a way that one of its oxygen atoms occupies the $O^{\delta1}$ position whereas the S_pO_2H intermediate is formed when the attached oxygen atom occupies positions $O^{\delta1}$ and $O^{\delta2}$, while the SpO_3H intermediate is formed when the attached oxygen atom occupies positions $O^{\delta2}$ and $O^{\delta3}$. Following the occupation of the $O^{\delta1}$ site the binding of further peroxide substrate requires that the attached oxygen be rotated out of this and into the next site. The formation of the over-oxidised Prx states (S_pO_2H and S_pO_3H) is therefore dependent not only on the thermodynamics of the unfolding of the active site but also the ease with which the structure can accommodate oxygen atoms into the $O^{\delta2}$ and $O^{\delta3}$ positions (Sarma*, et al.*, 2005).

Although over-oxidation leads to inactivation of the enzyme, it appears that in some eukaryotes build-up of over-oxidised Prxs may serve a signalling function, alerting the cells to high levels of reactive oxygen species. Biteau and co-workers have identified sulfiredoxin (Srx) as able to reduce doubly oxidised peroxiredoxins (Biteau*, et al.*, 2003). Although the activity of Srx has only been reported for some of the Prx subgroups, it has been suggested that in instances where Srx is functional the rate at which the Prxs become hyperoxidised far exceeds the rate of reduction of its sulfinic acid forms (Biteau*, et al.*, 2003).

1.3 Tertiary structure of Prxs

The core structure of peroxiredoxins consists of a seven-stranded β-sheet (β_2-β_1-β_5-β_4-β_3-β_6-β_7) surrounded by five helices (α_1 to α_5) (Echalier*, et al.*, 2005). The β-sheet is twisted in such a way that a central sheet made up of strands β_5-β_4-β_3-β_6-β_7 is covered on one face by β_1, β_2, α_1 and α_4 and on the opposite face by helices α_2, α_3 and α_5 (Fig 1.4) (Hall*, et al.*, 2011). The α_1 helix is a 3_{10}-helix in approximately half of the elucidated structures while the length of the α_5 varies from 2 to 5 turns in different sub-family members, although it starts in the same position across all the sub-family (Hall*, et al.*, 2011). Additional secondary structural elements such as insertions within the N- or C-termini or between loops of the protein occur in a sub-family specific manner (see Section 1.5 for details).

The α_2-helix contains the conserved active site cysteine residue C_P; in the words of Hall and co-workers helix α_2 is packed as a "baby lying in a cradle" relative to the rest of the structure where the bed of the cradle is formed by strands β_3 and β_4 and the walls by α_3 and α_5 (Fig 1.4A) (Hall*, et al.*, 2009b). The α_2-helix has been implicated in catalysis as local unfolding of the helix takes place during the catalytic cycle of the protein. The cradle that is formed around α_2 has been recognized to be important for stabilizing the fully folded and locally unfolded conformations of the protein and in facilitating a switch between the two conformations (Hall*, et al.*, 2011).

The FF conformation is required for productive binding of Prxs to substrates and is characterized by a number of features such as a fully folded active site pocket and C_p-loop. The C_p is found in the first turn of the conserved α_2 helix, while the resolving cysteine C_R may be buried as far away as 12 to 14 Å from the C_p in the FF

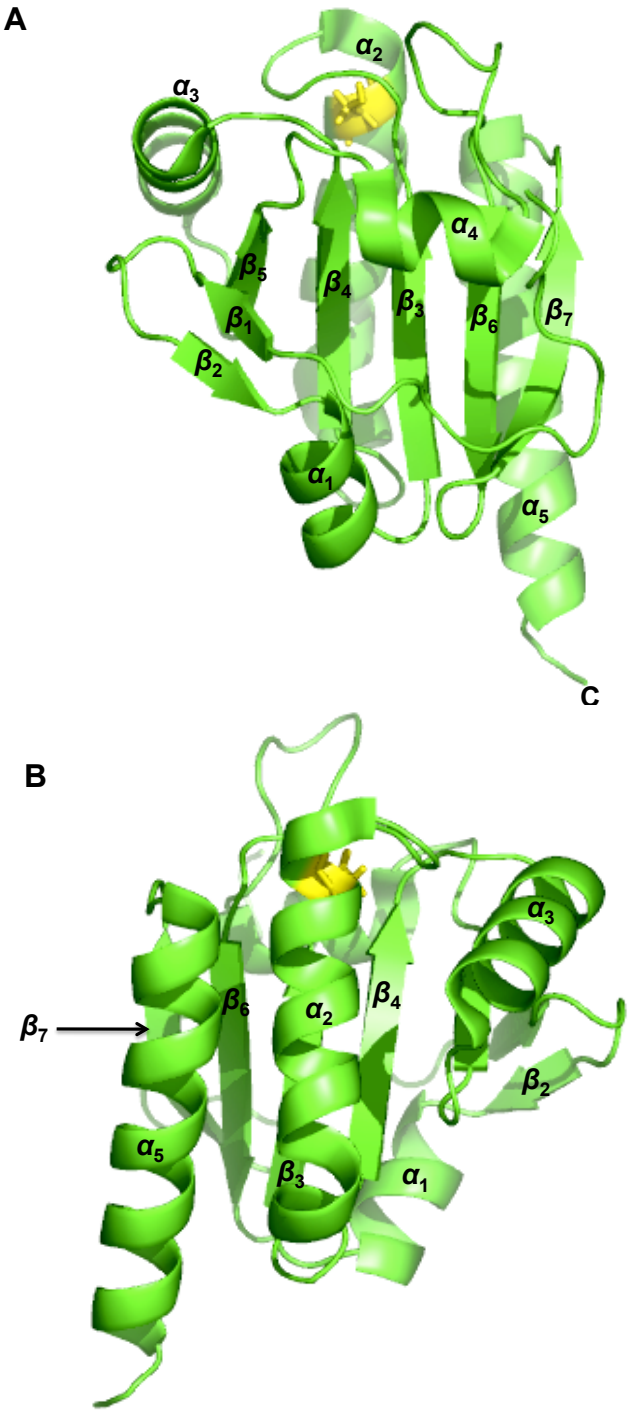

Fig 1.4: Core secondary structural elements of Prxs. (A) Shows the conserved core structure displayed such that the arrangement of the β-strands (2-1-5-4-3-6-7) and α helices (1 and 4) is visible. Rotation of the image (A) by 180 degrees around the y-axis such that helix α_2 appears in the words of Hall and co-workers "like a baby placed in cradle" with the sides of the cradle are formed by α_5 and α_3 and the base by β_3 and β_4 (Hall*, et al.*, 2011) as shown in (B). The C_p (displayed in sticks, yellow) is located within the first turn of the α_2 helix. The figure was generated based on the structure of *Sc*nTPx (PDB entry 2A4V) and has been visualized using the PYMOL Molecular Graphics System (2003) Delano Scientific, San Carlos, CA, USA.

conformation. The active site pocket contains a conserved catalytic C_P residue at the base of the pocket as well as three other residues: arginine, proline and threonine (replaced by serine in a few instances). The C_p-loop is a contiguous segment of conserved sequence motif ($PXXXTXXC_p$) containing three of the conserved residues found in the loop preceding the α_2-helix and shown to undergo conformational changes during the catalytic cycle (Wood*, et al.*, 2002). The FF structures show little variation within the C_p-loop conformation (Hall*, et al.*, 2010).

The locally unfolded conformation is characterized by the unfolding of the first turn of the α_2-helix and the C_p-loop allowing the C_p to move out of the protected site and becoming exposed and close to the S_RH so as to form a disulphide bridge. Prxs which react with the 2-Cys mechanism also experience the unfolding of the C-terminal end which allows the resolving cysteine to move closer in the exposed C_P to form disulphide with it (Wood*, et al.*, 2003b).

The role of active site residues in the reactivity of Prxs

The roles of the active site residues in the reactivity of Prxs have recently been characterized based on insights gleaned from enzyme-complex structures. Specific hydrogen bonding interactions between some backbone and side chain residues within the active site as well as some residues of the C_p-loop, α_2-helix and main chain backbone have been recognized to stabilize and activate not only the C_p but also the transition state of the substrate. H_2O_2-bound Prx structures show that the H_2O_2 molecule is well positioned in the active site to allow for a peroxidatic in-line S_N2 displacement reaction (Hall*, et al.*, 2010). In S_N2 displacement reactions, the nucleophile is expected to be within the length of a hydrogen bond away and

positioned about 180 degrees in the direction of the center of the electrophile. The presence of a partially formed bond at approximately 3.4 Å between the C_p (nucleophile) and O_A (electrophilic center) as well as the positioning of the C_p at about 172 degrees from the O_A contributes to the formation of the transition state (Fig 1.5). In addition to the positioning of the C_p, specific hydrogen bonding interactions involving residues of the active site play a role in the stabilising the transition state complex (Fig 1.5). For example, the active site proline residue shields the C_p from unwanted reactions while positioning the following two residues for hydrogen bonding. The threonine positions and activates the O_A atom of the peroxide while the arginine positions and activates the O_A atom and the C_p (Fig 1.5). The conserved arginine is stabilized by further interactions involving either a glutamine, glutamic acid or histidine residue, which is one turn away from the C_p with additional interactions occurring with backbone carbonyl groups in the β_7-α_5 loop (Hall*, et al.*, 2010) (Fig 1.5 and 1.2).

1.4 Quaternary structures of Prxs

Prxs structures have been reported to exist in a number of oligomeric states including monomers, dimers and decamers (Echalier*, et al.*, 2005; Hall*, et al.*, 2009b). The presence of higher order oligomeric states suggests that the monomer units interact with each other in an organized manner.

1.4.1 Prx-Prx structural interfaces

Two types of dimer interfaces have been recognized in Prxs referred to as the B-type (parallel) and A-type (perpendicular) (Sarma*, et al.*, 2005). The B-type interface is formed through the interaction of the β-sheets of the respective monomer units along

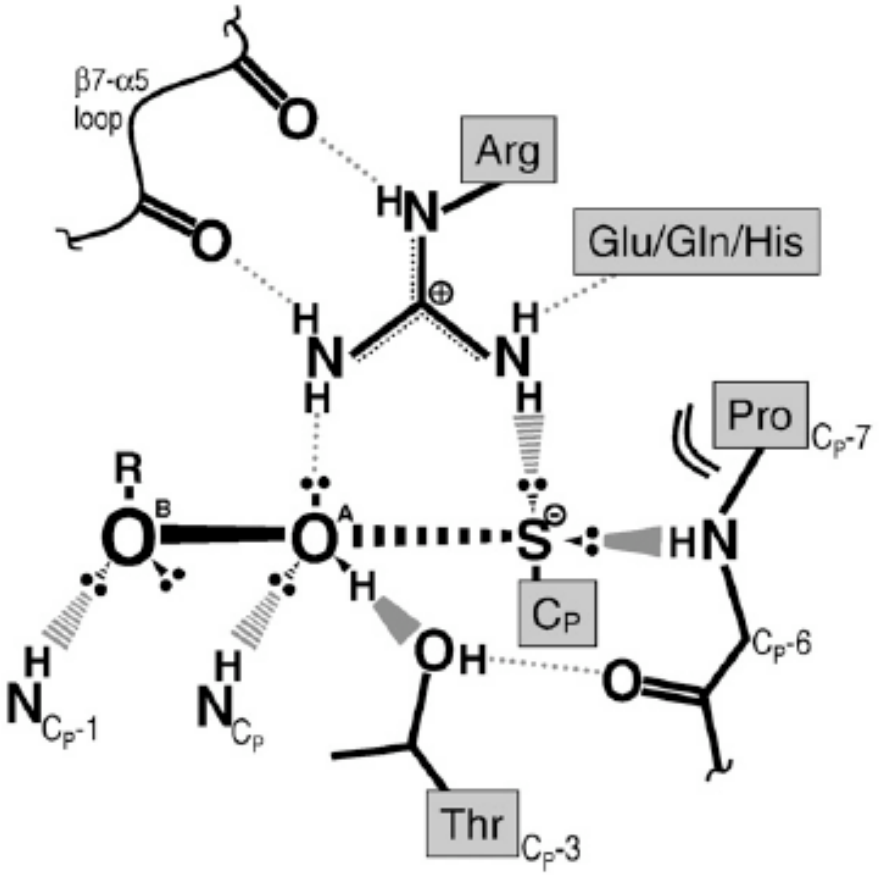

Fig 1.5: Interactions in the Prx active site Michaelis complex. The diagram shows the schematic drawing of the peroxide bound active site with emphasis on hydrogen-bonding interactions. The in-line geometry for S_P allowing it to attack O_A for the peroxidatic SN_2 reaction (bold broken line) and key hydrogen-bonding interactions (pale broken, dotted, and continuous lines have been indicated. This diagram complements the image shown in Fig 1.2. Backbone atoms in the C_P-loop are identified by their sequence position relative to C_P based on the Cp-loop motif (PXXXTXXC_p) (Fig 1.2). The negative charge on the C_P-thiolate has been indicated. The image has been directly taken from Hall*, et al.*, 2010.

strand β_7 (numbering based on the conserved secondary structural elements), resulting in a 10-stranded β-sheets (β_5-β_4-β_3-β_6-β_7-β_7-β_6-β_3-β_4-β_5) (Fig 1.6). The 2-fold axis of symmetry is oriented perpendicularly to the 10-stranded sheet, passing through (β_7-β_7) interface. B-type dimers are considered to be strong and stable and not prone to dissociation possibly due to extensive interaction of C-terminal extensions across the two fold axis of the respective monomer units (Hall*, et al.*, 2011). All Prxs which display B-type dimer interacting interfaces also show A type dimer interfaces, where the A-type interface is involved in the interaction of dimers (dimer-dimer interface), which results in the formation of higher ordered oligomers of four, five or six dimers (Fig 1.7) (Echalier*, et al.*, 2005).

The A-type (perpendicular dimer) interfaces result from the interaction of equivalent parts of the protein in four different regions including region 1 (β_3-α_2), region II (β_4-α_3), region III (β_5-α_4) and region IV (α_4-β_8) (Fig 1.8) (Echalier*, et al.*, 2005). The central β-sheet of each monomer is perpendicular to the interface unlike in the B-type where it is parallel to the interface (Fig 1.7) (Dietz, 2011). The A-type interface is prone to dissociation possibly due to the absence of C-terminal extensions, which provide stability in B-type interfaces (Echalier*, et al.*, 2005). The dissociation of the A-type interface has been reported for some Prxs resulting in the transition of the oligomeric states from higher ordered oligomers to dimers or dimers to monomers suggesting that the A-type interface plays a role in the formation of higher ordered oligomeric state of some Prxs (Echalier*, et al.*, 2005; Noguera-Mazon*, et al.*, 2006b). Poole and co-workers have shown furthermore that the catalytic activity of Prxs is reduced when they transition from decamers to dimers on the basis that the decamer

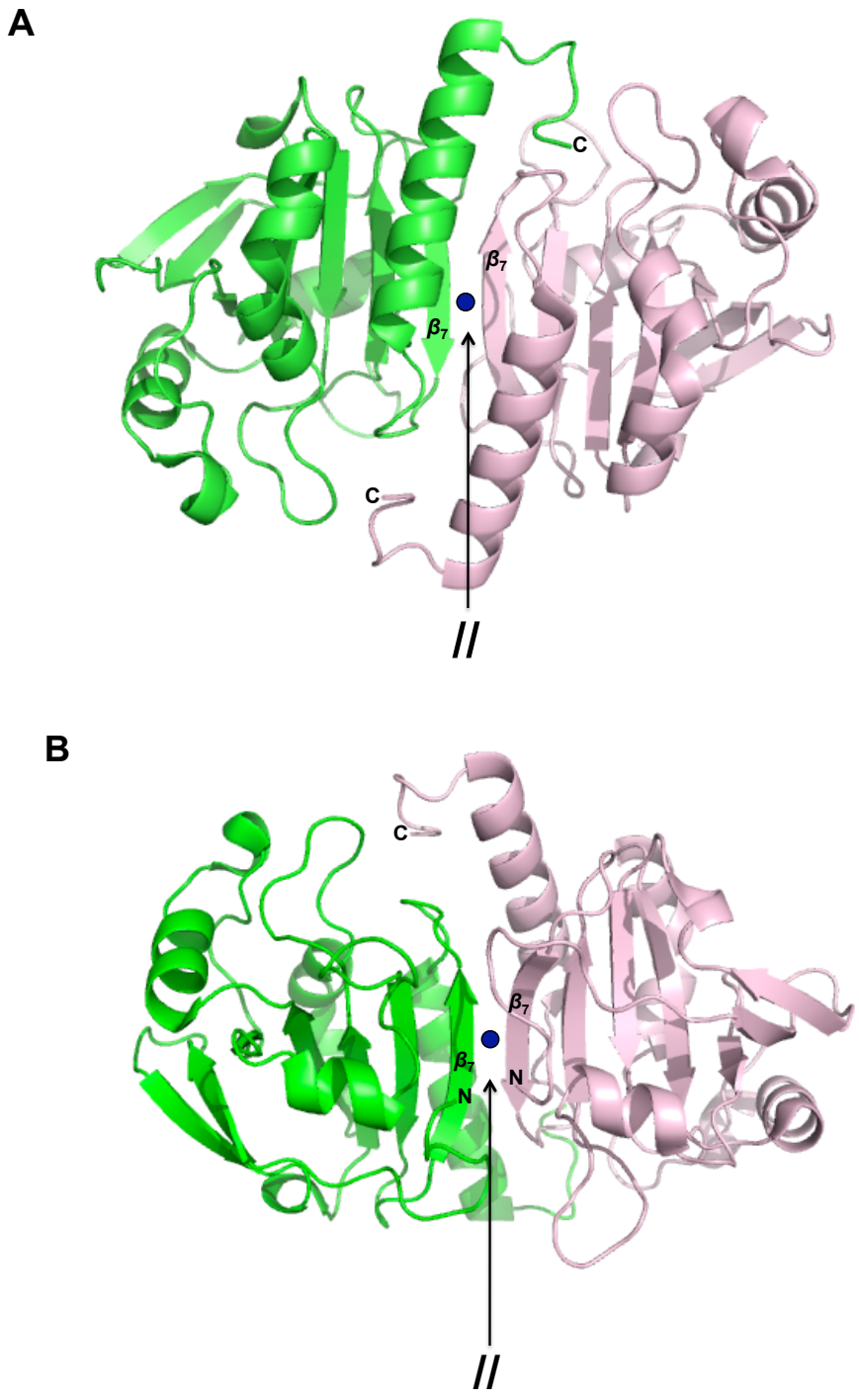

Fig 1.6: Cartoon representation of the B-type dimer interface. The B-type interface has been displayed such that the C-terminus of the structure is visible in (A) while the N-terminus is visible in (B). The 2-fold axis is represented by a dot. Both images were generated based on the structure of *Rn*Prx1 (PDB entry 1QQ2) and the figure has been visualized using the PYMOL Molecular Graphics System (2003) Delano Scientific, San Carlos, CA, USA.

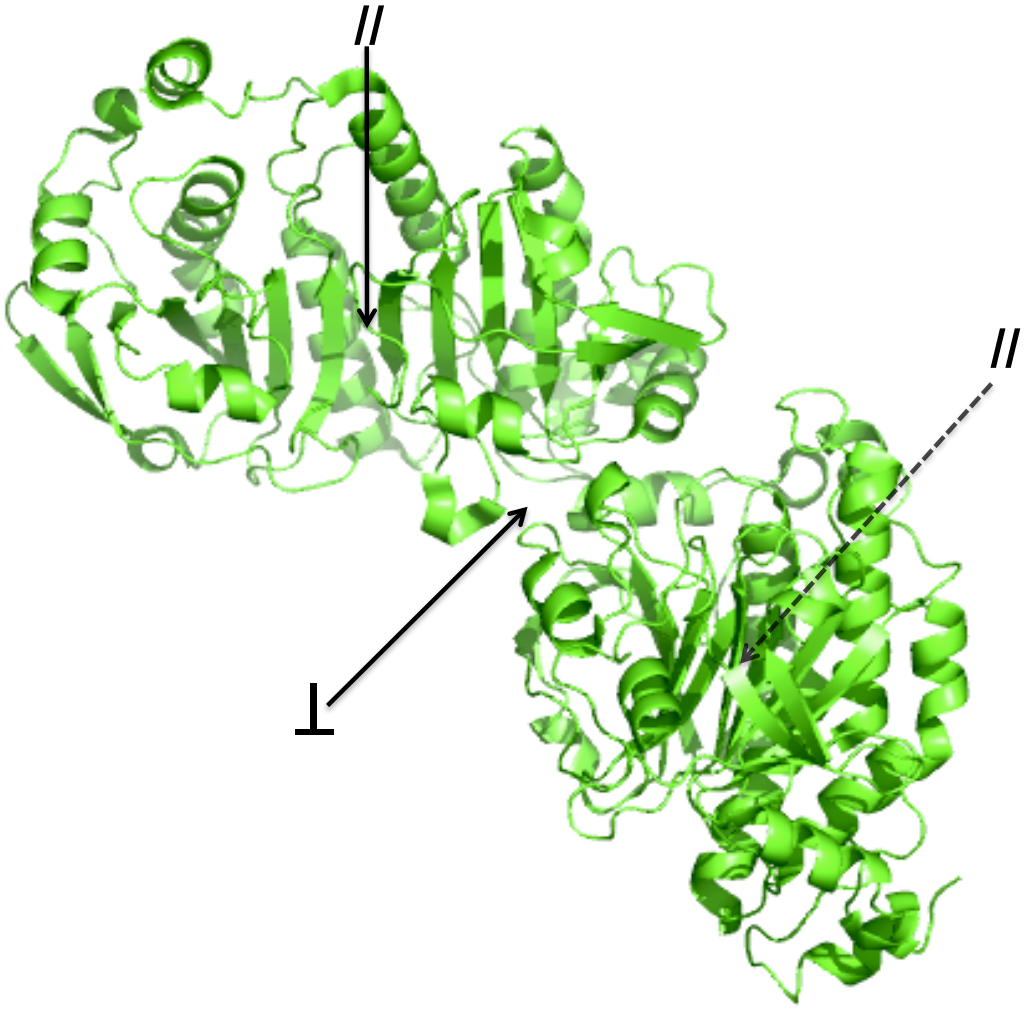

Fig 1.7: B-type and A-type dimer interfaces displayed in a higher order Prx oligomers. The B-type interface is represented using the (II) symbol and enables two monomer units to interact while the A-type interface is represented using ⊥ symbol and allows two B-type dimer units to interact. The figure was generated based on the structure of *Salmonella typhimuruim* AhpC (PDB entry 1N8J) and has been visualized using the PYMOL Molecular Graphics System (2003) Delano Scientific, San Carlos, CA, USA.

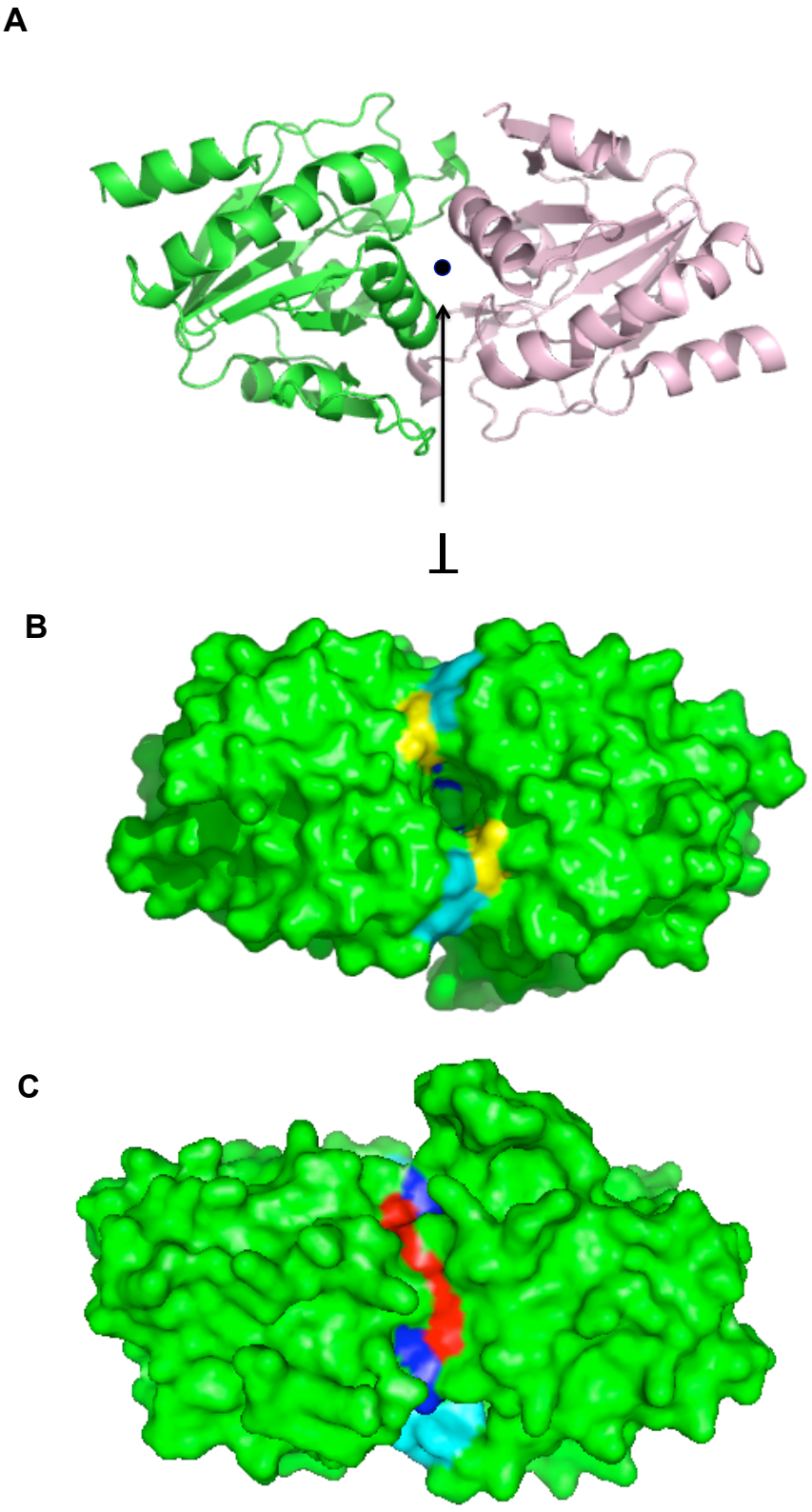

Fig 1.8: A-type dimer interface. Cartoon representation of the A-type dimer interface is shown in (A) while (B) and (C) show both sides of the surface representation of the A-type dimer interface. The 2-fold axis is represented by a dot shown in (A). The image shown in (B) and (C) have been colour coded to illustrate the four different interacting regions: 1 (β3-α2, red), II (β4-α3, blue), III (β5-α4, yellow) and IV (α4-β8, cyan) that make up the A-type interface (Echalier*, et al.*, 2005). The figure was generated based on the structure of P*f*AOP (PDB entry 1XIY) and has been visualized using the PYMOL Molecular Graphics System (2003) Delano Scientific, San Carlos, CA, USA.

contributes to the stability of the folded conformation of the active site (Parsonage*, et al.*, 2005).

1.4.2 Factors affecting the quaternary structure of Prxs

A range of factors including the oxidation state of the catalytic cysteine (C_p) (Wood*, et al.*, 2002), ionic strength (Chauhan & Mande, 2001), low pH (Kristensen*, et al.*, 1999), high magnesium or calcium concentrations (Plishker*, et al.*, 1992), reduction of redox active disulphide center (Schröder*, et al.*, 2000) and over oxidation of the peroxidatic cysteine (Wood*, et al.*, 2002), have been reported to play a role in the stability of the quaternary structures of Prxs.

1.4.2.1 Oxidation and quaternary structure Prxs

The state of oxidation of Prxs has been reported to lead to changes to their quaternary structures (Barranco-Medina*, et al.*, 2009). Prx structures containing A-and B-type dimer interfaces (Prx1) appear as decamers in the FF conformation and as dimers in the LU conformation (Wood*, et al.*, 2002). The first turn of the α_2-helix containing the C_p unwinds following the formation of disulphide bridges (LU), shifting the residues preceding the C_p forward resulting in the disruption of the perpendicular interface and the dissociation of the decamer into dimers (Wood*, et al.*, 2002). It was further observed that the quaternary structure of the protein was a decamer when overly-oxidised although the decamer associated with the overly-oxidised form is poorly recycled by reducing agents like thioredoxins while the dimeric form display low peroxidase activity (Wood*, et al.*, 2002).

The decamer to dimer transition on oxidation has been noted particularly for the Prx1 subfamily. However in a recent study Cao and co-workers showed that the reduced and

oxidised forms of a Prx1 subfamily member existed as decamers despite the fact that the C_p-loop adopted the LU conformation following oxidation (Cao, *et al.*, 2011). In this example the increased stability of the decamer in the oxidised form appeared to be a consequence of the replacement of proline at position 260 with phenylalanine (Cao, *et al.*, 2011).

Members of the Prx5 subfamily of peroxiredoxins have been reported to occur as non-covalent homodimers (Echalier, *et al.*, 2005; Evrard, *et al.*, 2004; Trivelli, *et al.*, 2003a). Kim and co-workers showed using analytical ultracentrifugation, light scattering and size exclusion experiments that the oligomerization state of human Prx5 is independent of its redox state (Kim, *et al.*, 2003). The oxidised and reduced forms of human Prx5 eluted at the same volume in size exclusion analysis, although the oxidised form of the protein did display features such as the unfolding of the α_2-helix, consistent with structural changes observed for the LU conformation.

A change in the oligomeric state of a Prx5 member has been reported following glutathionylation. Glutathionylation is a reversable covalent modification of protein cysteine thiols through the formation of mixed disulphides between the oxidised form of the protein and glutathione, a tri-peptide consisting of glycine, cysteine and glutamic acid. Cellular levels of glutathione are raised under elevated stress and glutathione plays an important role in preventing protein cysteine thiols from undergoing irreversible oxidation (Gallogly & Mieyal, 2007). Reversible glutathionylation modulates the activities of diverse protein substrates *in situ*, with effects on multiple physiological events (Gallogly & Mieyal, 2007).

Glutathionylation can occur either directly as observed for the 1-Cys "D" type Prxs (Prx5) or indirectly as in the case of the 1-Cys "B" type Prxs (Prx6 subfamily) (Manevich*, et al.*, 2004; Noguera-Mazon*, et al.*, 2006b). In indirect glutathionylation, the GSH is not able to access the C_P of the oxidised protein. However this barrier is broken following the formation of a heterodimeric complex between the oxidised protein and πGST. It appears that both in the case of direct and indirect glutathionylation the protein needs be oxidised prior to the attachment of glutathione. Whilst glutathionylation strictly refers to the attachment of the GSH molecule to proteins, the prior requirement that the protein be first oxidised has resulted in some researchers referring to glutathionylation as a redox reaction.

Noguera-Mazon and co-workers showed that the glutathionylation of Prx from *Populus tremula* led to unfolding of the α_2-helix, leading to the disruption of the dimer interface and the dissociation of the non-covalent homodimer to monomers (Noguera-Mazon*, et al.*, 2006b). They demonstrated furthermore that glutathionylation can be reversed by addition of DTT at 10-fold excess oxidised glutathione (GSSG) to protein concentration. However, at 20-fold excess GSSG the DTT dependent reversal was incomplete suggesting that the dimer-monomer transition was based on non-covalent interactions between GSSG and the protein.

The transition of the Prx5 subfamily (dimer to monomer) observed following glutathionylation has been likened to the decamer to dimer switch in the Prx1 proteins (Noguera-Mazon*, et al.*, 2006b).

1.4.2.2 The effect of pH on the oligomeric state of Prxs

A role for pH in determining the oligomeric state of Prxs was suggested through the study of calpromotin, a Prx1 subfamily member. Using gel filtration analysis over a range of pH from 5 to 8.5 Kristensen and co-workers showed that calpromotin was present as a large aggregate of about 300 kDa at pH 5.4 and a dimer of about 50 kDa at pH 8.53 (Kristensen*, et al.*, 1999). This result led the authors to propose that an ionisable group (not identified) that titrates between pH 7 and 8 was responsible for the effect. This represents the only report suggesting a role for pH in the oligomeric state of the Prxs. However, the effect of pH on the oligomeric state of Prxs has not been rigorously investigated. A role for pH in the oligomeric state of *Xv*Prx2 has been examined in this thesis and the findings presented in Chapter 4 of this work.

1.5 Classification of Prxs

Prxs have been classified into six distinct groups named Prx1, Prx6, Prx5, TPx, BCP and AhpE based on the structural alignment of conserved residues found within the vicinity of the active site as well as other residues found within a distance of 10Å to key conserved residues (Hofmann*, et al.*, 2002; Nelson*, et al.*, 2011; Noguera-Mazon*, et al.*, 2006a; Trivelli*, et al.*, 2003b). Phylogenic analysis of Prx sequences using representative members from all subfamilies is shown in Fig 1.9.

1.5.1 Prx1 subfamily

The Prx1 subfamily, previously referred to as the "A" group, are highly expressed peroxiredoxins that are found in various organisms. Representative members include yeast TSA proteins, bacterial AhpC proteins, several plant proteins and human Prxs numbered I to IV (Baier & Dietz, 1997; Dietz*, et al.*, 2002; Hofmann*, et al.*, 2002; Rhee*, et al.*, 2001; Trivelli*, et al.*, 2003b; Wood*, et al.*, 2002; Zhou*, et al.*, 1997).

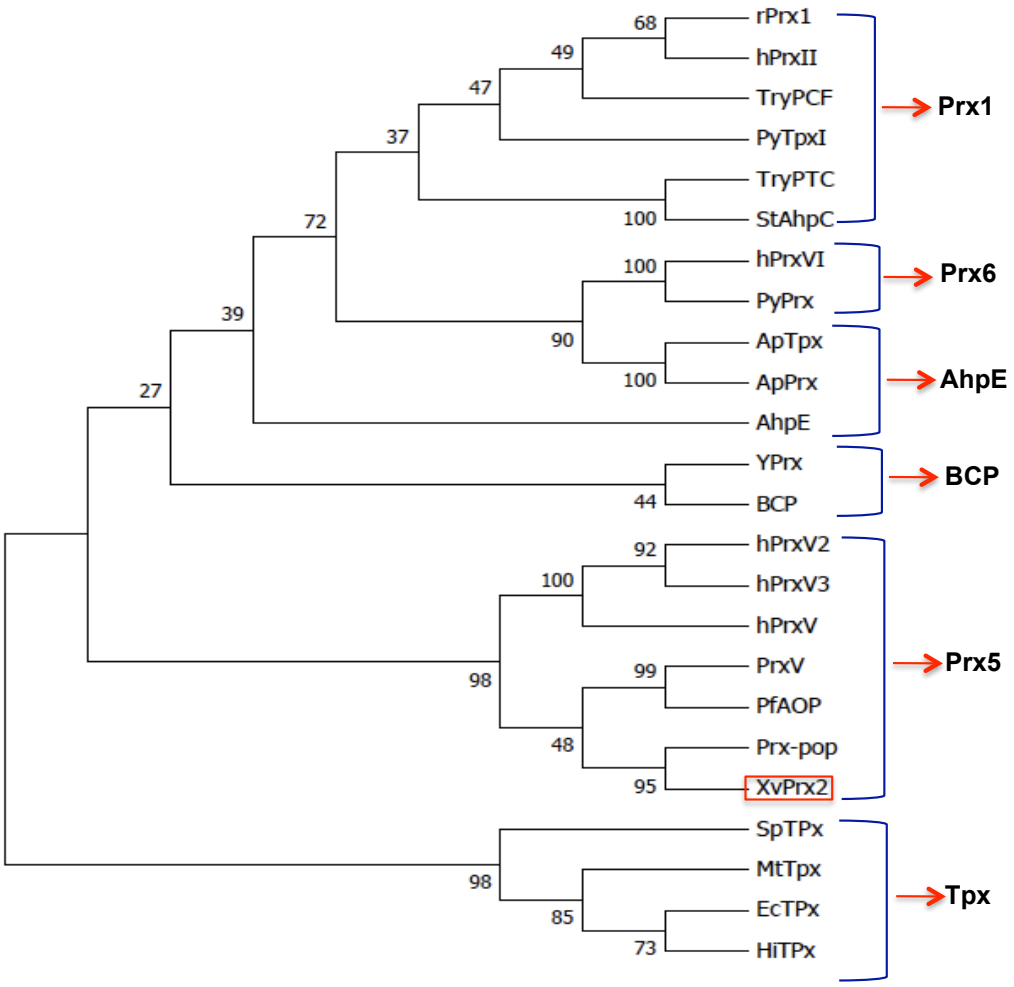

Fig 1.9: Family tree of representative members from all Prx subfamilies. The tree shows that Prxs can be classified into six subfamilies (Prx1, Prx6, AhpE, BCP, Prx5 and Tpx). *Xv*Prx2 (the sequence of this study, boxed in red) falls into the Prx5 subfamily and is closest with Prx-pop (*Populus tremula* Prx, PDB entry 1TP9). The tree was visualized using TreeView X (Page, 1996).

In addition to their roles as anti-oxidants, other roles including signalling and chaperone activity have been proposed for the Prx1 subfamily of peroxiredoxins (Hall, *et al.*, 2009a). Hall and co-workers have reported that proteins of the Prx1 subfamily can assume signalling roles through disulphide exchanges with other down-stream sensor proteins, following exposure to high concentrations of H_2O_2. They also noted that the exposure of members of the Prx1 subfamily to high concentrations of H_2O_2 results in the formation of higher ordered oligomers that have chaperoning activity. In both instances the exposure of members of the Prx1 subfamily to high concentrations of H_2O_2 results in their temporarily inactivation enabling a local build up of H_2O_2 which ensures that peroxides serve a signalling role (Hall, *et al.*, 2009a).

A number of structures of Prx1 members have been determined either in the FF or LU conformations (Fig 1.10). Comparison with the conserved common-core structure reveals the presence of two additional secondary structural elements in the form of helices α_4 and α_7 (Fig 1.11). Prx1 structures contain a longer loop between helices α_6 and α_7, as well as a 40 - 50 amino acid extension in the C-terminus following α_7 (Figs. 1.9 and 1.11). Members of the Prx1 subfamily are 2-Cys Peroxiredoxins. The C_p of Prx1 is located in the first turn of α_2-helix in the FF conformational while the resolving cysteine (C_R) is located at the C-terminus of the protein, in a conserved position with reference to the primary representative structure of this sub-family of proteins (Hall, *et al.*, 2011).

The C_R is buried within the C-terminal extension at approximately 14 Å away from the C_p in the FF conformation. Poole and co-workers have reported that the Cp-loop forms a helix (α_2), positioning the peroxidatic cysteine (C_P) in the active site in

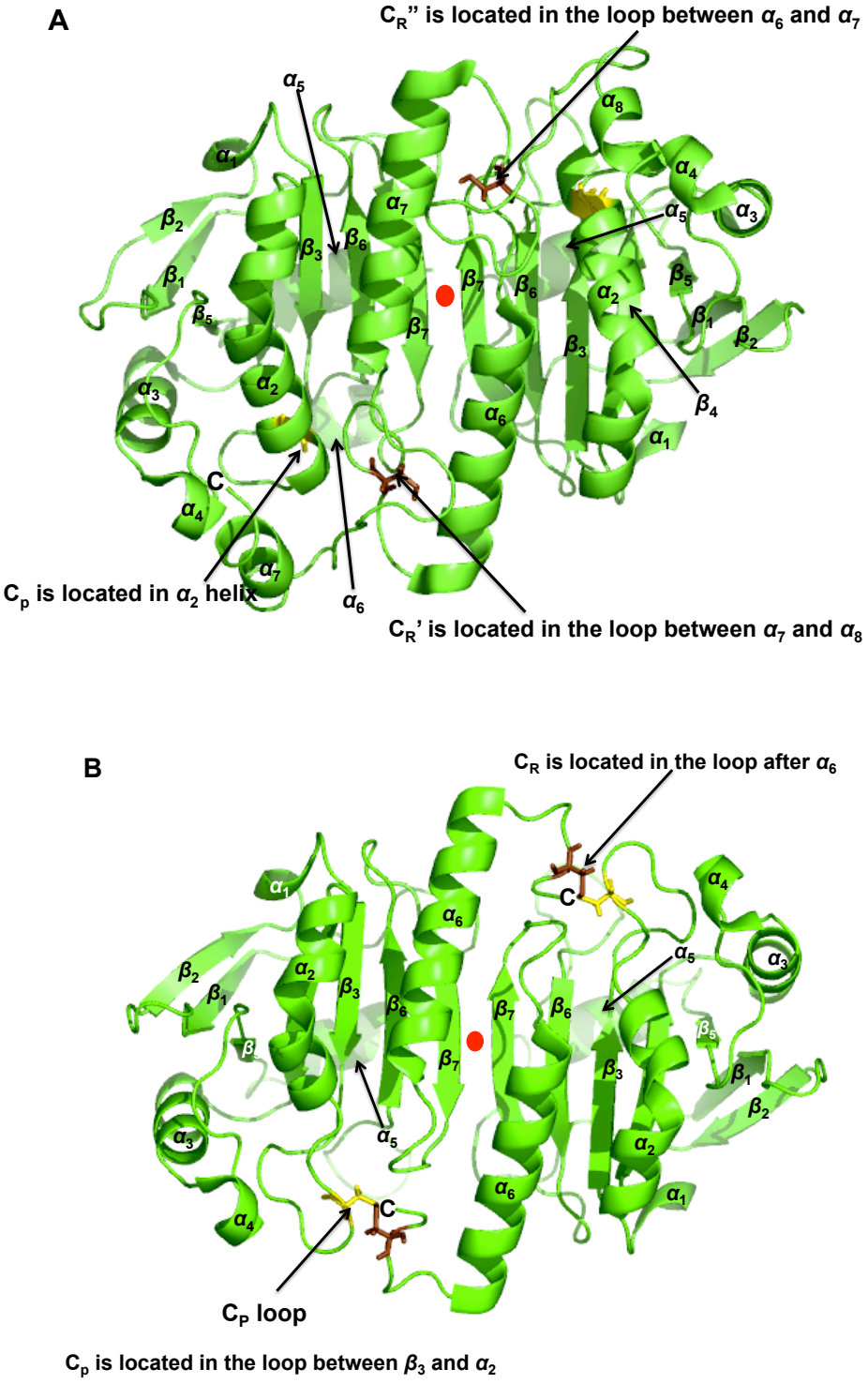

Fig 1.10: Core secondary structural elements of representative Prx1 structure. (A) FF Prx1 structure showing the presence of the C_p (displayed as sticks, yellow) within the first turn of α_2-helix while the C_R is located in a loop between helices α_7 and α_8. The image was generated based on the structure of *Rn*Prx1 (PDB entry 2Z9S). (B) LU Prx1 structure showing an exposed C_p (displayed as sticks, yellow) following the unfolding of the α_2-helix and the C-terminus of the protein. The C_R (displayed as sticks, brown) is located in a loop after α_6. A close contact can be seen between the C_p and C_R after the unfolding event, which allows the two residues to be disulphide bonded and thereby locking the structure in the LU conformation. The red dot indicates the position of the dimer interface and the dimer involves β-strand 7 from both monomer units. The image was generated based on the structure of *Rn*Prx1 (PDB entry 1QQ2). The figure has been visualized using the PYMOL Molecular Graphics System (2003) Delano Scientific, San Carlos, CA, USA.

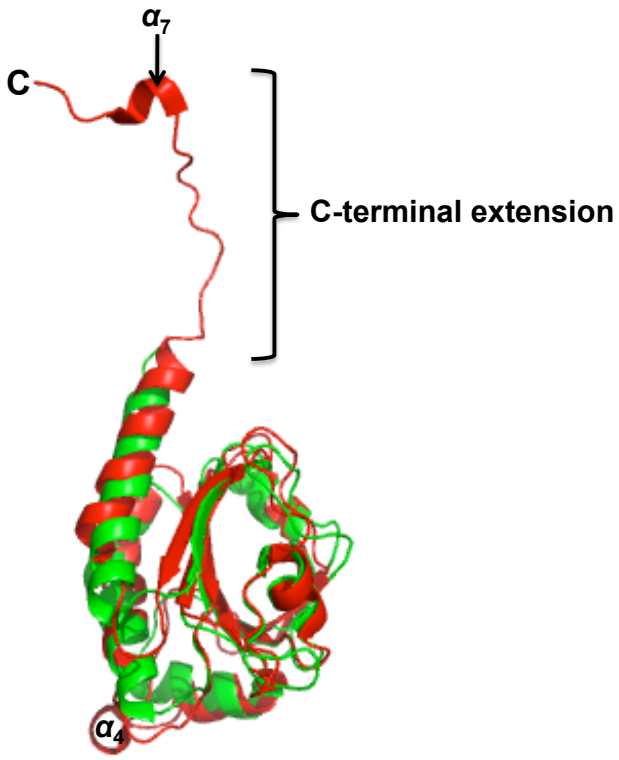

Fig 1.11: Overlay of Prx1 and the conserved Prx core structure. The overlay shows that Prx1 (red) has an extended C-terminal end, which gives rise to α_7 helix (Prx1 numbering). An additional α_4 helix (Prx1 numbering) is present in the structure of Prx1 but not in the conserved Prx core structure (green). The C-terminal extension is consistent with sequence alignment shown in Fig 1.4, suggesting a sequence to structural relation with implications for function. The conserved core structure of Prxs was generated based on the structure of *Sn*TPx (PDB entry 2A4V) while the structure of Prx1 (red) was based on the structure of *Hs*Prx1 (PDB entry 3HY2). The figure has been visualized using the PYMOL Molecular Graphics System (2003) Delano Scientific, San Carlos, CA, USA.

the reduced state. Peroxide decomposition results in the oxidation of the C_P to sulphenic acid resulting in the burying of the sulphur by the sulphenic acid oxygen (Wood*, et al.*, 2003b). A local unfolding event occurs at the active site resulting in the conversion of the C_p-loop into a solvent-exposed loop and thereby exposing the sulphenic sulphur for disulphide bond formation. Disulphide bond formation requires the C-terminal end of the protein to undergo unfolding resulting in positioning of the C_P and C_R at a distance that will allow disulphide bond to be formed between the C_P and C_R. This change results in the dissociation of the oligomeric state of the Prx1 from decamer to dimers (Wood*, et al.*, 2003b). The regeneration of the protein requires the presence of a reducing agent that can break the disulphide bonds and restore the fold of the C_p-loop.

Structures of Prx1 members have revealed that they dimerise along a B-type interface (Fig 1.12), with the C-terminal extension reaching across the dimer and making extensive contacts with the other subunit (Hall*, et al.*, 2011). Higher order oligomeric states of B-type homodimers interacting through the inter-dimer A-type ⊥ interfaces occur in the Prx1 subfamily (Section 1.4.1, Fig 1.7). A link between the oxidation and the oligomerization state has been reported in which the protein is a decamer when C_p is in the S_pH, S_pOH, S_pO_2H or S_pO_3H oxidative states and as a dimer when C_p is disulphide bonded with the C_R (LU) (Wood*, et al.*, 2003b).

The decamer to dimer transition occurs in part due to the unfolding of the C_p-loop, which disrupts the A-type interface. The decamer to dimer dissociation in turn affects the catalytic activity of the Prx1 subfamily because the decamer contributes to the stability of the folded conformation of the active site (Parsonage*, et al.*, 2005).

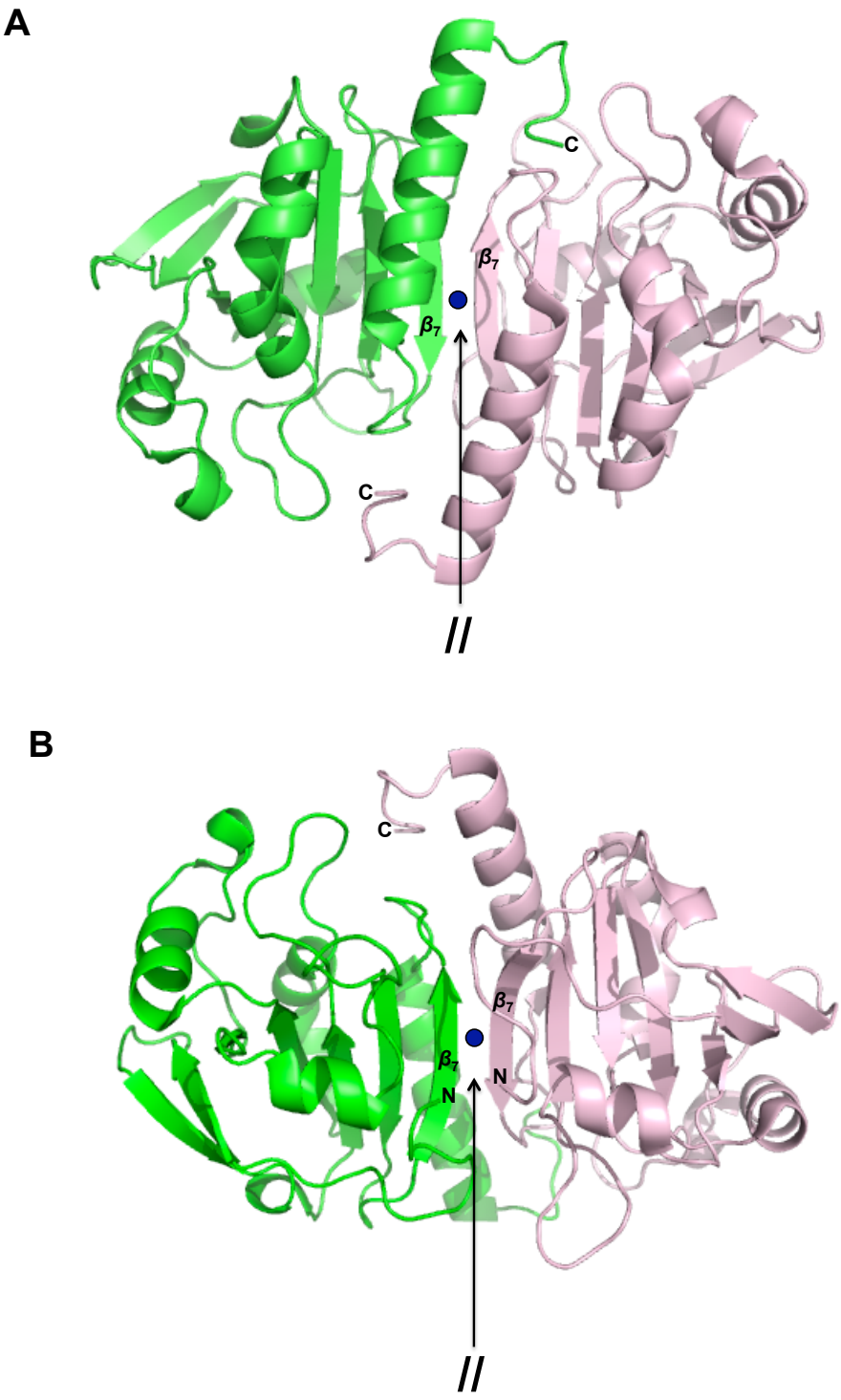

Fig 1.12: Cartoon representation of the B-type dimer interface. The B-type interface has been displayed such that the C-terminus of the structure is visible in (A) while the N-terminus is visible in (B). The 2-fold axis is represented by a dot. Both images were generated based on the structure of *Rn*Prx1 (PDB entry 1QQ2) and the figure has been visualized using the PYMOL Molecular Graphics System (2003) Delano Scientific, San Carlos, CA, USA.

The Prx1 subfamily can be further divided into two groups based on the robustness or sensitivity of the proteins to over-oxidation by peroxides (Wood, *et al.*, 2003a). Members sensitive to over-oxidation contain a YF-motif in the C-terminal extension, which packs against the C_P-loop stabilising the α_2-helix and blocking access to the C_P. This prevents formation of the disulphide bridge between the C_p and C_R, creating the opportunity for further oxidation of the S_pOH side chain to higher oxidation states (Wood, *et al.*, 2003a). Over-oxidised forms of Prx1 can no longer be regenerated by the normal catalytic mechanism (Section 1.2 Fig 1.2). However special repair enzymes known as sulfiredoxins (Srx) act in conjunction with ATP, Mg^{2+} and a thiol-containing reductant to regenerate the sulphenic acid forms of Prx1 to active Prx (Jonsson & Lowther, 2007).

1.5.2 Prx6 subfamily

The Prx6 subfamily was previously referred to as the "B", the "1-Cys" or the ORF6 group. The name is taken from human PrxVI, which was the first structure from the family to be elucidated (Choi, *et al.*, 1998). Prx6 have been found in all kingdoms of life (Baier & Dietz, 1997; Dietz, *et al.*, 2002; Hofmann, *et al.*, 2002; Noguera-Mazon, *et al.*, 2006b; Rhee, *et al.*, 2001; Stacy, *et al.*, 1999; Trivelli, *et al.*, 2003b; Wood, *et al.*, 2002; Zhou, *et al.*, 1997). Prx6 is predominantly made up of 1-Cys peroxiredoxins, although a number of 2-Cys Prxs have also been reported (Barranco-Medina, *et al.*, 2009; Hall, *et al.*, 2011). Reactivating reducing agents identified for recycling of Prx6 members include glutathione S-transferase, thioredoxin and ascorbate (Manevich, *et al.*, 2004; Monteiro, *et al.*, 2007; Pedrajas, *et al.*, 2000; Ralat, *et al.*, 2005).

Prx6 members form homodimers in solution, associating across a B-type interface. (Section.1.4.1). Each monomer is composed of two domains: a large N-terminal domain containing a thioredoxin-fold similar to the core Prx structure and a smaller C-terminal domain (Fig 1.13). The N-terminal domains dimerise through the anti-parallel interaction of their β_9-strands, stabilized by folding of the C-terminal domain of one monomer over the N-terminal domain of another monomer (Fig 1.14). It has been proposed that the C-terminal domain binds in the vicinity of the active site and contributes to substrate specificity by narrowing the entrance of the active site (Echalier*, et al.*, 2005).

A hallmark of Prx6 family is the C-terminal domain which, unlike in the case of the Prx1 family, is structured, incorporating up to 4 β-strands (β_{10}, β_{11}, β_{12}, β_{13}) and an α helix (α_6). Prx6 members also contain an insertion comprising β-strands β_6 and β_7. An overlay of a representative Prx6 structure and the core Prx structure is shown in Fig 1.15.

Prx6 peroxiredoxins have been reported in a number of oligomeric states, including monomers, dimers and tetramers (Bystrova*, et al.*, 2007; Choi*, et al.*, 1998; Smeets*, et al.*, 2008). However, unlike Prx1, Prx6 subfamily members do not appear to form decamers. This is due to the presence of the loop between α_4 and β_6 (Fig 1.16), which disrupts the A-type interface responsible for higher order associations in the Prx1 member proteins. The inability of Prx6 to form higher order structures (teroid-shaped-decamer) suggests that they will not have chaperone activity but more likely serve as peroxidases.

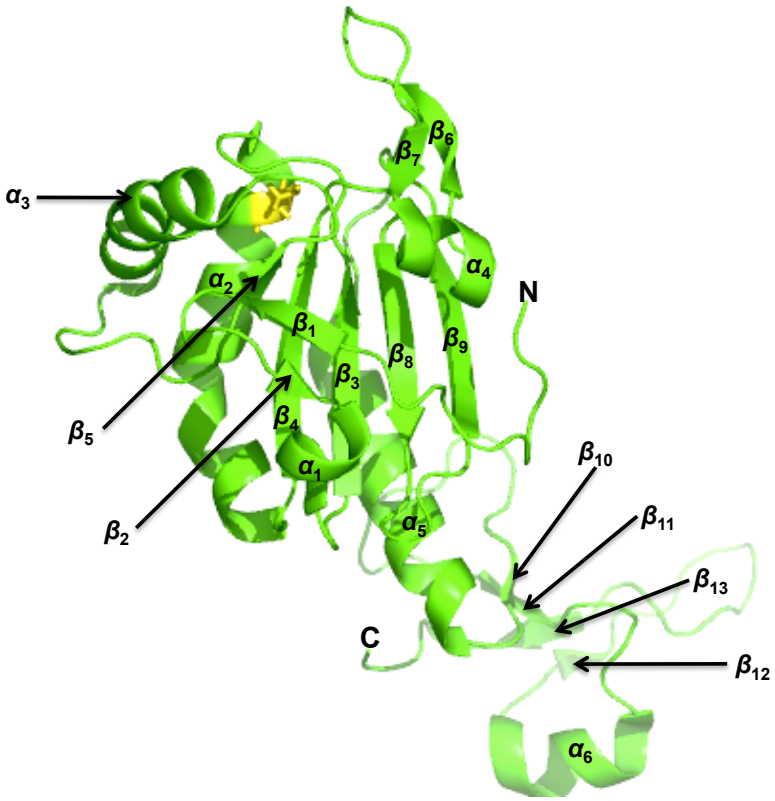

Fig 1.13: Cartoon representation of secondary structural elements of Prx6. A representative FF Prx6 structure with the C_p (represented as sticks, yellow) shown within the first turn of the α_2 helix. The diagram shows that Prx6 has 13 β-strands and 6α-helices (Prx6 numbering). The diagram was generated based on the structure of *Am*PRDX6 (PDB entry 2V2G) and the figure has been visualized using the PYMOL Molecular Graphics System (2003) Delano Scientific, San Carlos, CA, USA.

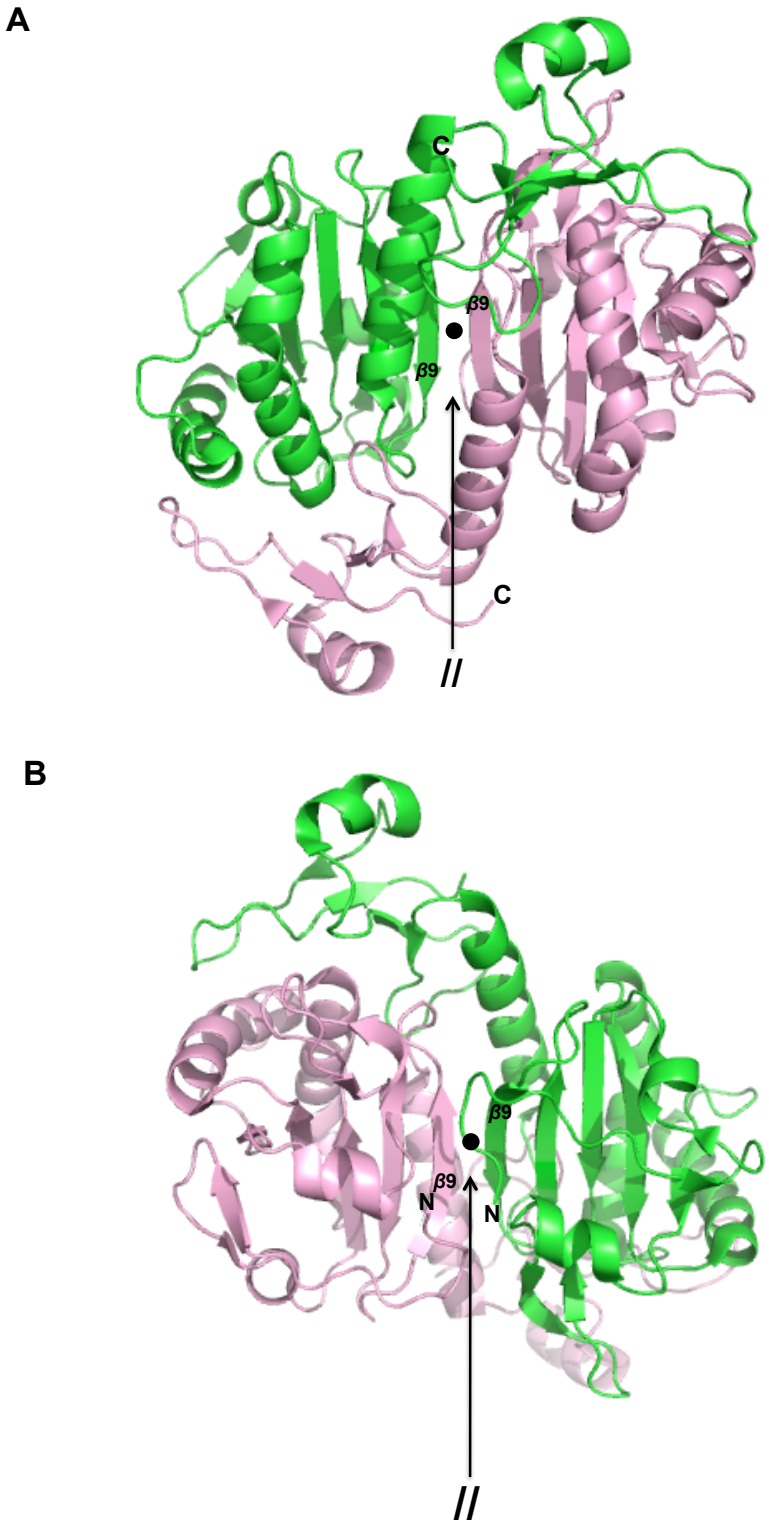

Fig 1.14: Cartoon representation of the B-type dimer interface of Prx6. The B-type interface has been displayed such that the C-terminus of the structure is visible in (A) and the N-terminus in (B). The 2-fold axis is represented by a dot. Both images were generated based on the structure of *Am*PRDX6 (PDB entry 2V2G) and the figure has been visualized using the PYMOL Molecular Graphics System (2003) Delano Scientific, San Carlos, CA, USA.

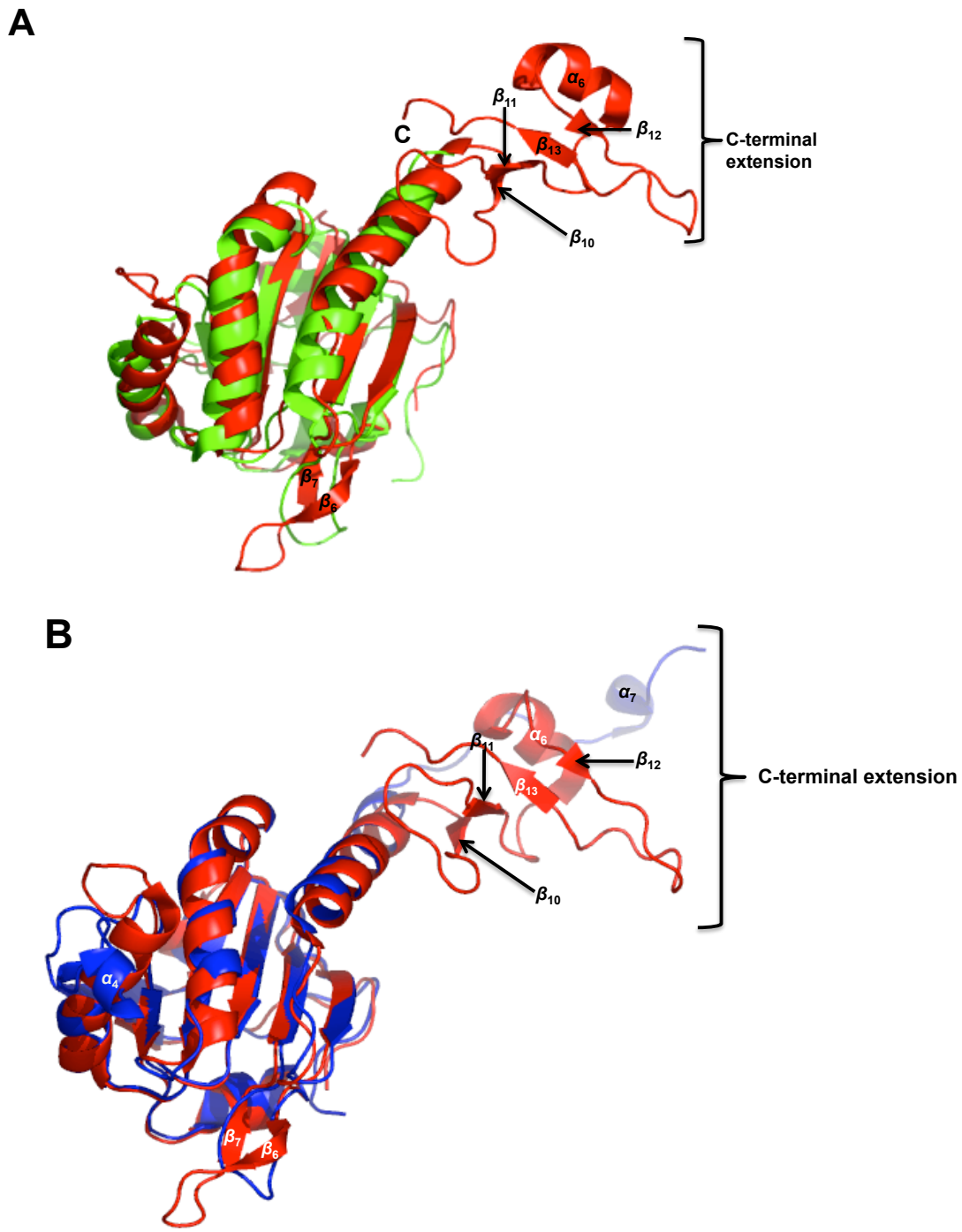

Fig 1.15: Overlay of core Prx, Prx1 and Prx6 structures. (A) Shows overlay of Prx core structure (PDB entry 2A4V, green) and Prx6 structure (PDB entry 2V2G, red) while (B) shows overlay of Prx1 (PDB entry 3HY2, blue) and Prx6 (PDB entry 2V2G, red). (A) shows that Prx6 has C-terminal extension which gives rise to a number of secondary structural elements including β-strand (β_{10}, β_{11}, β_{12}, β_{13}) and helix α_6. Prx6 incorporates a β-hairpin (β_6 and β_7) which is not present in the core Prx structure while both Prx1 and Prx6 have C-terminal extensions as shown in (B). The figure has been visualized using the PYMOL Molecular Graphics System (2003) Delano Scientific, San Carlos, CA, USA.

1.5.3 TPx subfamily

The TPx subfamily (previously referred to as the "E" group) are predominantly found in Gram-positive and Gram-negative eubacteria (Baier & Dietz, 1997; Dietz*, et al.*, 2002; Hofmann*, et al.*, 2002; Noguera-Mazon*, et al.*, 2006b; Rhee*, et al.*, 2001; Stacy*, et al.*, 1999; Trivelli*, et al.*, 2003b; Wood*, et al.*, 2002; Zhou*, et al.*, 1997). TPxs are cytoplasmic proteins released during osmotic shock that serve as main agents for the removal of hydrogen peroxides resulting from oxidative stress in bacteria (Tao, 2008). Most Tpx members use the 2-Cys reaction mechanism with the C_R positioned within its α_3 helix (Fig 1.17) although a small number of 1-Cys Tpx's have been reported (Hall*, et al.*, 2011).

The representative FF structure of Tpx peroxiredoxins contains 6 α-helices and 9 β-strands (Fig 1.17). Tpxs contain an extended N-terminus incorporating a β-hairpin comprised of β-strands β_1 and β_2, which appears to play a role in substrate specificity (Hall*, et al.*, 2011). Compared to the common-core structure of peroxiredoxins, an extra α helix (α_5), which folds toward the N-terminus, is present in Tpx structures (Fig 1.18). Tpxs form homodimers across an A-type interface although its dimer interface does not dissociate with a change in oxidative state (Baker & Poole, 2003). Analysis of representative Tpx structures both in the FF and LU states reveal that the reaction cycle requires the unfolding of the N and C-terminus of the α_2-helix. It appears the unfolding of the N-terminal end of the α_2-helix results in changes in the packing interaction of the α_2 and α_3, leading to the destabilization of the C-terminal end of α_3, allowing the exposed C_p and C_R (now in close proximity) to form disulphide bridges between the S_POH and S_RH (Fig 1.19A). The change in conformation of Tpxs from FF to LU during their reaction cycle results in massive structural changes especially at the α_2 and

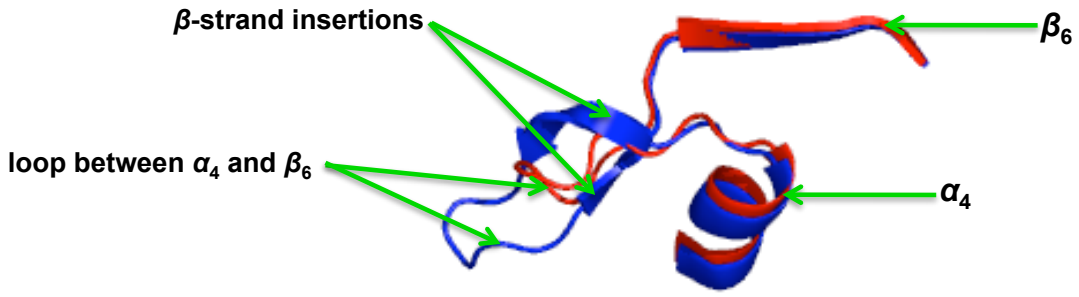

Fig 1.16: Overlay of regions corresponding to α_4 and β_6 of Prx1 and Prx6 structures. The image shows the presence of two β-strands in the loop between α_4 and β_6 in Prx6 but not Prx1 (PDB entry 3HY2, red). Prx1 contains A-type dimer interface through which it forms higher ordered structures (teroid-shaped decamer). The loop between α_4 and β_6 is one of the sites used to form the A-type interacting interface (Smeets, *et al.*, 2008). The loop between α_4 and β_6 of Prx6 (PDB entry 2V2G, blue) contains two β-strand insertions which crowd out this region ensuring that it is not available for the formation of the A-type dimer interface (Smeets, *et al.*, 2008). All Prx6 have been classified as B-type dimers and although some Prx6 structures have been shown to be tetramers, the interaction that allows for higher oligomers to form is not based on the A-type interface. The figure has been visualized using PYMOL Molecular Graphics System (2003) Delano Scientific, San Carlos, CA, USA.

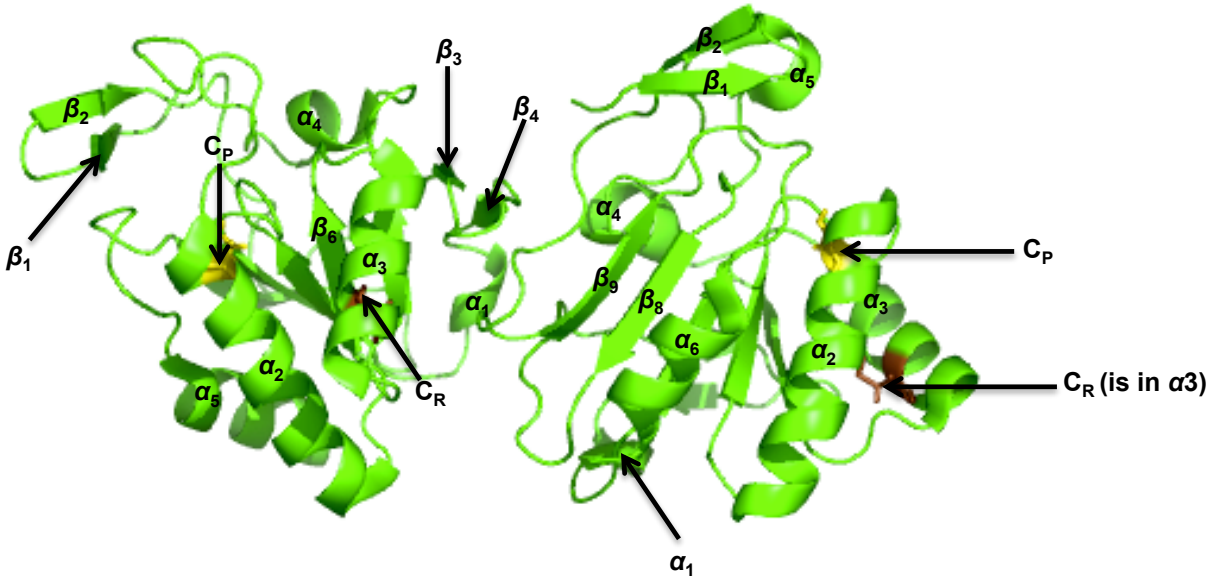

Fig 1.17: Cartoon representation of structural elements of Tpx. The diagram shows that Tpxs have 6 α-helices and 9 β-strands. The C_p (displayed as sticks, yellow) is found within the first turn of α_2-helix while the C_R (displayed as sticks, brown) is located within α_3 helix with C_p and C_R separated by a distance of 15 Å (Choi*, et al.*, 2003). The image was generated based on the structure of *Mt*Tpx (PDB entry 1Y25) and the figure has been visualized using PYMOL Molecular Graphics System (2003) Delano Scientific, San Carlos, CA, USA.

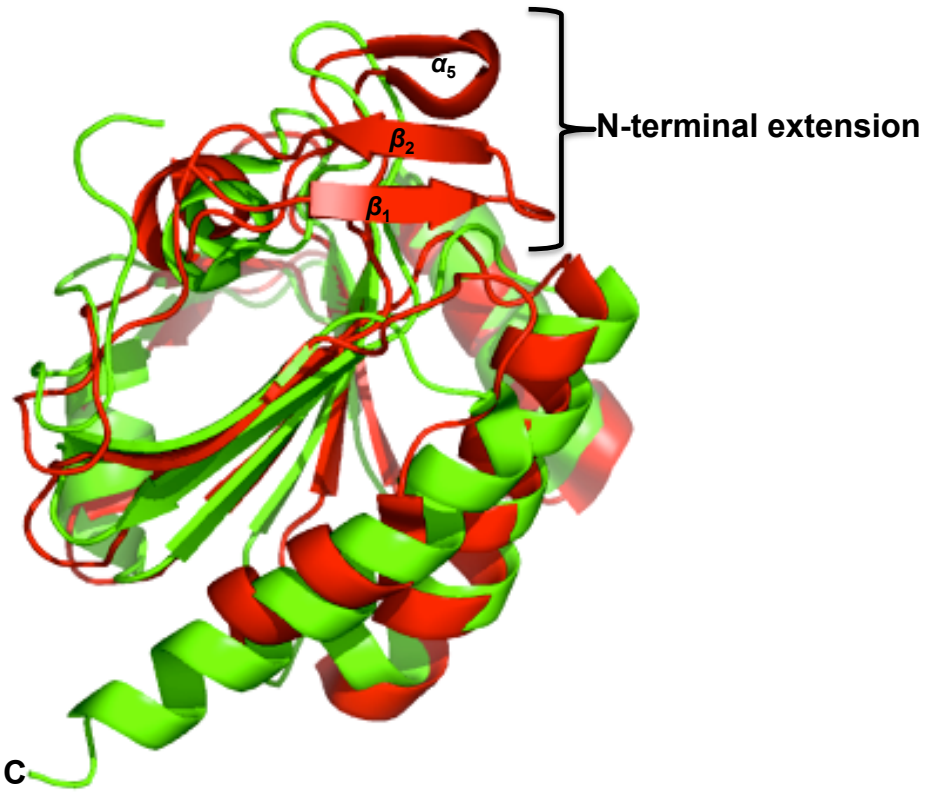

Fig 1.18: Overlay of the common core Prx structure with Tpx. The image shows that Tpxs (red) have an extended N-terminal end which gives rise to three additional secondary structural elements including 2 β-strands (a β-hairpin consisting of β-strands 1 and 2 (Tpx numbering) and an α helix (α5) compared to the conserved common-core structure (green) of Prxs. The N-terminus β-hairpin of Tpxs are involved in the formation of a hydrophobic collar that likely tailors substrate specificity to alkyl peroxidases (Hall*, et al.*, 2011). The image was generated based on structures of *Mt*Tpx (PDB entry 1Y25, red) and the conserved core Prxs structure was generated based on PDB entry 2A4V (green). The figure has been visualized using the PYMOL Molecular Graphics System (2003) Delano Scientific, San Carlos, CA, USA.

α_3 helices (Fig 1.19B).

1.5.4 AhpE

The AhpE subfamily are homologues of AhpC from *Mycobacterium tuberculosis* and closely related bacteria (Cole & Barrell, 1998; Li, *et al.*, 2005; Soito, *et al.*, 2010). AhpE shares approximately 34 and 25 % sequence identity with AhpC and BCP respectively (Hall, *et al.*, 2011; Li, *et al.*, 2005). There is no conserved C_R, on the basis of which AhpE is classified as a 1-Cys peroxiredoxin. As yet no physiologically relevant reductant has been identified (Soito, *et al.*, 2010).

Structures of AhpE members have been determined in reduced and oxidised states (Li, *et al.*, 2005) and they crystallize as homodimers with A-type interfaces (Fig 1.20). Each of the monomers consists of nine 9 β-strands and 5 α-helices (Fig 1.20). Size exclusion chromatography suggests that *Mt*AhpE may form octamers in solution (Li, *et al.*, 2005). A unique feature of AhpE is an extended N-terminal loop parallel to strand β_9 (Fig 1.20A) that makes hydrogen-bonding interactions with it and ensures that β_9 cannot participate in a B-type interface of the kind seen in Prx1 and Prx6 (Li, *et al.*, 2005). The C-terminal end of AhpE lacks a C-terminal extension like those found in Prx1 and Prx6 subfamilies. AhpE includes a β-hairpin insertion comprising of strands β_6 and β_7 between helix α_4 and strand β_6 and a longer loop between β_7 and α_5 as compared to the core Prx structure (Hall, *et al.*, 2011) (Fig 1.21).

Comparison of the oxidised and reduced forms of the AhpE structures reveals that in the sulphenic acid state (S_pOH) the arginine and threonine, which together stabilize the thiolate C_p, swing away allowing the loop between β_7 and α_5 to shift in position, resulting in opening up of the active site (Li, *et al.*, 2005).

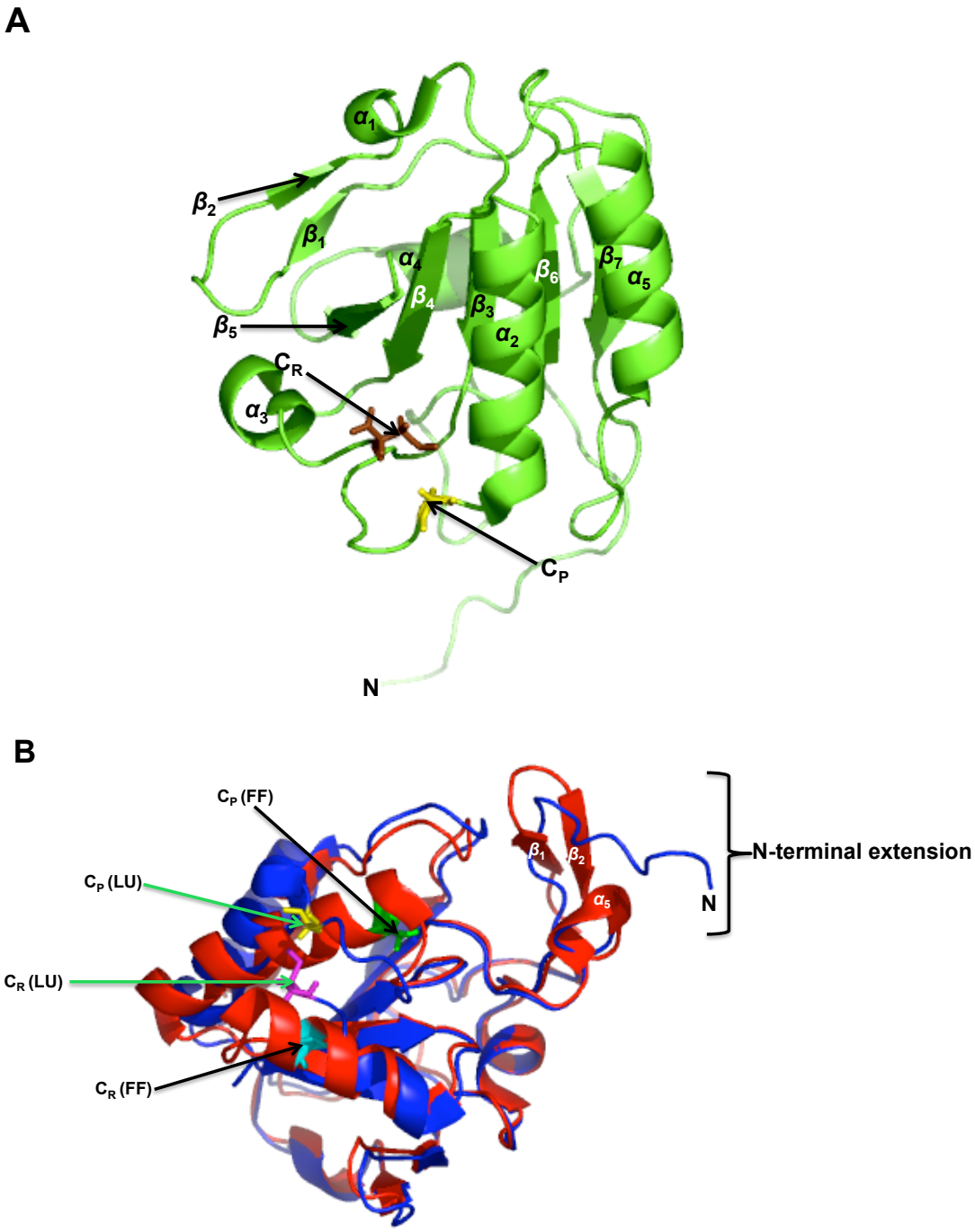

Fig 1.19: Cartoon representation of Tpx structure. (A) Shows the structure of TPX in fully folded (FF) conformation while (B) shows an overlay of FF (red) and the LU (blue) TPx. The FF Tpx structure shows that the catalytic cysteine (C_p) (green sticks) is located within the 1st turn of helix α_2 but become exposed in the LU conformation (yellow sticks) due to unfolding of the N terminus of α_2 helix. The C_R is located in helix α_3 in the FF conformation (cyan sticks) but becomes exposed in the LU conformation (pink sticks). The C_p and C_R become aligned and come into close proximity to form a disulphide bond and lock the structure in the LU conformation following structural changes associated from the unfolding of the N and C termini of α_2 and α_3 helices respectively. The FF Tpx structure was generated based on the structure of *Mt*Tpx (PDB entry 1Y25) while the LU Tpx structure was generated based on the structure of *Mt*Tpx (PDB entry 1XVQ). The figure has been visualized using the PYMOL Molecular Graphics System (2003) Delano Scientific, San Carlos, CA, USA.

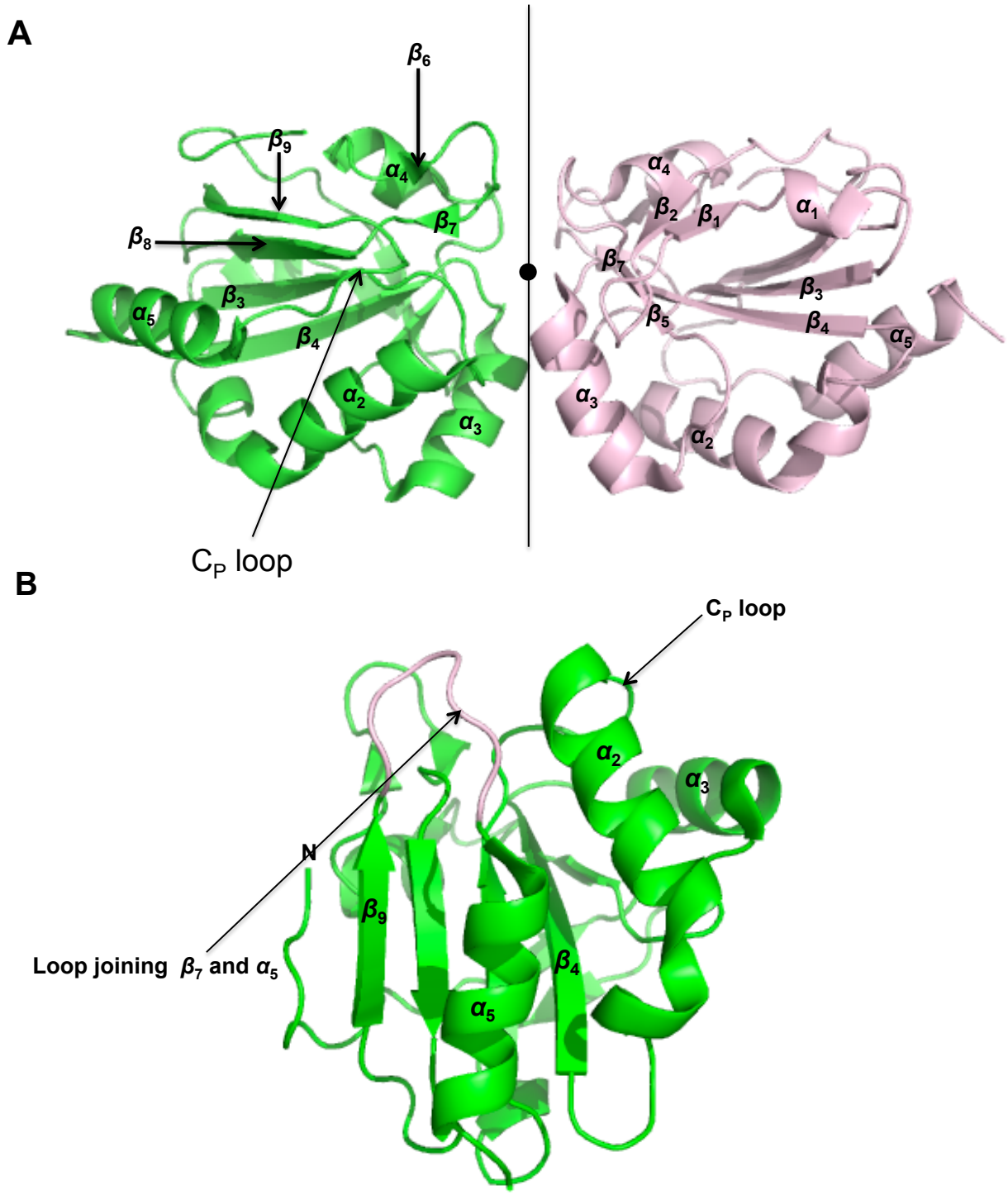

Fig 1.20: Cartoon representation of the structure of a representative member of AhpE. The A-type dimer interface is shown in (A) while the monomer structure containing 5 α-helices and 9 β-strands is shown in (B). The C_p is found within the first turn of α_2-helix and is preceded by the Cp-loop. The oxidation of the catalytic thiolate to SOH is accompanied re-arrangement of the loop joining β_9 and helix α_5. The image was generated based on the structure of *Mt*AhpE (PDB entry 1XXU) and the figure has been visualized using the PYMOL Molecular Graphics System (2003) Delano Scientific, San Carlos, CA, USA.

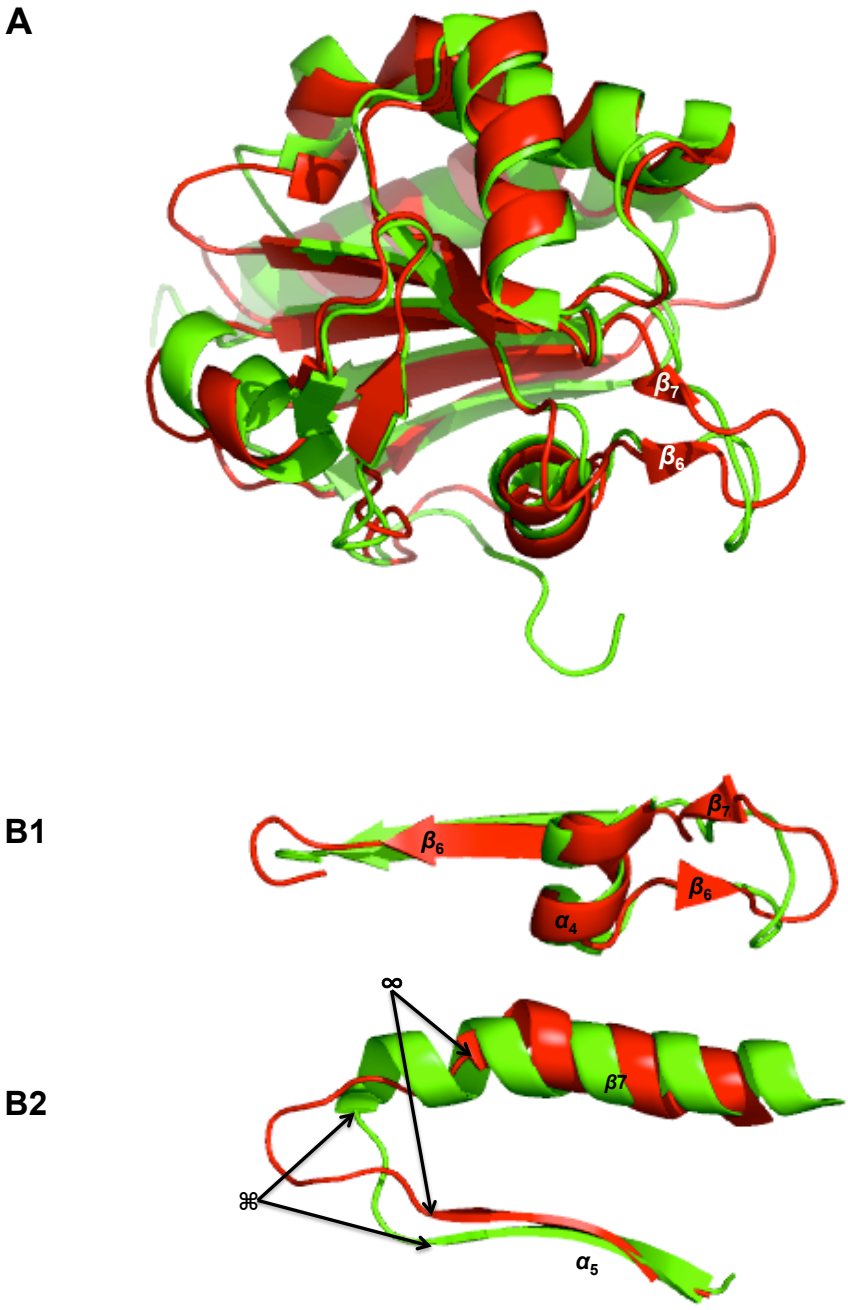

Fig 1.21: Overlay of the conserved core Prxs and AhpE structures. (A) Shows the overlay of both structures (core Prx structure has been coloured green, while AhpE structure has been coloured red) while an expanded view of regions between α_4 and β_6 and α_5 and β_7 (core Prx structure numbering) can be seen in (B1) and (B2). The region between α_4 and β_6 in AhpE has a β-hairpin insertion (β_6 and β_7, AhpE numbering), which is absent in the conserved core structure while the region between α_5 and β_7 show an extended loop in AhpE (∞) compared to the same region in the core structure (⌘). The re-arrangement of the extended loop between α_5 and β_7 is associated with the oxidation of the catalytic thiolate to SOH. These images where generated based on the core structure (PDB entry 2A4V, green) and AhpE (PDB entry 1XXU, red) respectively and have been visualized using the PYMOL Molecular Graphics System (2003) Delano Scientific, San Carlos, CA, USA.

This re-arrangement of the structure is thought to represent the first stage of the resolution of the 1-Cys Prx. Subsequent conformational changes are expected to occur involving helix α_2, which should expose and position the C_p for a reaction with a partner protein or small molecule (Hall, *et al.*, 2011).

1.5.5 BCP

Bacterioferritin comigratory protein (BCP) is representative of a subfamily of Prxs which were previously commonly referred to as the "C" group (Hofmann, *et al.*, 2002). They were originally identified largely in pathogenic bacteria but have been subsequently been shown to be widely distributed in fungi and plants (PrxQ) (Jeong, *et al.*, 2000; Kong, *et al.*, 2000; Rouhier, *et al.*, 2004). BCPs are divided into two main groups consisting of 2-Cys and 1-Cys members respectively (D'Ambrosio, *et al.*, 2009). The 2-Cys group has been further divided into the PrxQα and PrxQβ members based on the position of the C_R (Wakita, *et al.*, 2007). Hall and co-workers have recently suggested that this method of classification may not suffice for all members of the BCP subfamily in Prxs (Hall, *et al.*, 2011).

BCP structures have been reported to exist both as monomers and dimers (A-type interface) (Fig 1.22) (Hall, *et al.*, 2011) with the β-hairpin (β_6 and β_7) insertion suggested to play some role in preventing the formation of stabilising hydrogen bonds that can affect the oligomeric state of the protein as well in the regulation of the accessibility of the substrate channel (Echalier, *et al.*, 2005).

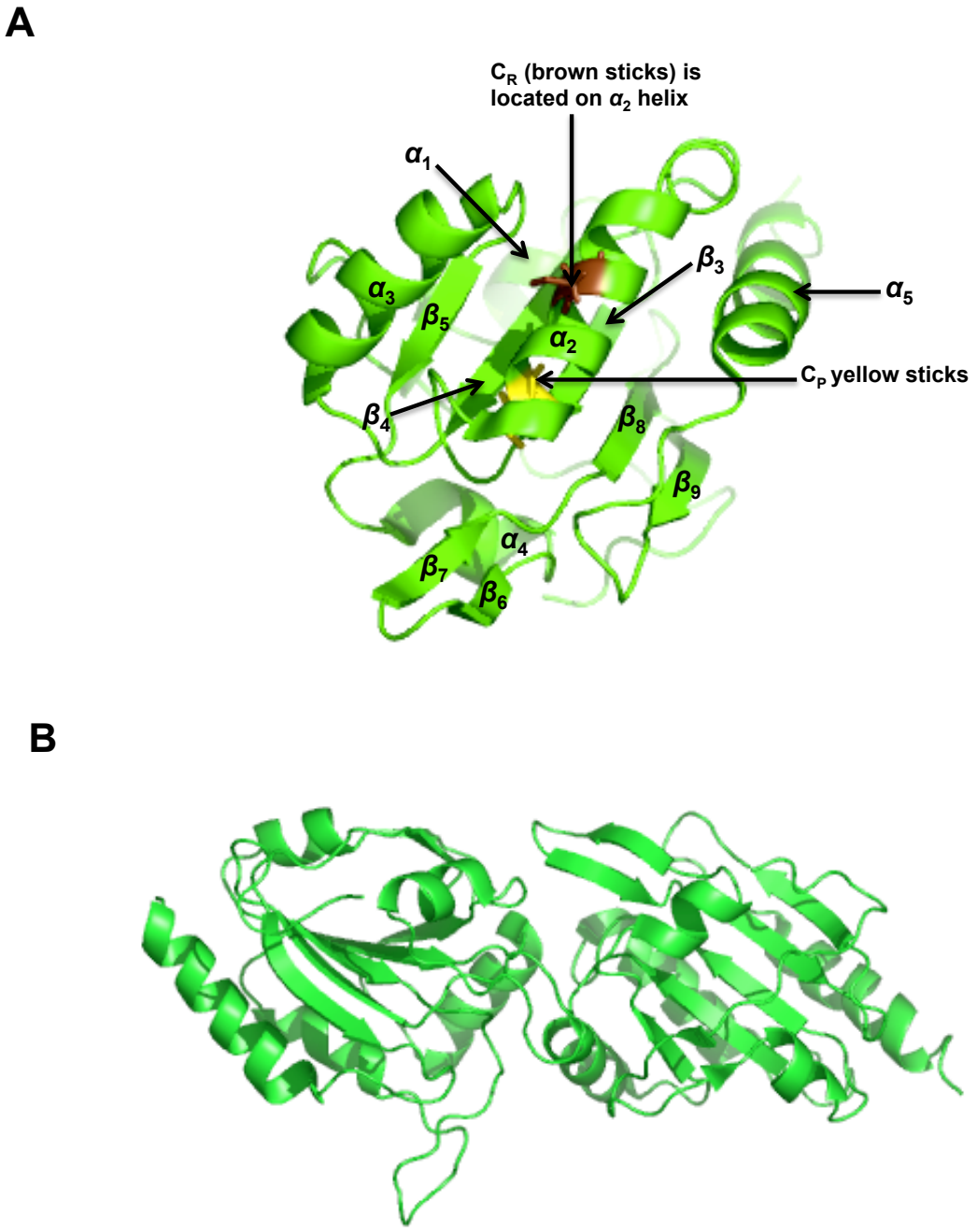

Fig: 1.22: Cartoon representation of the structure of *Ap*BCP. (A) The FF BCP structure with the C_p (yellow sticks) and C_R (brown sticks) located on the α_2-helix is shown in (A). The C_p and C_R are at about 10 Å apart in the FF conformation (D'Ambrosio, *et al.*, 2009) while the dimeric structure (A-type interface) of BCP is shown in (B). Image shown in (A) was generated based on the structure of *Ap*BCP (PDB entry 2CX4) and while image (B) was generated based on the structure of *Ap*BCP (PDB entry 2CX4). The figure has been visualized using the PYMOL Molecular Graphics System (2003) Delano Scientific, San Carlos, CA, USA.

1.5.6 Prx5 subfamily

The Prx5 subfamily (previously referred to as the "D" group) has been identified in mammals, fungi, bacteria and higher plants (Dietz, 2011; Knoops*, et al.*, 1999; Seo*, et al.*, 2000; Soito*, et al.*, 2010; Zhou*, et al.*, 1997). It is named after the Human PRDX5, the first structure belonging to this subfamily to be elucidated (Declercq*, et al.*, 2001). Human PRDX5 is present in a number of compartments including the mitochondria, peroxisomes, nucleus and cystosol (Declercq*, et al.*, 2001; Seo*, et al.*, 2000; Zhou*, et al.*, 1997). 83 % of Prx5 proteins use the 1-Cys mechanism, but 17 % use the 2-Cys, with the C_R located in the loop preceding helix α_5. A number of agents including glutaredoxin and thioredoxins have been shown to function as proton donors (Hall*, et al.*, 2011; Rouhier*, et al.*, 2001; Soito*, et al.*, 2010).

Structures of a number of Prx5 members have been resolved in both the FF and the LU conformations. The FF human Prx5 structure is made up of 6 α-helices and 7 β-strands (Fig 1.23A). A number of structural changes have been observed upon the oxidation of the human Prx5 structure including the unfolding of the N-terminus of the α_2-helix and the swinging away of the α_6 helix which leads to the exposure and positioning of the C_p and C_R for disulphide bridge formation (Fig 1.23B).

A feature of the Prx5 subfamily is the presence of an extra residue immediately after the C_p within its α_2-helix, which results in a bulging of the C-terminal end of the α_2-helix or "α-aneurysm" (Sarma*, et al.*, 2005). Prx5 proteins have a much shorter α_5 helix compared to the core Prx structure (Fig 1.24).

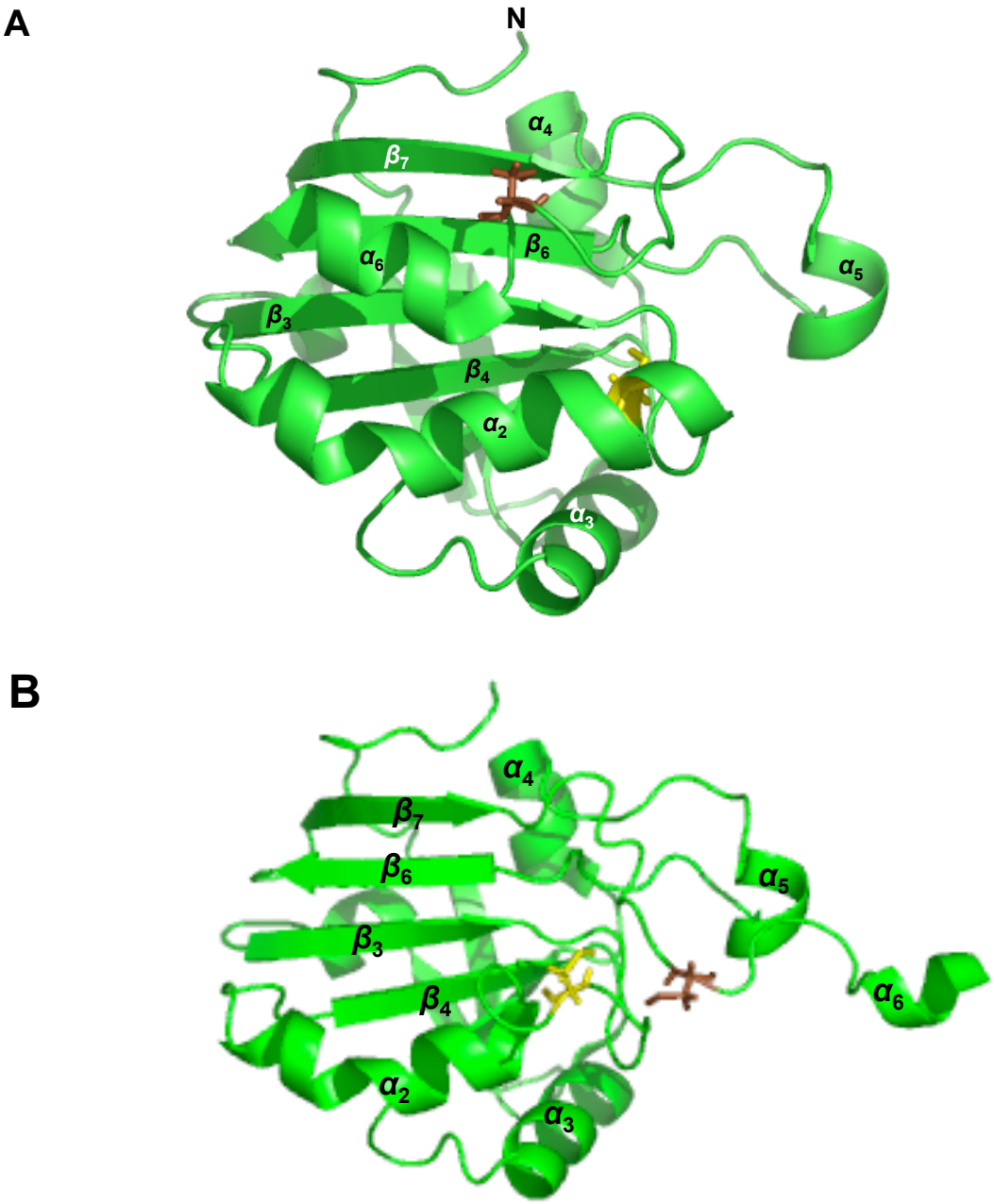

Fig 1.23: Cartoon representation of *Hs*PrxV structure. (A) *Hs*PrxV (FF) structure (PDB entry 1HD2) with the C_P (yellow sticks) and C_R (brown sticks). The C_P and C_R are at a distance of about 13 Å in the FF structure and cannot therefore form disulphide bridges (Evrard*, et al.*, 2004) (B) LU structure of *Hs*PrxV (PDB entry 1OC3 chain C) with the C_P (yellow sticks) in positioned closer to each other which allows disulphide bridges to be formed between the C_P and C_R. A number of changes occur to the structural features of *Hs*PrxV upon oxidation including the unfolding of the first two turns of the α_2-helix and the swinging away of the α_6 helix allowing the C_P and C_R to be positioned near each other at a distance that allows disulphide bridges to be formed between these residues. The figure has been visualized using PYMOL Molecular Graphics System (2003) Delano Scientific, San Carlos, CA, USA.

Fig 1.24: Overlay of *Populus tremula* Prx5 and core Prx structure. The Prx5 structure was generated based on PDB entry 1TP9 (red) while the core Prx structure was generated based on PDB entry 2A4V (green). The presence of a β-hairpin (β_6 and β_7) can be seen between α_4 and β_6 (core Prx structure numbering) in Prx5 but not in the core Prx structure. The length of helix α_5 is shortened in the Prx5 structure compared to that of the core Prx structure. The figure has been visualized using the PYMOL Molecular Graphics System (2003) Delano Scientific, San Carlos, CA, USA.

Prx5 members form homodimers across an A-type interface. The active site is located very close to the dimer interface and each site contains parts of both monomers, in particular the β-hairpin $\beta_6\beta_7$, suggesting that homo-dimerisation may be essential for catalytic activity (Echalier*, et al.*, 2005).

The effect of oxidation on the oligomeric state of Prx5 peroxiredoxins has been examined by Evrard and co-workers and more recently by Noguera-Mazon and co-workers (Evrard*, et al.*, 2004; Noguera-Mazon*, et al.*, 2006b). Evrard and co-workers reported that reduced and oxidised forms (sulphenic acid form) of human Prx5 eluted at the same volume in size exclusion analysis suggesting that the oligomeric state of Prx5 is not affected by oxidation. However the crystal structure of the oxidised protein showed structural changes including the unwinding of the N-terminus of the α_2 helix. Noguera-Mazon and co-workers showed that the non-covalent homodimer of *Populus tremula* Prx is dissociated by glutathionylation of the C_P. Results from NMR relaxtion analysis revealed that glutathionylation resulted in the complete unfolding of the α_2 helix, disrupting the interface and dissociating the homodimer into monomers (Noguera-Mazon*, et al.*, 2006b).

Glutathionylation followed by the rescue of the glutathionylated protein by glutaredoxin (Fig 1.25) has been proposed to represent the regeneration mechansim of the Prx5 subfamily. It is important to address the issue of the oligomeric state of *Xv*Prx2 and to investigate the effect of oxidation and glutathionylation on the oligomeric state of *Xv*Prx2.

Based on the similarity of the decamer to dimer transition of the Prx1 subfamily and

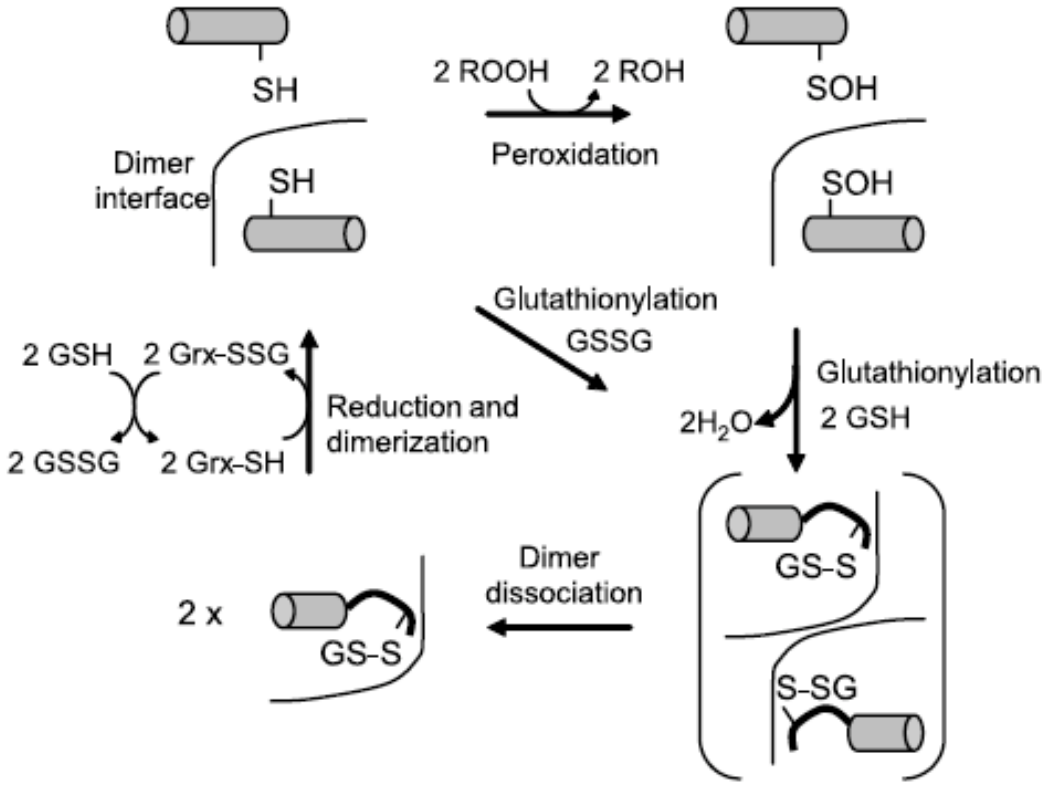

Fig 1.25: Reaction mechanism for the Prx5 subfamily. The model proposes that glutathionylation induces the unwinding of the α_2-helix resulting in the dissociation of the dimeric structure into monomers. The glutathionylated protein is then regenerated through its interaction with glutaradoxin. This figure was taken from Noguera-Mazon*, et al.*, 2006b.

the dimer to monomer transition of the Prx5 subfamily, we can assume that the monomeric form of Prx5 corresponds to the LU structure. At this present time, there are no reports of LU structures of the Prx5 subfamily with the 1-Cys reaction mechanism (Hall, et al., 2011) and we assume that this is partly due to the difficulty encountered in generating a stable monomeric form of the protein. pH is another factor which has been shown to affect the oligomeric state of Prx1 from decamer to dimer. Kristensen and colleagues showed that Prx1 decamers dissociated into dimers at a narrow range (pH 7 and 8) with the dimer observed at pH 8.53 and the decamer at pH 5.4. There are no reports of the effect of pH on the oligomeric state of any other Prx subfamily. In an attempt to understand the factors that govern the interaction responsible for the oligomeric state of *Xv*Prx2 we will investigate the effect of pH on the oligomeric state of *Xv*Prx2.

*Xv*Prx2, the subject of this work, is a close homologue of Prx isolated from *Populus tremula* (*Pt*PrxD). The structure of *Populus tremula* revealed an active site containing a histidine residue (H55), which is involved in hydrogen bonding network with $N^{\eta 1}$-$H^{\eta 12}$ of Arg129 and with the carbonyl group of S153 (Echalier*, et al.*, 2005). The H55 is important as a hydrogen-bond acceptor positioning the conserved arginine in the active site of the Prx5 (Hall*, et al.*, 2010). A comparison of the active sites of Prx5 and Prx6 revealed the presence of H39 (Prx6), which was closer to the C_p in Prx6 than the H55 is to the C_p in Prx5 (Choi*, et al.*, 1998; Echalier*, et al.*, 2005).

H39 makes important interactions with C_p following the disruption of hydrogen bonds between the C_p and conserved arginine and upon the formation of the sulphenic acid group in Prx6 (Choi*, et al.*, 1998).

H55 makes hydrogen-bonding interactions with the active site cysteine and arginine (see Fig 1.2B) and may play some role in the stability of deprotonated form of Prx5 and contribute to the pK_a of Prx5 proteins. In the later chapters of this work, we investigate the role of H55 in determining the pK_a of the protein and the stability of the ionized state of the thiol group.

1.6 Aims of the study

*Xv*Prx2 is a member of the Prx5 subfamily of peroxiredoxins found to be over-expressed in *Xerophyta viscosa* under desiccation conditions suggesting it may play a role in the protection of proteins or cellular components against reactive oxygen and nitrogen species. Support for this was found in a previous study that revealed the presence of multiple homologues of *Xv*Prx2 in *X. viscosa*, which were involved in ROS scavenging and thereby protecting nucleic acids from oxidative damage by ROS (Govender, 2006). No structure of *Xv*Prx2 is available, although a structure of the closely related Prx from *Populus tremula* (*Pt*PrxD) has been determined by X-ray crystallography. This structure and associated studies showed that *Pt*PrxD forms non-covalent homodimers across the A-type interface. Noguera-Mazon and co-workers showed that *Pt*PrxD could form disulphide bonds with glutathione, and that this process led to unfolding of the C_p-loop and α_2-helix and disruption of the homodimer. Noguera-Mazon and co-workers suggested furthermore that glutathionylation may play a physiological role in regeneration of peroxiredoxins of this subfamily and proposed a model for the reaction of the Prx5 subfamily (Fig 1.25) whereby Prx5 proteins undergo oxidation followed by glutathionylation and the glutathionylated species are rescued by glutaredoxin.

The objectives of the study are as follows:

1. The structure of *Xv*Prx2 will be determined using X-ray crystallography. This requires that milligram quantities of *Xv*Prx2 be produced and purified to homogeneity. The fragment coding for peroxiredoxin will be amplified using Polymerase Chain Reaction and cloned into the pGEX-6P-2 expression plasmid for expression in *E. coli*. Purification will be achieved by glutathione affinity chromatography using the GST tag after which GST will be removed using 3C protease.

2. The oligomeric state of *Xv*Prx2 will be investigated using size exclusion chromatography (SEC), nuclear magnetic resonance spectroscopy (NMR) and mass spectrometry, to confirm that it forms a non-covalent homodimer like *Pt*PrxD. ^{15}N-HSQC NMR spectra of both the monomeric and homodimer states will be assigned using triple resonance experiments on ^{13}C- and ^{15}N-enriched samples and used to determine the position of the dimerization interface.

3. The effect of glutathionylation and oxidation on the structure will be investigated using SEC and NMR.

4. The model proposed by Noguera-Mazon and co-workers for the regeneration of members of the Prx5 subfamily of peroxiredoxins will be tested by adding reduced glutathione to oxidised *Xv*Prx2 or oxidized glutathione to reduced *Xv*Prx2 and then attempting to reduce the resulting mixed disulphide either with DTT or glutaredoxin.

The rest of the thesis is organized as follows:

- Chapter 2 describes the materials and methods used in this work.

- Chapter 3 describes the generation of the pGEX-6P-2-*Xv*Prx2 expression construct and the development of a protocol for large-scale production of *Xv*Prx2 in bacteria and the purification of *Xv*Prx2 to homogeneity.
- Chapter 4 describes the preliminary characterization of *Xv*Prx2 using 1D and ^{15}N-HSQC NMR spectra, the investigation of the effect of pH on the oligomeric state of *Xv*Prx2 and the full and partial assignment of backbone and side chain resonances of the dimeric state respectively.
- Chapter 5 investigates the contribution of His55 and Cys51 to the stability of the dimeric state of *Xv*Prx2 as a function of pH and the effect of oxidation and glutathionylation of *Xv*Prx2 on the oligomeric state of the protein.
- Chapter 6 highlights our findings and outlines future lines of investigation.

Chapter 2: Materials and methods

2.1 Bacterial strains used

Escherichia coli (E. coli) BL21 (DE3) pLysS: F-*omp* T *hsd*S_B (rB-mB-) *gal dcm rne131*

MC1061 F^- *araD139* Δ*(ara-leu)7696 galE15 galK16* Δ*(lac)X74 rpsL* (Str^r) *hsdR2* (r_K^- m_K^+) *mcrA mcrB1*

2.2 General stock solutions, buffers and media

Ammonium Persulphate: 10 % stock solution was prepared in deionised water, stored at -20 °C.

Ampicillin: 100 mg/ml stock solution was prepared in deionised H_2O, sterilized by filtration using a 0.22 micron filter, stored at -20 °C.

Bradford Dye Stock: 0.1 % Coomassie brilliant blue G 250, 8.5 % phosphoric acid and 4.75 % ethanol. The solution stored at 4 °C was diluted 5 times with deionized water prior to use and filtered using a 0.45 micron filter.

Cell Lysis Buffer: 1 % Triton X-100, 50 µg/ml DNAse 1, 100 µg/ml lysozyme, 1 mM PMSF, 1 mM DTT, and 1 tablet of Complete™ EDTA-free protease inhibitor cocktail in 50 ml of PBS.

Coomassie Staining Solution: 0.025 % Coomassie Blue R-250, 40 % methanol and 7 % acetic acid in 2000 ml deionised water.

De-staining Solution: 10 % (v/v) acetic acid and 7 % (v/v) methanol.

10X DNAse 1 Buffer: 0.5 M Tris-HCl pH 7.5, 0.1 M $MnCl_2$, 0.5 mg/ml bovine serum albumin (BSA), sterilized by filtration, stored at -20 °C.

DNAse free RNAse buffer: 0.1 M sodium acetate anhydrate, 0.1 mM EDTA, pH 4.8, stored at -20 °C.

DTT: 1 M stock solution was prepared in 10 mM sodium acetate, pH 5.2, sterilized by filtration and stored at -20 °C.

ESI-MS buffer (non-denaturing): Ammonium acetate pH 5 to 8, filter sterilized using 0.22 micron filter, stored at room temperature.

Ethidium Bromide: 10 mg/ml stock solution was prepared in water, and stored in the dark at 4 °C.

GTE: 50 mM glucose, 50 mM Tris-HCl and 10 mM EDTA pH 8.0.

Glutathionylation buffer: 100 mM GSSG stock solution prepared in 10 mM ammonium acetate pH 7, stored at 4 °C

IPTG: A 1 M stock solution was prepared in deionised water, sterilized by filtration and stored at -20 °C.

Luria agar: 10 g/l tryptone powder, 5 g/l yeast extract, 5 g/l NaCl and 14 g/l bacteriological agar.

Luria broth: 10 g/l tryptone powder, 5 g/l yeast extract, and 5 g/l NaCl

Lysis Solution: 200 mM NaOH containing 1 % SDS.

Minimal media: 12.8 g/l Na_2HPO_4-$7H_2O$, 3 g/l KH_2PO_4, 1 g/l NH_4Cl and 0.5 g/l NaCl. The media was pH adjusted to 7.0 with NaOH and the solution was autoclaved. Immediately prior to use, the solution was supplemented with 2 ml of autoclaved 1 M $MgSO_4$, 100 µl of autoclaved 1 M $CaCl_2$ and 20 ml of filter-sterilized 20 % glucose. The solution was stored at room temperature.

Neutralization solution: 3 M potassium acetate, pH 5.0.

NMR buffer: 50 mM Sodium phosphate buffer pH 5.0, 6.0, 7.2, and 8.0 containing 20 mM NaCl, 10 mM DTT and 1 mM NaN_3.

PBS: 137 mM NaCl, 2.7 mM KCl, 8 mM Na_2HPO_4-$7H_20$ and 1.5 mM KH_2PO_4. The solution was pH adjusted to 7.4.

PBS-T: PBS containing 1 % Triton X-100, stored at 4 °C.

Phenol: chloroform: isoamlyalcohol: 25 parts Tris-saturated 24 parts phenol and 1 part chloroform.

PMSF: A 10 mM stock solution was prepared in isopropanol, stored at -20 °C.

3C protease cleavage buffer: 50 mM Tris pH 7.0 containing 150 mM NaCl, 1 mM DTT and 0.01 % Triton X-100. The solution was prepared fresh prior to use.

Protein elution buffer: 10 mM reduced glutathione in 50 mM Tris pH 9.0 containing 150 mM NaCl, 1 mM EDTA and 1 mM NaN_3.

2X SDS PAGE Sample buffer: 4 % SDS, 0.150 M Tris pH 6.8, 20 % glycerol and 1 mg/ml Bromophenol Blue, stored at 4 °C.

5X SDS Electrophoresis Buffer: 25 mM Tris, 25 mM glycine and 0.1 % SDS, pH 8.3.

Separating buffer: 1.5 M Tris pH 8.8, stored at 4 °C.

4X Stacking buffer: 0.5 M Tris pH 6.8, stored at 4 °C.

10X TBE: 0.9 M Tris-HCl, 0.89 M boric acid and 25 mM EDTA, pH 8.3. The solution was diluted 10-fold with deionised water prior to use.

TBS: 20 mM Tris-HCl and 150 mM NaCl, pH 7.4.

TE: 10 mM Tris-HCl and 1 mM EDTA, pH 7.4.

Tfb1 buffer: 30 mM potassium acetate, 50 mM $MnCl_2$, 0.1 M KCl, 6.7 mM $CaCl_2$ and 15 % glycerol (v/v).

Tbf2 buffer: 9 mM MOPS, 50 mM $CaCl_2$, 10 mM KCl and 15 % glycerol (v/v).

TYM broth: 20 g/l Tryptone powder, 5 g/l Yeast extract, 3.5 g/l NaCl and 2 g/l $MgCl_2$.

2.3 Primer design

PCR primers were designed based on the sequence of *Xv*Prx2*,* isolated from *Xerophyta*

viscosa (Baker) (accession number EU333003). The forward and reverse primers included BamHI and XhoI restriction sites respectively, allowing for the sub-cloning of the *Xv*Prx2 insert from pGEM®-t Easy vector into the BamHI and XhoI restriction sites of the multiple cloning cassette of the pGEX-6P-2 vector. A TAG stop codon was included in the design of the reverse primer (Fig 3.1).

2.4 PCR amplification

Polymerase Chain Reaction (PCR) was used to amplify *Xv*Prx2 using a template kindly provided by Dr Kershini Govender. The PCR reaction mix consisted of template DNA, 1 X PCR reaction buffer, 200 µM dNTPs, 1.5 µM $MgCl_2$, 2.5 U/50 µl Taq, and 0.4 µM of the forward and reverse primers respectively. PCR reactions were carried out by adding appropriate volumes of the reaction mix (Table 2.1) into PCR tubes followed by gentle flicking of tube content and brief centrifugation. PCR tubes were placed in a pre-heated (94 °C) thermal cycler (Gene Amp® 2700 PCR System, Applied Biosystems, USA) and the reaction performed using the following program: 94 ºC for 2 minutes to denature the double stranded DNA, followed by 35 cycles each consisting of the following steps: 94 ºC for 30 seconds to denature the double stranded DNA, 55 ºC for 40 seconds to anneal the double strands, 72 ºC for 45 seconds to extend the DNA and a final elongation step at 72 ºC for 10 minutes. The reaction products were analyzed on a 1 % agarose/ethidium bromide (EtBr) gel and purified using the QIAquick® PCR Purification kit (QIAGEN) according to the manufacturer's instruction.

Reagents	Final concentrations	Volumes (μl)
Forward Primer	0.4 μM	8
Reverse Primer	0.4 μM	8
DNTPs	200 μM	8
$MgCl_2$	1.5 mM	6
10 X PCR Buffer	10 X	20
Template	20 ng	8
Taq polymerase	2.5 u/50 μl	2
H_2O		140
Total		200

Table 2.1: Polymerase Chain Reaction (200 μl) Master Mix. All PCR reactions were carried out using final concentrations of reagents as shown in the Table.

2.5 Agarose gel electrophoresis of DNA

DNA fragments were resolved using 1 % agarose gels. Gels were prepared by pouring appropriate amounts of agarose in 1 X TBE or TE, cooling to 55 - 60 ºC, adding EtBr to 0.5 µg/ml and allowing it to set in a gel tray. DNA samples were mixed with appropriate volumes of loading buffer prior to loading onto gels. Molecular weight markers loaded onto gels were used to estimate the size of DNA fragments. Electrophoresis was carried out in 1 X TBE at 10 V/cm until the dyes migrated an appropriate distance. DNA was visualized under UV light using a transilluminator operating at 254 nm. DNA to be recovered was visualized using a long wavelength (360 nm) to avoid damage to the DNA.

2.6 Plasmids

2.6.1 pGEM®-T Easy vector

The pGEM®-t Easy vector system (Fig 2.1) (Promega) is suited for direct cloning of DNA fragments amplified using *Taq* polymerase, based on the fact that *Taq* polymerase adds an extra dATP nucleotide to the 3' end of amplicons (extendase activity), resulting in 3' A-overhangs at both ends of a double-stranded amplicon (Clark, 1988). The pGEM®-t Easy vector is supplied in a linearised form with a single 3' T-overhang at both ends, allowing direct sticky-end cloning of PCR products.

2.6.2 pGEX-6P-2 Expression vector system

The pGEX gene fusion system (Amersham Pharmacia Biotech) gives high-level inducible expression of target proteins fused to the C-terminus of glutathione-S-tranferase (GST) from *Schistosoma japonicum* and is used for expression, purification and detection of recombinant GST fusion protein.

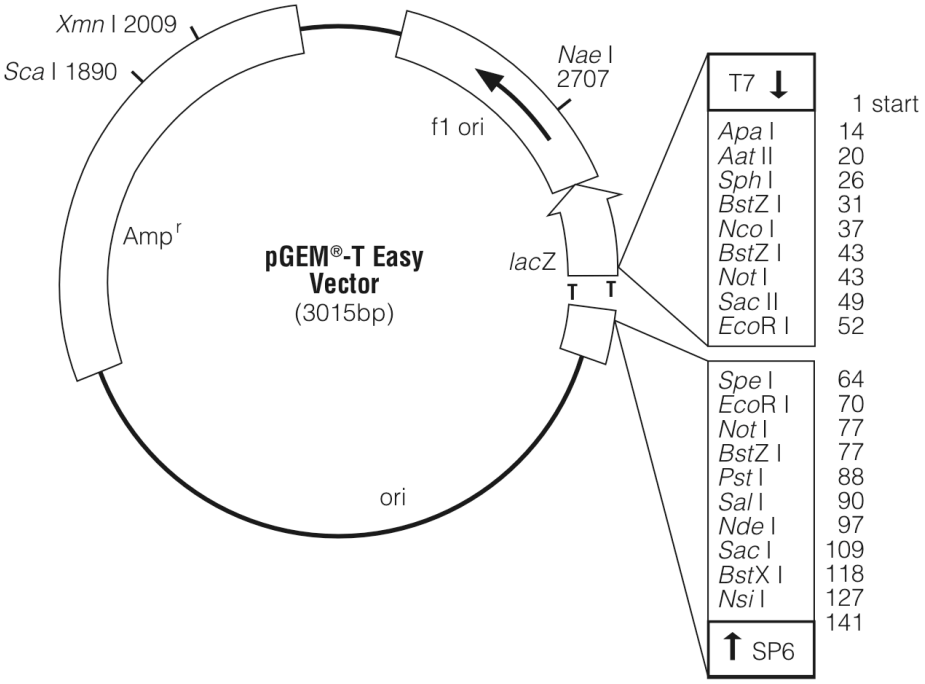

Fig 2.1: Map of pGEM®-T Easy Vector System. T-overhangs and a number of restriction sites can be seen within its *lac*Z gene.

The pGEX-6P-2 expression vector (Fig 2.2) contains a *tac* promoter, which drives high levels of IPTG inducible expression of the recombinant fusion protein in *E. coli*. GST acts as an affinity tag that allows for affinity purification of recombinant fusion protein using glutathione sepharose (Sigma). The pGEX plasmid contains a recognition sequence for 3C protease from human rhinovirus, which allows for the removal of the GST domain following purification of recombinant fusion protein. 3C protease is also expressed as a GST-tagged fusion, allowing for removal of both 3C and cleaved GST in a second round of glutathione affinity purification.

2.7 Cloning of PCR products into pGEM®-T Easy Vector

PCR products were cloned into the pGEM®-T-Easy Vector System (Promega) (Fig 2.1). Ligation reactions were set up as shown in Table 2.2 using various insert to vector ratios, calculated according to the formula shown in below Table 2.2. Ligation reactions were incubated at 4 ºC for 18 hours and products used to transform competent *E. coli* MC1061 cells which had been thawed on ice for 5 minutes. Transformation of the ligation products was carried out by adding 10 µl of the products to 100 µl of competent *E. coli* MC1061, followed by brief flicking of the tubes and incubation on ice for 25 minutes. Thereafter, the cells were heat-shocked at 42 ^{o}C for 45 seconds followed by incubation on ice for 5 minutes following which 900 µl of pre-warmed LB was added to the transformed cells and the cells incubated at 37 ^{o}C for 1 hour. 50 µl of competent *E. coli* MC1061 cells, which had been transformed with the ligation products, was spread on LB agar plates containing 100 µg/ml ampicillin and incubated at 37 ºC for 18 hours.

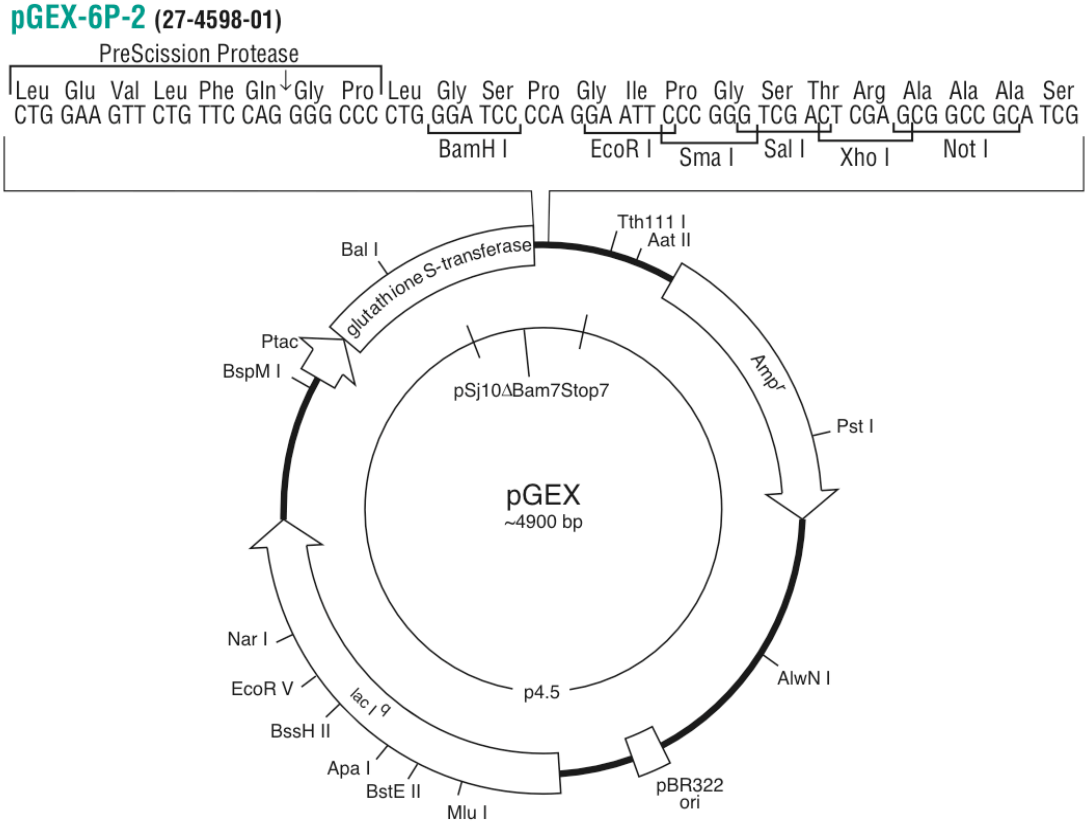

Fig. 2.2: pGEX-6P-2 expression vector map. The map shows the Glutathione-S-transferase domain immediately upstream of the multiple cloning cassatte. The position of the PreScissionTM protease clevage site is shown between the GST domain and the multiple cloning site.

2.8 Screening colonies for the presence of insert using Colony PCR

Colony PCR was carried out by suspending single colonies in 20 µl of distilled water. 1 µl of each suspension was added to the PCR reaction to serve as template and the reaction carried out using the set up shown in Table (2.1), using M13 and gene specific primers respectively. Colonies positive for the presence of inserts were inoculated into LB medium containing 100 µg/ml ampicillin and incubated at 37 ºC for 18 hours.

2.9 Isolation of Plasmid DNA

Small scale plasmid DNA isolation was performed using the alkaline lysis method (Birnboim & Doly, 1979). 10 µl of a suspension of cells was inoculated into 15 ml LB broth containing 100 µg/ml ampicillin and incubated at 37 ºC for 18 hours. The overnight culture was harvested by centrifugation at 6000 x *g* for 10 minutes. The supernatant was discarded and the bacterial pellet re-suspended in 200 µl GTE. The mixture was incubated at room temperature for 5 minutes after which 400 µl of Lysis Solution was added. The mixture was gently mixed and incubated at room temperature for a further 5 minutes.

The mixture was neutralized by the addition of 300 µl Neutralizing solution, mixed gently by inverting a few times and centrifuged at 10000 x *g* for 15 minutes. The pellet was discarded and the supernatant transferred into a fresh tube into which 0.7 volume of isopropanol was added. The mixture was incubated at -20 °C for 30 minutes to precipitate nucleic acids after which it was centrifuged at 10000 x *g* for 10 minutes. The resulting pellet was washed twice with 70 % ethanol, air-dried and then dissolved in 100 µl of 1 X TE. 100 µg/ml of RNAse was added to the plasmid and incubated in a water bath at 37 °C for 60 minutes. The nuclease-treated plasmid was extracted

Ligation Reaction Reagents	Standard Reaction	Positive Control	Back ground Control
2X Rapid Ligation Buffer, T4 DNA Ligase	5 μl	5 μl	5 μl
pGEM®-t Easy vector (50ng/μl)	1 μl	1 μl	1 μl
PCR product	X μl *	-	-
Control Insert DNA	-	1 μl	-
T4 DNA Ligase (3 Weiss units/μl)	1 μl	1 μl	1 μl
deionized water to a final volume of	10 μl	10 μl	10 μl

3:1 and 1:3 PCR product: Vector molar ratio was used for ligation reactions

Table 2.2: Experimental setup for cloning of PCR products into pGEM®-T Easy vector. The table shows generic setup of ligation reactions for pGEM®-T Easy vector-XvPrx2 inserts. 3:1 and 1:3 PCR product: Vector molar ratios were used for optimal cloning. All ligation reactions were carried out at 4 ^{o}C for 18 hours.

$$\frac{\text{ng of Vector x Kb size of Insert}}{\text{Kb size of vector}} \text{ x insert: vector molar} = \text{ng of insert}$$

with equal volumes of 25 parts phenol: 24 parts chloroform: 1 part isoamyl-alcohol. The tube was centrifuged at 10000 x *g* for 5 minutes and the upper aqueous phase containing the DNA recovered. 0.3 M sodium acetate was added and the mixture incubated at -20 °C for 30 minutes to precipitate the plasmid DNA. The precipitate was centrifuged at 10000 x *g* for 15 minutes, washed with 70 % ethanol, air-dried and re-dissolved in 100 µl 1 X TE.

2.10 Double digest of DNA constructs

Double digest reactions were set up by transferring appropriate volumes of the reaction mix (Table 2.3) into 0.5 ml tubes followed by incubation of the mixture at 37 ^{o}C for 1 hour. The digestion products were analyzed by electrophoresis on a 1 % agarose/ethidium bromide (EtBr) gel. Fragments corresponding to *Xv*Prx2 inserts were purified from the gel using QIAquick® PCR Purification kit (QIAGEN), according to the manufacturer's instruction. All double digest reactions were set up as shown in Table 2.3, using 10 units of enzyme for 1µg DNA concentrations.

2.11 DNA Sequencing

DNA sequencing of constructs was carried out at Inqaba Biotechnical Industries (Pty) Ltd. The experimentally determined sequences were compared with the expected sequences using the Blast2 sequence alignment tool (http://www.ncbi.nlm.nih.gov/BLAST/bl2seq/wblas2.cgi) (Tatusova & Madden, 1999). Validation of base calling was performed by inspection of the raw sequencing trace, using the Finch TV software suite (http://www.geospiza.com/finchtv). Nucleotide sequences were translated to protein sequences using the ExPASy translation Tool (http://au.expasy.org/tools/dna.html).

Double Digest Reagents	Reaction Volumes (µl)
BamHI	1 µl
XhoI	1 µl
DNA	X µl = (1ug)
Buffer R	1 µl
H_2O	X µl H_2O (to make up reaction volume to 10 µl)
Total reaction volume	10 µl

Table 2.3: Generic setup used for all double digest reactions. Double digest reactions carried out at various points differed with respect to volumes of reagents required for particular reactions. All digests were carried out at 4 ^{o}C for 18 hours.

2.12 Generation of pGEX-6P-2-*Xv*Prx2 expression plasmid

*Xv*Prx2 was digested out of pGEM®-T-Easy-*Xv*Prx2 using the flanking BamHI and XhoI sites and subcloned into pGEX-6P-2 using the procedure described in Section 2.7. The resulting pGEX-6P-2-*Xv*Prx2 construct was transformed into *E. coli* BL21 (DE3) pLysS cells as described in Section 2.7.

2.13 Expression screen of *E. coli* BL21 (DE3) pLysS cells transformed with expression construct for recombinant protein expression

E. coli BL21 (DE3) pLysS cells transformed with pGEX-6P-2-*Xv*Prx2 were plated out on LB plates containing 100 µg/ml ampicillin and incubated at 37 ºC for 18 hours. Single colonies were picked and sub-cultured in LB broth containing 100 µg/ml ampicillin and incubated with vigorous shaking at 37 ºC for 4 hours. 1 ml aliquots were transferred into two separate 15 ml tubes with 1 mM isopropyl *β*-D-thiogalactopyranoside (IPTG) added to one of the cultures (induced cells), whereas no IPTG was added to the other culture (un-induced cells). Both tubes were incubated for a further three hours at 37 ºC with vigorous shaking.

Cells were harvested by centrifugation at 10000 x g for 6 minutes and the pellets re-suspended in 100 µl of Sample Treatment Buffer. The suspension was incubated at 95 ºC for 5 minutes, following which samples were analyzed by SDS-PAGE gel electrophoresis and the clone demonstrating the highest level of recombinant protein expression selected for large-scale expression.

2.14 Recombinant expression of double labelled ^{13}C, ^{15}N-GST-*Xv*Prx2 fusion protein

2.14.1 Expression

Large-scale expression of GST-*Xv*Prx2 was carried out either in LB or in minimal medium supplemented with 1g/ L $^{14}NH_4Cl$ and 2g/L ^{12}C-glucose as the sources of nitrogen and carbon respectively. For ^{15}N-enriched samples the $^{14}NH_4Cl$ was replaced with $^{15}NH_4Cl$ (Cambridge Isotope Laboratories, Andover MA, USA) and for ^{15}N, ^{13}C-enriched samples ^{12}C-glucose was additionally replaced with ^{13}C-glucose (Cambridge Isotope Laboratories, Andover MA, USA).

Large scale expression was achieved by inoculating 100 µl of culture from the highest expressing clone of *E. coli* BL21 (DE3) pLysS cells containing pGEX-6P-2-*Xv*Prx2 expression construct into 10 ml of LB or 100 ml of Minimal Media supplemented with 1g/l NH_4Cl and 2g/l glucose and 100 µg/ml ampicillin. Cells were incubated with vigorous shaking at 37 ºC for 18 hours following, which 990 ml of LB or 900 ml of Minimal Media containing 100 µg/ml of ampicillin was added to the primary culture and the cells incubated at 37 ºC until the OD_{600} was between 0.4 and 0.6. Expression of recombinant protein was induced by the addition of IPTG to a final concentration of 1 mM and the cells incubated under gentle shaking at 25 ºC for 18 hours.

2.14.2 Extraction

Cells were harvested by centrifugation at 6000 x g at 4 ºC for 10 minutes and the pellets re-suspended in 15 ml Lysis Buffer. Cells were lysed using 3 cycles of freezing at -80, followed by thawing at 37 ºC for 20 minutes respectively. 50 µg/ml DNase was added to the lysate and incubation carried out at 37 ºC for 45 minutes after which the

lysate was centrifuge at 10000 x g at 4 ºC for 30 minutes and clarified through a 0.45 µm filter (OSMONICS).

2.14.3 Affinity purification

Affinity purification of the GST-*Xv*Prx2 was carried out using a 20 x 1 cm Econo® Column packed with 10 ml glutathione-linked agarose (SIGMA® Aldrich), operated by gravity flow. The required amount of glutathione-linked agarose beads were suspended in deionised water and allowed to swell overnight at 4 °C after which the slurry was poured into a 20 x 1cm Econo® chromatography column (Amersham Pharmacia Biotech). The column was equilibrated with 5 column volumes (CVs) of equilibration buffer before use.

Lysate from disrupted cells was loaded onto the pre-equilibrated glutathione-agarose column and the flow through collected. The column was then washed with 5 CV of Equilibration Buffer following which the fusion protein was eluted in 3 CVs of Elution buffer.

2.14.4 3C Protease cleavage and recovery of *Xv*Prx2

Fractions containing eluted GST-*Xv*Prx2 were pooled and placed in a dialysis bag (SnakeSkin, Thermo Scientific) with a molecular weight cut off of 3500 Daltons and dialyzed for 1 hour at 4 ºC in Cleavage Buffer. PreScission Protease

3C protease was added to the protein solution and cleavage allowed to take place at 4 ºC for 24 hours. Following cleavage, protein fractions were analyzed by SDS-PAGE electrophoresis for the presence of GST and *Xv*Prx2 domains. The GST domain was removed by loading the cleaved protein solution back onto the glutathione agarose

column. The flow through, which contained *Xv*Prx2, was subjected to further purification.

2.14.5 Anion exchange chromatography

Anion exchange chromatography was carried out using a 1.6 ml column containing 20 HQ POROS media (Amersham Biosciences) on a BioCAD® SPRINT™ Perfusion Chromatography system (PerSeptive Biosystems) at a flow rate of 10 ml/minute. The instrument was operated using a pre-programmed sequence consisting of the following steps: 10 CV Equilibration Step (10 mM Tris-HCl pH 7 +10 mM NaCl), Injection of sample, 10 CV Wash Step (10 mM Tris-HCl pH 7.0 + 10 mM NaCl), 15 CV gradient (10 mM Tris-HCl pH 7.0 + 0-0.5 M NaCl), 10 CV Clean Step (10 mM Tris-HCl pH 7.0 + 2M NaCl) and 10 CV Re-equilibration Step (10 mM Tris-HCl pH 7.0 + 10 mM NaCl). Eluted protein was monitored at 280 nm using an in-line UV meter and NaCl concentration was monitored using an in-line conductivity meter. The presence of eluted protein was confirmed by subjecting the fractions to SDS-PAGE analysis. Fractions containing *Xv*Prx2 were pooled and concentrated to 900 µl using Amicon® Ultra centrifugal devices (Millipore) for size exclusion chromatography.

2.14.6 Size exclusion chromatography

Size exclusion chromatography was used as a final polishing step. Size exclusion chromatography was carried out using a 100 x 1.8 cm Econo® Column packed with 150 ml HiPrep™ 16/100 Sephacryl S-100 High resolution gel (Amersham Pharmacia Biotech) on a BioCAD® SPRINT™ Perfusion Chromatography system (PerSeptive Biosystems). The column was equilibrated with 1.5 CV of phosphate buffer pH 7.2 containing 20 mM NaCl, 1 mM NaN_3 and 10 mM DTT, at a flow rate of

0.5 ml/minute. The protein sample was injected into a 1 ml injection loop using a Hamilton syringe and fractions collected using a Gilson® 203B fraction collector and eluted protein monitored using absorbance at 280 nm. Fractions were subjected to analysis by SDS-PAGE after which fractions containing *Xv*Prx2 were concentrated to 600 µl using an Amicon® Ultra Centrifugal Device (Millipore) with a molecular weight cut off (MWCO) of 3000 Daltons.

2.15 SDS-polyacrylamide gel electrophoresis (SDS-PAGE)

Proteins samples were separated on SDS-PAGE gels according to Laemmli's method (Laemmli, 1970), which utilizes a stacking gel to focus the proteins into a thin line before they enter the separating gel, which then separates them according to their molecular weight. 8 x 10 cm gels of 1.5 mm thickness were cast using Hoefer Mighty Small™ SE 245 Dual Gel casters (Hoefer), using 40 % premixed acrylamide: bis-acrylamide 37.5:1 solution. 16 % separating gels were made up as follows: 3.2 ml de-ionized H_2O, 2.625 ml 1.5 M Tris pH 8.8, 4 ml 40 % premixed acrylamide: bis-acrylamide 37.5:1, 105 µl 10 % SDS, 60 µl of 10 % ammonium persulphate (APS) and 7.5 µl TEMED (N, N, N', N'-tetramethylenediamine). 4 % stacking gels were prepared using 3.050 ml de-ionized H_2O, 1.25 ml 0.5 M Tris pH 6.8, 0.75 ml 40 % premixed acrylamide: bis-acrylamide 37.5:1, 50 µl 10 % SDS, 25 µl of 10 % APS and 7.5 µl TEMED (Table 2.4).

Samples were diluted with an equal amount of 1 x sample treatment buffer and boiled at 95 ºC for 5 minutes followed by centrifugation at 6000 x g for 30 seconds. Pre-mixed protein molecular range marker was diluted 5 times before being subjected to the same treatment. Electrophoresis was carried out in 1 x SDS electrophoresis running buffer at an initial field strenght of 10 V/cm using a Mighty Small II Gel

Reagents	16 % Separating gel	4 % Stacking gel
Separating buffer	2.625 ml	-
Stacking buffer	-	1.25 ml
Deionised water	3.2 ml	3.050 ml
40 % Bis Acrylamide 37.5:1	4.0 ml	0.75 ml
10 % SDS	105 µl	50 µl
APS 0.05 %	60 µl	25 µl
TEMED	7.5 µl	5.0 µl

Table 2.4: Composition of 16 % SDS PAGE gel

Electrophoresis System (Hoefer). The field strenght was adjusted to 15 V/cm when the Bromophenol blue dye reached the separating gel. Electrophoresis was stopped when the dye reached the bottom of the separating gel after which the gel was stained in Coomassie staining solution for 30 minutes and de-stained in de-staining solution for an appropriate length of time for visualization.

2.16 Native Gel Electrophoresis

Separating, stacking and polymerization solutions for native gel electrophoresis were prepared exactly as in the case of SDS-PAGE. SDS and reducing agents (DTT and β-mercaptoethanol) were omitted from the sample and electrophoresis buffers. Protein samples were mixed with sample buffer prior to loading onto gels but were not subjected to heating. Electrophoresis was carried out at 2.5 V/cm and the gel tank was placed in an icebox to avoid over-heating. Electrophoresis was stopped when the dye reached the bottom of the separating gel after which the gel was stained in Coomassie staining solution for 30 minutes and de-stained for visualization.

2.17 Determination of protein concentrations

Protein concentrations were determined using two independent methods: the Bradford colorimetric assay method (Bradford, 1976) and absorption at 280nm.

Bradford assay

Bradford dye was diluted 5 fold immediately prior to use and filtered through a 0.45 μM filter (OSMONICS) while incubating on ice. Serial dilutions of a 1mg/ml stock solution of bovine serum albumin (BSA) were prepared in NMR Buffer to give final concentrations ranging between 2 - 8 μg/ml, to serve as standards. Dilutions 1 in 5000, 1 in 7500 and 1 in 10000 of the protein samples were made in NMR buffer and

briefly centrifuged. The Bradford dye was added to the standards and diluted protein samples were briefly centrifuged, transferred to cuvettes and incubated for 5 minutes at room temperature.

The absorbance value was measured at 595 nm (A_{595}), using a Labsystems Multiskan®-BIOCHROMATIC Spectrophotometer. The standard absorbance curve was constructed by plotting the absorbance of the BSA standards at 595 nm (A_{595}) as a function of concentration in μg/ml, using Excel (Microsoft Corporation). An estimation of protein concentration was obtained by measuring absorbance values and extracting corresponding concentrations with the use of BSA standard curve. Final protein concentrations were calculated by multiplying the calculated values by sample dilution factors.

Absorbance at 280 nm

The protein sample was diluted four-fold in NMR buffer and the absorbance at 280 nm (A_{280}) measured using a NanoDrop® *ND-1000* Spectrophotometer (NanoDrop Technologies Inc.). The protein concentration C (in mM) was determined using the Beer Lamberts Law, $A_{280} = \varepsilon CL$, where ε is the molar extinction coefficient (in units of mM^{-1} cm^{-1}) and L=1cm is the path length. ε was estimated from the amino acid sequence of *Xv*Prx2 using the Expert Protein Analysis System server (http://www.expasy.ch/cgi-bin/pi_tool) and found to be 13.980 mM^{-1} cm^{-1}.

2.18 Preliminary crystallization trials of *Xv*Prx2

A rigorous search for *Xv*Prx2 crystallization conditions was pursued using protein concentrations in the range of 10-20 mg/ml. Crystallization trials were set up using the

hanging and sitting-drop vapour-diffusion methods at 277, 289 and 295K in 24 and 96 well VDX plates (Hampton Research), by manual and semi automated methods (Mosquito 4B, Labtech). Typically, hanging drop vapour-diffusion methods required 2 µl of protein samples, which was added onto siliconized cover slides (Hampton Research), followed by the addition of a pre-determined volume of precipitating solution depending on the intended final concentration of the protein. Cover slides were gently inverted over wells containing 700 µl of precipitating solutions (Reservoir solutions) and sealed with vacuum grease (Sigma). A total of about 1500 precipitating solutions, including commercial screens Crystal Screen 1 and 2, Crystal Screen Lite, PEG Ion Screen, Grid Screen NaCl, Grid Screen PEG 6000, JCSG Core I, II, III, IV, and other JCSG screens as well as home made precipitating buffers, were screened to identify conditions that allowed for growth of protein crystals. Conditions giving hits were optimized to improve the size of protein crystals by varying a number of factors including the pH of crystallization buffers, the ionic strength of protein buffer solutions, protein cncentration and temperatures under which the trials were set up.

Attemps at data collection were pursued using the Rigaku RUH3R copper-rotating anode X-ray source operated at 40 KV, 22MA, located at University of the Western Cape, South Africa and the synchroton facility in Soleil, France.

2.19 NMR spectroscopy

Samples used to record NMR data were concentrated to 600 µl in 50 mM phosphate pH 7.2 or 8 and transferred to 5 ml NMR tubes (Wilmad). 10 % D_2O was added to samples to serve as an internal reference to lock the spectrometer carrier frequency.

Complete triple resonance datasets were acquired using the 600 MHz Bruker Spectrometer (Bruker Billerica, MA) located at Institute of Genetics Molecular and Cellular Biology (IGBMC), Strasbourg, France and the Varian Unity Inova 600 MHz spectrometer in the Chemistry Department of Stellenbosch University, South Africa (Table 2.5). The Bruker instrument was equipped with a triple resonance cryoprobe whereas the Varian instrument was equipped with room temperature triple resonance probe. Triple resonance experiments were recorded with 128 increments in the carbon dimension, 64 increments in the nitrogen dimension and 4 transients per FID. Strip plots were generated in NMRViewJ (Johnson, 2004) and Cara (Rochus, 2004) using a peak list picked from the HNCO spectrum. Spectra were processed with the NMRPipe software package (Delaglio *et al.,* 1995) and visualized using NMRViewJ (Johnson, 2004) and Cara (Rochus, 2004).

2.20 Sequential assignment of backbone resonances

HNCA and HN(CO)CA experiments

HNCA and HN(CO)CA spectra reviewed by (Bax & Ikura, 1991; Farmer*, et al.*, 1992; Grzesiek & Bax, 1992; Kay*, et al.*, 1990) constitute a pair of 3D NMR experiments commonly used for sequential backbone assignment of proteins. The magnetic transfer pathways of the HNCA and HN(CO)CA experiments are shown in Fig 2.3. The transfer of magnetization in HNCA starts with the large magnetization of the H^N proton, following which the signal is transferred to the attached nitrogen nucleus and then either to the C_α nucleus of the same residue, referred to here as the "ith residue" or to the C_α nucleus of the preceding residue (i-1), through the CO group. The signal is then transferred back via the nitrogen to the H^N proton for detection during t_3. During the pseudo-evolution periods t_1 and t_2 the signal is amplitude modulated by the

precession frequencies of the C_α and the nitrogen nuclei respectively where as during the real time interval t_3 the signal is amplitude modulated by the H^N nucleus. Fourier transformation with respect to t_1, t_2 and t_3 results in a three dimensional spectrum in which the ω_1 dimension corresponds to the ^{13}C chemical shifts, the ω_2 dimension to the ^{15}N chemical shifts and the ω_3 dimension to the H^N chemical shifts.

The HN(CO)CA spectrum, on the other hand, contains only one resonance corresponding to each (δH^N, δN) frequency pair, corresponding to coordinates (δH^N, δN, $\delta C_\alpha(i-1)$), since magnetic energy only flows from the H^N to the $C_\alpha(i-1)$ and not the $C_\alpha(i)$ (see Fig 2.3B). Since in the HNCA experiment magnetic energy flows from an H^N to both $C_\alpha(i-1)$ and $C_\alpha(i)$ (see Fig 2.3A) and the signal is therefore modulated by the procession frequencies of both C_α nuclei, the resulting spectrum contains two resonances corresponding to each (δH^N, δN) frequency pair, at coordinates (δH^N, δN, $\delta C_\alpha(i-1)$) and (δH^N, δN, $\delta C_\alpha(i)$) respectively.

HNCACB and HN(CO)CACB experiments

The HNCACB and HN(CO)CACB (reviewed by (Grzesiek & Bax, 1992), constitute a pair of triple resonance experiments, which offer alternative information for establishing sequential backbone connectivity than that provided by the HN(CO)CA / HNCA pair. The flow of magnetic energy is shown in Fig 2.4. The resulting spectra are essentially the same as for the HN(CO)CA / HNCA pair except that resonances corresponding to the C_β nuclei appear as (δH^N, δN, $\delta C_\beta(i-1)$) and (δH^N, δN, $\delta C_\beta(i)$) in the case of HNCACB and (δH^N, δN, $\delta C_\beta(i-1)$) in the case HN(CO)CACB. In the HNCACB the C_β resonances appear with opposite sign to the C_α resonances, which greatly facilitates identification of serine and threonine resonances, for which $\delta C_B >$

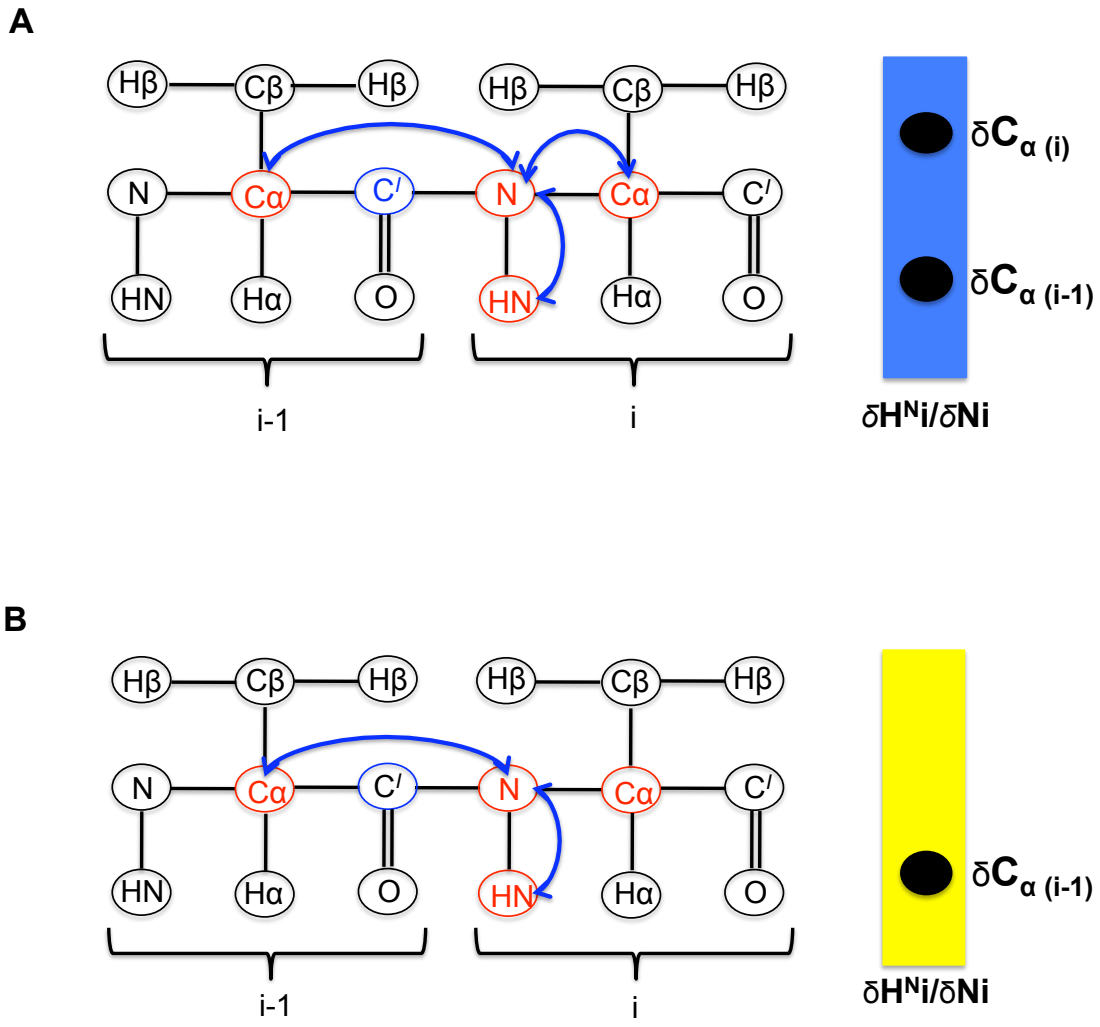

Fig 2.3: Coherence transfer pathway of HNCA and HN(CO)CA experiments for a pair of consecutive residues (i-1) and (i). In the HNCA experiment (A) magnetic energy is transferred from the C_α of both residues (i-1) and (i) to the N and H^N proton of residues (i-1) and (i). In the HN(CO)CA (B) magnetic energy is transferred from the C_α of residue (i-1) to the N and H^N proton of residue (i) through the CO group of residue (i-1). The resonance of the C_α of residue (i-1) is generally weaker in the HNCA compared to the C_α resonance of residue (i). Schematic strips corresponding to residue (i) are shown on the right hand side.

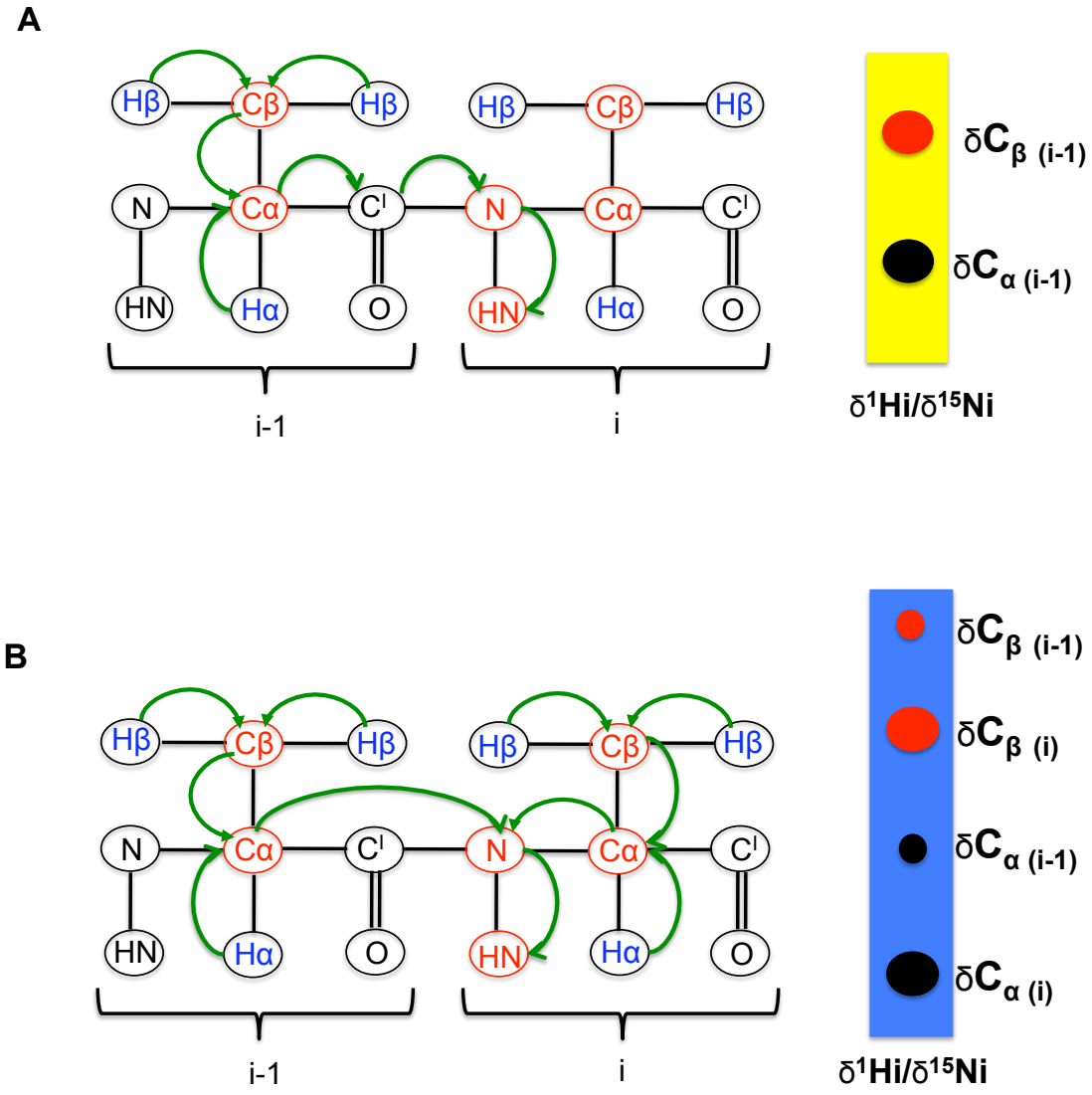

Fig 2.4: Coherence transfer pathways for HN(CO)CACB and HNCACB experiments for a pair of consecutive residues. In HN(CO)CACB depicted in (A), magnetization is transferred from the C_β to the C_α of residue (i-1) to the N and H^N proton of residue (i) through the CO group of residue (i-1), which is not observed in the spectra. In the HNCACB experiment shown in (B), magnetization is transferred from the C_β and C_α of residues (i) and (i-1) to the N and H^N proton of residues (i) and (i-1). In the HNCACB the C_β resonances have opposite sign from the C_α resonances, indicated here by red for negative, black for positive.

δC_A, compared to other residues.

2.21. Sequential assignment of side chain resonances

HCCH-TOCSY and HCCH-COSY spectra

Side-chain carbon proton resonances were assigned using HCCH-TOCSY and HCCH-COSY experiments. Here the transfer of magnetic energy between atoms occurs via J coupling. The magnetic energy is transferred between the side-chain hydrogen nuclei and their attached ^{13}C nuclei following which there is an isotropic ^{13}C mixing and a final transfer back to the side-chain hydrogen atoms for detection. The pathway for the transfer of magnetic energy in HCCH-TOCSY and HCCH-COSY experiments is shown in Fig 2.5.

The strategy used for side chain assignment is summarized as follows: Read off the C_α and C_β carbon shifts from the HN(CO)CACB and HNCACB.

1 Display planes of the HCCH-TOCSY and HCCH-COSY spectra and insert the C_α and C_β of interest into the z-dimension of the spectra. Look for peaks on the diagonal, which are found mostly in the expected regions based on the table shown in Fig 4.7B, which should have charateristic peaks displayed on the same line as the diagonal of peaks. Use the HCCH-TOCSY to check the spin system and confirm the topology using HCCH-COSY.

2 Read off the proton shifts and note these. Change the dimensions of the panels such that the carbon dimension is now on the y-axis and one of the proton dimensions on the z-axis. Choose the range of the carbon shift to be ± 5ppm based on the expected shifts on Fig 4.7B and enter proton shift values obtained previously into the z-axis. The correct carbon shift should contain a number of

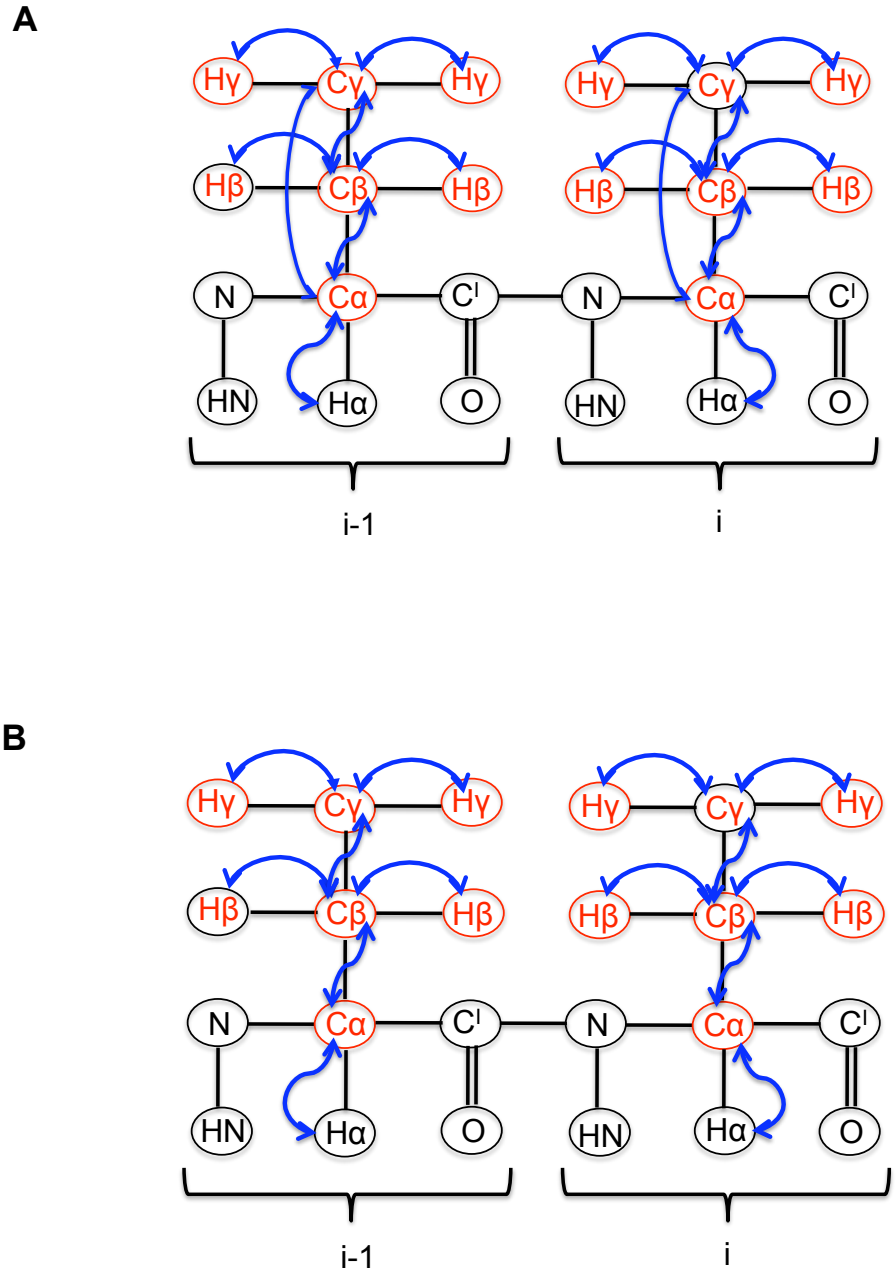

Fig 2.5: coherence transfer pathway in HCCH-TOCSY and HCCH-COSY experiments. (A) Shows the coherence transfer pathway in HCCH-TOCSY while (B) shows the coherence transfer pathway in HCCH-COSY experiments respectively. The blue arrows show the direction of transfer of magnetic energy, which starts, from a side-chain proton (coloured red) to the directly attached carbon atom via the small ^{1}J coupling (35-55 Hz) and then to the neighbouring carbon atoms and their attached protons. HCCH-TOCSY yields strips at each carbon frequency in the side chain in which all side-chain hydrogen resonances are visible. HCCH-COSY is a slightly less crowded version of HCCH-TOCSY but here only the hydrogen resonances of their own and neighbouring carbons are visible.

peaks based on the expected spin system and topology of the residue. The full list of NMR experiments performed appears in Table 2.5.

2.22 Protein analysis by mass spectrometry

Part of the MS data presented in this thesis was generated using the LTQ Orbitrap Velos instrument (Thermo Scientific) located at Stellenbosch University Health Faculty, Tygerberg Campus, Cape Town. The rest of the data and development of the method was carried out using the API Ultima Q-TOF spectrometer (Waters Corporation, Massachusetts, USA) at Stellenbosch University. Both instruments employed an electrospray ionisation source (ESI).

Electrospray (ES) ionisation spectrometry was performed under both denaturing and non-denaturing conditions. For non-denaturing conditions, samples were injected in 40 mM ammonium acetate. Denaturing conditions were achieved by the addition of 50 % HPLC-grade acetonitrile and 0.2 - 1% formic acid at a flow rate of between 5 and 100 µl/min. Spectra scanning was done in ESI positive mode, capillary voltage 3 kV, cone voltage 4-60 V positive ion mode from m/z 100 to m/z 1990 or 1000 to 4000 m/z at a cone voltage of 35 V. Deconvolution of m/z traces was performed using MaxInt3 (API ultima) and ProMass Deconvolution software (Orbitrap).

2.23 Analytical Size Exclusion Chromatography (SEC)

Analytical SEC was carried out using a HiLoad 16/60 Superdex 75 prep grade column (GE Healthcare UK Limited) on an ÄKTA^{TM}FPLC system. 0.5 ml protein samples were applied to the system and analysis carried out at a flow rate of 0.5 ml/min. 1.5 ml fractions were collected and analyzed by SDS-PAGE and native PAGE electrophoresis. The column was calibrated by measuring the elution volumes of a

NMR Experiment	Function of Experiment
1D ^{1}H homonuclear	Evaluation of sample integrity and state of folding.
^{15}N-HSQC	Evaluation of sample integrity and state of folding; ^{1}H and ^{15}N chemical shifts
^{1}H-^{15}N NOE	Characterization of folded state of backbone
HNCO	Carbonyl carbon chemical shifts
HN(CA)CO	Carbonyl carbon chemical shifts
HN(CO)CACB	Sequential assignment of backbone resonances; $^{13}C_{\alpha}$ and $^{13}C_{\beta}$ chemical shifts
HNCACB	Sequential assignment of backbone resonances; $^{13}C_{\alpha}$ and $^{13}C_{\beta}$ chemical shifts
HNCA	Sequential assignment of backbone; $^{13}C_{\alpha}$ chemical shifts
HN(CO)CA	Sequential assignment of backbone; $^{13}C_{\alpha}$ chemical shifts
HC(C)H-TOCSY	Side-chain ^{1}H and ^{13}C chemical shift assignments
HC(C)H-COSY	Side-chain ^{1}H and ^{13}C chemical shift assignments

Table 2.5: List of some NMR experiments performed on *Xv*Prx2

number of proteins of known molecular weight and plotting them as a function of log(MW) and fitting the graphs to a straight line of the form $V = m \times Log_{10}(MW) + C$ where V is the elution volume, from which values of constants m and C were extracted. The expression was inverted to give $MW = 10^{(v-c)/m}$ which was used to determine the effective molecular weight of *Xv*Prx2 corresponding to the elution volume V.

2.24 Mutants

Mutants were synthesized by Genscript (GenScript USA Inc. 860 Centennial Ave. Piscataway, NJ 08854 USA) by replacing histidine 55 with alanine (H55A) and cysteine 51 with serine (C51S) in pGEX-6P-2-*Xv*Prx2 to create pGEX-6P-2-*Xv*Prx2-H55A and pGEX-6P-2-*Xv*Prx2-C51S respectively. The expression and purification of the mutants was achieved using the protocol applied for the expression of the wild-type *Xv*Prx2.

2.25 Fitting of pH titrations

Fitting of pH data was carried out using Profit (QuantumSoft, Bühlstr. 18, CH-8707 Uetikon am See, Switzerland), using equation in Appendix II. Fitting of the wild type data was carried out by allowing the Ve^d, Ve^m and pK_a to vary.

2.26 Glutathionylation

Gluathionylation was carried out by adding a 10-fold excess of oxidised glutathione (GSSG) to *Xv*Prx2 in 40 mM ammonium acetate buffer, pH 7. The pH of the sample was adjusted back to 7 following the addition of GSSG using acetic acid.

Chapter 3: Expression and purification of *Xv*Prx2

3.1 Introduction

Structural and functional studies of protein molecules by X-ray crystallography and nuclear magnetic resonance spectroscopy (NMR) require the use of highly purified protein samples with a concentration in the range of 0.5 mM and above. Heterologous expression in bacteria is a cheap and rapid method for producing milligram quantities of proteins and additionally offers the capability of uniformly enriching with ^{13}C and ^{15}N for triple resonance NMR studies. The pGEX-6P-2 expression system allows high-level expression of heterologous proteins from a *tac* promoter, induced by IPTG. The protein is expressed as a GST fusion, allowing one-step purification using glutathione-linked agarose beads. The GST can be conveniently removed using the 3C protease from rhinovirus, for which a recognition site is located in the linker region between GST and the multiple cloning cassette. 3C protease cleaves optimally at 4 °C, and can be expressed in-house fused to GST. Following cleavage the GST, uncleaved fusion protein and the 3C protease can be removed by a second round of glutathione affinity purification, leaving the target protein in the flow through.

This chapter describes the generation of the pGEX-6P-*Xv*Prx2 expression construct and the recombinant expression and purification of unlabelled and isotopically enriched *Xv*Prx2 for structural studies.

3.2 Generation of pGEX-6P-2-*Xv*Prx2 expression construct

3.2.1 PCR amplification of *Xv*Prx2

PCR amplification of *Xv*Prx2 was carried out as described in Section 2.4, using primers designed based on the sequence of *Xv*Prx2 (NCBI accession number EU333003),

isolated from *Xerophyta viscosa* (Baker). The primer sequences are shown in Fig 3.1. The forward and reverse primers included BamHI and XhoI restriction sites, respectively, allowing for sub-cloning of the amplicon into the BamHI and the XhoI sites of the pGEX-6P-2 vector. A stop codon (TAG) was included in the reverse primer (Fig 3.1). The result of PCR amplification of *Xv*Prx2 is shown in Fig 3.2. Lane 2 shows an amplicon of approximately 516 bp, which corresponds to the expected size of *Xv*Prx2.

3.2.2 Cloning of PCR product into pGEM®-T Easy and pGEX-6P-2 vectors

The *Xv*Prx2 PCR amplification product was cloned into the pGEM®-t Easy vector (Fig 2.1) as described in Section 2.7. Colony PCR was carried out to screen recombinant pGEM®-t Easy vector clones for the presence of the *Xv*Prx2 insert (Fig 3.3), using gene specific and M13 primers. The sizes of the amplicons were consistent with the expected sizes of 516 bp for the gene specific primers (Lanes 3-7) and 872 bp for the M13 primers (Lanes 8-11).

pGEM®-T Easy recombinant vector clones containing *Xv*Prx2 inserts were transformed into MC1061 competent cells and spread on LB agar plates containing ampicillin (100 μg/ml). Individual colonies were used to inoculate enriched media for small-scale DNA isolation as described in Section (2.9). Isolated plasmid DNA was digested with BamHI and XhoI restriction enzymes to release the *Xv*Prx2 insert and separated on a 1 % agarose gel. Fig 3.4, lane 2, shows two bands of approximately 500 bp and 3300 bp corresponding to *Xv*Prx2 and parental pGEM®-t Easy vector respectively. The released insert was purified using a 1 % agarose/ethidium bromide (EtBr) gel using the QIAquick® PCR Purification kit (QIAGEN), according to the manufacturer's

Fig 3.1: Primers used for PCR amplification of *Xv*Prx2. BamHI (GGATCC) and XhoI (CTCGAG) restriction recognitions sites were included in the forward and reverse primers and have been highlighted in red and blue respectively. A stop codon (**TAG**) shown in bold was included in the reverse primer.

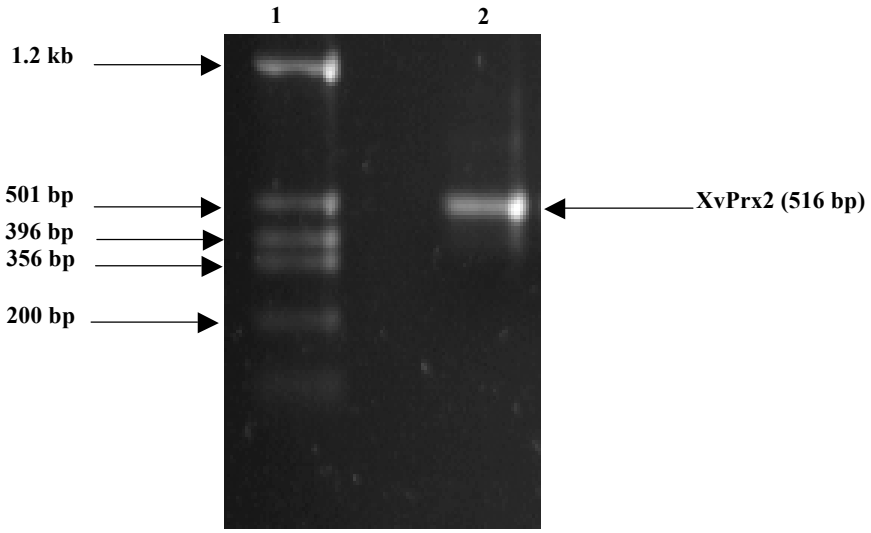

Fig 3.2: 1 % agarose gel electrophoresis of *Xv*Prx2 PCR amplification product. Lane 1 shows Mass Ruler DNA while lane 2 shows an amplicon of approximately 500 bp corresponding to *Xv*Prx2 (516 bp).

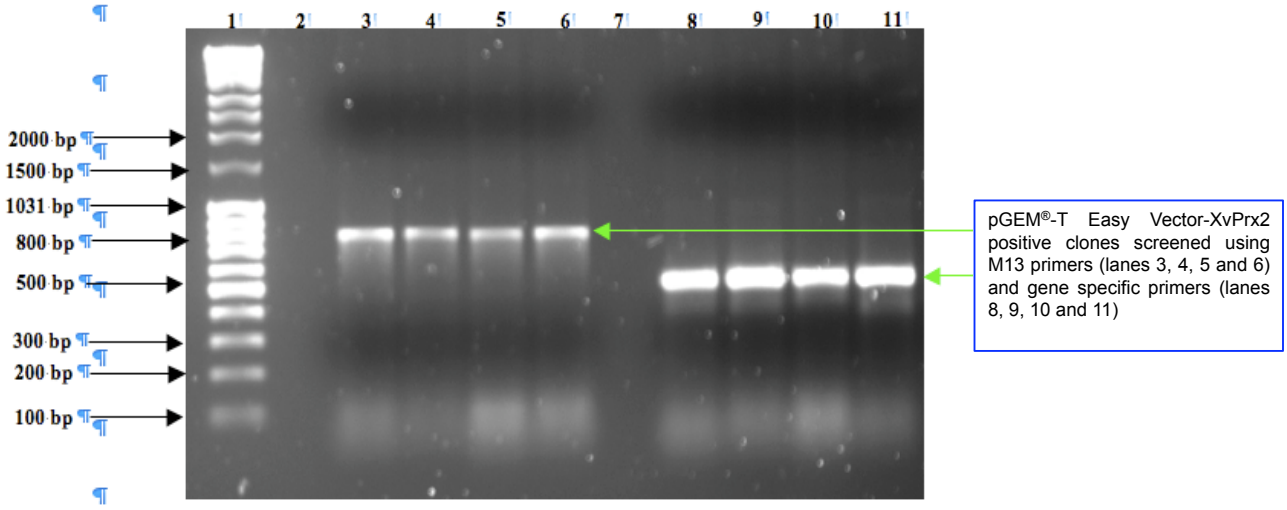

Fig 3.3: 1% agarose gel electrophoresis of colony PCR screening of recombinant pGEM®-t Easy vector clones for the presence of *Xv*Prx2 insert. Lane 1 shows Mass Ruler DNA Ladder™ Mix, lanes 3, 4, 5 and 6 show clones positive for *Xv*Prx2 screened using M13 forward and reverse primers, while lanes 8, 9. 10 and 11 show clones positive for *Xv*Prx2 inserts screened using gene specific primers.

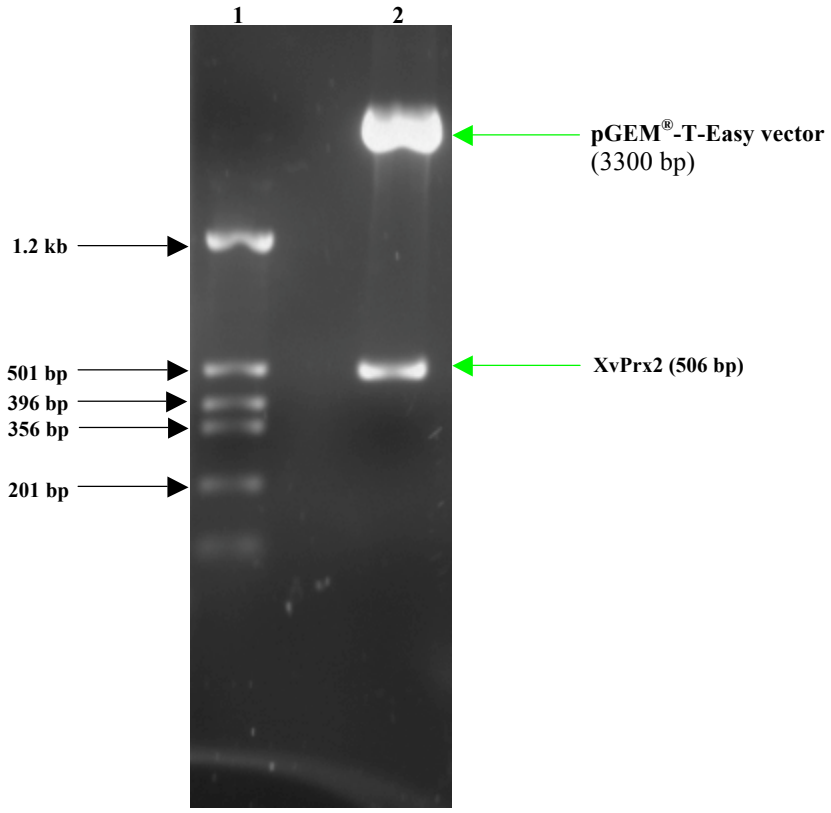

Fig 3.4: 1 % agarose gel electrophoresis of double restriction digestion of recombinant pGEM®-T-Easy-XvPrx2 plasmid DNA. Lane 1 shows molecular weight marker while lane 2 shows double restriction digestion products of pGEM®-T-Easy-XvPrx2 plasmid DNA. Lane 2 shows two bands, a higher band at approximately 3300 bp, which corresponds to pGEM®-t-Easy vector, and a lower band approximately 506 bp, which corresponds to the released insert (*Xv*Prx2).

instruction and ligated into the BamHI and XhoI sites of pGEX-6P-2 to create the pGEX-6P-2-*Xv*Prx2 expression construct.

Ligation products of *Xv*Prx2 and pGEX-6P-2 were transformed into competent MC1061 cells (Section 2.7), plated out on LB plates containing 100 µg/ml ampicillin and incubated at 37 ºC for 18 hours. Colonies were screened for the presence of *Xv*Prx2 inserts using colony PCR following which plasmid DNA was isolated from the positive clones. The plasmid DNA was subjected to double restriction digest using BamHI and XhoI restriction enzymes to positively confirm the presence of *Xv*Prx2 inserts. Fig 3.5, lane 2, shows two bands: a higher band at approximately 4900 bp, which corresponds to pGEX-6P-2, and a lower band approximately 502 bp in size, corresponding to the released insert (*Xv*Prx2).

3.2.3 DNA sequencing

Five clones containing pGEX-6P-2-*Xv*Prx2 plasmid DNA were subjected to sequencing by Inqaba Biotech. The clones in which the forward and reverse sequences matched exactly to the expected sequences (see Appendix 1) were used for heterologous expression of *Xv*Prx2.

3.3. Heterologous expression of *Xv*Prx2

*Xv*Prx2 was expressed as a recombinant GST fusion protein using the pGEX-6P-2 expression system. The expected amino acid sequence of *Xv*Prx2 following the removal of GST is shown below.

GPLGSMAPIAVGETIPDGTLGWFDEKDELKQISIHSLAAGKKIVLIGV
PGAFTPTCSMQHVPSFIEKAEELKAKGVDEFLVISVNDPFVMKAWSKT
YPENKHVKFLADGSGKYTQALGVELDLSEKGLGLRSRRFAILVDDLKV
KVANVEEGGAFTISGADEILKAV

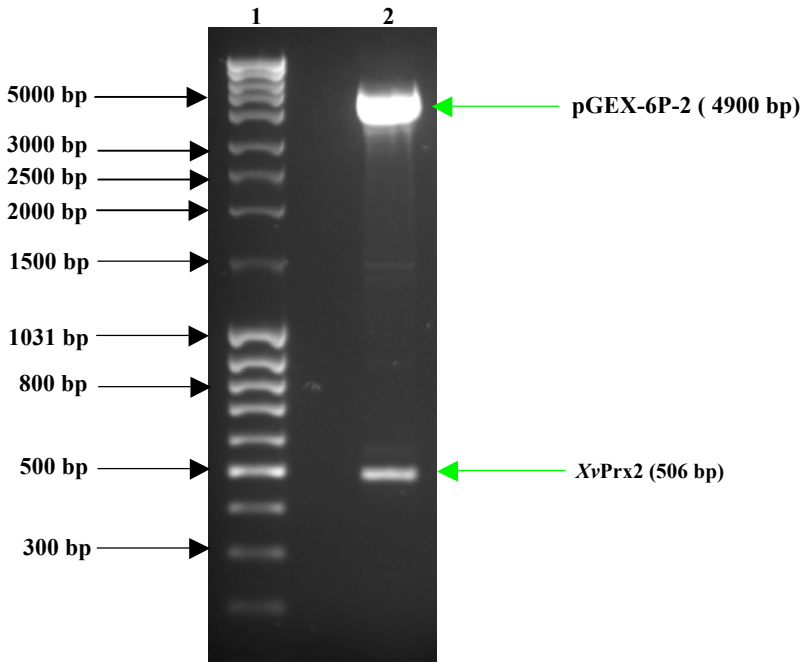

Fig 3.5: 1% agarose gel electrophoresis of double restriction digestion of recombinant pGEX-6P-2-*Xv*Prx2 plasmid DNA. Lane 1 shows Mass Ruler DNA Ladder^{TM} Mix while lane 2 shows pGEX-6P-2-*Xv*Prx2 double digestion products. Lane 2 shows two bands, a higher band at approximately 4900 bp, which corresponds to pGEX-6P-2, and a lower band approximately 506 bp in size, corresponding to the released insert (*Xv*Prx2).

The first five residues (underlined above) represent an artifact of the expression system. The expected molecular weight of *Xv*Prx2, as calculated using the ExPASy PROTPARAM server (*http://ca.expasy.org/cgi-bin/protparam*), is approximately 17.9 kDa with an isoelectric point (pI) of 5.43 (Appendix 3). Since the molecular weight of GST is 26.7 kDa, the expected molecular weight of the GST-*Xv*Prx2 fusion protein is approximately 45 kDa.

E. coli BL21 (DE3) pLysS cells transformed with pGEX-6P-2-*Xv*Prx2 were screened for expression of recombinant GST-*Xv*Prx2 fusion protein using SDS-PAGE, as described in Section 2.13. Pairs of samples from induced and un-induced 1 ml cultures are shown in Fig 3.6. Strong expression of an approximately 45 kDa protein is visible in the induced lanes (2, 4, 6 and 8) but not in the un-induced lanes (3, 5, 7 and 9) indicating that successful expression of recombinant GST-*Xv*Prx2 fusion protein had been induced.

Large-scale expression of GST-*Xv*Prx2 fusion protein was carried out as described in Section 2.14.1. Cell lysis, extraction and affinity purification of recombinant GST-*Xv*Prx2 fusion protein were carried out as described in Sections 2.14.2 and 2.14.3. A representative SDS-PAGE analysis of extraction and affinity purification of recombinant fusion protein is shown in Fig 3.7. The quantity of fusion protein eluted from the column, as well as the absence of significant amounts of degradation products, indicates that both the expression and purification were highly efficient.

The fusion protein was subjected to 3C protease cleavage (Section 2.14.4) and cleaved protein samples were analyzed using SDS-PAGE as shown in Fig 3.8. Two bands are

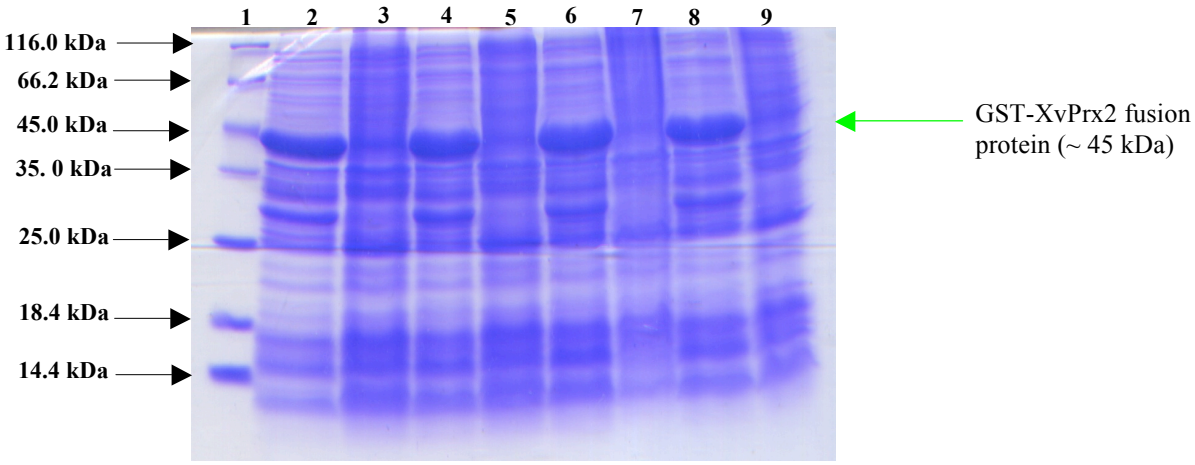

Fig 3.6: Expression screen results of colonies transformed with pGEX-6P-2-XvPrx2. Lane 1 shows molecular range maker, lanes 2, 4, 6 and 8 show induced samples while lanes 3, 5, 7 and 9 show un-induced samples. All induced samples demonstrate the presence of a strong band of approximately 45.0 kDa, corresponding to the expected combined size of GST-XvPrx2 fusion protein.

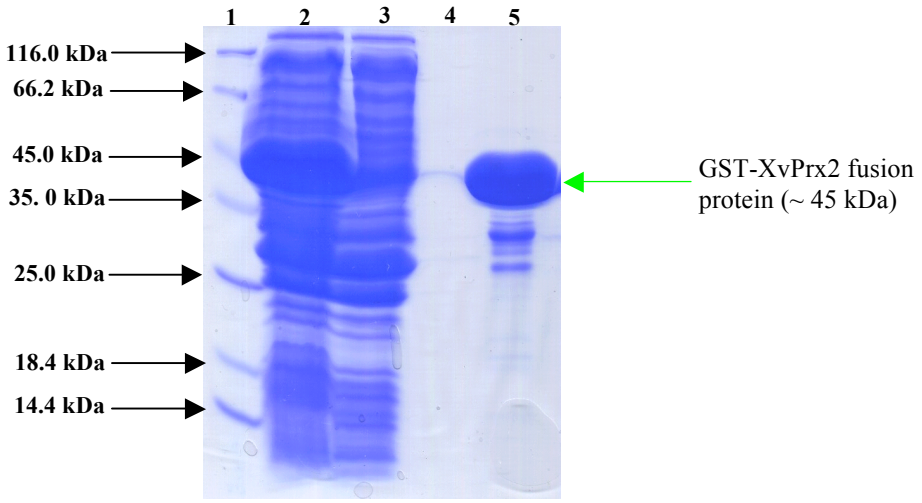

Fig 3.7: SDS-PAGE analysis of expression and affinity purification of GST-*Xv*Prx2 fusion protein. Lane 1 shows molecular range maker, lane 2 shows total protein extract from induced cells, lane 3 shows the flow through from glutathione affinity column, lane 4 shows the column wash and lane 5 shows the eluted GST-fusion protein.

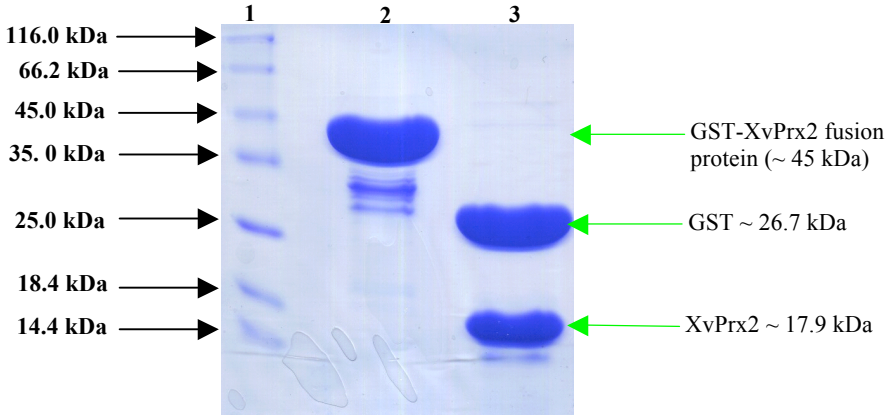

Fig 3.8: 3C protease cleavage of GST-*Xv*Prx2 fusion protein. Lane 1 shows molecular range marker, lane 2 shows un-cleaved GST-*Xv*Prx2 fusion protein while lane 3 shows the fusion protein following cleavage. Two bands are observed in lane 3, a higher band at approximately 27 kDa which corresponds to GST, and a lower band approximately 18 kDa in size corresponding to *Xv*Prx2.

visible, corresponding to GST (top) and *Xv*Prx2 (bottom) respectively. No more than trace amounts of the original fusion protein (45 kDa) remain, indicating that cleavage of the GST-*Xv*Prx2 fusion protein was completed within 24 hours. The intensities of the bands corresponding to GST and *Xv*Prx2 are consistent with the relative sizes of both protein molecules indicating minimal loss of protein samples during cleavage of fusion protein. A second round of affinity purification was used to remove the separated GST domain. The chromatogram and associated SDS-PAGE in Fig 3.9 show that most of the *Xv*Prx2 was found in the flow through (peak A) and almost all the GST was retained on the column (peak B).

An alternative method for removing trace amounts of GST following affinity purification of the cleaved fusion was developed involving the use of anion exchange chromatography (Section 2.14.5). Although the pIs of GST (5.7) and *Xv*Prx2 (5.43) are close, pH scouting using a 20HQ column showed that good separation was achieved at pH 7 using 10 mM Tris, as shown in Fig 3.10. *Xv*Prx2 was not retained by the column (with the exception of a small fraction in peak 6) whereas GST was retained by the column (peak 7 and 8), as confirmed by the associated SDS-PAGE in (B). The introduction of an additional purification step (anion exchange chromatography) following affinity purification therefore resulted in the removal of residual GST from *Xv*Prx2 leading to significant purification of the *Xv*Prx2 protein samples.

Fractions containing *Xv*Prx2 were pooled and concentrated to 900 µl using an Amicon® Ultra Centrifugal Device (Millipore) with a 5000 Dalton cut off. Size exclusion chromatography was carried out using a 100 x 1.8 cm Econo® Column

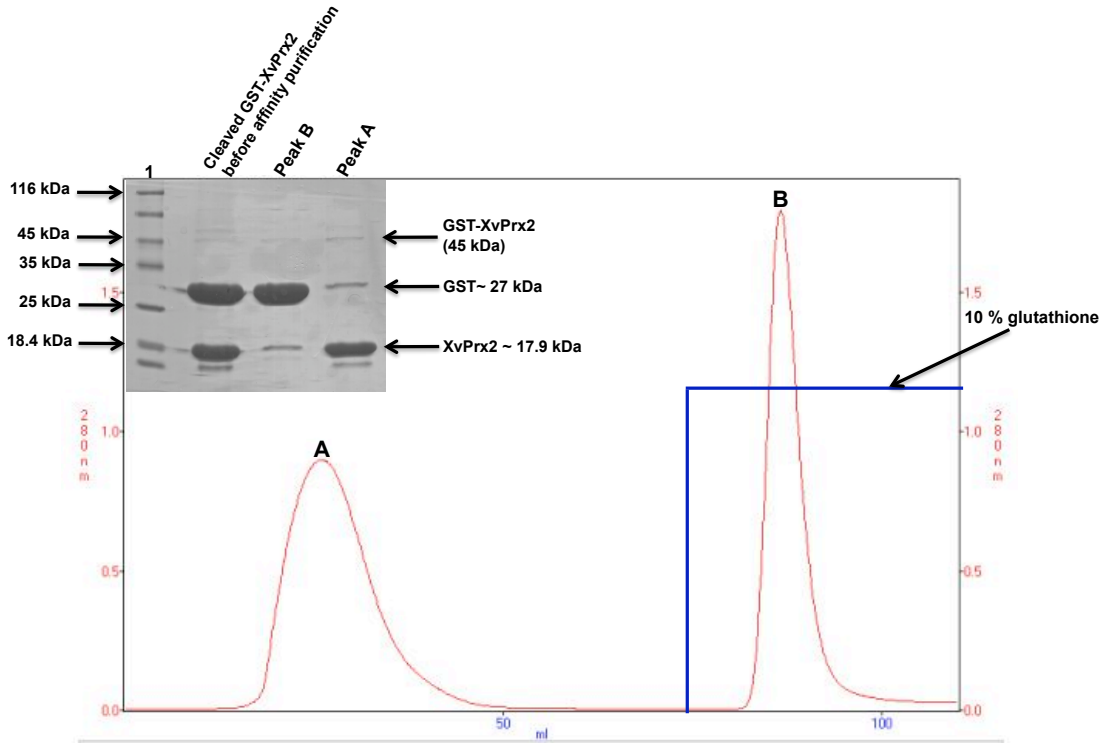

Fig 3.9: Affinity purification chromatogram of cleaved GST-*Xv*Prx2 purified over glutathione-linked agarose column. The top left hand insert shows SDS-PAGE analysis of the cleaved GST-*Xv*Prx2 sample before and after glutathione-linked agarose column purification. Lane 1 shows molecular weight marker, lane 2 shows the cleaved sample (GST-*Xv*Prx2) before affinity purification, lane 3 shows GST domain (peak B) and lane 4 shows *Xv*Prx2 (peak A). Residual traces of the GST-*Xv*Prx2 fusion protein (45 kDa) and GST domain can be seen in the flow through (peak A). The sample labelled A was subjected to further purification to remove traces of both the fusion protein and GST domain.

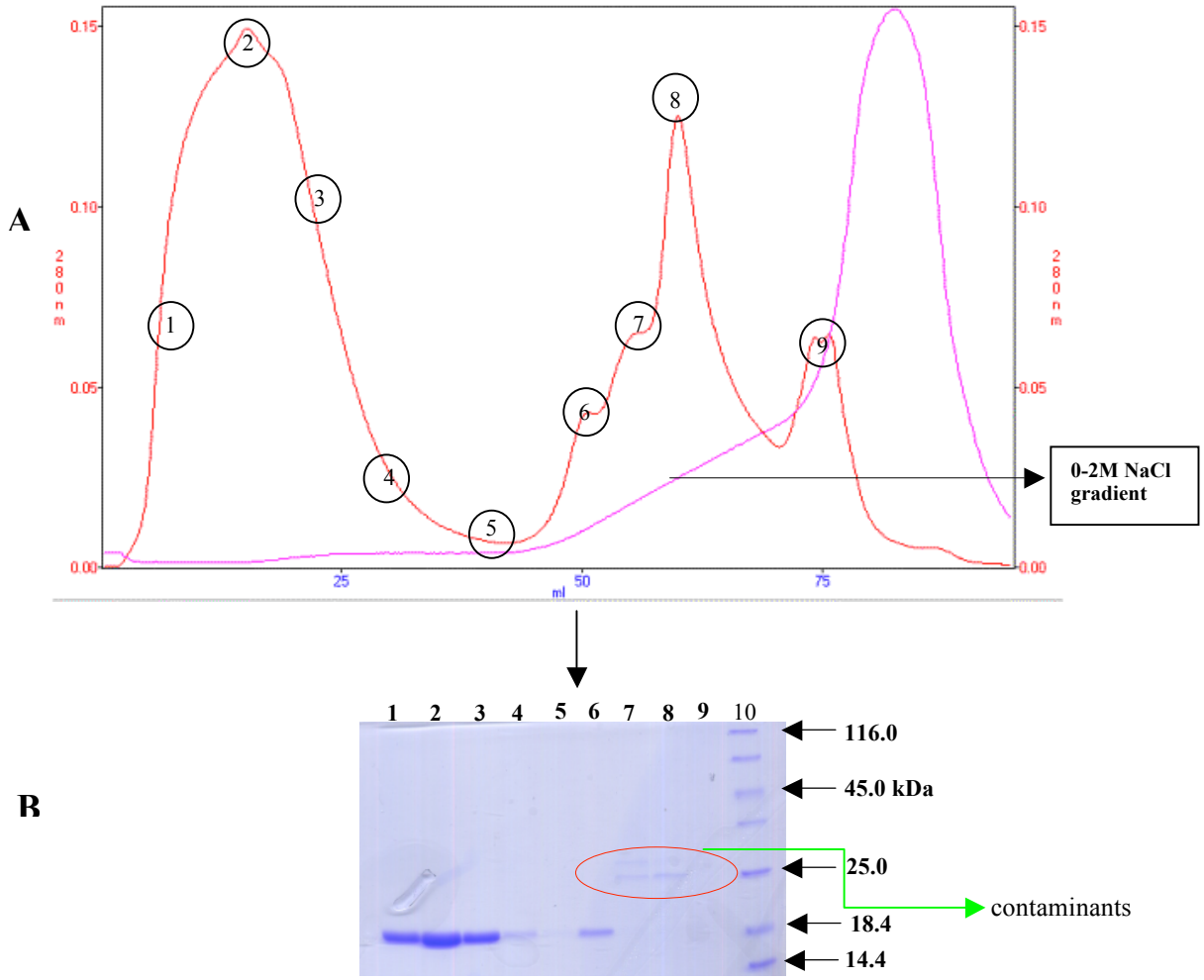

Fig 3.10: Removal of residual GST by anion exchange. (A) *Xv*Prx2 sample containing small amounts of GST, corresponding to peak A in Fig 3.9, was applied to 20HQ anion exchange column in 10 mM Tris, pH 7. With the exception of a small amount in fraction 6, the majority of the *Xv*Prx2 was found in the flow through whereas the GST was retained on the column. (B) SDS-PAGE analysis of fractions to confirm constituent proteins.

packed with 150 ml Sephacryl S100 gel operated using a BioCAD® SPRINT™ Perfusion chromatography system (PerSeptive Biosystems), as described in Section 2.14.6. The SEC chromatogram (see Fig 3.11A) contains one major peak which SDS-PAGE (Fig 3.11B) confirms corresponds to highly purified *Xv*Prx2. Fractions containing *Xv*Prx2 were pooled and concentrated to a final volume of 600 µl. SDS-PAGE analysis of the concentrated *Xv*Prx2 sample (Fig 3.12) shows no evidence of degradation products or contaminating protein suggesting that the sample was sufficiently pure and homogenous for crystallization trials or NMR analysis.

3.4. Determination of protein concentration

The concentration of *Xv*Prx2 was calculated using the Bradford calometric assay and absorption at 280 nm as described in Section 2.17. Absorbance values for both the standard (BSA) and the *Xv*Prx2 sample are presented in Table 3.1 and the corresponding straight-line plots are shown in Fig 3.13. Using the analysis described in Section 2.18;

$$[Xv\text{Prx2}(1/10000)] = 0.155/0.0433 = 3.580\ \mu g/ml$$

Multiplying by the dilution factor yields the final concentration of *Xv*Prx2:

$$[Xv\text{Prx2}] = 35.80\ mg/ml$$

Since the molecular weight of *Xv*Prx2 is 17.9 kDa, 1mM is equivalent to 17.9 mg/ml. Hence the final concentration is 35.80/17.9 = 2.0 mM.

The protein concentration was independently determined using a NanoDrop® *ND-1000* Spectrophotometer (NanoDrop Technologies Inc.). The UV absorption spectrum of the sample at 5-fold dilution is shown in Fig 3.14; $A_{280} \sim 7.4$. (Note that the Nano-

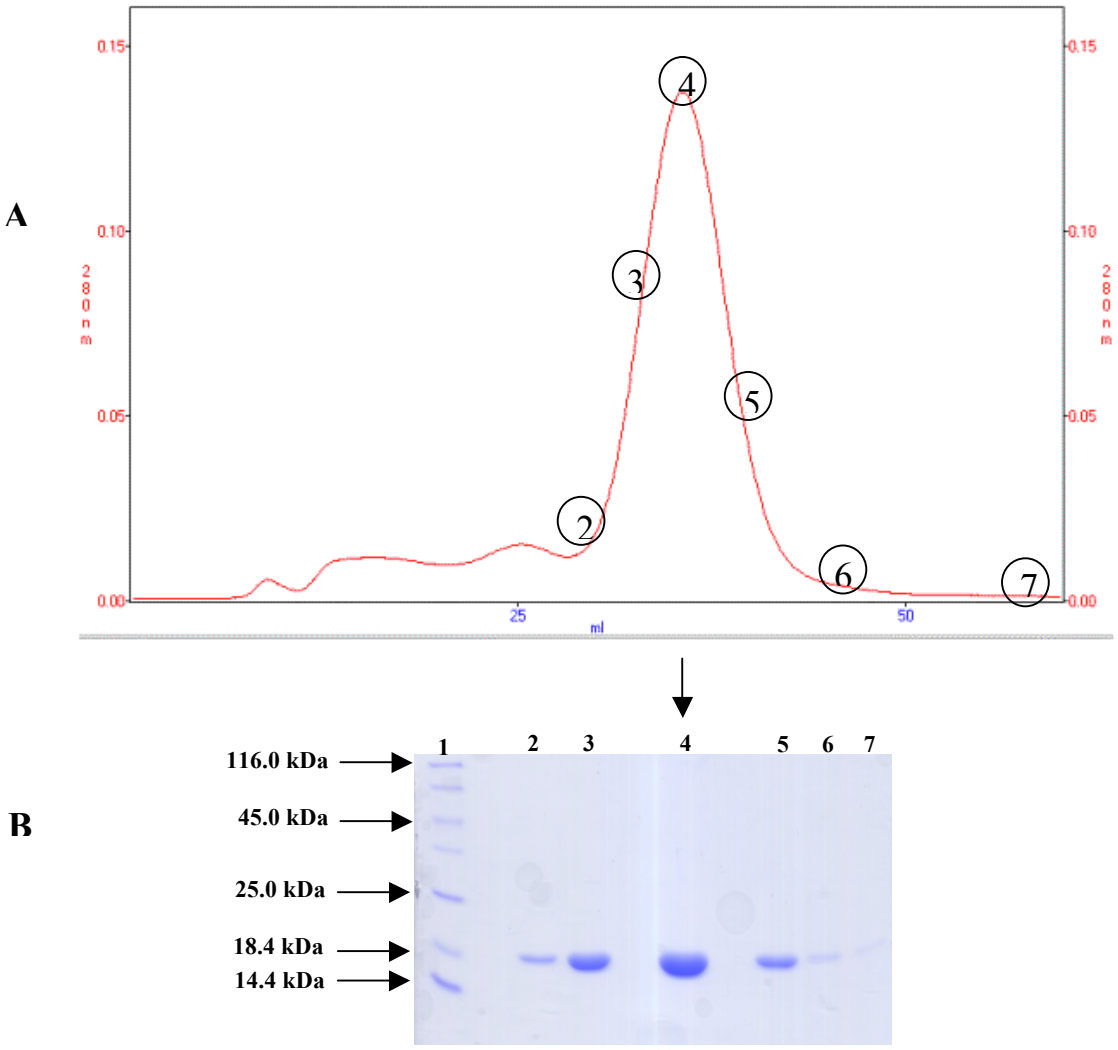

Fig 3.11: Size exclusion chromatogram of *Xv*Prx2. (A) Shows the chromatogram of *Xv*Prx2 sample while (B) shows SDS-PAGE analysis of the corresponding regions of the chromatogram. SEC was carried out to acahevie two purposes: (1) to polish *Xv*Prx2 samples and (2) to exchange the protein buffer environment. The numberig of the SDS-PAGE lanes (B) corresponds to the numbering shown in the chromatogram (A). The SEC was carried out over a 100 x 1.8 cm Econo® column packed with 150 ml HiPrepTM 16/100 Sephacryl S-100 High Resolution gel.

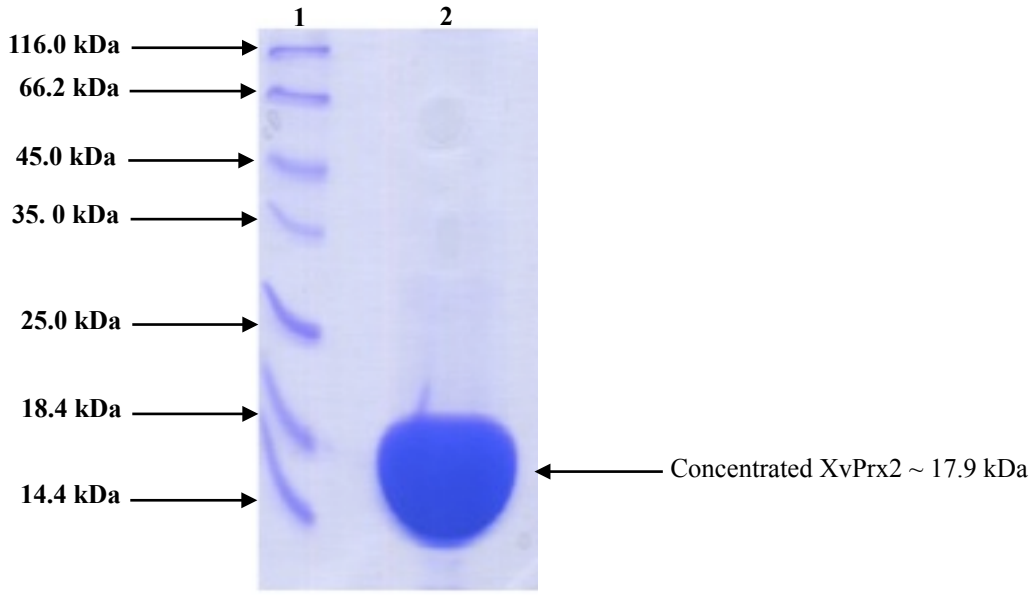

Fig 3.12: SDS-PAGE of concentrated *Xv*Prx2 following size exclusion chromatography. Lane 1 shows molecular range marker while lane 2 shows concentrated *Xv*Prx2. The absence of additional bands corresponding to degradation products or contaminating proteins shows that the sample is highly homogenous.

Table (3.1)

BSA Concentration (ug/ml)	Absorbance (595nm)
2	0.072
4	0.159
6	0.266
8	0.344
10	0.440
XvPrx2	Absorbance (595nm)
1/5000	0.308
1/10000	0.155

Table 3.1: A_{280} readings for known concentrations of BSA and *Xv*Prx2 at 1/5000 and 1/10000 dilutions. Absorbance values were used to generate the standard curve shown in Fig 3.13 from which the unknown concentration of *Xv*Prx2 was determined.

Fig. 3.13

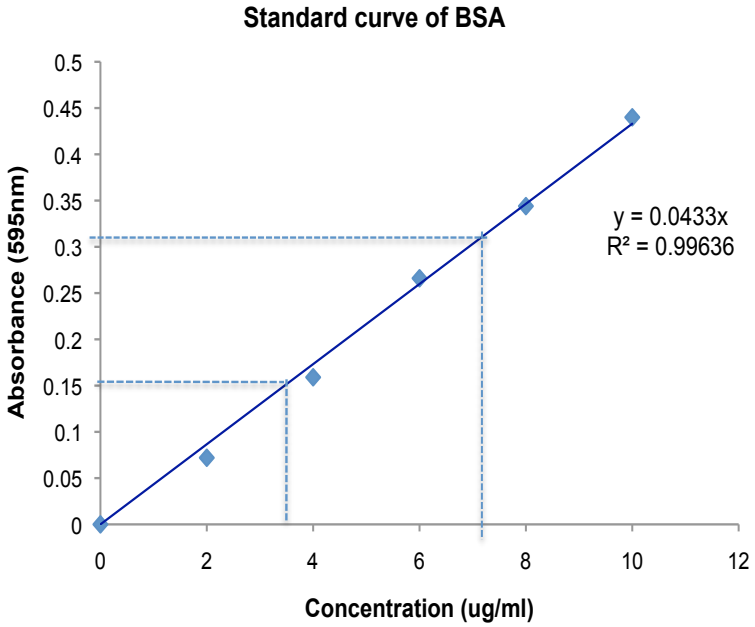

Fig 3.13: Extraction of *Xv*Prx2 concentration from BSA regression curve. The BSA regression curve was generated based on absorbance values (A_{595nm}) obtained from known concentrations of BSA. Absorbance values obtained from *Xv*Prx2 samples (diluted 1 in 5000 and 1 in 10000 times) were used to extract the concentration of the sample using dashed lines shown in Fig 3.13 or by substituting the absorbance values into the equation shown in Fig 3.13. The final concentration of *Xv*Prx2 was obtained by multiplying the concentration of the diluted sample by the dilution factor and found to be approximately 2.0 mM. *Xv*Prx2 concentration was sufficient to set up crystallization trials and the acquisition of NMR data, which typically require protein in the concentration range of 0.5 mM and above.

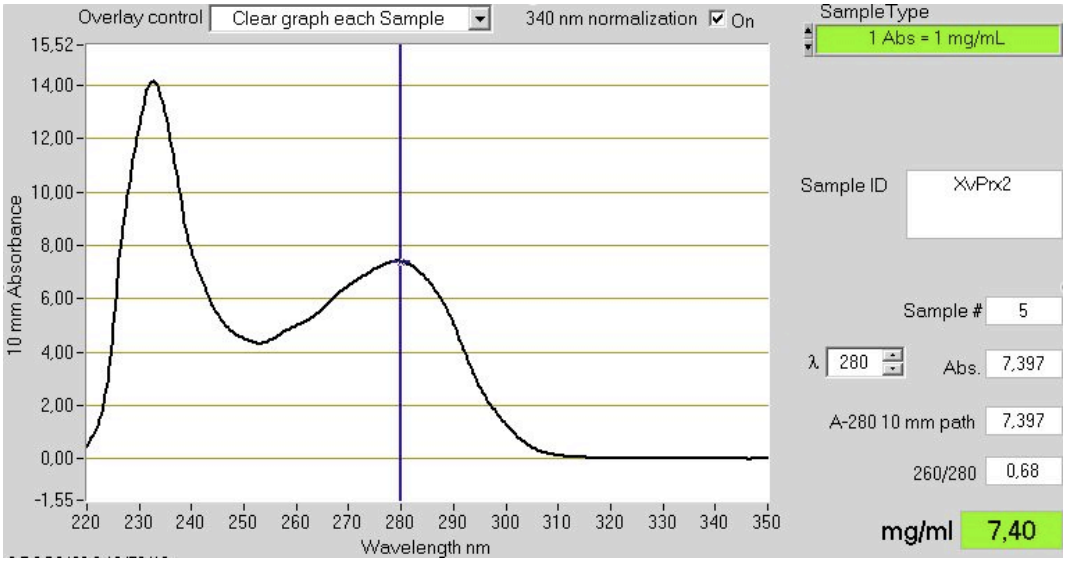

Fig 3.14: NanoDrop value of concentrated *Xv*Prx2 (diluted 1 in 4). The value obtained using NanoDrop was 2. 067 mM, consistent with values obtained using Bradford assay.

Drop automatically adjusts the optical path length so that the absorbance falls within the linear range and then extrapolates up to a path length of 1 cm, so the high value of A_{280} is not of concern). The Beer lambert law states that

$$A_{280} = \varepsilon CL,$$

where ε is the extinction coefficient of the protein (in units of $mM^{-1}cm^{-1}$), C is the total concentration and L = 1 cm. Using A_{280} = 7.4, L = 1 cm and ε = 13.98 mM^{-1} cm^{-1}, as determined by the ExPASy ProtParam server (*http://ca.expasy.org/cgi-bin/protparam*), C was calculated to be approximately 2.1 mM.

This value, which relies on prediction of the extinction coefficient from the amino acid sequence, is consistent with the value calculated using the Bradford assay, taking into consideration the uncertainties inherent in both methods. Since X-ray crystallization trials and NMR experiments both require concentrations of protein in the range of 0.5 mM and above, we concluded that the *Xv*Prx2 sample was of sufficient concentration and purity for structural studies using X-ray crystallography and NMR.

3.5. Crystallization trials of *Xv*Prx2

A rigorous search for conditions suitable for crystallization was pursued using protein concentrations in the range of 10 - 20 mg/ml, using the hanging-drop and sitting-drop vapour-diffusion methods, as described in Section 2.18. Figs. 3.15-3.19 shows some crystals of *Xv*Prx2 obtained using the crystallization conditions described in the legends on the associated figures.

A number of attempts were made to record diffraction data using some of these

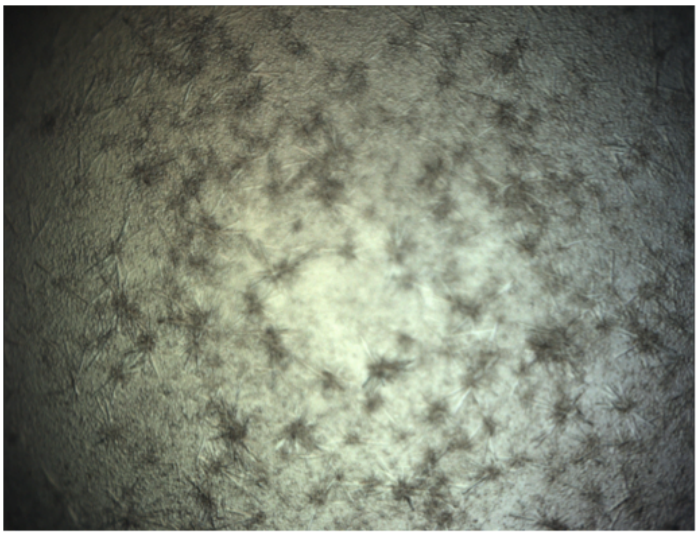

Fig 3.15: Showers of *Xv*Prx2 micro crystals obtained in 0.1M MES pH 6.0, 25 % PEG 10000 using 17mg/ml of protein. Crystals produced under this condition were not of sufficient size for data collection.

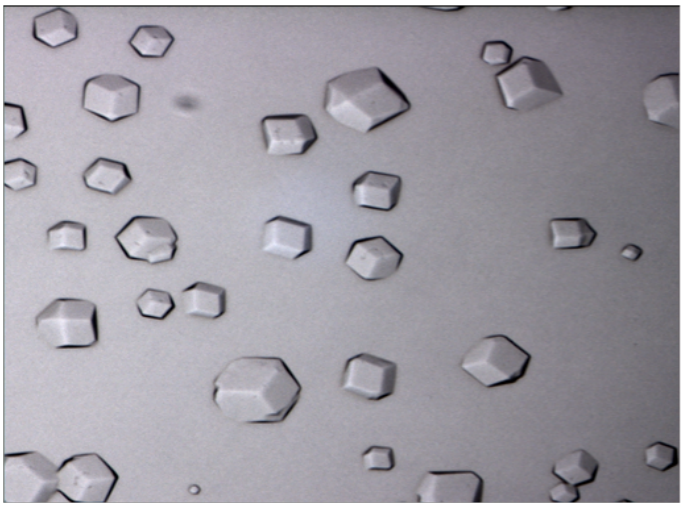

Fig 3.16: *Xv*Prx2 crystals obtained in in 0.1M MES pH 6.0, 25 % PEG 10000 using 11mg/ml of protein. Crystals produced under this condition did not produce sufficient reflections for structure solution using X-ray crystallography.

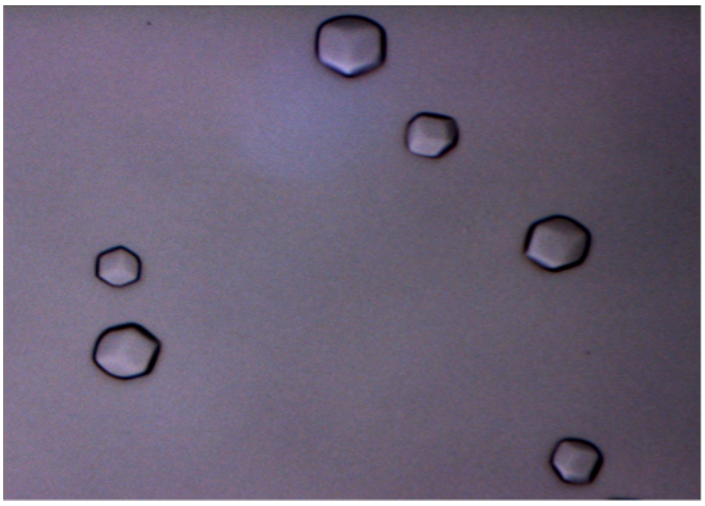

Fig 3.17: *Xv*Prx2 crystals obtained in 0.2 M di-potassium Phosphate using 17mg/ml of protein. Crystals produced under this condition did not produce sufficient diffraction spots for structure solution.

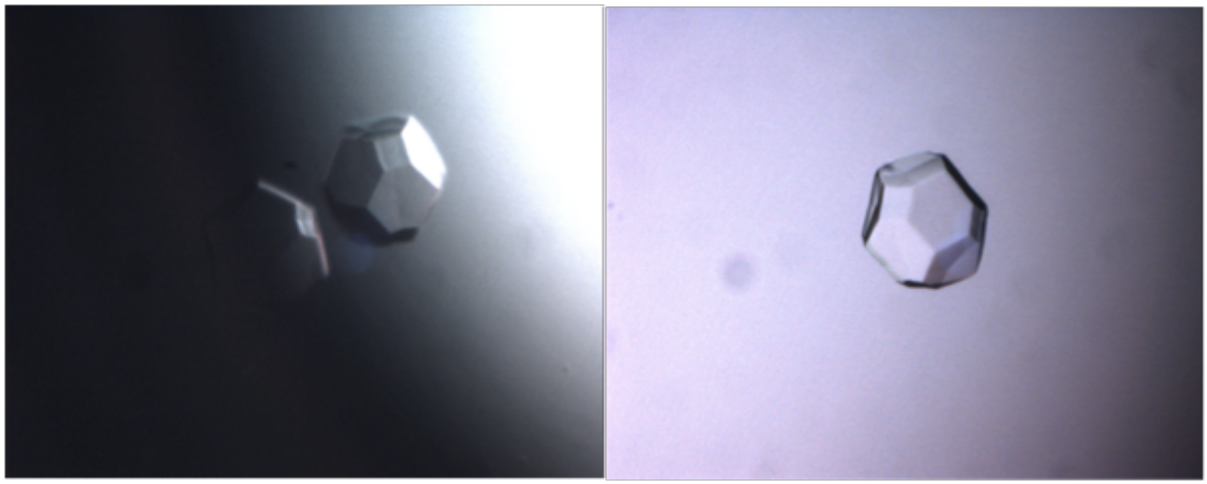

Fig 3.18: *Xv*Prx2 crystals obtained in 0.1M Tris pH 6.5 containing 20 % PEG 20000 using 17 mg/ml of protein. Crystals produced under this condition did not produce sufficient diffraction spots for structure solution.

crystals on the in-house X-ray source located University of the Western Cape, South Africa and the synchrotron facility in Soleil, France. However, in all the cases the data showed insufficient numbers of reflections for structure calculation.

Summary

In this chapter we reported the successful amplification of *Xv*Prx2 using PCR, generation of the pGEX-6P-2-*Xv*Prx2 expression construct, expression of unlabelled, ^{15}N-labelled and ^{15}N, ^{13}C-enriched *Xv*Prx2 samples in *E. coli* and their purification to homogeneity. The data relating to bacterial expression of *Xv*Prx2 presented in this work is representative of both labelled and unlabelled protein samples. The concentration of the resulting sample was of the order of 2 mM. More than two thousand crystallization conditions were screened using manual and semi-automated means and, while several crystals were obtained, none of them produced sufficient refections for structure determination. In the next chapter we describe the biophysical characterization of *Xv*Prx2 using a variety of methods as well as the backbone and side chain assignment of *Xv*Prx2 using heteronuclear nuclear magnetic resonance spectroscopy.

Chapter 4: Biophysical characterisation of *Xv*Prx2 using nuclear magnetic resonance spectroscopy, electrospray ionisation mass spectrometry and analytical size exclusion chromatography

Peroxiredoxins (Prxs) have been classified into six distinct groups, namely Prx1, Prx6, Prx5, TPx, BCP and AhpE, based on structural alignment of conserved residues found within the vicinity of the active site as well as other residues found within a distance of 10Å to key conserved residues (Section 1.5). *Xv*Prx2 belongs to the Prx5 subfamily, showing closest homology to PrxD from *Populus tremula* (*Pt*PrxD). PtPrxD and *Saccharomyces cerevisiae* alkylhydroperoxide reductase (Ahp1) both occur as non-covalent homodimers, with the homodimeric interface perpendicularly aligned to the central β-sheet (A-type dimer, see Section 1.4.1, Fig 1.8) (Echalier*, et al.*, 2005; Trivelli*, et al.*, 2003a). The residues involved in the interaction of the interface appear to be conserved in all Prx5 subfamily members suggesting that all proteins of this subfamily homodimerize using the same interface (Echalier*, et al.*, 2005). A functional role for the interface has been suggested on the basis of the fact that residues from each monomer are involved in forming the substrate binding pocket (Hall*, et al.*, 2011).

A number of factors including pH have been suggested to play a role in determining the oligomeric state of Prxs. A role for pH on the oligomeric state of Prxs has been reported in only one instance involving calpromotin, a Prx1 subfamily member protein derived from human red blood cells. Calmoprotin was observed to form large aggregates of about 300 kDa at pH 5.4 and a dimer of about 50 kDa at pH 8.53 (Kristensen*, et al.*, 1999). However, the effect of pH on the oligomeric state of Prx5 subfamily members has not been reported.

A number of tools including NMR, ESI-MS and analytical SEC have been used to investigate the oligomeric state of Prxs (Echalier*, et al.*, 2005; Evrard*, et al.*, 2004; Noguera-Mazon*, et al.*, 2006b; Trivelli*, et al.*, 2003a). NMR supplies direct structural data on biomolecules, as well as their state of folding, the presence of intra-and intermolecular bonding, the size of proteins as a function of their rate of tumbling and the signature of proteins associated with different oligomeric states. The presence of a number of isoforms of a protein, which may be associated with different oligomeric states, can be distinguished and their signatures assigned using NMR. Modern mass spectrometers serve as excellent tools to investigate the oligomeric state of proteins and have been used to determine the molecular weight of proteins or protein complexes with accuracies of less than 1Da, (Loo, 1997). MS data used to observe non-covalently linked protein complexes needs to be recorded under non-denaturing conditions. Analytical SEC allows the apparent molecular weight of proteins to be estimated based on the elution volumes of protein standards with known molecular weight. SEC is not dependent on the choice of buffer and is therefore ideal for investigating the molecular weight of complexes or the apparent molecular weight of molecules in exchange between different oligomeric states.

This chapter presents an investigation of the oligomeric state of *Xv*Prx2 using NMR, ESI-MS and analytical SEC. Furthermore, it examines the effect of pH on the oligomeric state of *Xv*Prx2 and concludes by presenting the full assignment of backbone resonances of *Xv*Prx2 in the homodimeric state.

4.1 Characterization of the folding properties of *Xv*Prx2 using NMR

1D proton spectrum

The 1D proton spectrum of a protein contains sufficient information for assessing the

state of folding of the protein (Rehm*, et al.*, 2002). Whereas the spectrum of an unfolded protein is essentially the sum of the random coil spectra of each amino acid within the protein, the spectra of folded proteins are shifted away from random coil values due to the structural diversity and the presence of different microenvironments within the interior of the structure. The most significant differences are the result of shielding from ring currents arising from aromatic side chains (Rehm*, et al.*, 2002). The degree of protein folding can thus be predicted on the basis of the chemical shift dispersion of proton signals compared to random coil values: in folded proteins backbone amide proton (H^N) chemical resonances are found between 6.5 and 10.5 ppm, H^α resonances between 3.2 and 5.5 ppm and methyl groups between 0.5 and -1.0 ppm (Cavanagh, 1996). In contrast, in unfolded proteins proton chemical shifts are more narrowly distributed, with backbone H^N resonances clustered around 8.3 ppm, methyl groups between 0.8 and 1.1 ppm (Wüthrich, 1986) and H^α protons in the region 4.1- 4.4 ppm (Cavanagh, 1996).

The 1D proton spectrum of *Xv*Prx2 (Fig 4.1) shows ample dispersion away from random coil values. A number of H^N resonances are shifted significantly up-field into the range 8.5-10.5 ppm, including one observed at approximately 11.1 ppm. A number of methyl group resonances have been downshifted into the range < 0.8 ppm, including one at approximately -0.52 ppm. The identity of this resonance is reported in Section 4.4 and the implication of its shift for the oligomeric state of *Xv*Prx2 is examined in Section 5.2.

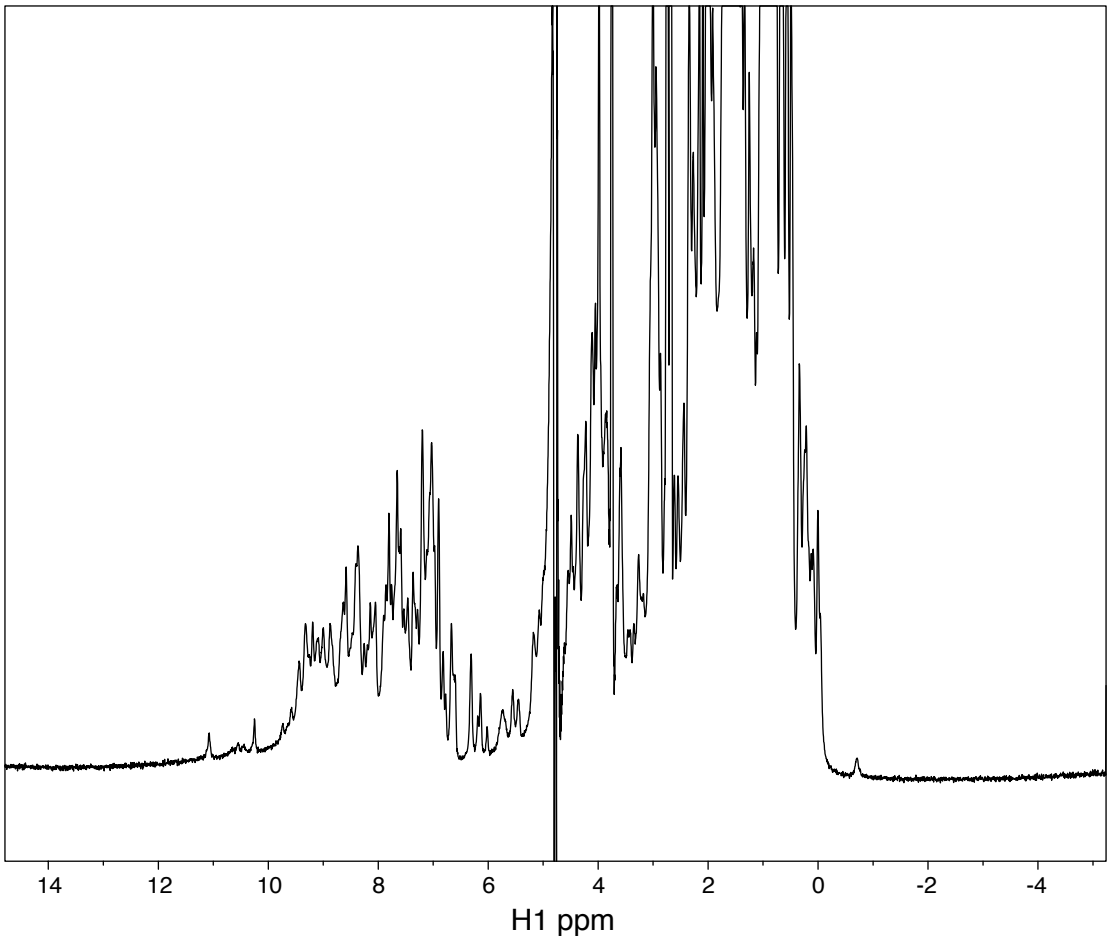

Fig 4.1: 1D ^{1}H spectrum of *Xv*Prx2 at pH 7.0, 25 °C recorded at 600 MHz. The spectrum shows a good dispersion of proton resonances suggestive of a folded protein. Of particular interest are the resonances at -0.52 ppm and > 10 ppm.

^{15}N HSQC spectrum

^{15}N-HSQC spectra are excellent tools for assessing the state of folding and integrity of proteins, providing data with improved resolution and higher information content compared to 1D NMR experiments (Rehm*, et al.*, 2002). The majority of resonances in a ^{15}N-HSQC spectrum correspond to backbone amide groups, with the horizontal coordinate corresponding to the H^N chemical shift and the vertical coordinate to chemical shift of the attached nitrogen. However other groups containing directly bonded to the nitrogen atoms also appear in the spectrum, including the ε-amino group of each arginine residue, the side chain indole group of tryptophan residues (although there are none in *Xv*Prx2) and the backbone NH_2 groups of arginine and asparagine residues. The latter appear as two peaks with the same nitrogen chemical shift and two different proton shifts; a number of them have been indicated using a horizontal lines in Fig 4.2. The $H^{\eta 1}$ and $H^{\eta 2}$ NH_2 groups of arginine residues may sometimes be observed but typically are not due to broadening resulting from rapid exchange with the solvent. Prolines lack NH groups and are thus not observed in ^{15}N-HSQC spectra. The degree of structure or disorderliness within proteins is indicated by the dispersion (spread) of resonances analogous to that observed in 1D NMR spectrum. Spectra of unfolded proteins show a characteristic clumping of resonances around H^N chemical shifts of approximately 8.3 ppm while the spectra of folded proteins show large dispersions of peaks in the range 6 -12 ppm and 105 - 135 ppm in the H^N and N dimensions respectively (Rehm*, et al.*, 2002).

The ^{15}N-HSQC spectrum of *Xv*Prx2 at pH 7 is shown in Fig 4.2. It shows a number resonances shifted significantly upfield in the ^{1}H dimension including those at (δ^{15}N, δ^1H) = (132.5, 9.64), (131, 10.25), (129, 11.03), (126.9, 9.72), (120.1, 9.55), (120.5,

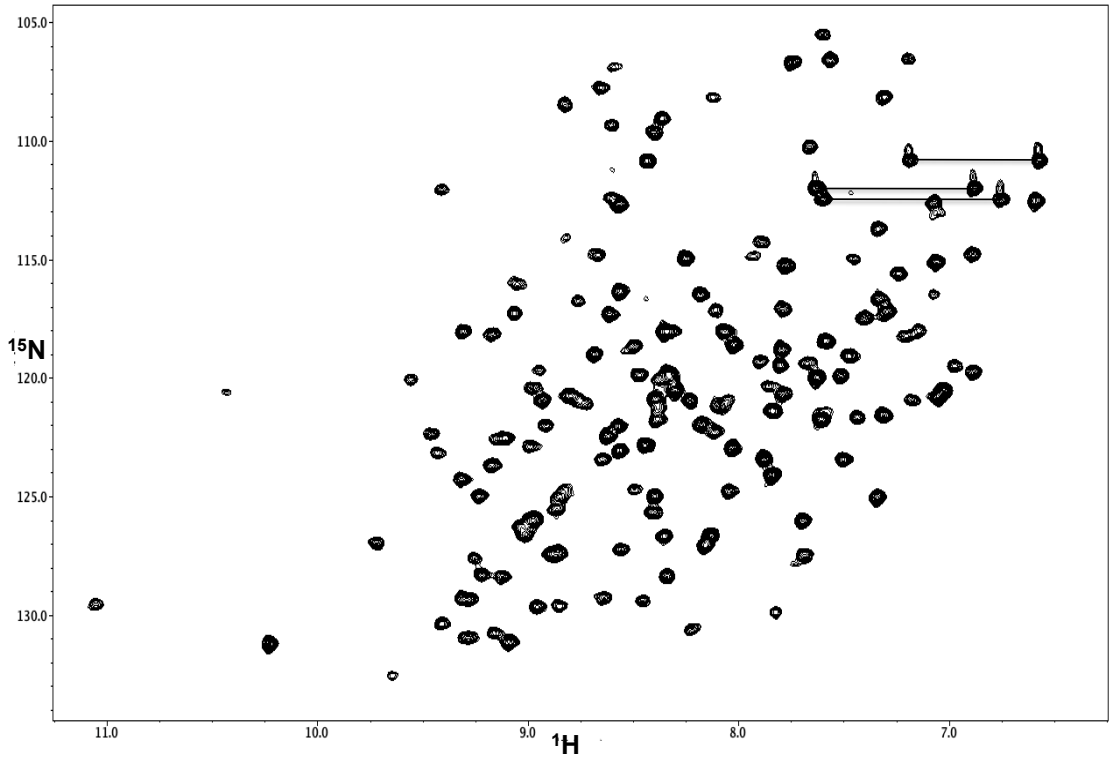

Fig 4.2: ^{15}N-HSQC spectrum of *Xv*Prx2 at pH 7, 25 °C, recorded at 600 MHz. The resonances are well dispersed in both the ^{1}H and the ^{15}N dimensions, which is indicative of a well folded, compact protein. Most of the resonances correspond to the backbone NH groups, although a number of side chain NH_2 groups can be seen joined by the horizontal lines in the top right-hand corner. The observed number of resonances (167) is consistent with the expected number (169).

10.4). The high degree of dispersion indicates that the protein is properly folded. The expressed protein is expected to contain 3 asparagine and 2 glutamine residues, each of which has a side chain NH_2 group, and 8 prolines which do not have backbone amide groups. Since the native protein is 162 residues long, with the inclusion of the 5 non-native residues at the N-terminus we expect a total of 167-8+2*5 = 169 resonances, which is consistent with the observed number of 167. On the whole, the spectrum appears to be a good representation of the protein with a reasonable degree of spread of its resonances suggesting a compact fold under these conditions.

4.2 Investigation of pH effect on the conformation *Xv*Prx2 using NMR

Changes in environmental factors of a protein such as pH and temperature can affect the shape and conformation of a protein, which may affect the number, dispersion and location of resonances in the ^{15}N-HSQC spectrum. The pH of a protein environment can affect its ability to make covalent or non-covalent interactions, which are often responsible for holding a protein in a particular configuration. NMR studies have revealed pH dependent effects on a number of proteins, including the SH3 domain of Drosophila drk, Dynein light chain protein, a part of the cytoplasmic motor assembly and human thioredoxin (Andersen*, et al.*, 1997; Mohan*, et al.*, 2006; Zhang & Forman-Kay, 1995).

1D spectra of *Xv*Prx2 at pH 5 and 7 are shown in Fig 4.3. At pH 7 a highly shifted peak can be observed at -0.52 ppm, which is not present at pH 5.

Significant differences are also apparent in ^{15}N-HSQC spectra recorded at pH 5, 6, 7 and 8, which are shown in Fig 4.4. Two different conformations dominate at pH 5 and pH 8 respectively, and at pH 6 the spectrum contains approximately equal populations

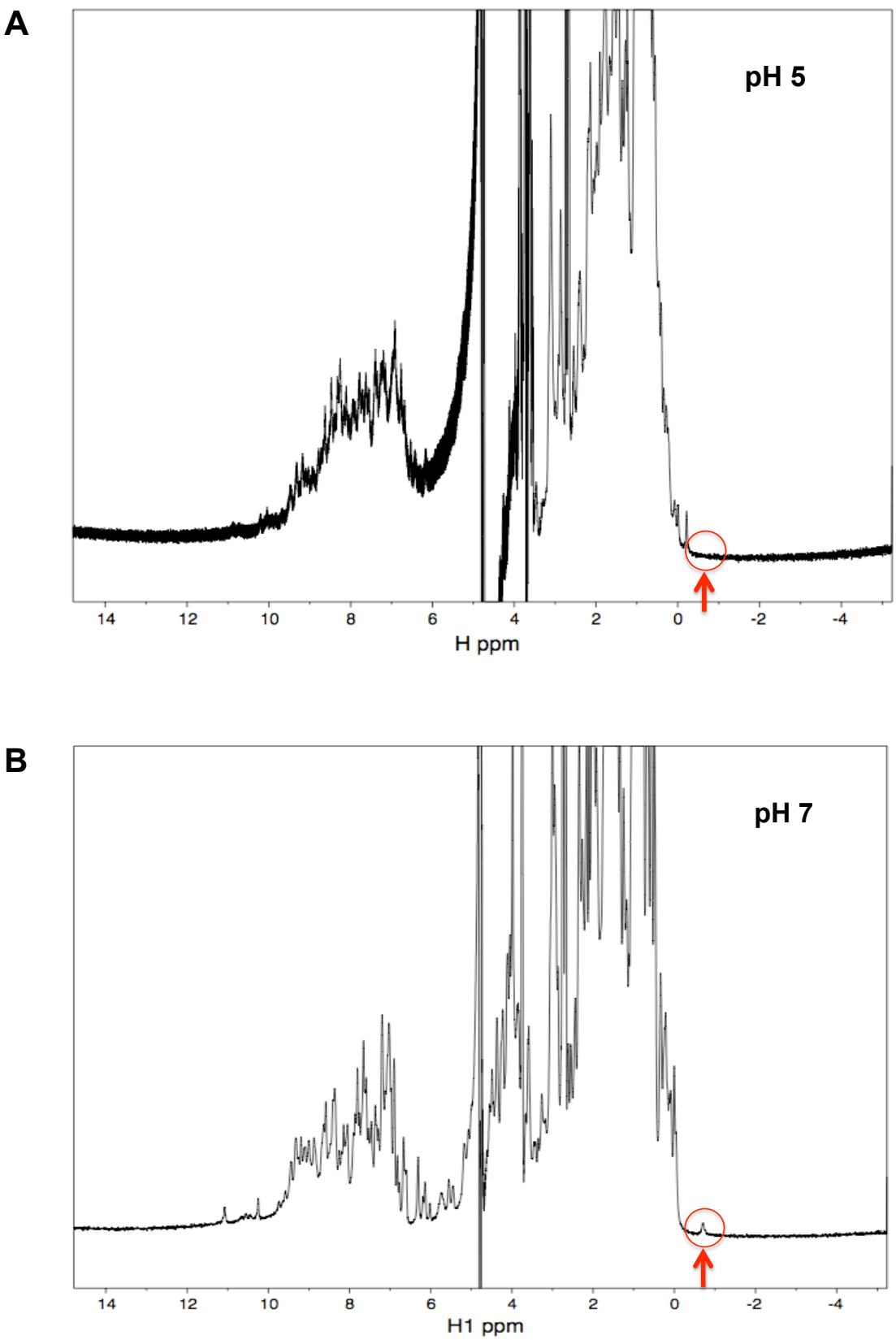

Fig 4.3: 1D proton spectra of *Xv*Prx2 at pH 5 and 7, recorded at 600 MHz at 25 °C. The degree of dispersion is consistent with folding at both pH values. However a significantly down-field shifted resonance is visible at pH 7 (indicated with arrow) which is not present at pH 5.

of each conformation. This is most clearly seen in the boxed regions in which a doubling of peaks occurs at pH 6. The effect is presented in more detail in Fig 4.5 where the same regions of pH 5 (blue), pH 6 (red) and pH 7 (black) are overlaid. The fact that both conformations are observed in the spectrum implies that the rate of interconversions between them is slow on the time scale of NMR.

The protein was found to be substantially less stable at pH 5 than at higher pH, starting to precipitate during the concentration step and precipitating significantly after 12 - 24 hours. The protein was also significantly less stable at 25 °C than at 4 °C. The poor stability at pH 5 significantly affected the quality of the data that could be obtained under these conditions and resulted in our inability to assign backbone and side chain resonances at pH 5.

^{15}N NMR dynamics experiments are excellent tools for investigating the effective mass of a protein and hence its oligomeric state. T1 and T2 values, which describes the time it takes for a nuclea spin to return to its equlibrium value, were measured at pH 8 (without needing to assign the protein) and analysed by Dr Andrew Atkinson, Kings College London, giving a value of 27 kDa for the effective molecular weight. Since this value is intermediate between monomer and homodimer it raised the possibility that the pH-dependent effect corresponded to a monomer-dimer transformation. However, which spectrum corresponded to the monomer and which to the dimer, was not yet clear. We were unable to measure the apparent molecular weight at pH 5 due to the instability of the protein at this pH. Non-denaturing mass spectrometry was used to investigate this question further, as described in Section 4.5.

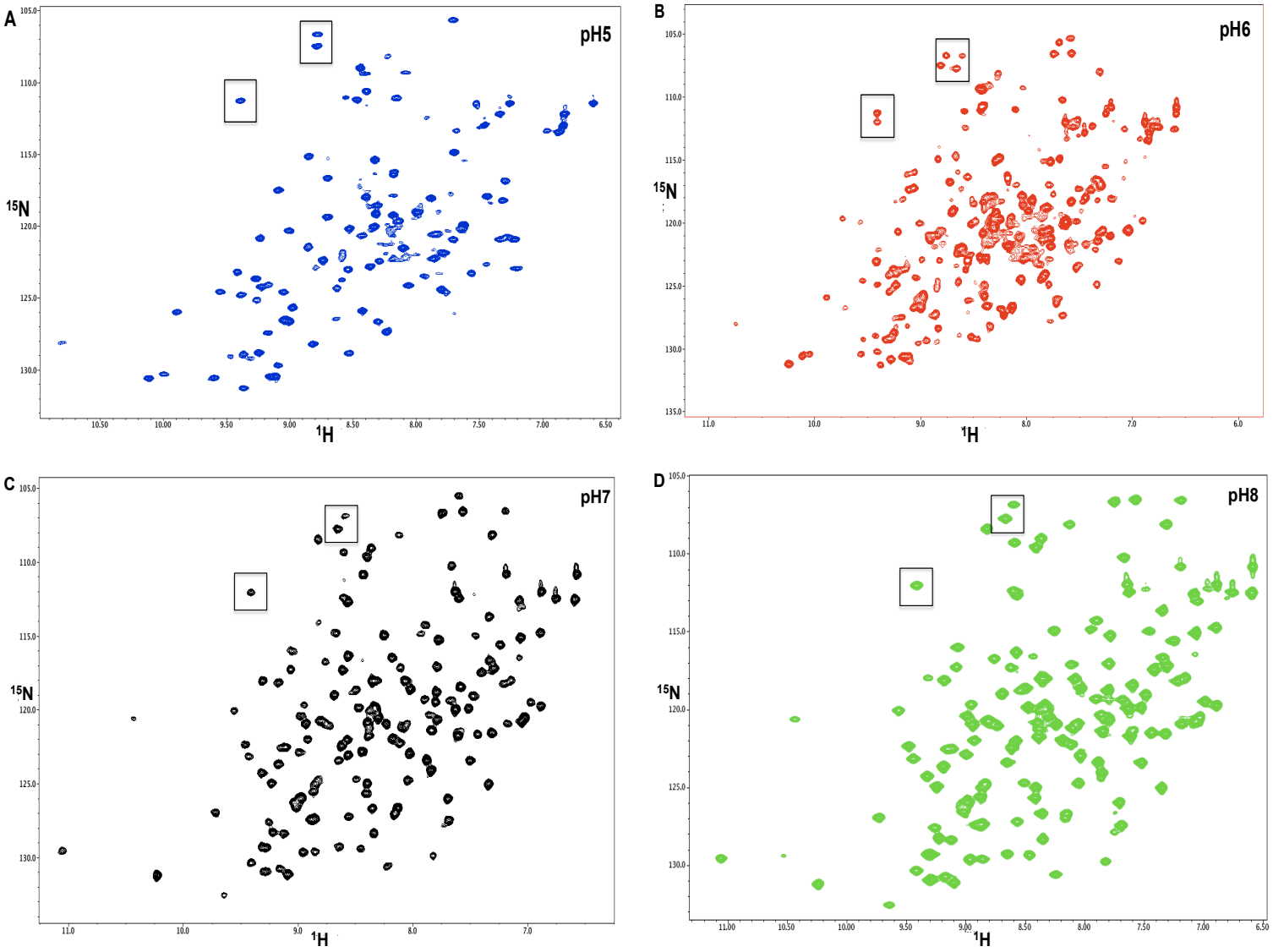

Fig 4.4: ^{15}N-HSQC spectra of *Xv*Prx2 at pH 5(A), 6(B), 7(C) and 8(D) at 25 °C, recorded at 600 MHz. Significant differences are apparent in the ^{15}N-HSQC spectrum recorded at pH 5, 6, 7 and 8. It is clear that two different conformations dominate at pH 5 and pH 8 respectively, and that the pH 6 data contains approximately equal populations of each conformation while the pH 7 data is very similar to the pH 8 data. This is most clearly seen in the boxed regions in which the doubling of peaks has occurred. This is shown in more detail in Fig 4.5 in which the same regions of pH 5 (blue), pH 6 (red) and pH 7 (black) are overlaid. The pH 7 and pH 8 spectra are almost identical.

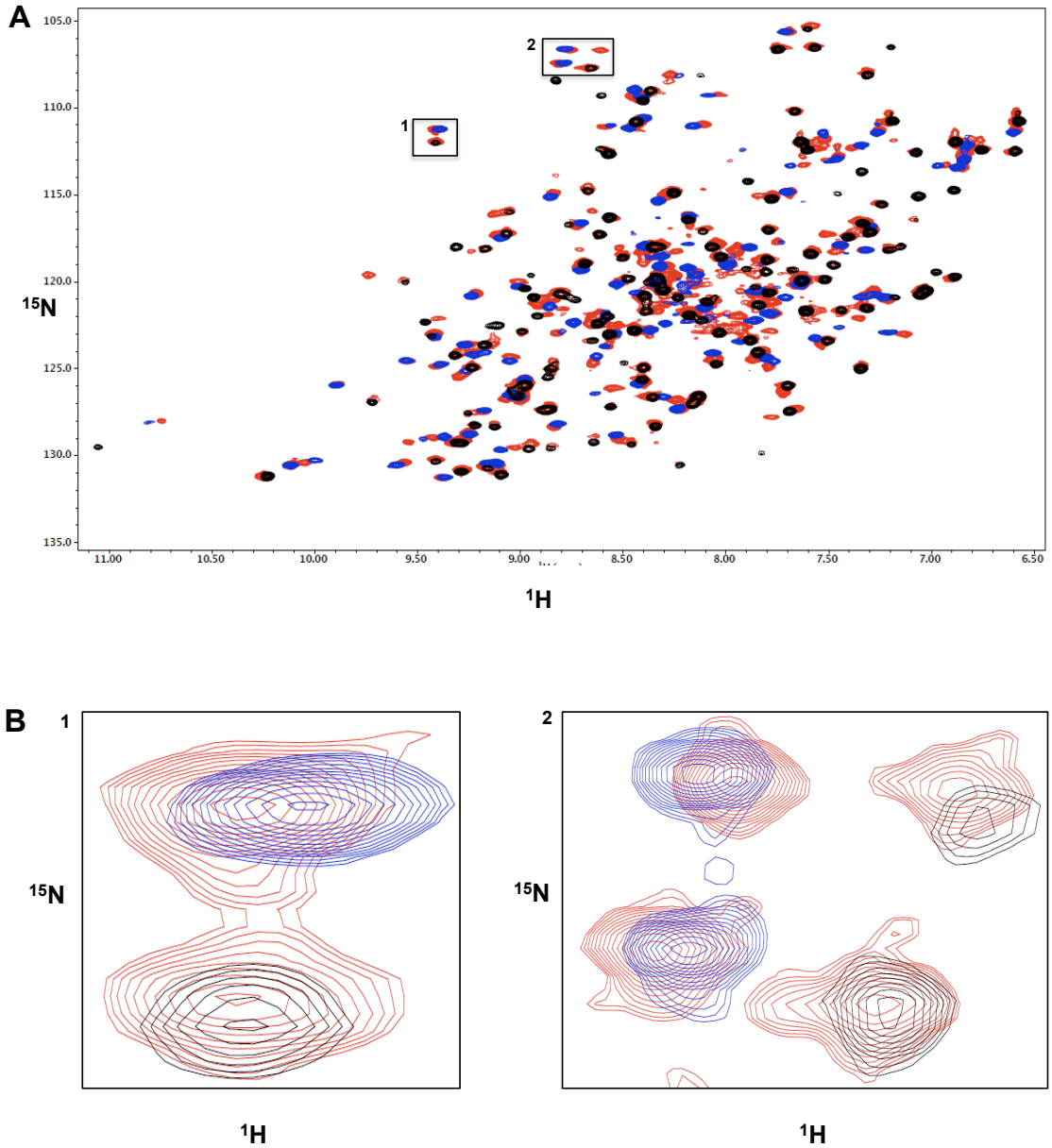

Fig 4.5: Overlay of ^{15}N-HSQC spectra of *Xv*Prx2 at pH 5, 6 and 7, recorded at 600 MHz at 25 °C. (A) shows the overlay of full spectra of *Xv*Prx2 at pH 5 (blue), pH 6 (red) and pH 7 (black) while (B) shows an expanded view of regions marked "1" and "2" in (A). The overlay shows that the two different conformations present at pH 5 and 7 are both present in approximately equal amounts at pH 6.

4.3 Sequential assignment of *Xv*Prx2 backbone resonances at pH 7.2

As a first step towards determination of the structure of *Xv*Prx2 at pH 8, as well as for interpretation of the pH dependent chemical shift changes discussed in the previous section, ^{13}C, ^{15}N-labelled samples were generated and used to record triple resonance spectra required for assignment of backbone chemical shifts.

A number of triple resonance experiments can be interpreted as separating the 2-dimensional ^{15}N-HSQC spectrum into a third frequency dimension, corresponding in this case to the ^{13}C dimension. The simplest example is the HNCO spectrum, in which the 3rd dimension corresponds to the frequency of the carbonyl carbon attached to each backbone NH group. Since the projection of the HNCO spectrum along the carbon dimension yields a spectrum identical to the ^{15}N-HSQC (with the exception of the non-backbone resonances), but with less overlap due to separation in the carbon dimension, resonances in the ^{15}N-HSQC spectra are usually picked using the HNCO spectrum. The resulting peak list contains coordinates δ^1H, $\delta^{15}N$, $\delta^{13}C$, of which only the δ^1H and $\delta^{15}N$ are used for generating strip plots.

Two-dimensional H-C and N-C strip plots were set up using the NMRView software package. H-C strip plots were generated from HN(CO)CA and HNCA by extracting strips of width 2δ in the ^1H dimension (where δ is a small fraction of the spectral width in the ^1H dimension) centered on each H^N resonance and extending across the full ^{13}C spectral width. N-C strip plots were generated similarly.

As has been described in Section 2.21, the HN(CO)CA generates only one peak corresponding to the preceding α-carbon $C^{\alpha(i-1)}$, whereas the HNCA generates two

peaks corresponding to the α-carbon of residue *i* ($C^{\alpha(i)}$) in addition to $C^{\alpha(i-1)}$. Comparison of HNCA and HN(CO)CA side-by-side using a strip plot allows the connectivities of the amides to be established; a double strip plot generated by interlinking strips from HN(CO)CA (gold) and HNCA (blue) is shown in Fig 4.6. The aim is to order the pairs of strips so that the $C^{\alpha(i)}$ of one pair (in the blue strip) has the same chemical shift as the $C^{\alpha(i-1)}$ (in the gold strip) of the next pair to the right. A similar strip plot for HNCACB and HN(CO)CACB is shown in Fig 4.7 while the table used to cross reference resonance shifts for identification is shown in Fig 4.8.

Initial attempts the assign the ^{15}N-HSQC at pH 6 were abandoned after the doubling seen in Fig 4.4(B) was identified. Initial promising triple resonance spectra recorded at Stellenbosch at pH 8 were followed up by more careful optimization under the guidance of Dr Andrew Atkinson at the Institute of Genetics Molecular and Cellular Biology (IGBMC) in Strasbourg, France. Thermofluor-based high-throughput stability optimization experiments revealed that our protein remained stable at low concentrations of salt (20 mM) in the complete absence of EDTA and at temperatures as high as 40 °C, allowing us to change sample conditions and the temperature used for data acquisition. A temperature of 38 °C resulted in increased molecular tumbling and thereby reduced the width of the spectral lines, improving the resolution of triple resonance experiments significantly. Using these conditions a full backbone assignment was achieved at pH 7.2. The assigned ^{15}N-HSQC spectrum of *Xv*Prx2 recorded at pH 7.2 is shown in Fig 4.9.

In total we were able to assign backbone resonances of 152 of the 162 residues of *Xv*Prx2 (ignoring the five artifactual residues (GPLGS) found at the N-terminus of the

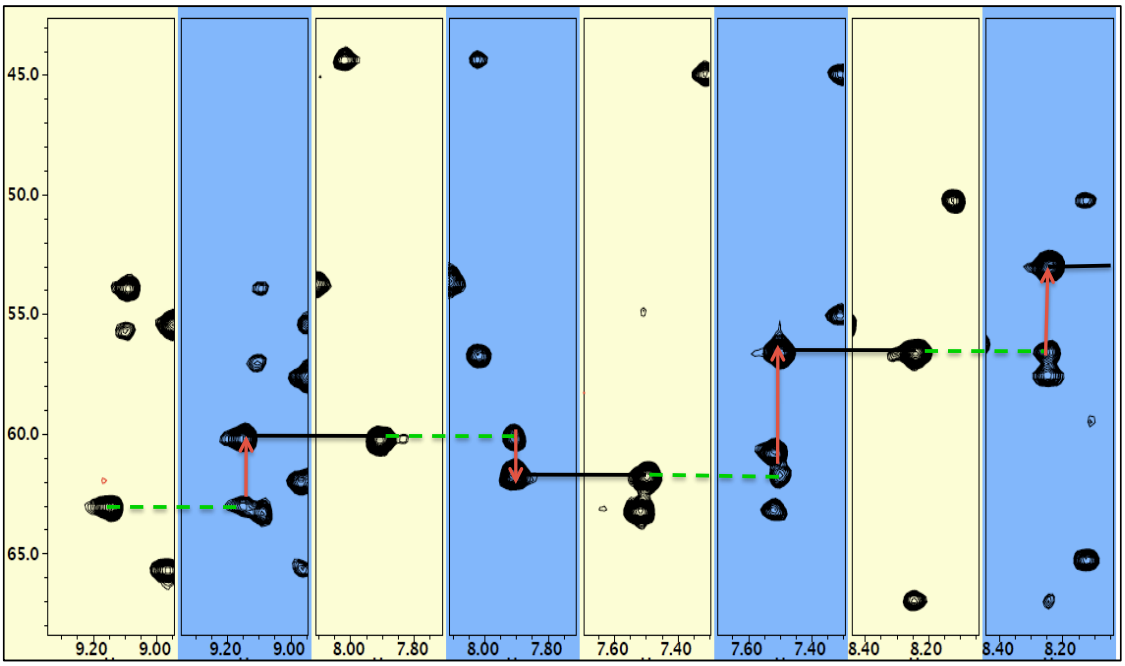

Fig 4.6: Double strip plots showing backbone sequential connectivities of some *Xv*Prx2 residues. The golden strips are taken from a HN(CO)CA spectrum while the blue strips are from the corresponding HNCA spectrum. The golden strips shows one peak corresponding to the C^{α} of the preceding residue *i-1* while the blue strips show 2 peaks corresponding to the C^{α} of residue *i* and *i-1* of which the peak of residue *i* is more intense. Peaks within the blue strip, which do not have corresponding equivalents in the golden strip, correspond to the C^{α} peak of residue i while peaks, which have equivalents in the golden strips correspond to the C^{α} of residue *i-1*. The red arrow shows connectivity of peaks during the assignment process. The red dashed line indicates magnetization transfer from the C^{α} of residue *i-1* to the H-N groups of residue *i*, while the black non-dashed lines indicate the transfer of magnetic energy from the C^{α} resonance of the residue *i* to adjacent HN groups of residue *i*, thus permitting residue-specific sequential connectivity. The strips have been arranged such that adjacent strips contain corresponding carbon shifts.

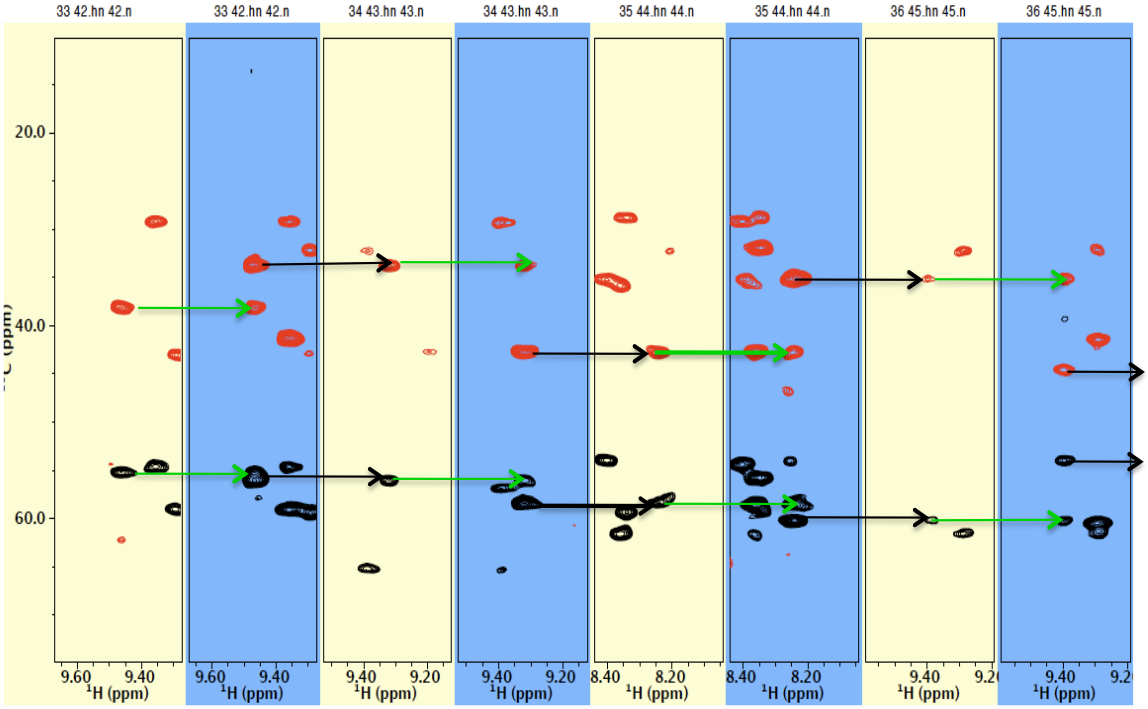

Fig 4.7: Double strip plots showing backbone sequential connectivities of some *Xv*Prx2 residues. Gold strips are taken from HN(CO)CACB spectrum while blue strips are from the corresponding HNCACB spectrum. Black arrows indicate transfer of magnetic energy from C^{α} or C^{β} resonance to adjacent H-N groups of residue *i*, while green arrows indicate the transfer of magnetic energy from the C^{α} or C^{β} resonance to adjacent HN groups of residue *i-1* thus permitting the establishment of sequential residue connectivity. The strips have been arranged such that adjacent strips contain corresponding carbon shifts.

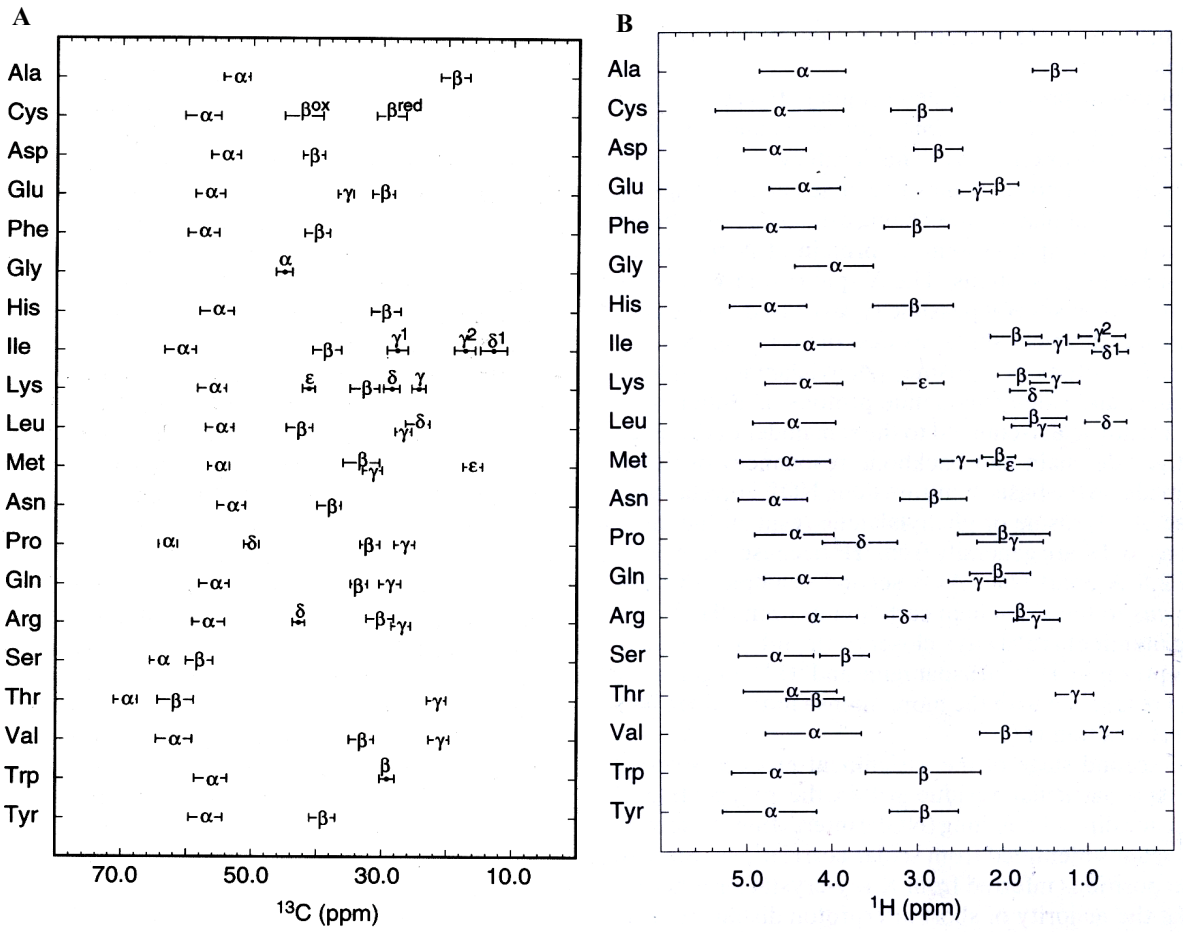

Fig 4.8: Chemical shifts for all 20 naturally-occurring amino acid residues. Average C^{α} and C^{β} chemical shifts are shown in (A) with the aliphatic side-chain amide ^{1}H chemical shifts in (B). Adapted from Cavanagh, 1996.

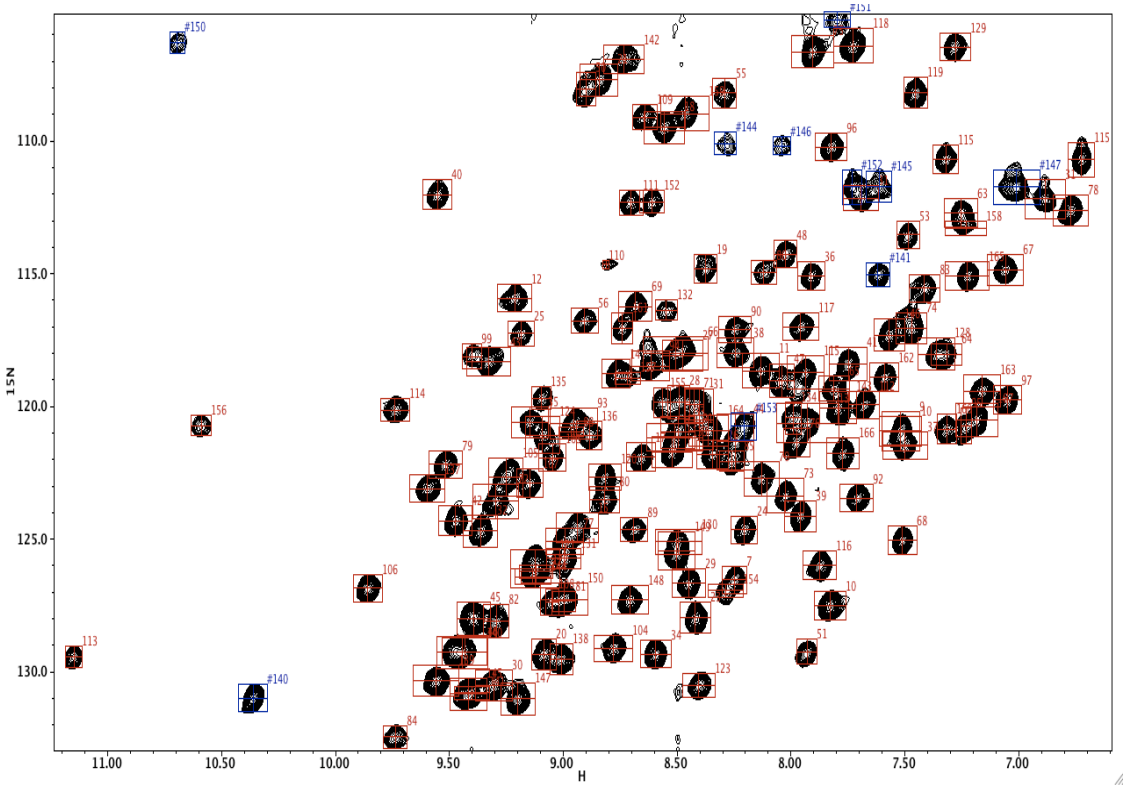

Fig 4.9: ^{15}N-HSQC spectrum of *Xv*Prx2 recorded at pH 7.2, 38 °C and 600 MHz. Each assigned peak is labelled with a numbering system in which the residues are counted from the initiation methionine. The initiation methionine is the 6th residue of the protein when the N-terminal sequence (GPLGS), which are artifacts of the cloning system, is considered (Section 3.3). The numbering system used in this Fig. differs by six when compared to those shown in Appendix IV. Labels beginning with # symbol (blue) are unassigned.

protein). The residues we were unable to assign were Met1, Ser52, Met53, Gln54, His55, Val56, Glu119 and Lys120, either because their corresponding resonances were not observable, most probably due to local chemical exchange, or due to poor connectivity to other residues. The H^N, N, C^α and C^β chemical shifts of all the assigned atoms were extracted from the spectra using NMRView and are tabulated in Appendix IV.

Only after assignment had been completed was it confirmed that *Xv*Prx2 is homodimeric at pH 7.2, giving it an effective molecular weight of 38 kDa. This places the protein near the upper limit of feasibility for backbone assignment using standard (non-TROSY) and non-deuterated triple techniques. Despite attempts at both pH 7.2 and 8 we were unable to assign enough side chain resonances for determination of the structure of the wild type protein. However we were able to assign the resonance at δH = -0.52 ppm that is present at pH 8 but not at pH 5. The procedure for doing that is reported in the remainder of this section and the structural implication of the presence or absence of the resonance at -0.52 ppm is discussed in chapter 5.

A 2D homonuclear TOCSY spectrum is a 2-dimensional spectrum in which cross-peaks between positions on the diagonal correspond to transfer of magnetic energy through covalent bonds between the protons corresponding to diagonal positions. The horizontal and vertical axes both correspond to proton chemical shifts. Energy transfer occurs among all protons in an amino acid, but cannot cross the peptide bond from one amino acid to another, making the experiments ideal for identifying protons belonging to a particular amino acid (colloquially referred to as a "spin system").

The 3D HC(C)H-TOCSY is a 3-dimensional version of the homonuclear TOCSY in which the over-crowded and overlapping cross-peaks have been separated into the 3rd dimension according to the chemical shifts of carbon attached to one of the diagonal protons. Since the un-bracketed "C" in "HC(C)H" refers to the vertical proton dimension, the nomenclature makes it clear that the cross peaks will be labelled (and hence positioned in the 3rd dimension) according to the chemical shift of the carbon directly bonded to the proton on the vertical axis (proton 2 in Fig 4.10A). Consequently, a 2D-plane corresponding to a particular carbon chemical shift will contain only the cross-peaks (appearing in the form of a horizontal line) in which the proton directly attached to the carbon in question lies on the diagonal (see Fig 4.10(C)). Identical patterns are expected at carbon chemical shifts corresponding to each of the protons in the amino acid, allowing the chemical shifts of each carbon and each proton to be systematically determined.

The HC(C)H-COSY is essentially the same as the HC(C)H-TOCSY, with the exception that magnetic energy is only transferred between protons joined by up to 3 covalent bonds. In the case of amino acids this means either H-C-C-H or H-C-H. As well as being less crowded and of increased sensitivity, the HC(C)H-COSY is useful in establishing covalent topology that is not clear from the HC(C)H-TOCSY.

The procedure for assigning side chains of protons is illustrated here for the case of Ile41. Fig 4.11 shows sections of 2-D planes from the HC(C)H-COSY spectrum corresponding to the C^{α}, C^{β}, $C^{\gamma 1}$, $C^{\gamma 2}$ and $C^{\delta 1}$ carbons of Ile41. A diagram of the topology of isoleucine is shown in Fig 4.11 (B). Since this is a COSY spectrum, the C^{α} plane contains only the H^{α} and H^{β}, with H^{α} on the diagonal. The C^{β} plane however,

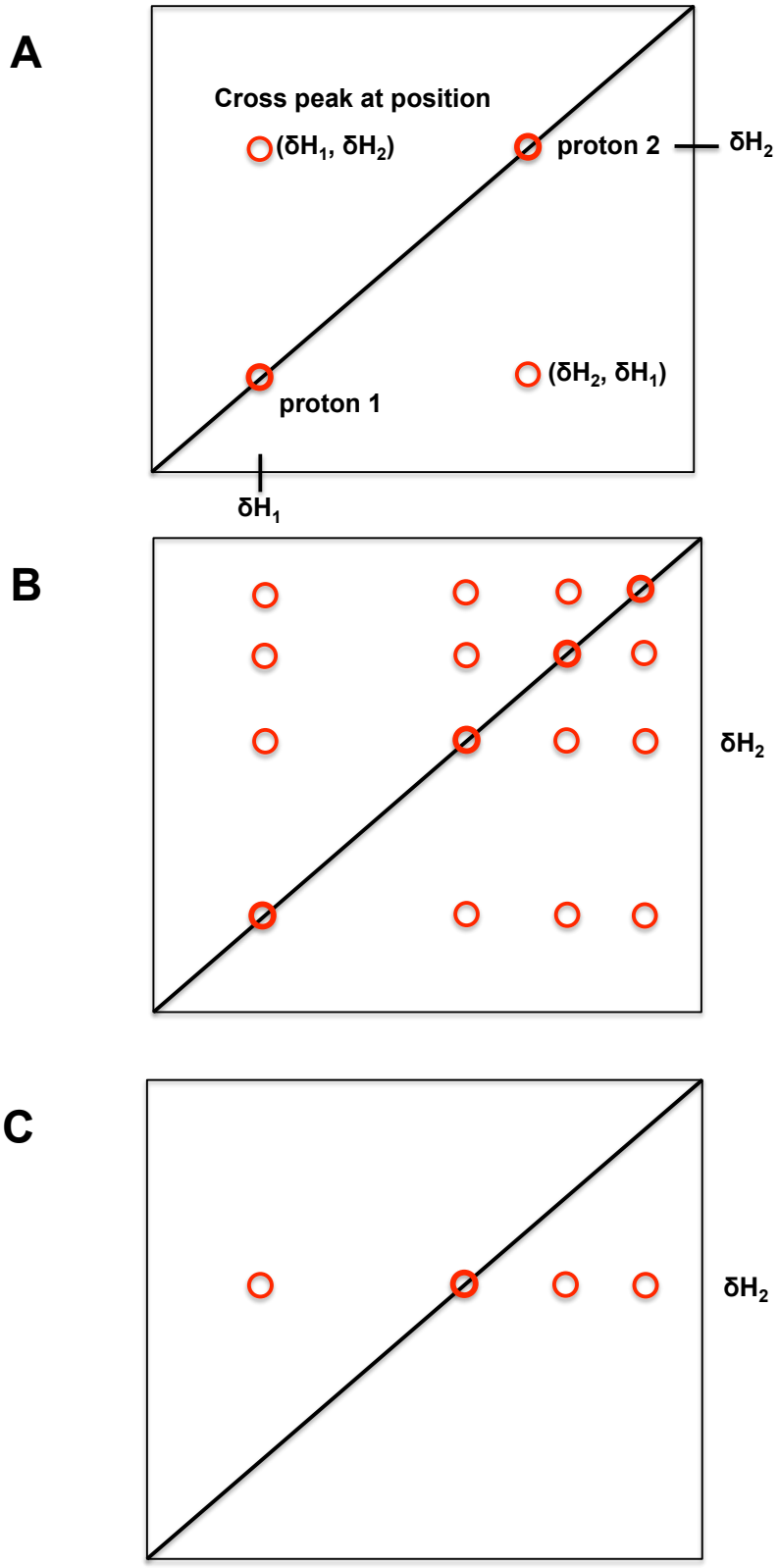

Fig 4.10: Proton cross peaks in a 2-proton, 2D-TOCSY and HC(C)H-TOCSY spin system. (A) Shows cross peaks between proton 1 and 2 in a 2-proton system. **(B)** 2D-TOCSY of a typical 4 - proton amino acid residue is shown in **(B)** while **(C)** shows a plane of HC(C)H-TOCSY spectrum single resonance, do not appear because the $C^{\delta 1}$ is not directly coupled to the C^{β}. The $C^{\gamma 2}$ plane contains only H^{β} and the $H^{\gamma 2}$ methyl resonance on the diagonal, again as expcted, since the $C^{\gamma 2}$ is connected only to the C^{β} .corresponding to the chemical shift of the carbon directly attached to proton 2.

contains H^{α}, the $H^{\gamma 2}$ methyl and the $H^{\gamma 11}$ and $H^{\gamma 12}$ methylenes, as well as H^{β} on the diagonal. This is because $C^{\gamma 2}$, $C^{\gamma 1}$ and C^{α} are all directly connected to C^{β}. However the $H^{\delta 1}$ methyl protons, which (as with all methyl groups in protein NMR) appear as a single resonance, do not appear because the $C^{\delta 1}$ is not directly coupled to the C^{β}. The $C^{\gamma 2}$ plane contains only H^{β} and the $H^{\gamma 2}$ methyl resonance on the diagonal, again as expcted, since the $C^{\gamma 2}$ is connected only to the C^{β}.

The $C^{\gamma 1}$ plane contains two rows of identical cross-peaks, one in which $H^{\gamma 11}$ is on the diagonal and one in which $H^{\gamma 12}$ is on the diagonal. Both sets contain H^{β} and $H^{\delta 1}$ as well as a cross peak between the two $H^{\gamma 1}$ protons. The $C^{\delta 1}$ plane contains $H^{\gamma 21}$ and $H^{\gamma 22}$ with $H^{\delta 1}$ on the diagonal.

The same information is contained in the HC(C)H-TOCSY spectrum in Fig 4.12, although the spectral quality is poorer. However the conclusion to be drawn from Figs. 4.11 and 4.12 is that the carbon chemical shifts of the planes (shown at the right) unambiguously identify the amino acid giving rise to the resonances as Ile 41. The structural significance of this result will be discussed in Chapter 5.

4.5. Investigation of pH-dependent oligomerisation of *Xv*Prx2 using ESI-MS

NMR analysis revealed a significant pH-dependent effect consistent with large conformational changes or changes of oligomeric state. It had been previously reported that a number of factors, including pH, play a role in the change of the oligomeric state of the Prx1 subfamily proteins from dimer to decamer or vice versa (Kristensen*, et al.*, 1999). However, there are no reports of pH dependent effects on the oligomeric state

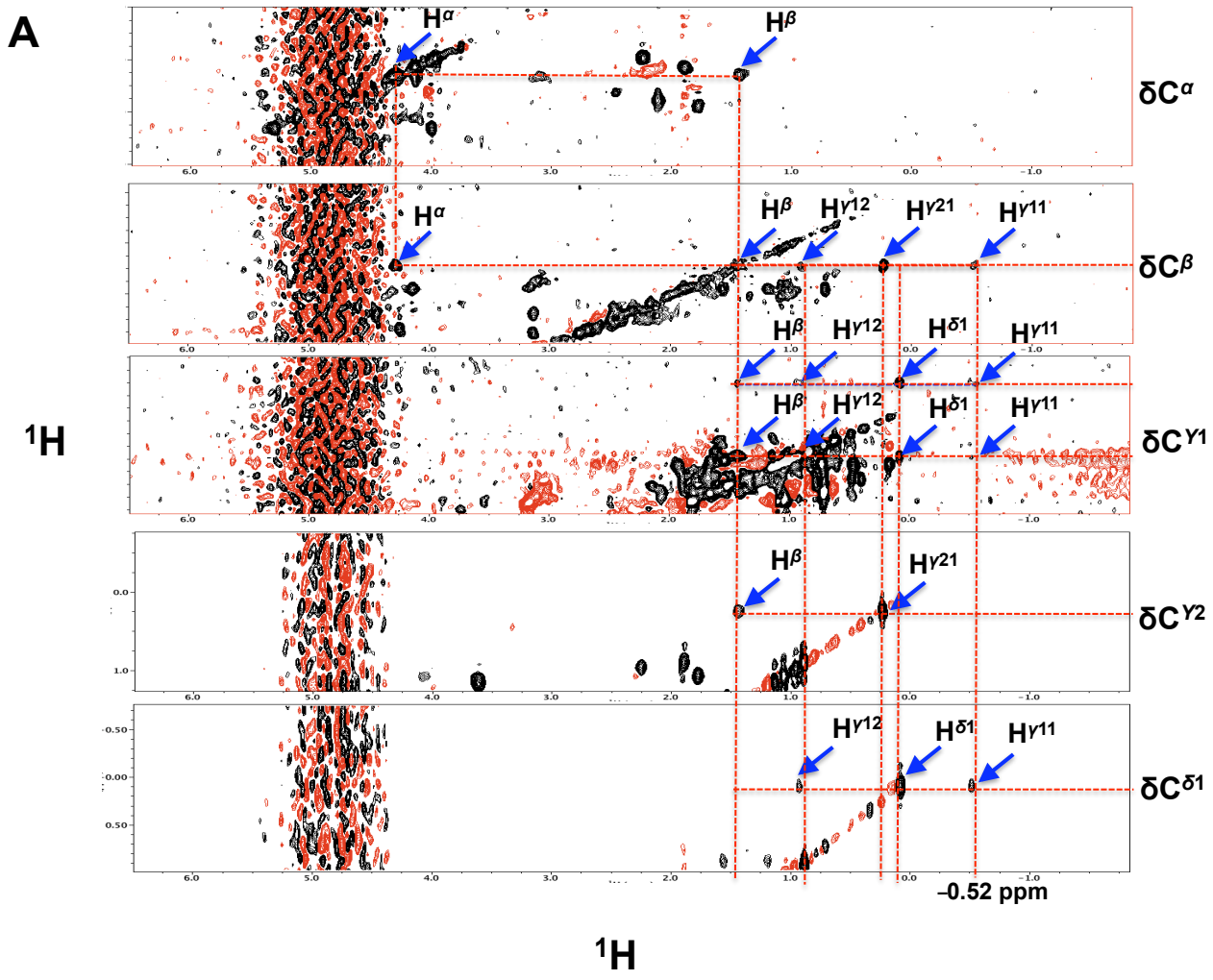

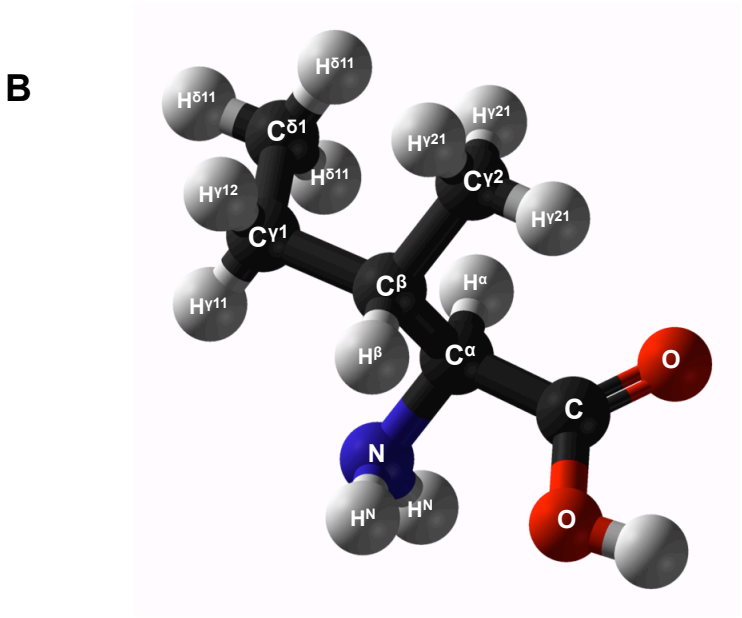

Fig 4.11: Selected planes of the HC(C)H-COSY spectrum of *Xv*Prx2 at pH 7.2. (A) Planes correspond to the chemical shifts of carbon atoms of Ile 41. The same proton resonances occur in each plane, filtered by the three-bond rule appropriate to COSY spectra, as explained in the text. (B) Topology of isoleucine.

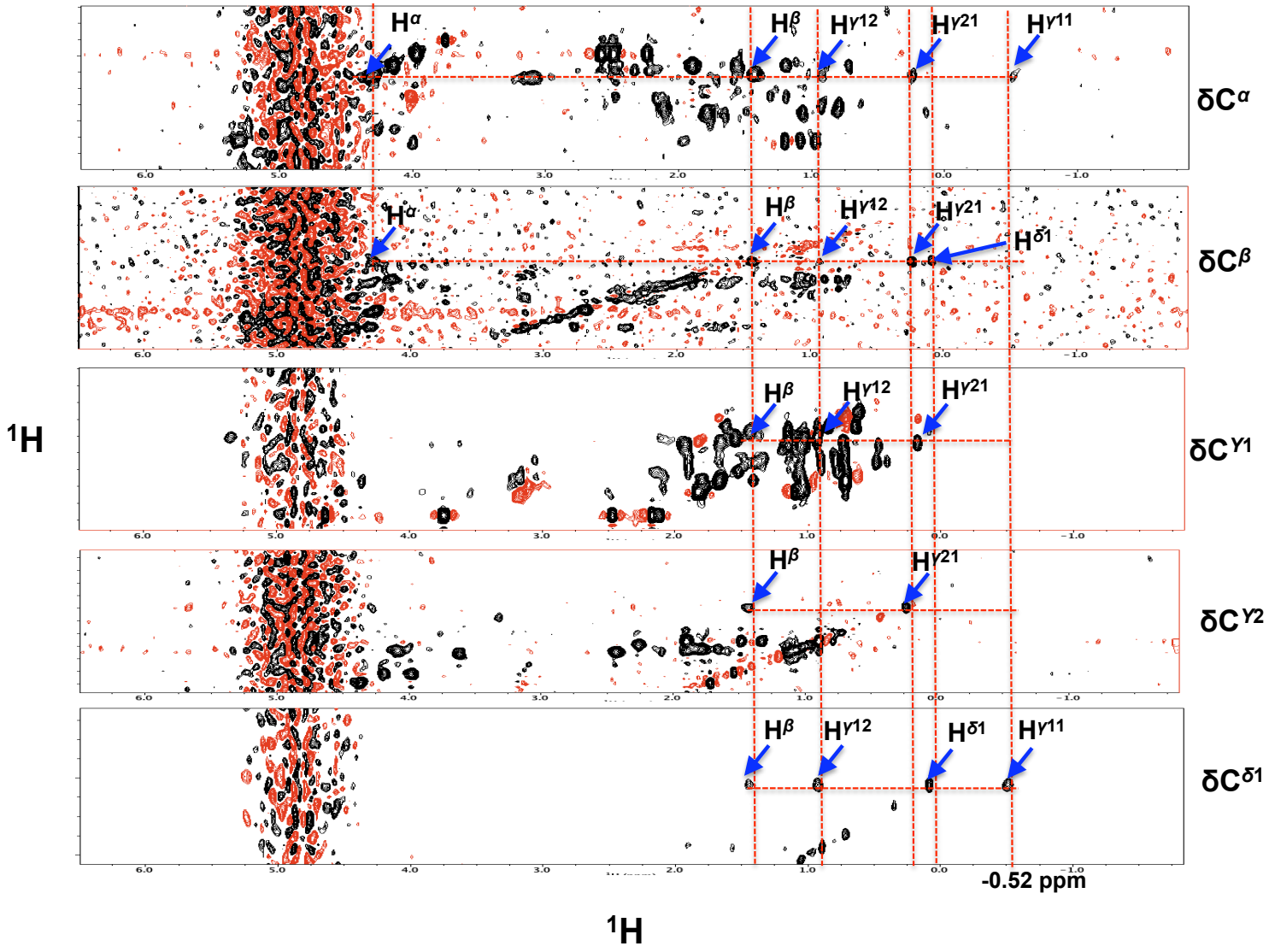

Fig 4.12: Selected planes of the HC(C)H-TOCSY spectrum of *Xv*Prx2.

of Prx5 subfamily proteins although they have been reported to form non-covalent homodimers at pH 7.0 (Echalier*, et al.*, 2005). Non-denaturing mass spectrometry has been used to explore pH dependent changes in a number of proteins and a link to their oligomeric states (Hanefeld*, et al.*, 2001; Kashiwagi*, et al.*, 2000).

Commercial mass spectrometers utilize a range of different technologies for detection, including Time-Of-Flight (TOF), Quadru9pole and Orbitrap, as well as for the ionisation of the sample, of which the most common are the Matrix Assisted Laser Desorption Ionisation (MALDI) and Electrospray Ionisation (ESI). Whereas MALDI tends to produce only singly and doubly ionized species, ESI produces a spectrum of different ionisations, each of which contains the same information. The resulting spectrum of resonances can either be analysed directly (the "raw" data) or can be integrated to give a spectrum containing a single resonance corresponding to the mass of the protein.

Mass spectrometry (MS) conventionally determines only the mass to charge ratio of an ionised species, requiring the charged state (and therefore the mass) to be inferred from additional factors. However the resolution of modern mass spectrometers allows for detection of the complete isotope spectrum of each ionisation, from which the mass of each ionisation can be unambigously determined.

MS is most commonly carried out under denaturing conditions, typically achieved by addition of 0.2 % formic acid. While denaturing conditions tend to increase the number of charges acquired by the protein in ESI, the unfolded state of the protein means that non-covalent interactions cannot be observed. In recent years MS has been used to

study proteins in non-denaturing conditions by the use of volatile solvents such as ammonium acetate, and soft ionisation conditions such as low cone voltages (Hanefeld, *et al.*, 2001; Kashiwagi, *et al.*, 2000).

Fig 4.13 shows the "raw" mass spectrum of *Xv*Prx2 at pH 7 under non-denaturing conditions. The resonances marked "8+", "7+", and "6+" have been identified by the instrument as containing 8, 7 and 6 positive charges respectively, based on their isotopic spectra. The m/z values of 2238.5793, 2557.8013 and 2983.9717 therefore correspond to independent estimations of the mass of the protein. The overall mass of the protein is obtained by multiplying the m/z value by the number of charged ions followed by the subtraction of the mass of the charged ions as shown in the formular below:

$$m/z = \frac{[M + xH]^{x+}}{x}$$

where m/z represents the mass to charged ratio, M the overall mass of the protein and x the number of charged ions or states.

Using the argument above the m/z values of 2238.5793, 2557.8013 and 2983.9717 corresponding to the 8th, 7th and 6th states respectively, corresponding to protein masses of 17900.6 (2238.5793 x 8 - 8), 17897.6 (2557.8013 x 7 - 7) and 17897.8 (2983.9717 x 6 - 6) Da respectively, which are all consistent with the expected value of 17899 Da.

Using the same reasoning the resonance at m/z = 2754 should correspond to 17899/2754 ≈ 6.5 positive charges. However, since half-integral charges are not physically possible, this resonance can only correspond to 13 charges on the homodimeric state, giving an m/z value of (2 × 17899)/13 = 2754. This resonance was independently identified as carrying 13 charges based on its isotopic spectrum, in agreement with the above argument. Similarly the resonance at m/z = 3256 corresponds to the 11^{th} ionisation of the homodimer. The resonances marked 8+, 7+ and 6+ will also contain contributions from the 16^{th}, 14^{th} and 12^{th} ionisations of the homodimer respectively, but it is difficult to separate the contributions; however the 13^{th} and 11^{th} ionisations can only arise from the homodimer, and therefore constitute independent evidence that the protein is at least partly homodimeric at pH 7. When the "raw" data was deconvoluted using the MaxInt1 and MaxInt3 algorithms the expected two mass species were identified, corresponding to the monomeric (17899 Da) and homodimeric (35797 Da) forms of the protein respectively (Fig 4.13B).

Similar mass spectra acquired at pH 5, 6 and 8 are shown in Figs. 4.14 - 4.16 (the corresonding deconvoluted spectrum is shown only for pH 5). At pH 8 the relative heights of the peaks indicative of the homodimer (m/z = 2754 and 3256) appear similar to those at pH 7. However, the same peaks (the 13^{th} and 11^{th} ionisations of the homodimer appear to have decreased in height at pH 6 and have disappeared completely at pH 5, which suggests that the protein is entirely monomeric at pH 5.

Our ESI-MS data suggests that the fraction of *Xv*Prx2 molecules involved in homodimerization increases as the pH increases from 5 to 8, from zero at pH 5 to around 1/3 at pH 8. Since it is likely that at least some of the homodimers have

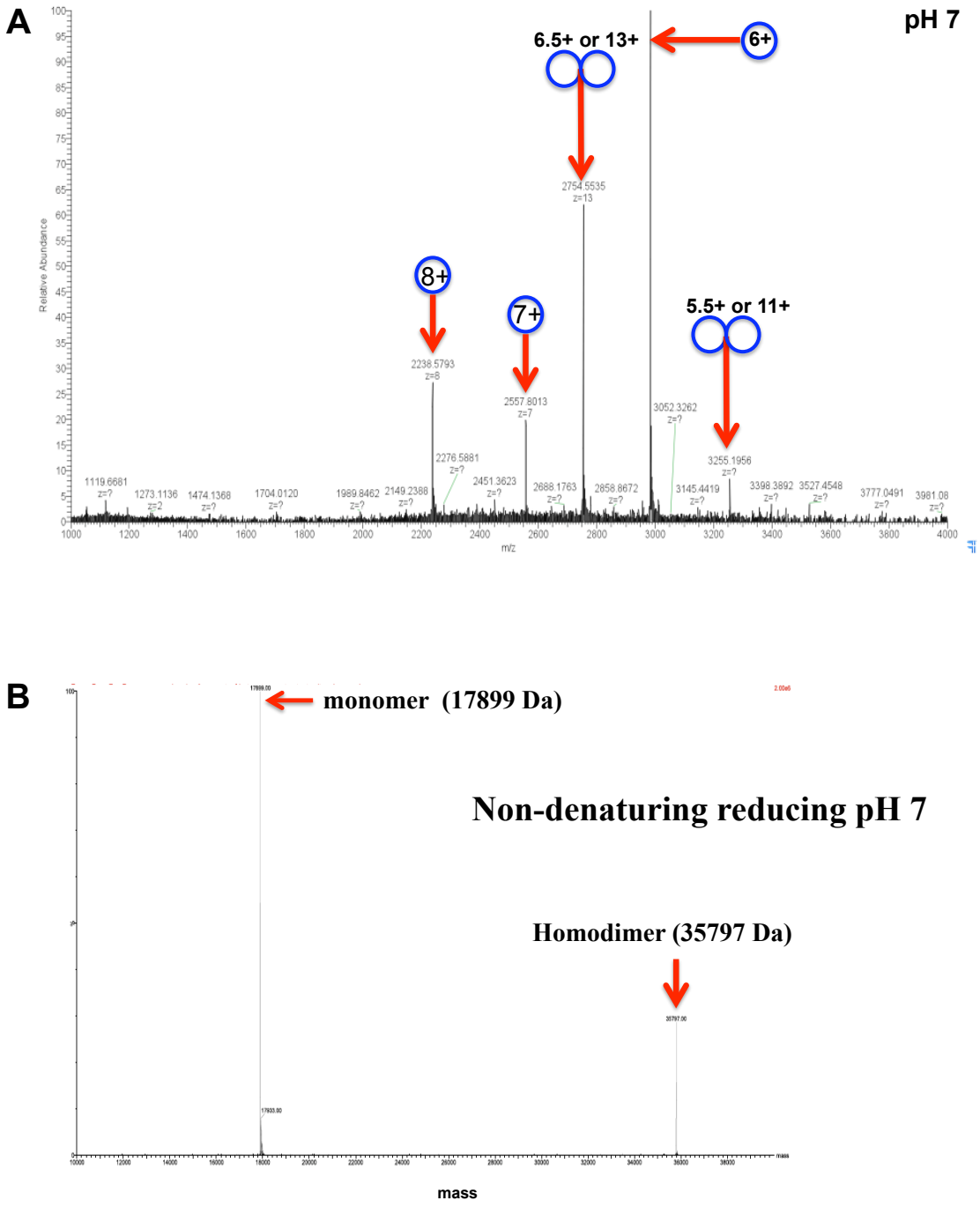

Fig 4.13: ESI-MS spectrum of *Xv*Prx2 acquired at pH 7 under non-denaturing reducing conditions. (A) The "raw" data exhibits a spectrum of different ionisations which are indicated by the numbers above. Single circles represent a sum of the 9th, 8th, 7th and 6th ionisations of the monomer and the 18th, 16th, 14th and 12th ionisations of the homodimer, respectively. Peaks denoted with double circles can only correspond to the 11th and 13th ionisations of the homodimer, as half integral charges (6.5 and 5.5 respectively) are not physical. These resonances confirm that the homodimeric state is present at pH 7. The deconvoluted spectrum is shown in (B), confirming the conclusion drawn from the raw data that a significant fraction of the protein is homodimeric at pH 7.

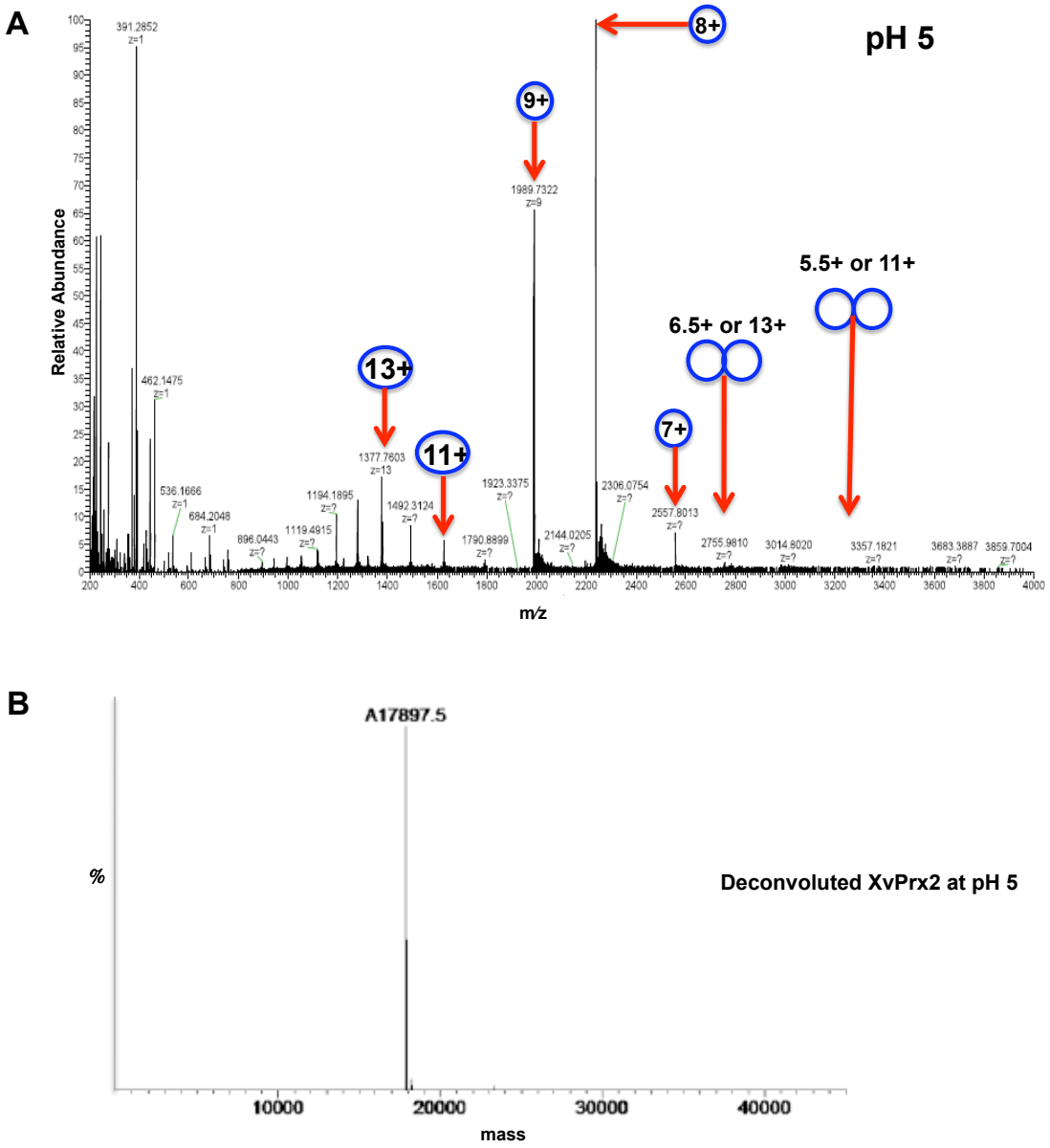

Fig 4.14: ESI-MS spectrum of *Xv*Prx2 acquired at pH 5 under non-denaturing reducing conditions. (A) shows the "raw" ESI-MS spectrum of *Xv*Prx2 at pH 5 acquired under non-denaturing conditions; displaying a number of peaks (circled and denoted with arrows) respresenting the respective charged ion states of the protein and collectively corresponding to the monomeric configuration of *Xv*Prx2. Arrows pointing in from below the spectrum (Fig 4.14A), which have not been circled, show the positions that would have been occupied by peaks corresponding to the homodimeric configuration of the protein. The deconvoluted form of the same data shown in Fig 4.14A is shown in (B), showing one peak (17897.5 Da) corresponding to the monomeric form of the protein. The fact that the peaks representative of the homodimeric form of the protein are completely absent in Fig 4.14A coupled with the presence of only the monomer peak (17897.5 Da) in Fig 4.14B indicates that *Xv*Prx2 is completely monomeric at pH 5.

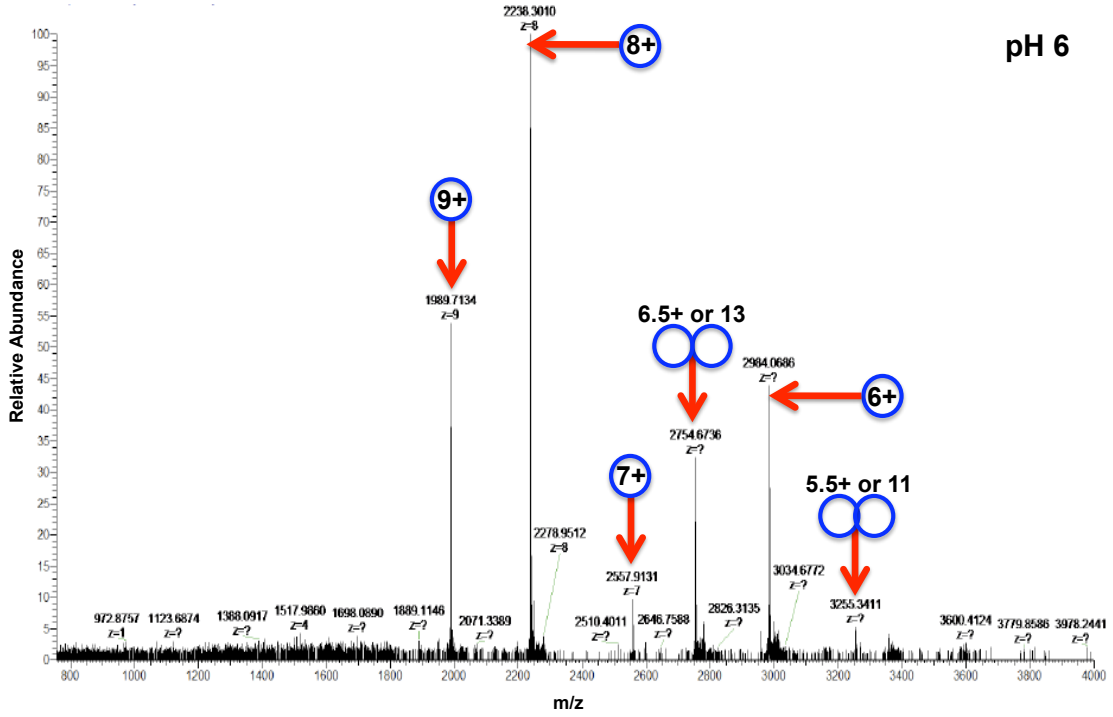

Fig 4.15: ESI-MS spectrum of *Xv*Prx2 acquired at pH 6 under non-denaturing reducing conditions. The spectrum show peaks (circled and denoted with arrows) indicating the number of charged ionic states. Single circles represent peaks that correspond to the monomeric configuration (9^{th}, 8^{th}, 6^{th}) while double circles represent homodimeric peaks. The 13^{th} and 11^{th} ionizatons infact correspond to (17899/2754.4609 ≈ 6.5+ and 17899/3255.2625 ≈ 5.5+ ionisations). However since half integral charges are not physical, the 13^{th} and 11^{th} resonances can only correspond to charges on the homodimeric state, giving an m/z value of (2 × 17899)/13 = 2754, (2 × 17899)/11 = 3255. The ionisations marked 6.5+ or 13+, and 5.5+ or 11+ are independent evidence that the homodimeric states are present at pH 6 although the resonances marked 9+, 8+, 7+ and 6+ could also contain contributions from the 18^{th}, 16^{th}, 14^{th}, and 12^{th} ionisations of the homodimer, but it is difficult to separate the contributions of the homodimer to the monomer for such ionisation states.

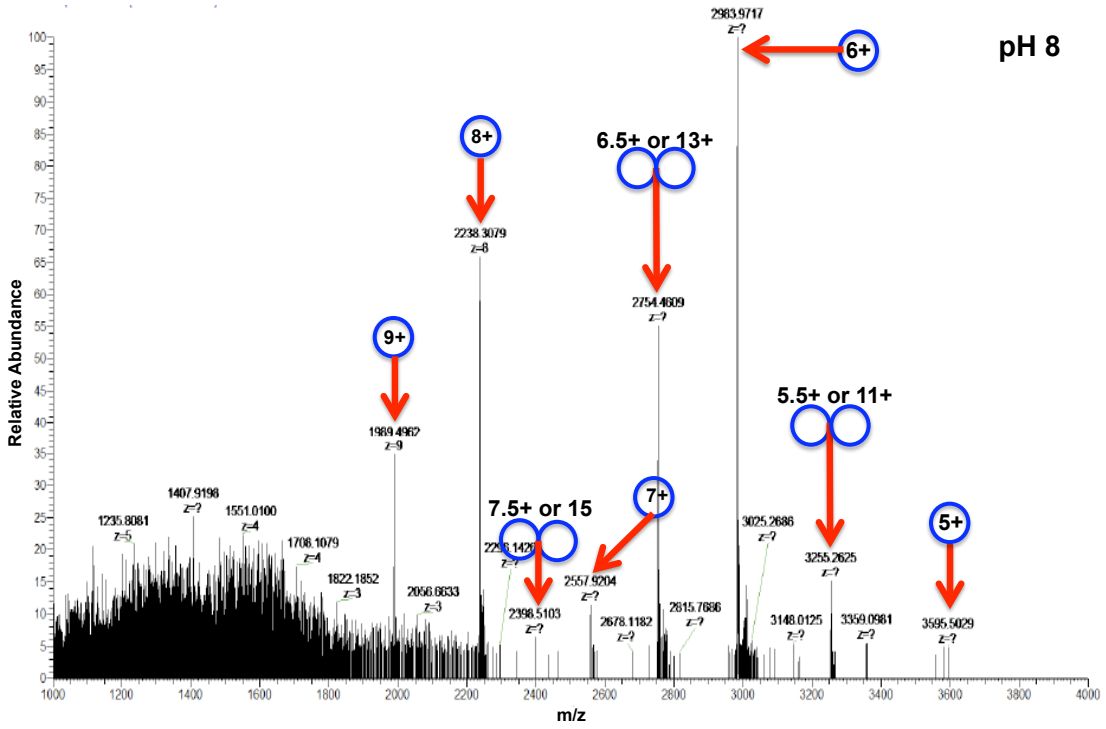

Fig 4.16: ESI-MS spectrum of *Xv*Prx2 acquired at pH 8 under non-denaturing reducing conditions. The mass spectrum show peaks (circled and denoted with arrows) indicating the number of charged ionic states. Single circles indicate peaks that correspond to the monomeric form of the protein while double circles indicate peaks which have been determined to correspond to the 15th, 13th, and 11th ionizatons (2398.5103, 2754.4609, 3255.2625 Da). The 15th, 13th, and 11th resonances can only correspond to (17899/2398.5103 ≈ 7.5+, 17899/2754.4609 ≈ 6.5+, and 17899/3255.2625 ≈ 5.5+. However, since half integral charges are not physically possible, the 15th, 13th and 11th resonances can only correspond to charges on the homodimeric state, giving an m/z value of (2 × 17899)/15 = 2398, (2 × 17899)/13 = 2754, (2 × 17899)/11 = 3255. The presence of dimer peaks as well as monomer peaks suggests that *Xv*Prx2 appears as monomers and dimers at pH 8. We notice a gradual increase in the population and intensity of dimeric peaks as the protein buffer pH increase (pH 6 to 8) suggesting that the protein is more dimeric at pH 8 compared to pH 6.

dissociated during ionisation, despite the soft ionisation conditions, the fraction involved in homodimerisation at pH 8 is likely to be an underestimate. Dimers are also known to ionise less effectively than monomers (Loo, 1997), which would lead to further underestimation of the homodimerisation fraction. On the basis of the above evidence, we conclude that the NMR spectra recorded at pH 5 and pH 8 (Fig 4.4) correspond to the monomeric and homodimeric forms of *Xv*Prx2 respectively. On the basis of the NMR data we conclude furthermore that by pH 8 *Xv*Prx2 is entirely homodimeric, rather than the 30% suggested by MS (Fig 4.13B), which is therefore deemed to be an underestimate.

Since all of the above ESI-MS and NMR spectra were recorded in the presence of 10 mM DTT, we conclude that the homodimers from the high pH conformation are non-covalent, rather than being the result of intermolecular disulphide bonds.

To confirm this conclusion, 1% formic acid was added to denature the protein, as shown in Fig 4.17 (B). The homodimeric peak completely disappeared, indicating that it was entirely dependent on the folded state of the protein, i.e it corresponded to non-covalent homodimers. The effect of omitting DTT from the original spectrum is shown in Fig 4.17 (C). The fraction of homodimers appears to be slightly larger than when DTT is present (A), indicating that in non-reducing conditions most of the protein is in the form of non-convalent homodimers, but a smaller fraction are in the form of covalent dimers. This conclusion is supported by the fact that when the non-reduced protein is denatured (Fig 4.17D) a small fraction of homodimers remain, which therefore correspond to covalent homodimers.

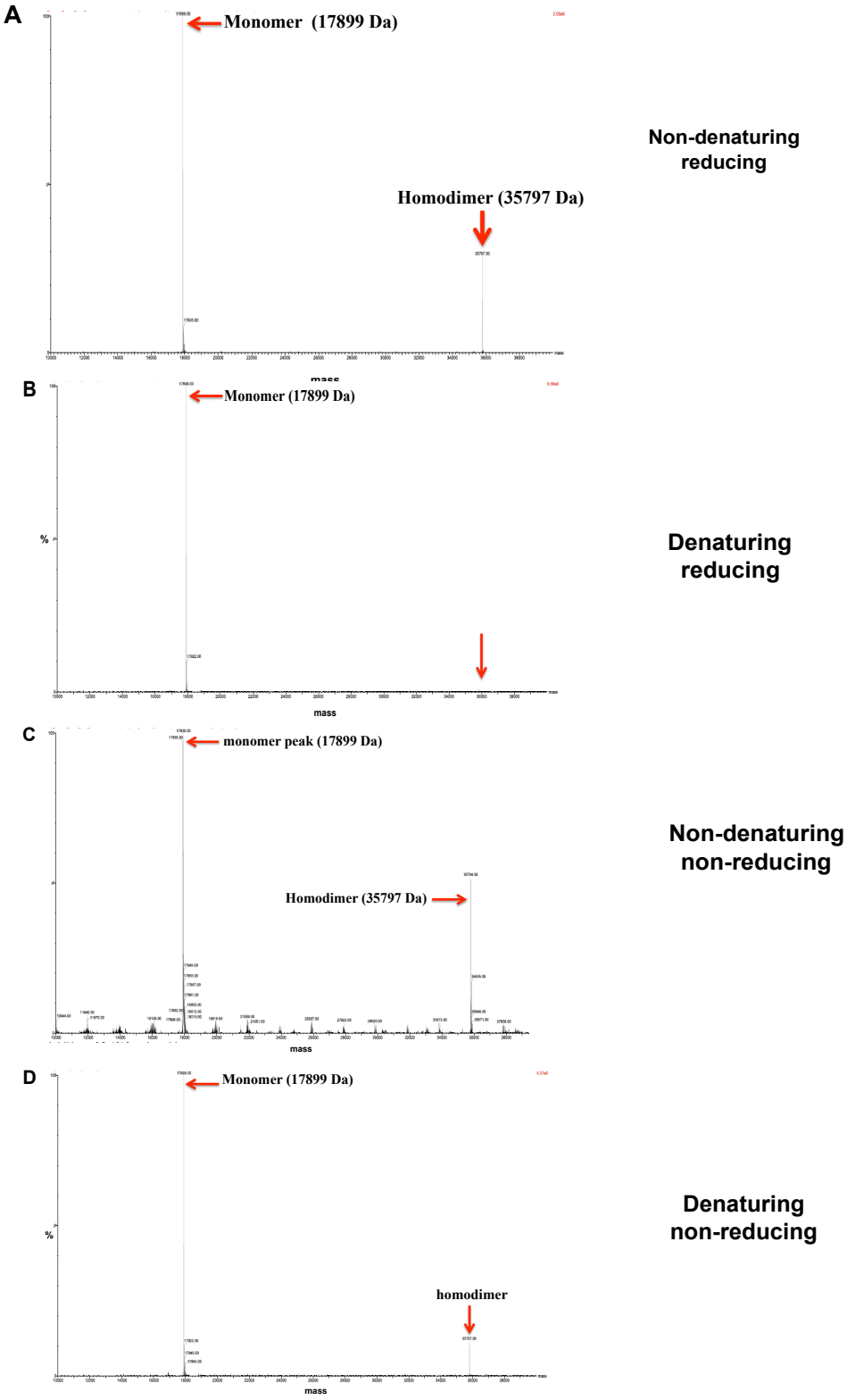

Fig 4.17: Deconvoluted ESI-MS spectrum of *Xv*Prx2 acquired at pH 7 under non-denaturing and denaturing conditions. (A) Under non-denaturing, reducing conditions a significant fraction of the protein is in the form of homodimers, which must be non-covalent due to the present of 10 mM DTT. (B) Confirm this, when the sample used in (A) is denatured the homodimeric fraction disappears, confirming that the homodimers in (A) are indeed non-covalent. (C) When DTT was omitted from the sample used in (A) the fraction of homodimers increases, presumably corresponding to non-covalent plus covalent homodimers (inter-molecular disulphide bridges). (D) Confirming this, when the sample used in (C) is denatured a small fraction of homodimers remain, which must covalent due to the denaturing conditions.

The effect of DTT on the formation of covalent homodimers was further investigated using denaturing SDS-PAGE. Lane 2 of Fig 4.18 shows that when DTT is omitted a significant fraction of *Xv*Prx2 migrates as covalent dimers (upper band at approximately 36 kDa), whereas when DTT is included the upper band disappears completely (lane 3). We conclude that 10 mM DTT is sufficient to suppress all inter-molecular disuphide bonds and therefore that the homodimers detected both by ESI-MS and NMR in the presence of 10 mM DTT are entirely due to non-covalent interactions.

Since all of the above ESI-MS and NMR spectra were recorded in the presence of 10 mM DTT, we conclude that the homodimers from the high pH conformation are non-covalent, rather than being the result of intermolecular disulphide bonds.

4.6 Investigation of the effect of pH on the oligomeric state of *Xv*Prx2 using SEC

NMR and non-denaturing ESI-MS provided evidence that *Xv*Prx2 is monomeric at pH 5, forms a non-covalant homodimer at pH 8 and exits in a mixture of monomer and dimer at pH values in between. The mechanism by which pH changes affected the dimerisation state was, however, still unclear. To address this, *Xv*Prx2 was subjected to analytical size exclusion chromatography (SEC) at a range of different pH values.

SEC provides a convenient method for estimating apparent molecular weight of proteins. The column used was a HiLoad 16/60 Superdex 75 prep grade, which means that protein of molecular weight > ~70 kDa will have access only to the volume excluded by the beads, whereas those with molecular weight < ~70 kDa will have access to spaces within the beads, with the result that they will take longer to transit the column. An approximately linear relationship has been found to hold between the volume at which proteins elute and the logarithm of the molecular weight of the

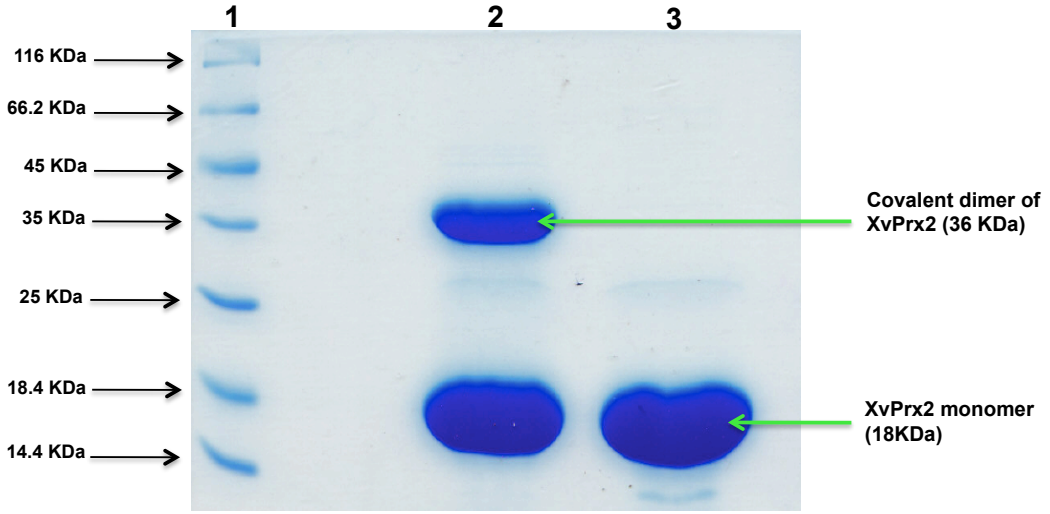

Fig 4.18: SDS-PAGE gel of *Xv*Prx2 under non-reducing and reducing conditions. *Xv*Prx2 at pH 7 is shown in non-reducing conditions (lane 2) and reducing conditions (10 mM DTT) (lane 3). The top band in lane 2 corresponds to covalent homodimers (inter-molecular disulphide bridges). The complete absence of the top band in lane 3 shows that 10 mM DTT is sufficient to suppress all inter-molecular disulphide bridges.

protein. This relationship can be calibrated using standard proteins of known molecular weight, after which the relationship can be used to infer the molecular weight of proteins of unknown molecular weight based on the volume at which they elute. The method is ideal for investigating the apparent molecular weight of proteins involved in oligomerization. In addition, the fact that the pH of the buffer plays no role in the chromatographic separation makes it ideal for the current investigation of pH-dependent oligomerization.

SEC was carried out at range of pH values from 5 to 8, yielding the elution volumes shown in Table 4.1. An overlay of the chromatograms (Fig 4.19) reveals a decrease in elution volume, or equivalently an increase in effective molecular weight, with increasing pH.

Superposition of the chromatograms with those of a number of standards of known molecular weight (see Table 4.2 for details of elution volumes) shows that the apparent molecular weights are greater than 13.7 kDa (RNAse A) but less than 44 kDa (Ovalbumin) (Fig 4.20). A more quantitative analysis of the effective molecular weights is provided in Table 4.3, based on the calibration of the SEC column using the standard proteins, shown in Fig 4.21, as described in Section 2.24. The molecular weights are entirely consistent with the conclusion derived from NMR and ESI-MS that *Xv*Prx2 exists as a monomer at pH 5 and a non-covalent homodimer at pH 8.

The presence of 10 mM DTT in both sample and SEC buffer further guarantees that that homodimer is non-covalent. When the DTT was omitted it had no effect at pH 7, as shown in Fig 4.22, which is consistent with our previous conclusion that at pH 7 the protein is almost completely dimeric, whether covalent or non-covalent cannot be

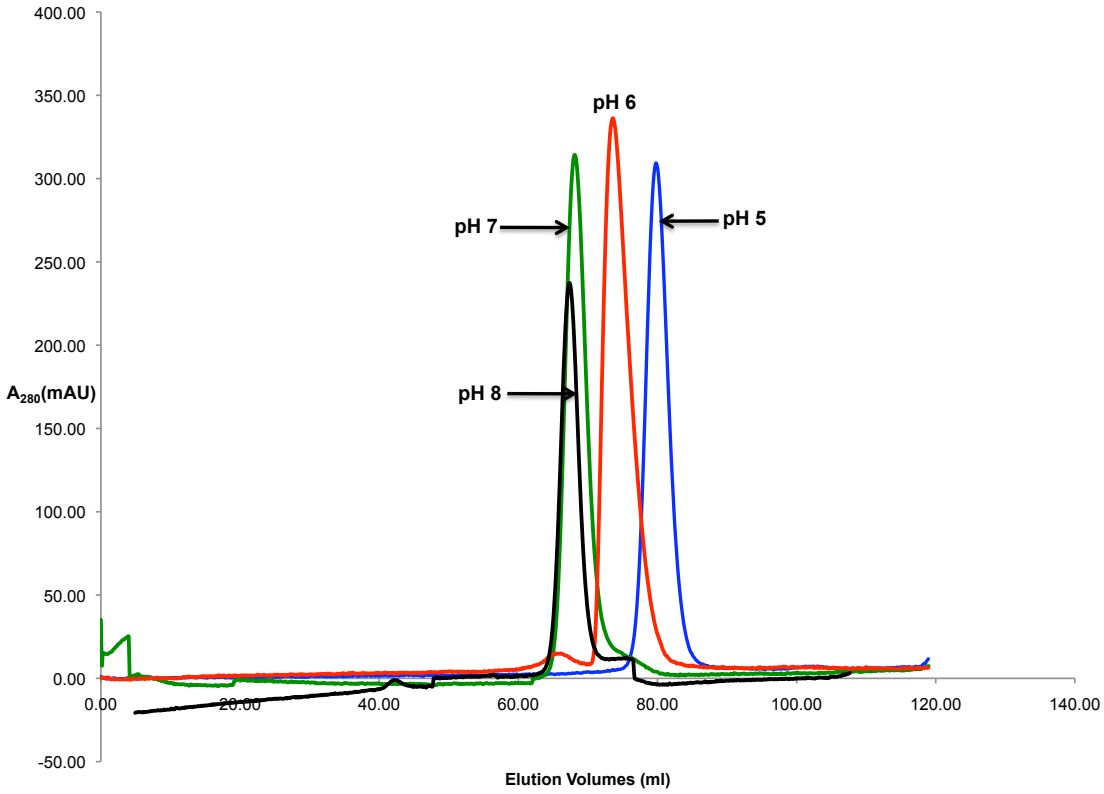

Fig 4.19: Overlay of SEC of *Xv*Prx2 under different pH conditions. The elution times of *Xv*Prx2 at pH 8, 7, 6 and 5 are given in Table 4.1. The overlay reveals that the effective volume of the protein increases with increasing pH. The effective size of the protein as a function of pH is shown in (Table 4.3) based on the elution volumes of protein standards of known molecular (Fig 4.20).

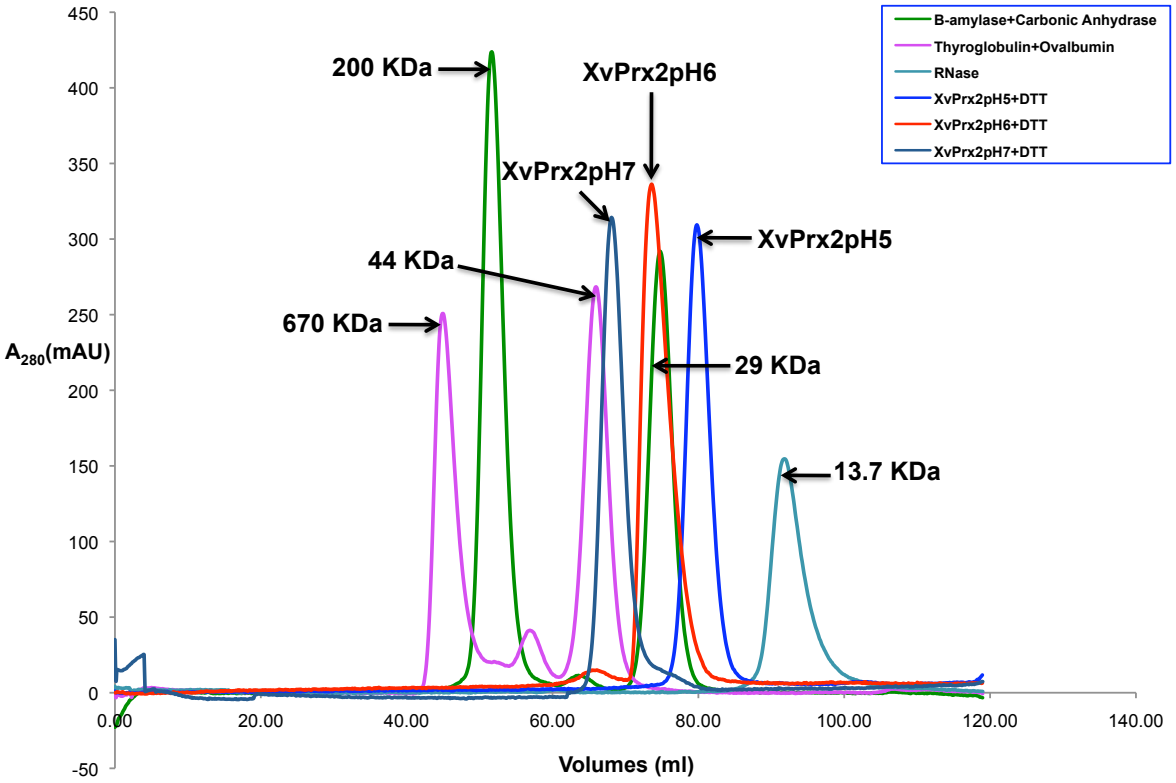

Fig 4.20: Overlay of *Xv*Prx2 SEC under different pH conditions with protein standards. *Xv*Prx2 elutes at volumes between 44 kDa (ovalbumin) and 13.7 kDa (RNase), indicating that it is a mixture of monomer and homodimer. The effective size of the protein at different pH values is shown in Table 4.3, based on the standard curve shown in Fig 4.21.

pH	Elution Volume (ml)
5.0	79.14
5.5	78.26
6.0	73.62
6.5	69.40
7.0	68.10
8.0	67.35

Table 4.1: Elution volume of *Xv*Prx2 at different pHs. *Xv*Prx2 samples were separated under the same condition and buffer environment (50 mM ammonium acetate containing of 10 mM DTT), with a variation of pH (5 - 8). The elution volumn at each pH was used to estimate the effective molecular weight (Table 4.3) based on a calibration curve (Fig 4.21) generated using values presented in Table 4.2.

Protein standards	Elution Volume (ml)	Molecular weight (kDa)
Conalbumin	62.09	75
Bovine Serum Albumin	61.42	67
Ovalbumin	65.97	44
Carbonic Anhydrase	74.73	29
RNAse	91.75	13.7

Table 4.2: Elution volume of protein standards separated through a HiLoad 16/60 Superdex 75 Prep grade column. All standards were separated under the same condition and buffer environment (50 mM ammonium acetate pH 8 in the presence of 10 mM DTT). The elution volume was obtained by noting the values from the point of injection to the centre of the peak.

pH	Elution Volume (ml)	Molecular weight (kDa)
5.0	79.14	24.1
5.5	78.26	25.1
6.0	73.62	30.9
6.5	69.40	37.4
7.0	68.10	39.6
8.0	67.35	41.0

Table 4.3: Effective molecular weight of *Xv*Prx2 at different pH values, based on the standard curve shown in Fig 4.21.

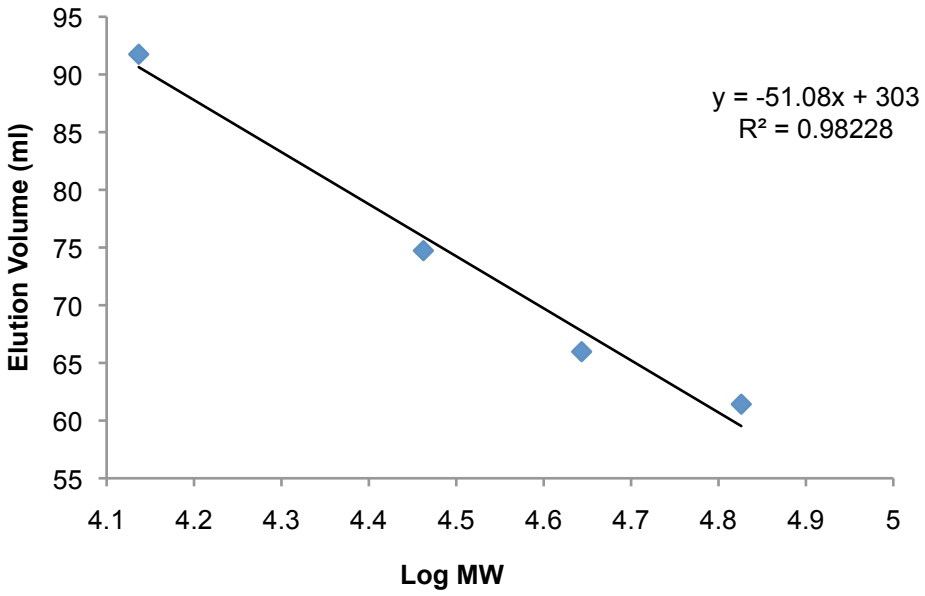

Fig 4.21: SEC standard curve. The SEC standard curve was generated based on the data shown in Table 4.2.

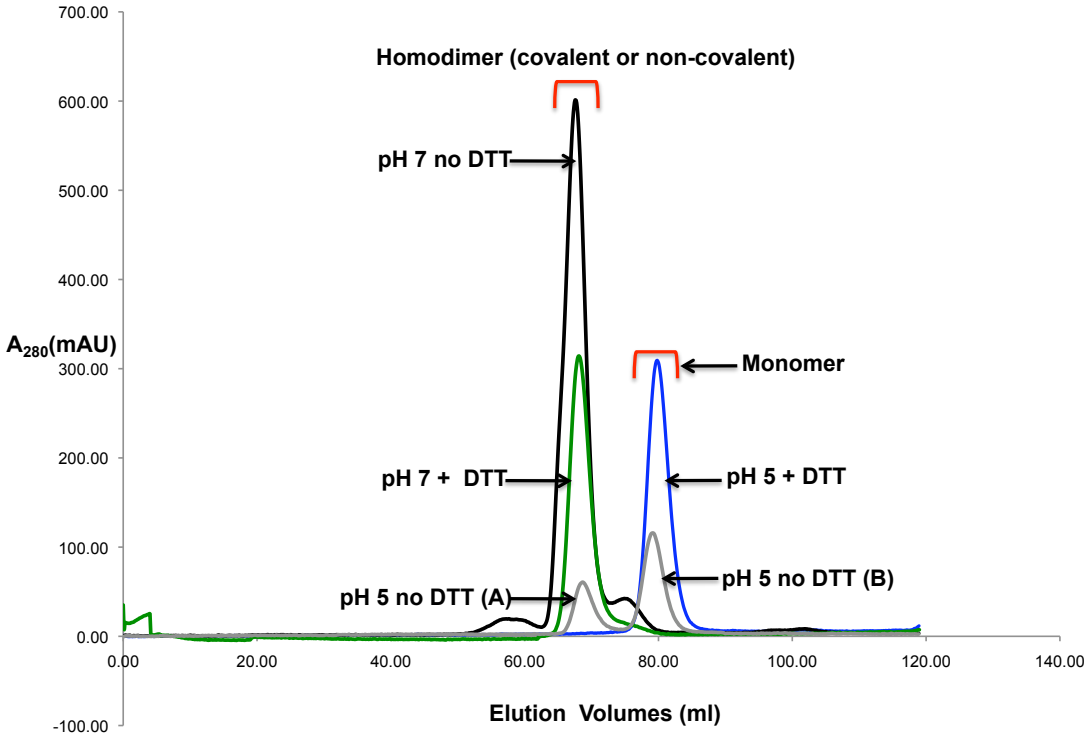

Fig 4.22: Overlay of SEC of *Xv*Prx2 at pH 7 and pH 5 in the presence and absence of DTT. pH and reducing conditions are as indicated. Omission of DTT had a large effect at pH5, with almost half of the sample eluting at the volume expected for homodimers, which must therefore correspond to inter-molecular disulphide bonds. However omission of DTT had little effect at pH 7, where the protein forms non-covalent homodimers under reducing conditions and presumably a mixture of covalent and non-covalent dimers under reducing conditions.

determined by this method. At pH 5, on the other hand, where the protein is known to be completely monomeric, when DTT is omitted a significant fraction of the protein becomes disulphide bonded, producing a second peak at the position expected for the homodimeric state, as shown in Fig 4.22. The fact that the protein elutes at volumes between those expected for the dimer or the monomer can be explained by a model in which the protein flips repeatedly between monomer and dimer during its passage down the column. If we assume that a fraction α are monomeric at any one time ($0 \leq \alpha \leq 1$) then, as shown in Appendix II, the protein will elute at $Ve = Ve^d + \alpha\left(Ve^m - Ve^d\right)$, where Ve^d is the elution volume at which pure dimer elutes and Ve^m the volume at which pure monomer elutes.

If we assume further that the transition between the monomer and dimer corresponds to the ionisation or protonation of a single group in the interface, with dimerisation only being possible when the group is ionized then, as is also shown in Appendix II, the Henderson-Hasselbalch equation gives the following expression for the elution volume in terms of the pH and the pK_a of the ionisable group:

$$Ve = Ve^d + \frac{Ve^m - Ve^d}{1 + 10^{pH - pKa}}$$

Fitting this expression to a graph of Ve as a function of pH (Fig 4.23) allows extraction of values for the pK_a, as well as for Ve^d and Ve^m. The fit is in excellent agreement with the data and yields a value for the pK_a of 6.0 ± 0.1. This value suggests that at pH 5.0 the protein is only 90% monomeric $\left(\alpha = \frac{1}{1 + 10^{5-6}} = 0.9\right)$, whereas at pH 8.0 it is 99% homodimeric. If the values of Ve^m = 81.1 and Ve^d = 66. 9 ml are used to calculate the

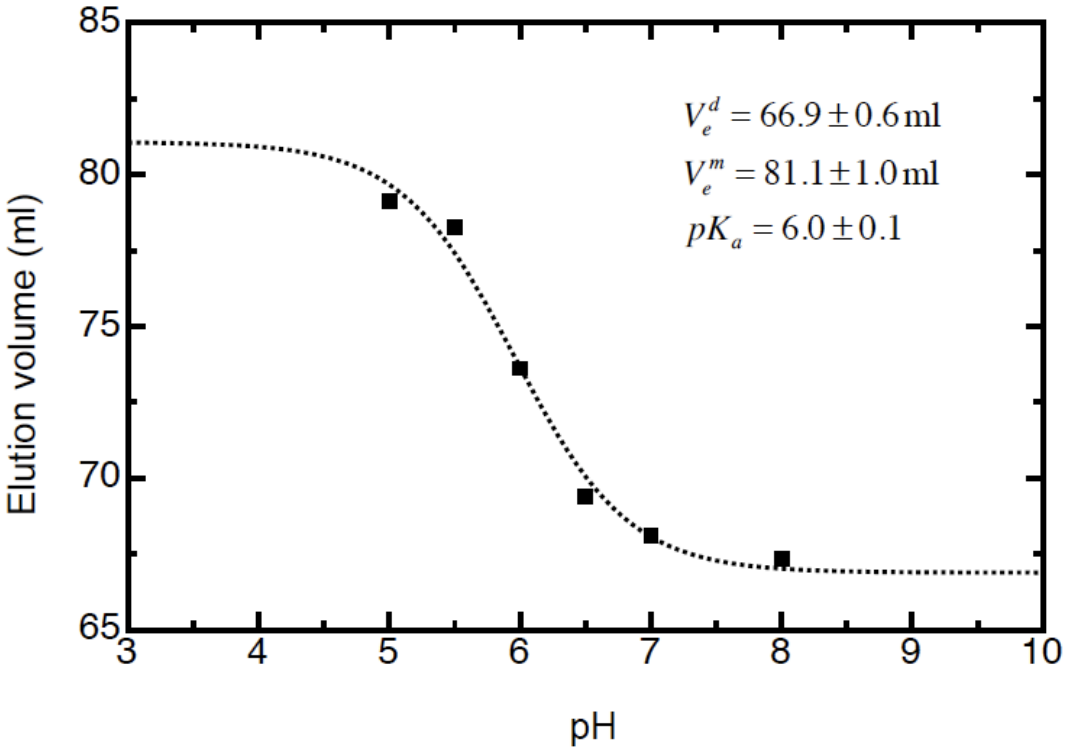

Fig 4.23: *Ve* (elution volume) plotted as a function of pH. The filled squares correspond to the values given in Table 4.1 and the dotted line to the theoretical expression given in the text. The fit allowed for the extraction of pK_a, Ve^d and Ve^m. *Xv*Prx2 has a pK_a of 6, which is consistent with the pK_a extracted from a number of Prxs (ranging from 5.4 to 6.0) (Nelson, *et al.*, 2008; Ogusucu, *et al.*, 2007).

effective molecular weights of the monomer and dimer using the standard curve shown in Fig 4.21, the corresponding values are 22.1 kDa for the monomer and 41.8 kDa for the dimer. These are in satisfactory agreement with the expected values of 18 kDa and 36 kDa respectively.

Chapter 5: Investigation of the role of Cys51 and His55 in the monomer to dimer pH-dependent shift and the effect of oxidation and glutathionylation on the stability of the non-covalent homodimer

In the previous chapter it was shown that *Xv*Prx2 forms a non-covalent homodimer above pH 6, and monomeric below. The fact that Prx5 subfamily ("D-type") peroxiredoxins form non-covalent homodimers has been previously reported for *Pf*AOP from *Plasmodium falciparum* (Sarma*, et al.*, 2005) and *Pt*PrxD from *Populus tremula* (Echalier*, et al.*, 2005), which is highly homologous to *Xv*Prx2 (see Fig 5.1 for an alignment). That study was carried out at pH 7 and no attempt was made to investigate the effect of pH on the stability of the homodimer. However attachment of a glutathione group to the catalytic cysteine of *Pt*PrxD was shown to lead to dissolution of the non-covalent homodimer, an effect that Noguera-Mazon and co-workers suggested may play a role in the catalytic mechanism of the enzyme (Noguera-Mazon*, et al.*, 2006b).

The *Pt*PrxD homodimer forms across an A-type ("perpendicular") interface, with helix α_2 well structured and packing against the central β-sheet. Since the N-terminal end of the helix forms part of the dimersation interface it has been suggested that unfolding of the α_2-helix would not be compatible with formation of the homodimer (Noguera-Mazon*, et al.*, 2006b). The helix is stabilized by a network of hydrogen bonds donated by Arg129 and accepted by the thiolate group of Cys51 and the side chain nitrogen of His55 (see Fig 1.2B). Both Cys51 and His55 are located near the N-terminal end of helix α_2, facing in towards Arg129, which lies between the central β-sheet and the α_2-helix. His55 is replaced in some other members of the Prx5 family by glutamine and glutamic acid, both of which are able to accept hydrogen bonds. In *Pf*AOP from *Plasmodium falciparum* this position is occupied by a methionine which is able to

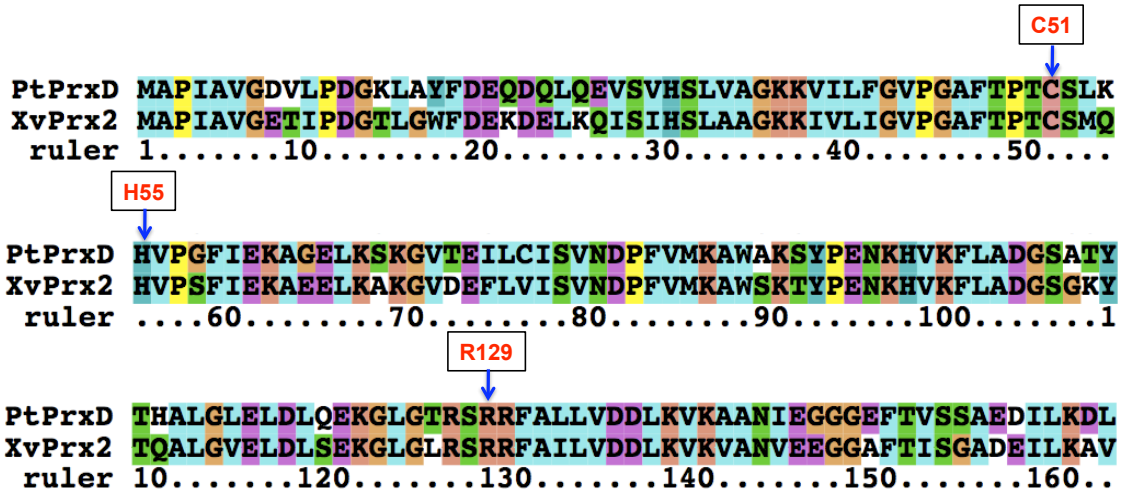

Fig 5.1: Sequence alignment of *P. tremula* Prx (*Pt*PrxD, PDB entry 1TP9) and *X. viscosa* Prx (*Xv*Prx2). The alignment was generated using MUSCLE (Edgar, 2004) and shows a high conservation of residues between *Pt*PrxD and *Xv*Prx2. Cys51 (catalytic cysteine), His55 and Arg129, which are involved in hydrogen bonding interaction (Fig 5.2) have all been boxed (black) and highlighted (red).

accept hydrogen bonds, although it rarely does so (Gregoret, L. M., Rader, S. D., Fletterick, R. J. & Cohen, F. E. (1991). In the monomeric form, in contrast, helix α_2 was found to be unstructured, presumably swinging out, away from the core of the protein. Abolition of the dimer by glutathionylation was accompanied by unfolding of the α_2-helix, supporting the assertion that the dimer can only form when the α_2-helix is structured.

Cys51 and His55 are also present in *Xv*Prx2, as can be seen from the alignment in Fig 5.1. Since they are both ionisable they were the obvious places to begin looking for the cause of the pH-dependent effects reported in the previous chapter. The pK_a of the imidazole group of histidine is very close to the value of 6.0 extracted from SEC data in Fig 4.23, and although the pK_a of the side chain thiol group of cysteine in solution is approximately 8.3 (Klomsiri*, et al.*, 2010), in folded Prxs it has been reported to be lowered to around 6 in a number of cases (Nelson*, et al.*, 2008; Ogusucu*, et al.*, 2007).

In order to define the structural context for our investigation of the pH-dependent dimerisation of *Xv*Prx2, we began by generating a model of the molecular structure using the close homologue from *P. tremula*. The 3D Jury server was used to generate a multiple alignment from which the sequence from *P.tremula* was selected for homology modeling using MODELLER (Sali and Blundell 1993). A cartoon representation of the model is shown in Fig 5.2A while an overlay of the model with the *Pt*PrxD structure is shown in Fig 5.2B.

Consistent with the *Pt*PrxD structure, the model of *Xv*Prx2 predicts that Arg129 is at the centre of a network of hydrogen bonds. As shown in Fig 5.3B the side-chain $N^{\eta 1}$

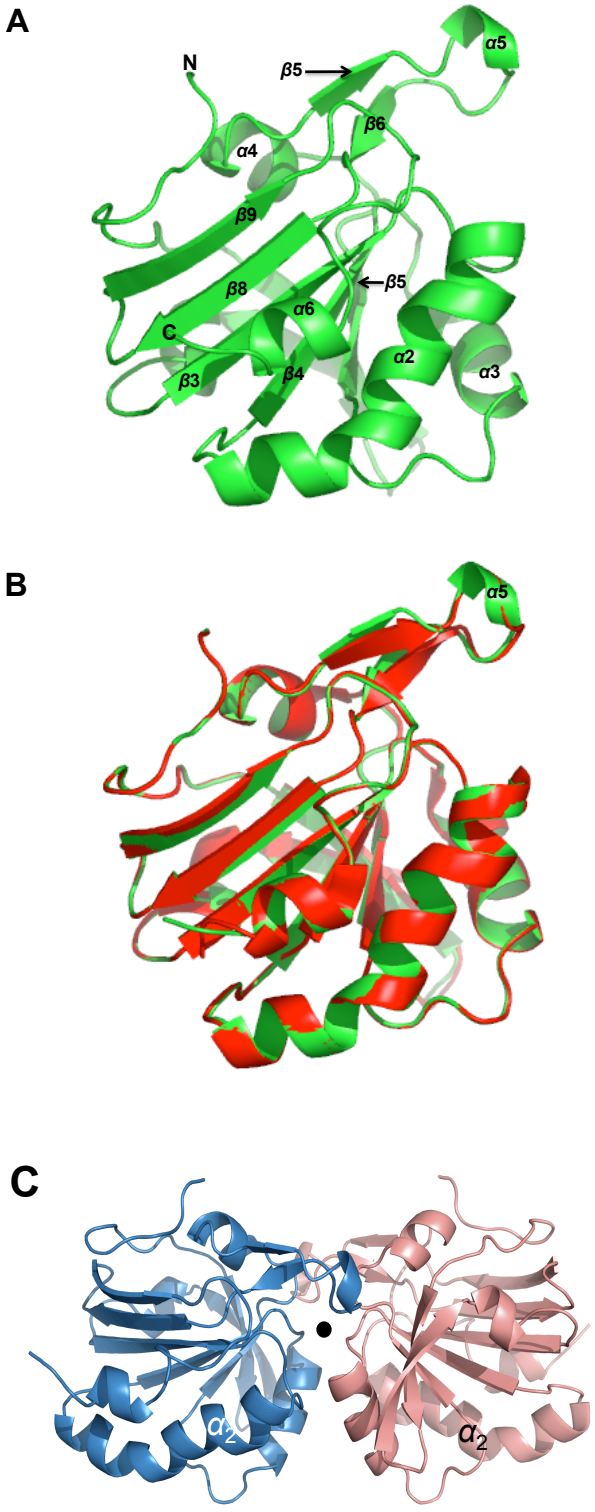

Fig 5.2: Cartoon representation of *Xv*Prx2. (A) Structural model of *Xv*Prx2 built using the close homologue PrxD from *Populus tremula* (PDB entry 1TP9). (B) The overlay of *Xv*Prx2 (green) and *Pt*PrxD (pink) reveals the high structural similarity (RSMD 0.266). Molecular fitting was performed using the DaliLite server (Holm & Park, 2000). (C) Cartoon representation of the *Xv*Prx2 homodimer, modeled on the structure of *Pf*AOP from *Plasmodium falciparum*. The figure has been visualized using the PYMOL Molecular Graphics System (2003) Delano Scientific, San Carlos, CA, USA.

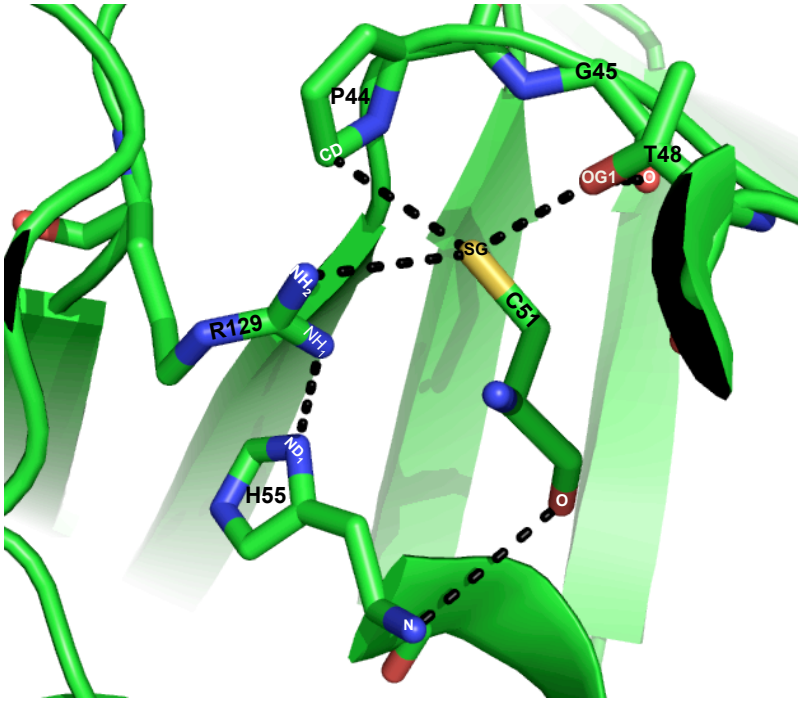

Fig 5.3: Hydrogen bonding interactions stabilising the α_2-helix in *Xv*Prx2. Expanded view of the active site of *Xv*Prx2 showing the hydrogen bonding network between R129, C51 and H55 which stabilize the α_2-helix and, by extension, the homodimeric state. The model was generated based on the structure of PrxD from *P. tremula* (PDB entry 1TP9) and the figure was visualized using the PYMOL Molecular Graphics System (2003) Delano Scientific, San Carlos, CA, USA.

and $N^{\eta 2}$ are predicted to donate hydrogen bonds to the side chain $N^{\delta 1}$ of His55 and the thiolate of Cys51 respectively.

Since His55 $N^{\delta 1}$ can only accept hydrogen bonds when it is ionized, which is the case when pH values are above its pK_a, our data suggests that the Arg129 - His55 hydrogen bond plays a dominant role in stabilising the α_2-helix at pH > 6. To test this model we mutated His55 to alanine and repeated the SEC analysis. The results are shown in Fig 5.4 and the elution volumes are tabulated as a function of pH in Table 5.1. As compared to the wild-type (solid curve, Fig 5.4), the elevated elution volumes in the pH region 6 - 9 show that the H55A mutant remains a monomer at higher pH values than the wild type. This confirms our model that the hydrogen bond between between Arg129 and His55 plays the major role in stabilising the α_2-helix and allowing the homodimer to form.

A surprising feature of Fig 5.4 is that at sufficiently high pH the H55A mutant again forms dimers. Since the major increase in dimerisation occurs between pH 8 and 9, in the vicinity of the cysteine thiol group, suspicion fell on Cys51, which our structural model predicts accepts a hydrogen bond from Arg129 $N^{\eta 2}$. Since the thiol group can only accept a hydrogen bond at pH values above its pK_a, this mechanism is likely to lead to stabilization of the homodimer above pH 8.3, which is consistent with what is observed.

However the H55A data in Fig 5.4 suggests that a greater fraction of homodimer is present in the pH range 6 - 8 than would be expected for a single ionisation with the pK_a of 8.3. The data lacks the sigmoidal shape seen in the wild-type data (solid line)

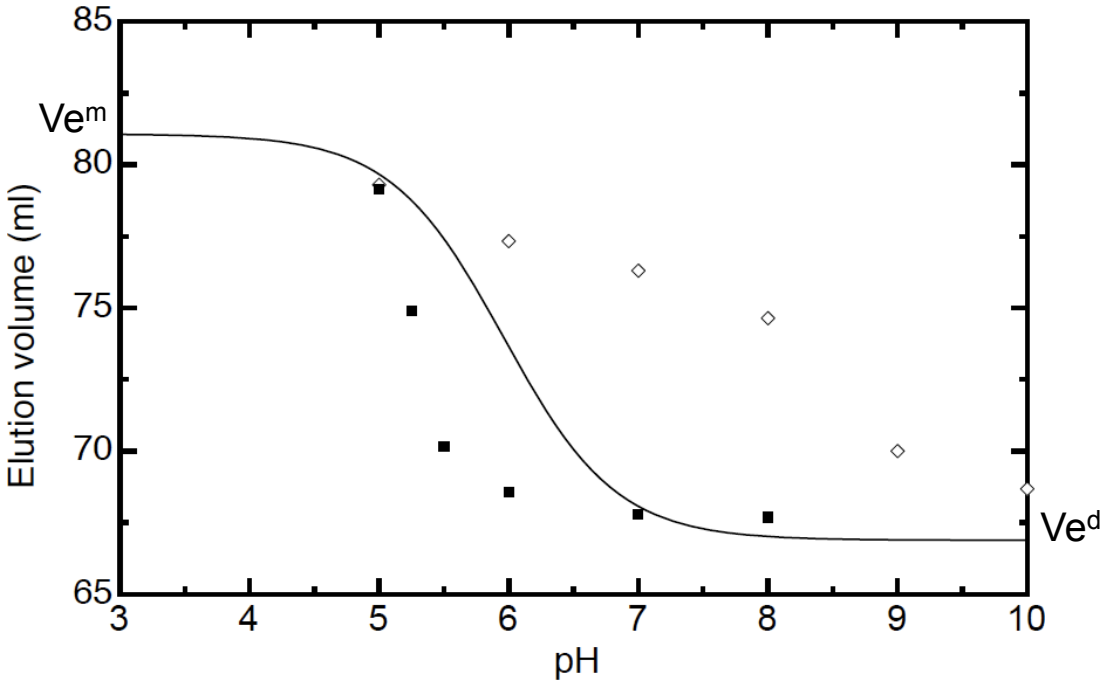

Fig 5.4: The effect of mutations H55A (open diamonds) and C51S (filled squares) on the pH-dependent transition from monomer to homodimer. The solid line represents the wild-type behaviour, which is shown for purposes of comparison. The H55A mutation is monomeric at higher pH values than the wild type, suggesting that the hydrogen bond between R129 and H55 plays an important role in stabilising the homodimeric state. Surprisingly the homodimeric state is still present at high pH values. Replacing C51 with a serine stabilizes the homodimer at lower H values than the wild type, an effect which is difficult to explain.

pH (H55A)	Elution Volume (ml)
5.0	79.30
6.0	77.33
7.0	76.30
8.0	74.64
9.0	70.00
10.0	68.68

Table 5.1: SEC elution volumes for *Xv*Prx2-H55A at various pH values. All other parameters were the same as for to the wild type protein.

pH (C51S)	Elution Volume (ml)
5.00	79.14
5.25	74.90
5.50	70.15
6.00	68.55
7.00	67.80
8.00	67.69

Table 5.2: SEC elution volumes for *Xv*Prx2-C51S at various pH values. All other parameters were the same as for to the wild type protein.

which may indicate a more complex mechanism than that assumed in Appendix II. However our NMR data (see later, Section 5.1, Fig 5.5) suggests that at pH 7 the H55A mutant is still almost entirely monomeric, and therefore we suspect that the SEC data over-estimates the amount of homodimer present.

To test our model that Cys51 plays a role in the stabilizing the homodimer at high pH we replaced it with serine. Although similar in size and chemical characteristics to cysteine, serine has a higher solution pK_a of 9.15. We therefore expected the replacement of cysteine by serine to have no effect on the stability of the homodimer at low pH. To our surprise it had the opposite effect, reducing the apparent pK_a from 6.0 to 5.3 (Fig 5.4, solid black squares).

The SEC results reported above are consistent with results generated using NMR. The 1D proton spectrum of H55A at pH 7 is shown in Fig 5.5A: the absence of the signature peaks at -0.5 ppm and 11.1 ppm shows that H55A is almost completely monomeric (compare with Fig 4.3(A)). However both peaks are present in the 1D spectrum of C51S (Fig 5.5(B)), confirming that it is homodimeric at pH 7.

Chemical shifts of -0.5 ppm represent large deviations from random coil values, and typically result from packing of the corresponding nucleus against an aromatic ring. The magnetic shielding produced by rings is known as “ring current effects” and is largest along the axis of the ring (the line through the centre of the ring and perpendicular to the plane of the ring). Analysis of the modelled structure shows that Ile 41 lies in the space between the central β-sheet and helix α_2, where it packs directly against the sidechain ring of Phe 59, as shown in Fig 5.6. Phe 59 lies on helix α_2, one

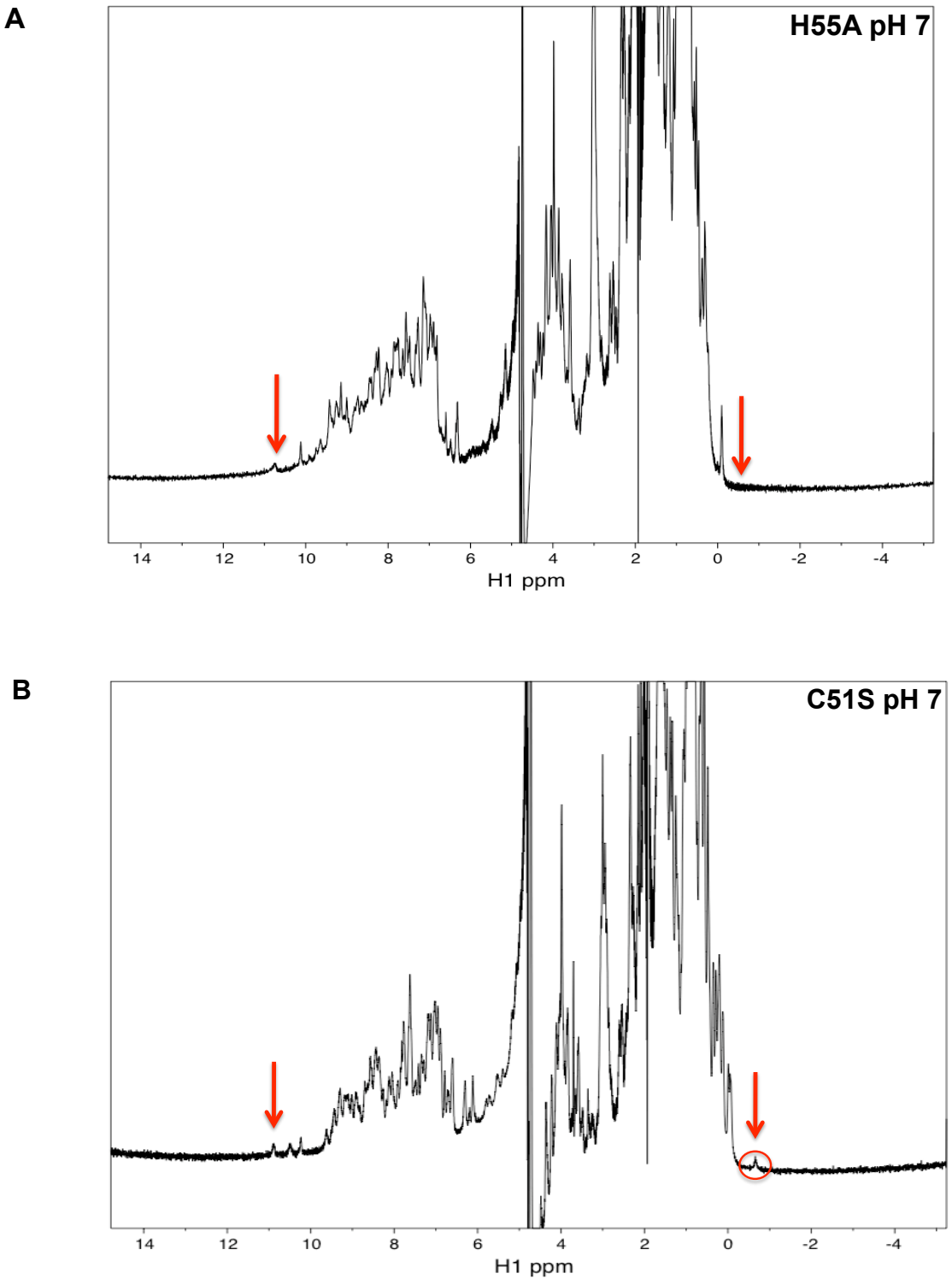

Fig 5.5: 1D proton spectra of *Xv*Prx2-H55A and *Xv*Prx2-C51S recorded at pH 7.0, 25 °C and 600 MHz. Red arrows indicate resonances which are expected in the homodimeric form, but not in the monomeric form. The spectra show that *Xv*Prx2-H55A is almost completely monomeric at pH 7 (A) whereas *Xv*Prx2-C51S is predominantly homodimeric (B), consistent with the SEC data shown in Fig 5.4.

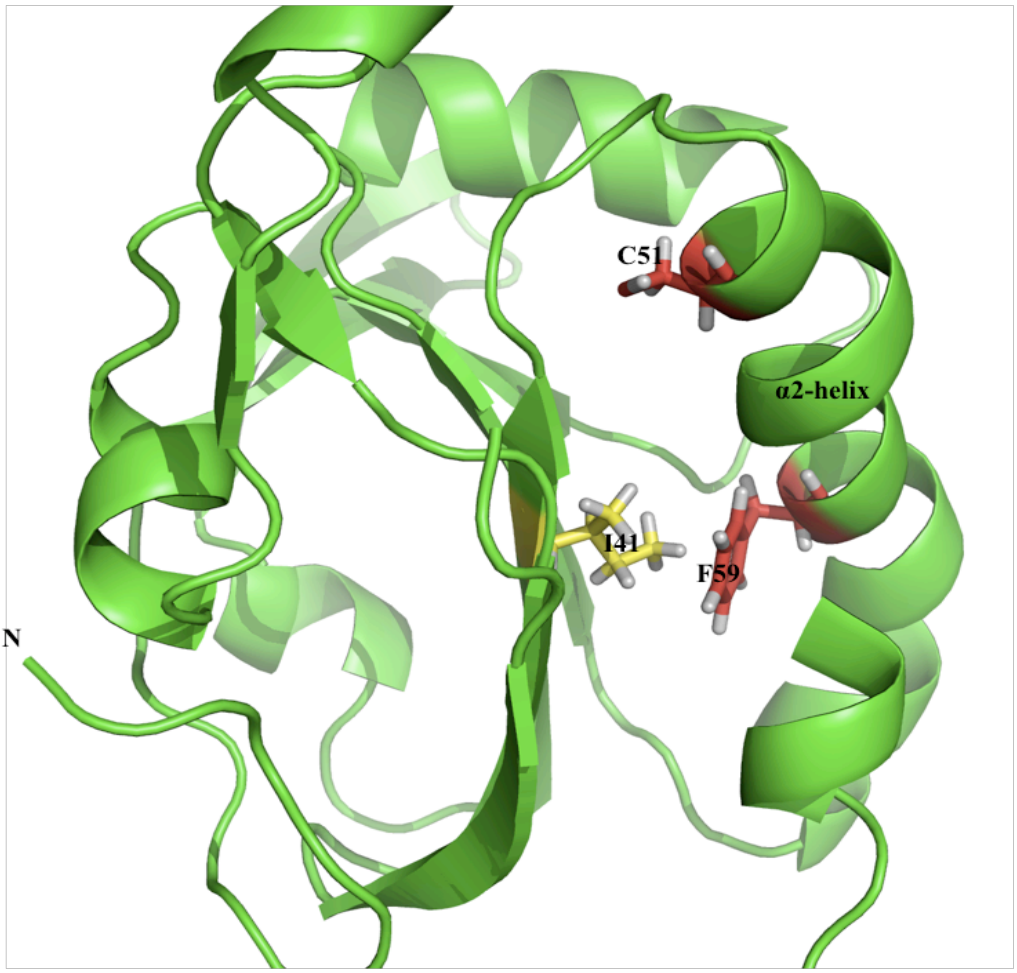

Fig 5.6: Ile41 packs directly against the ring of Phe 59, which explains the downfield shift of the $H^{\gamma 11}$ proton of Ile41 to -0.52 ppm when the α_2-helix is structured. The model was generated based on structure of *Populus tremula* Prx (PDB entry 1TP9) and the figure has been visualized using the PYMOL Molecular Graphics System (2003) Delano Scientific, San Carlos, CA, USA.

turn away from His55, and therefore is only expected to influence Ile 41 $H^{\gamma 12}$ when helix α_2 is structured. The 1D NMR spectrum therefore provides strong evidence that helix α_2 is structured when the protein is homodimeric, but unstructured when monomeric.

Additional evidence that H55A is monomeric at higher pH values than the wt is provided by ^{15}N-HSQC spectra. The overlay of H55A and wt in Fig 5.7 (A) at pH 7 confirms that H55A has contributions from the monomeric spectrum not seen in the wt at this pH. As expected the H55A spectrum at pH 7 overlays very well with the wt spectrum at pH 5 (Fig 5.7B), which has been shown to be almost entirely monomeric.

Fig 5.8 shows a comparison of ^{15}N-HSQC spectra of H55A at pH 7, 8 and 9. As the pH increases peaks associated with the monomer are increasingly replaced by peaks associated with the homodimer, as shown most clearly in the boxed resonances, which correspond to the backbone amide of Leu40. At pH 8 there are almost equal amounts of monomer and homodimer from which we can conclude that the pK_a of the H55A is in the vicinity of pH 8, which is in general agreement with the results shown in Fig 5.4. Expanded views of the boxed regions in Fig 5.8 are presented in Fig 5.9A and the volumes extracted from the peaks used to determine the monomeric fraction, which is plotted in Fig 5.9B. The solid curve corresponds to fitting on the expression shown in Appendix II. The monomer-homodimer transition is approximately at pH 8. Fig 5.9B is consistent with Fig 5.5A in suggesting that at pH 7 there is very little of the dimer present and that Fig 5.4 over-estimates the amount of homodimer present for H55A.

Our data shows that by replacing H55 by an alanine we have raised the maximium pH

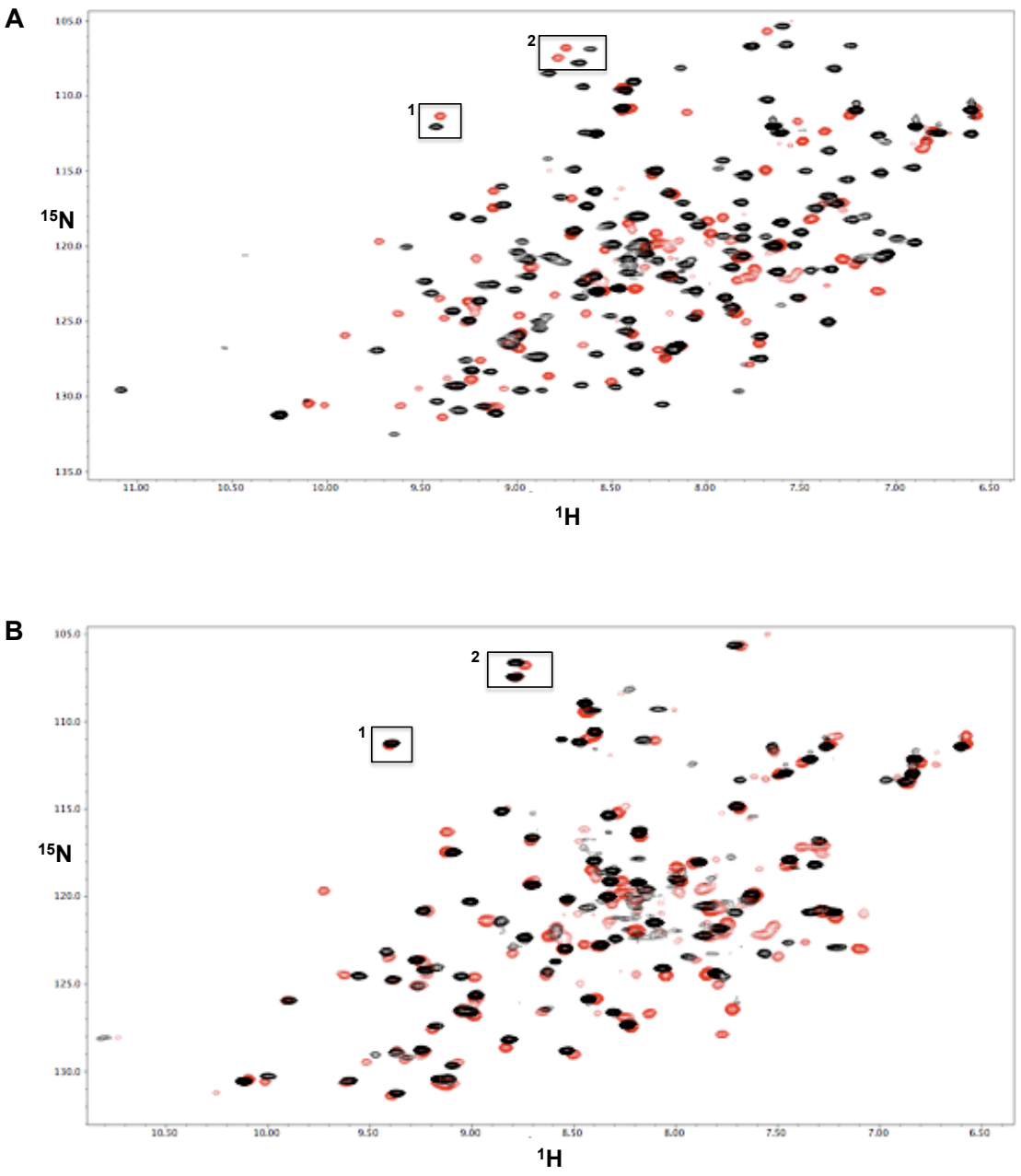

Fig 5.7: Overlay of ^{15}N-HSQC spectra of *Xv*Prx2 and *Xv*Prx2-H55A recorded at pH 7, 25 °C and 600 MHz. The spectrum of *Xv*Prx2-H55A pH 7 (red) is manifestly different to that of the wild type at pH7 (black) (A), which is homodimeric, but much more similar to that of the wild-type at pH5 whci is monomeric.

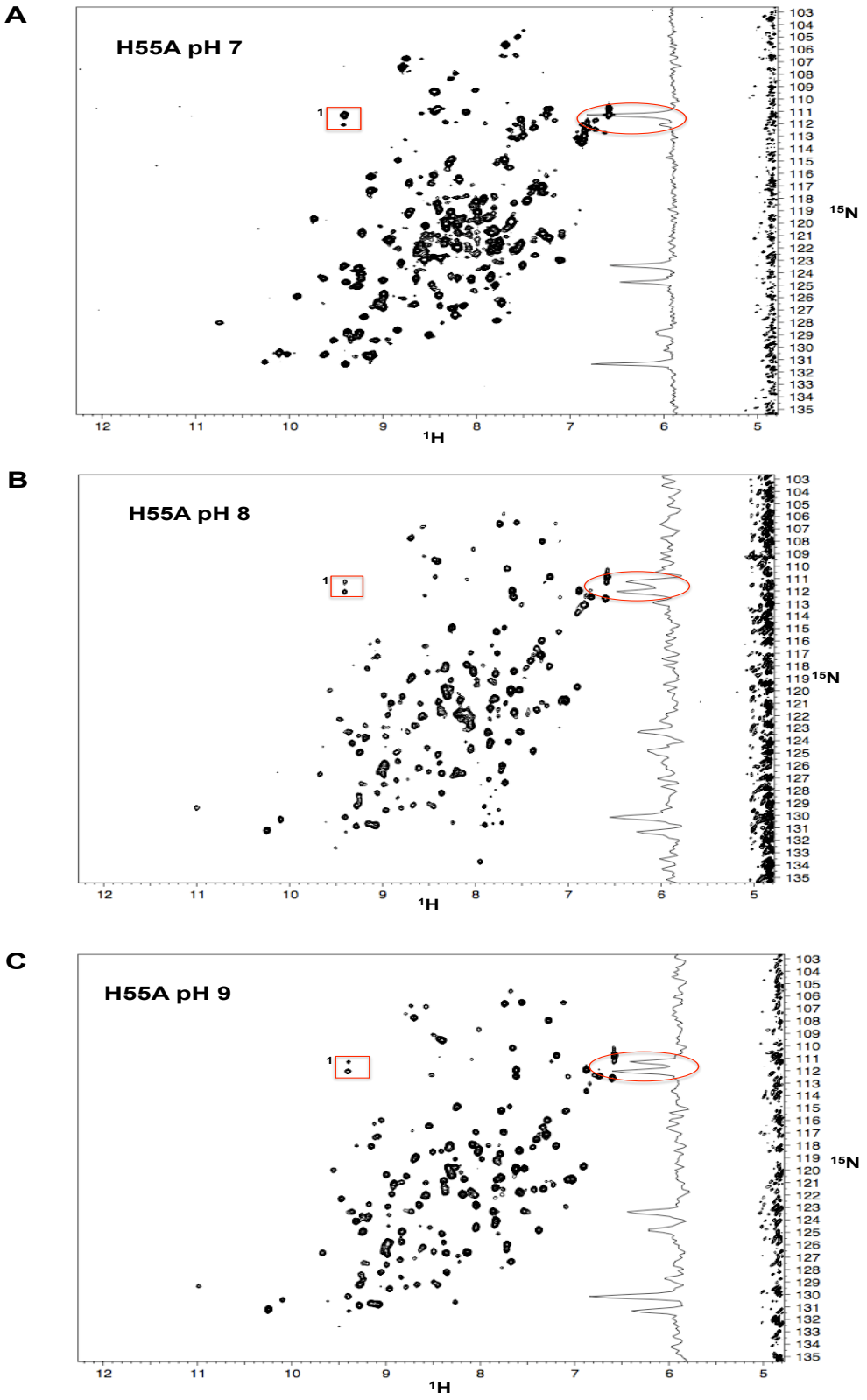

Fig 5.8: ^{15}N-HSQC spectra of *Xv*Prx2-H55A recorded at pH 7, 8 and 9, at 25 °C and 600 MHz. The boxed region shows two resonances associated with either the monomeric (top resonance) or dimeric (bottom resonance) configurations. Vertical cross sections (circled) through these resonances are shown at right. Increasing the pH from 7 to 9 results in an increase in the height of the bottom resonance and a corresponding decrease in the height of the top resonance, indicating a change from monomer to homodimer.

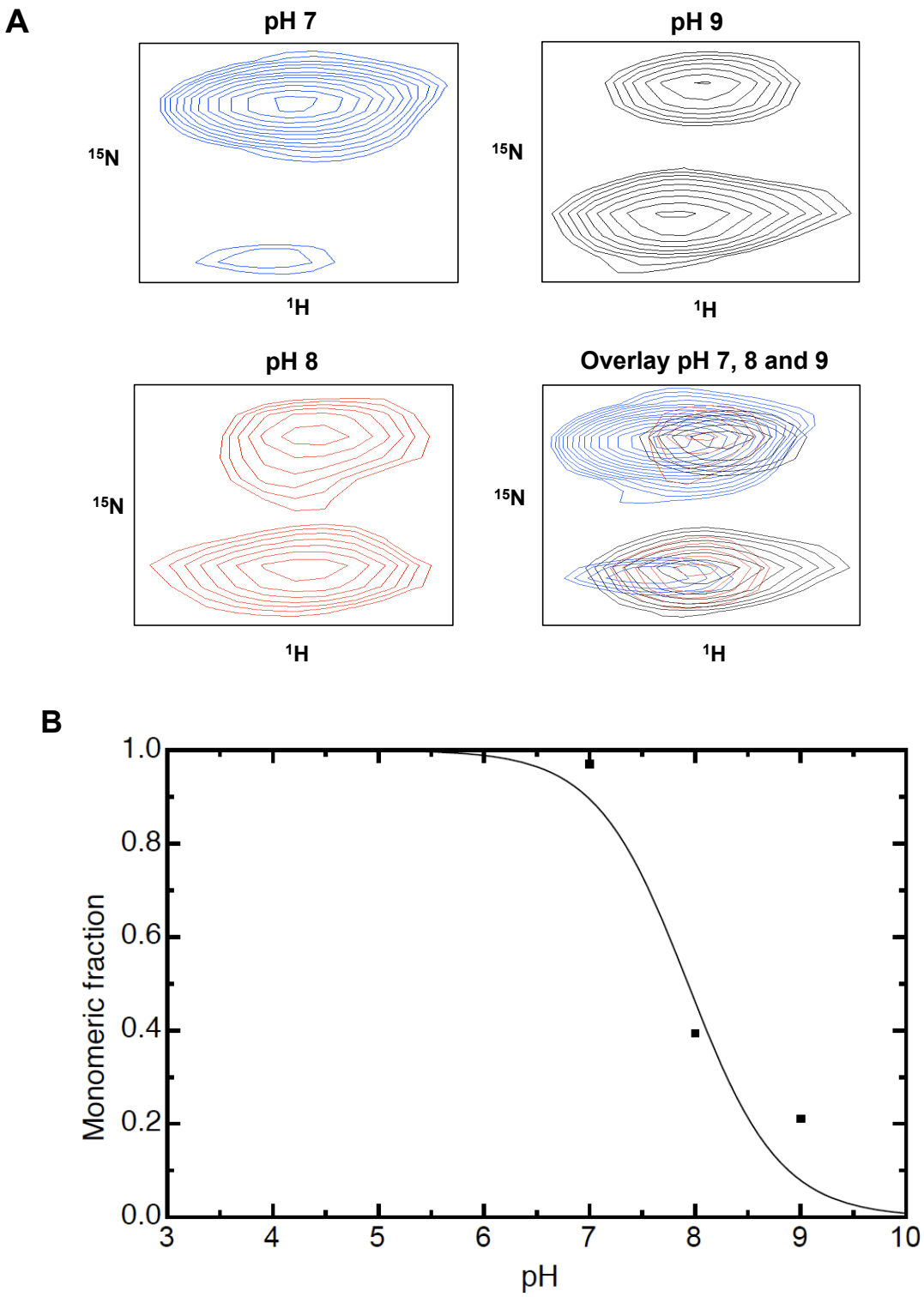

Fig 5.9: Expanded view of *Xv*Prx2-H55A mutant Leu40 resonance at pH 7, 8 and 9. (A) Increasing the pH from 7 to 9 results in an increase in the height of the bottom resonance and a corresponding decrease in the height of the top resonance, indicating a change from monomer to homodimer. (B) The monomeric fraction of the protein was calculated using the volumes of the peaks shown in (A) and the solid line represents a fit of the expression in Appendix II, giving an effective pK_a of 7.9. The data shows that *Xv*Prx2-H55A is almost entirely monomeric at pH 7 (97 %) while a mixture of monomers and dimers is observed at pH 8 (40 % monomeric) and pH 9 (20 % monomeric).

at which *Xv*Prx2 is monomeric from 5 to 7. Since wild type *Xv*Prx2 was found to be too unstable at pH 5 for NMR structural analysis, this opens the possibility that H55A will be sufficiently stable at pH 6 or 7 for structure determination. Preliminary data suggests that it is more stable at these pHs than the wild type at pH 5.

5.2 Oxidation of *Xv*Prx2

Peroxiredoxins protect proteins and other cellular components from oxidative damage induced by reactive oxygen (ROS) and nitrogen species. Their activity results in the reduction of hydroxyl radicals or peroxide substrates to water, alcohol and other break down products. The detailed overview of the catalytic cycle of Prxs has been presented in Section 1.2 (Fig 1.1). Briefly, it involves a nucleophillic attack of hydroxyl radicals or peroxides or other substrates using the catalytic cysteine residue (C_P) resulting in the oxidation of the sulfhydryl side chain ($-S_PH$) group to sulphenic ($-S_POH$) acid groups, which may be oxidised further to sulphinic ($-S_PO_2H$) and sulphonic ($-S_PO_3H$) states. The sulphinic and sulphonic acid forms have been reported to be resistant to reduction and therefore inactive, although reports by Biteau and co-workers suggest that S_PO_2H can be reduced by the thiol-containing protein sulphiredoxin (Biteau*, et al.*, 2003).

Some reports have suggested a link between the state of oxidation of the catalytic cysteine and the oligomeric state of Prxs. For example, Wood and co-workers showed that the Prx1 subfamily occurs as a decamer in reduced and overly-oxidised states but as a disulphide-bonded dimer in the oxidised state. The decamer associated with the overly-oxidised form is poorly recycled by electron donors like thioredoxins while the disulphide-bonded dimeric form displays low peroxidase activity (Wood*, et al.*, 2002). The effect of oxidation of the catalytic cysteine on two members of the Prx5 subfamily, the human Prx5 and *Saccharomyces cerevisiae* alkylhydroperoxide reductase (Ahp1),

has been reported. Both proteins contain two cysteine residues that form intra- and or intermolecular disulphide bond during their catalytic cycle and occur as dimers under reducing and oxidised (human Prx5) or overly oxidised (Ahp1) states (Evrard*, et al.*, 2004; Lian*, et al.*, 2012; Trivelli*, et al.*, 2003a). Some changes to the structures of the oxidised forms consistent with the unfolding of the N-terminus of the α_2-helix have been reported although the overall oligomeric state of both proteins remained unchanged following oxidation.

There are no reports of the effect of oxidation on the oligomeric state of 1-Cys Prx5 subfamily proteins. This section will focus on the effect of oxidation on the oligomeric state of *Xv*Prx2.

5.2.1 The effect of oxidation on the oligomeric state of *Xv*Prx2

In order to investigate the effect of H_2O_2 on *Xv*Prx2 we incubated it with various concentrations of H_2O_2, followed by denaturing mass spectrometry. The "raw" MS spectrum of the oxidised sample shown in Fig 5.10A shows that the protein has acquired an additional 32 Da, consistent with the sulphinic acid form of the protein (*Xv*Prx2-SO_2H). For example, the 8^{th} ionisation has m/z = 2242.3333, which corresponds to m = 2242.3333 x 8 - 8 = 17930.66 while the 9^{th} ionisation has m/z = 1993.2963 corresponding to m = 1993.2963 x 9 - 9 = 17930.66. This can be compared with the spectrum recorded in the absence of H_2O_2 (Fig 5.10B) in which m/z = 2238.18 and 1989.69 for the 8^{th} and 9^{th} ionization states, corresponding to m = 17897 and 17898 respectively. As expected the deconvoluted spectrum for the H_2O_2-exposed sample (Fig 5.10C) displays a major peak at 17930.6 Da, corresponding to the sulphinic acid form, and a smaller peak at 17898.6 Da corresponding to the non-

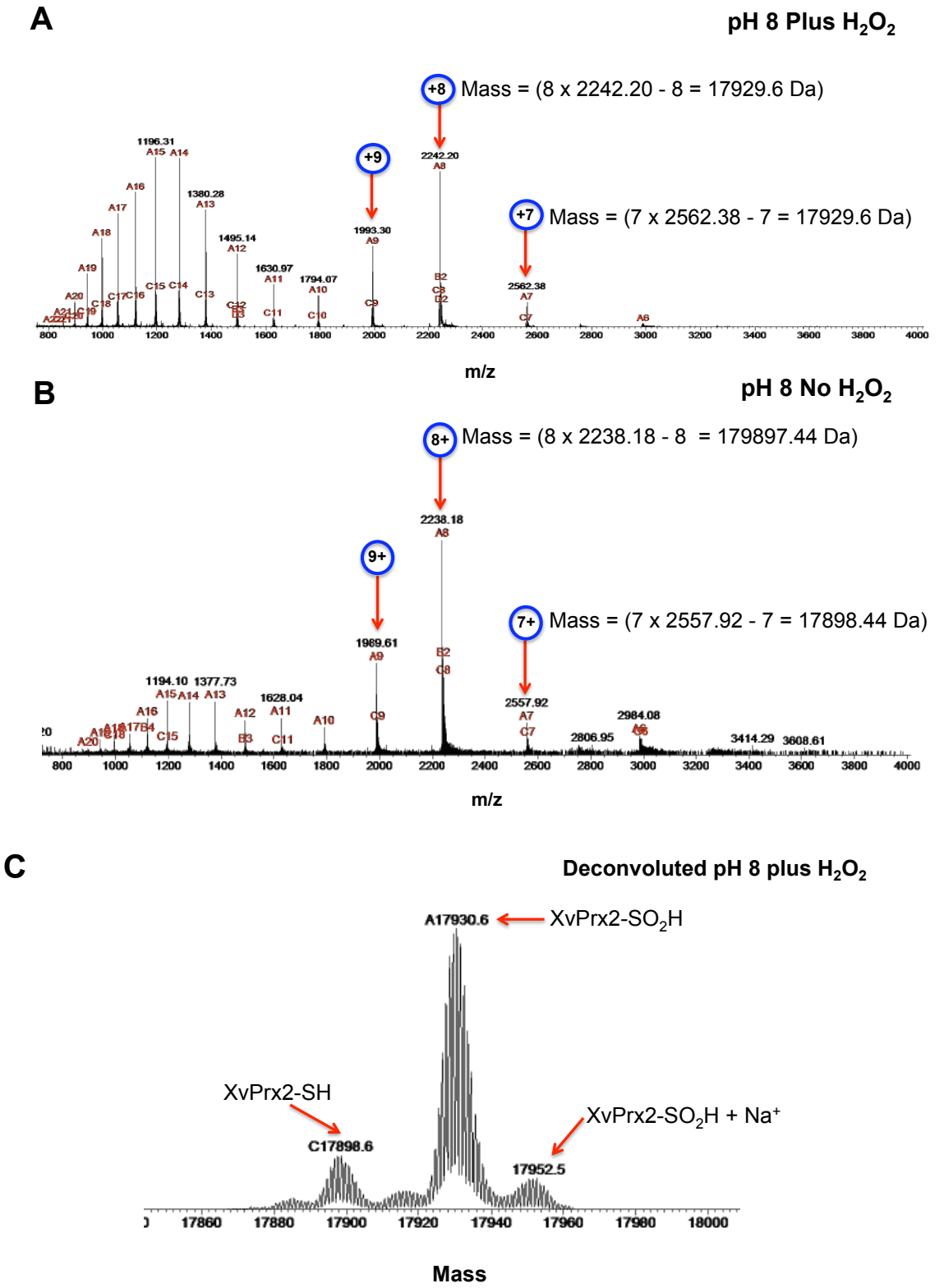

Fig 5.10: Mass spectra of oxidised and non-oxidised *Xv*Prx2 pH 8. (A) Shows the annotated "raw" mass spectrum of oxidised *Xv*Prx2 pH 8 while (B) shows a similar spectrum obtained from the sample prior to incubation with H_2O_2. The deconvoluted spectrum of the sample exposed to H_2O_2 is shown in (C). A shift in peak sizes by approximately 32 Da can be seen in the spectrum shown in (A) when compared to that shown in (B). The deconvoluted spectrum (C) shows 2 peaks, the one at 17930 corresponding to the sulphinic acid (*Xv*Prx2-S_2OH) form of the protein (17898 + 32 = 17930), and the non-oxidised form of the protein at 17898. The sulphinic acid form of the protein (*Xv*Prx2-SOH) is not observed.

oxidised form. The peak at 17952.5 Da corresponds to the sulphinic form complexed with a single Na^+ ion rather than the sulphonic acid form.

Despite several attempts we were unable to observe the sulphenic acid (singly oxidised) form of the protein. Figs. 5.11B and C show two scenerios observed following oxidation consisting of non-oxidised and doubly oxidised forms of the protein. The fact that non-oxidised and doubly oxidised forms of the protein were simultaneously observed suggests that the concentrations of H_2O_2 used were optimal for observing singly oxidised forms of the protein rather than being excessive. We conclude that the singly oxidised form of the protein is highly unstable with a high propensity to be further oxidised to the next oxidation state, as has been reported for a number of other 1-Cys peroxiredoxins.

The effect of oxidation was further investigated using NMR. 1D NMR spectra before and after addition of a 2-fold excess of H_2O_2 are shown in Fig 5.12. The most notably feature is the almost complete disappearance of the resonances at -0.5 ppm and 11.1 ppm. It was shown in Section 4.3 that the resonance at -0.5 ppm corresponds to Ile 41 packing against Phe 59, which is diagnostic of helix α_2 packing against the central β-sheet. The peak at 11.1 ppm is similarly diagnostic of fully folded state of the reduced protein at pH 8. The absence of these peaks therefore implies that oxidation leads to unfolding of the α_2-helix.

However an overlay of ^{15}N-HSQC spectrum of the oxidised sample with that of the non-oxidised sample at pH 8 (Fig 5.13), which has been shown to be homodimeric, and the non-oxidised sample at pH 5 (Fig 5.14) which is monomeric, suggests that the

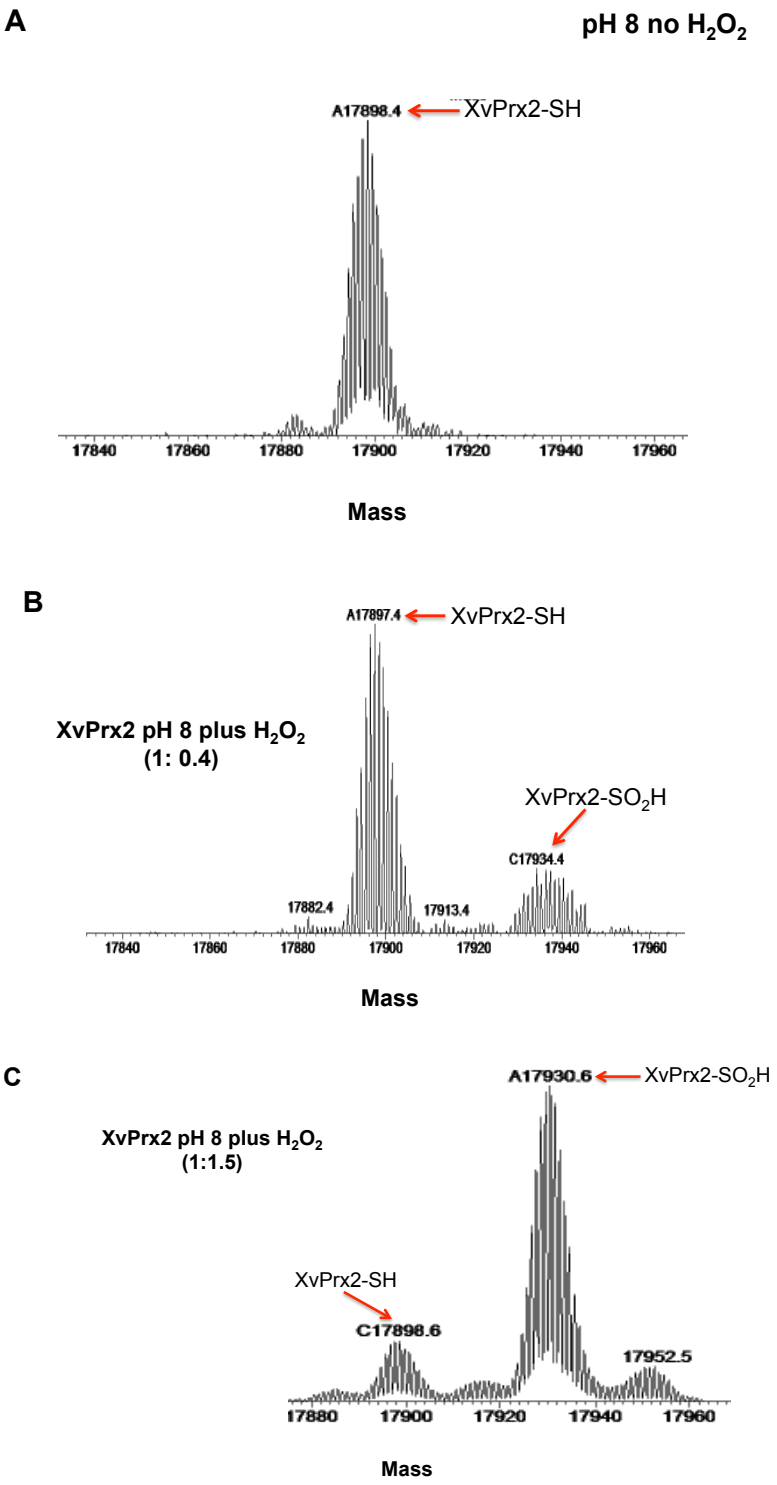

Fig 5.11: Deconvoluted MS spectra of non-oxidised and doubly-oxidised forms of *Xv*Prx2. (A) shows spectrum of non-oxidised *Xv*Prx2 while (B) and (C) show spectra of oxidised *Xv*Prx2 at 1:0.4 and 1:1.5 *Xv*Prx2 to H_2O_2 concentrations respectively. The spectrum shown in (B) is mostly non-oxidised while that shown in (C) is mostly doubly oxidised (-SO_2H). We could not observe the singly oxidised form of *Xv*Prx2 (-SOH) at all concentrations of H_2O_2 used.

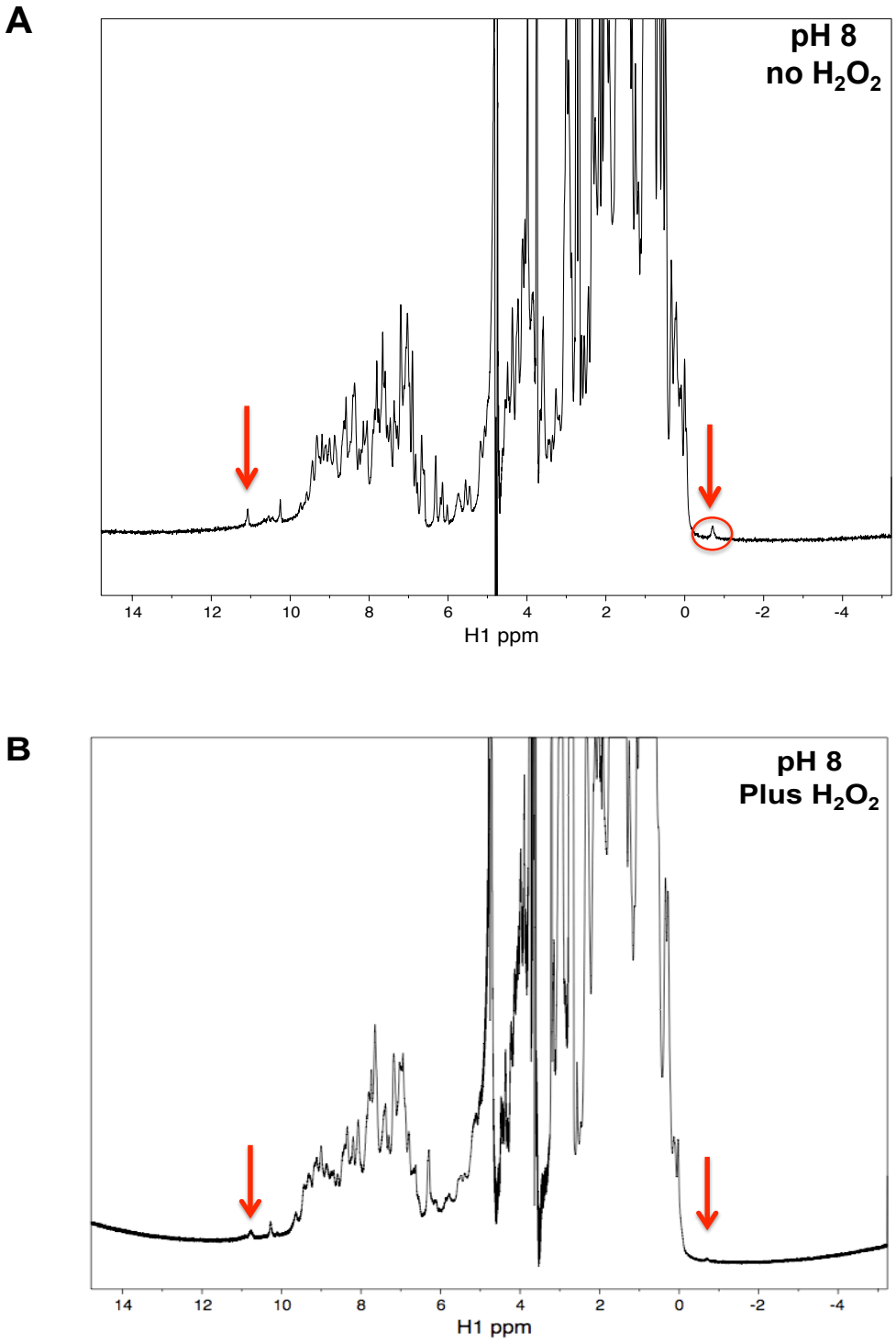

Fig 5.12: 1D ^{1}H spectrum of *Xv*Prx2 oxidised and non-oxidised at pH 8, 25 °C recorded at 600 MHz. (A) Shows the 1D proton spectrum of *Xv*Prx2 pH 8 non oxidised (no H_2O_2) while **(B)** shows the oxidised version of the same spectrum (+ H_2O_2). Both spectra are strikingly similar. Of particular interest is the absence of the resonances at -0.5 ppm and 11.1 ppm in the oxidised spectrum but not the non-oxidised spectrum. These peaks have been shown to be signatures of the dimeric form of the protein. The fact that these peaks are either reduced or changed in position in the oxidised but not the non-oxidised spectrum suggests that oxidation induces the partial or full unfolding of the α_2-helix.

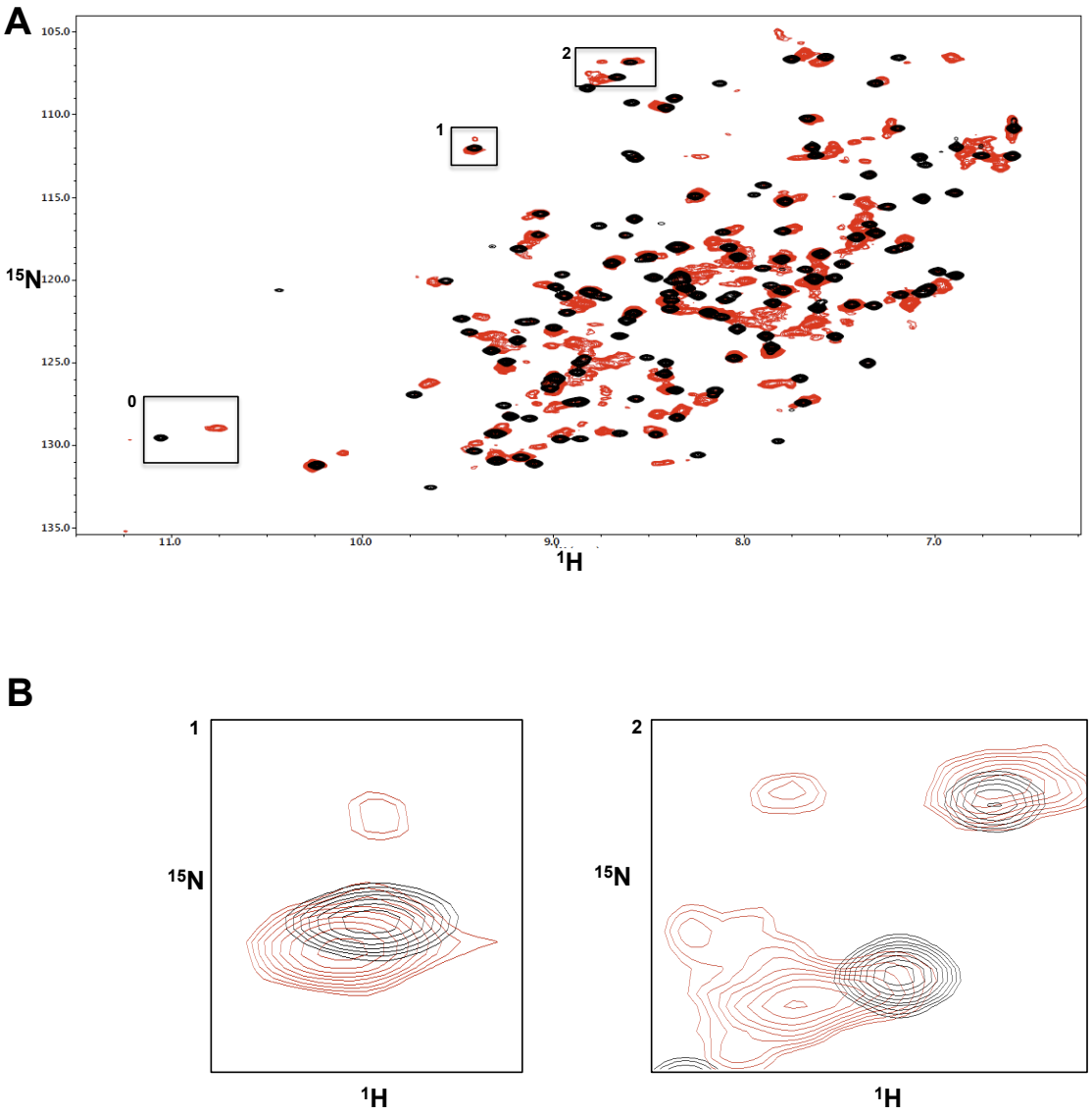

Fig 5.13: Overlay of ^{15}N-HSQC spectra of *Xv*Prx2 at pH 8 oxidised (red) and non-oxidised (black) at 25 °C, recorded at 600 MHz. (A) shows a full view of the overlay while (B) shows expanded view of regions "1" and "2" of the full view. The oxidised sample appears to have a small trace of the monomeric configuration appearing (small separate peaks). Overall both spectra overlay near perfectly suggesting that the oxidised sample is dimeric just like the non-oxidised sample.

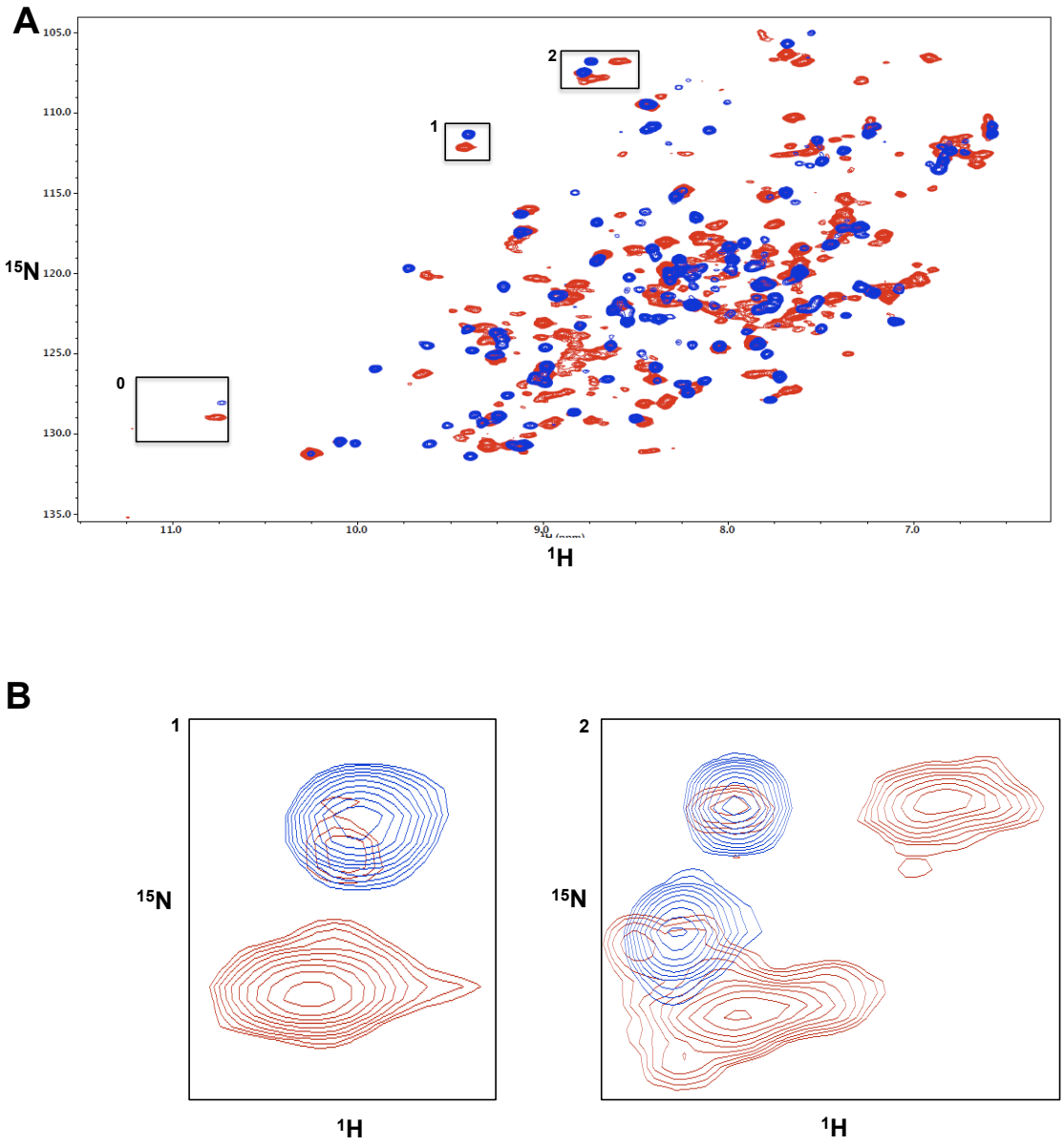

Fig 5.14: Overlay of ^{15}N-HSQC spectra of oxidised *Xv*Prx2 at pH 8 (red) and the monomeric pH 5 configuration (blue) at 25 °C, recorded at 600 MHz. (A) shows a full view of the overlay while (B) shows expanded view of regions "1" and "2" of the full view. The oxidised sample appears to have a small trace of the monomeric configuration appearing (small separate red peaks). A clear difference is seen in the resonance positions of the monomeric sample suggesting that the oxidised sample is not monomeric.

sample remains predominantly dimeric following oxidation. In a number of cases, such as the resonances in boxes marked “1” and “2”, the oxidized spectrum appears similar to the homodimeric spectrum (pH 8), with a small contribution from the monomeric spectrum (pH 5). But on the whole the spectrum does not look similar to either the homodimeric or the monomeric spectrum. The above data leads us to the hypothesis that oxidation unfolds the α_2-helix, and that this destabilizes the protein, causing a small fraction of molecules to dissociate into monomers. However the majoriy of the molecules remain homodimeric.

Analytical SEC provides additional support for this hypothesis. At pH 7 both oxidised (+ 2 fold H_2O_2) and un-oxidised (+ 10 mM DTT) *Xv*Prx2 elute at the same volume (Fig 5.15), which corresponds to the dimeric form, rather than at the position of the pH 5 sample, which corresponds to the monomeric form.

Hence we conclude that oxidation does not disrupt the homodimer at pH 7 although it does destabilize it to an extent, cause a small fraction of the molecules to unfold. We also suspect that the α_2-helix becomes unfolded. We are unable to account for the widespread changes brought about by oxidation, changes that do not correspond either to the monomeric or the homodimeric spectrum. A possible explanation is that it is due to conformational changes to the tertiary structure of each monomer, probably brought about by unfolding of the α_2-helix.

5.3 Glutathionylation

Glutathionylation is a covalent modification of cysteine thiol groups involving the

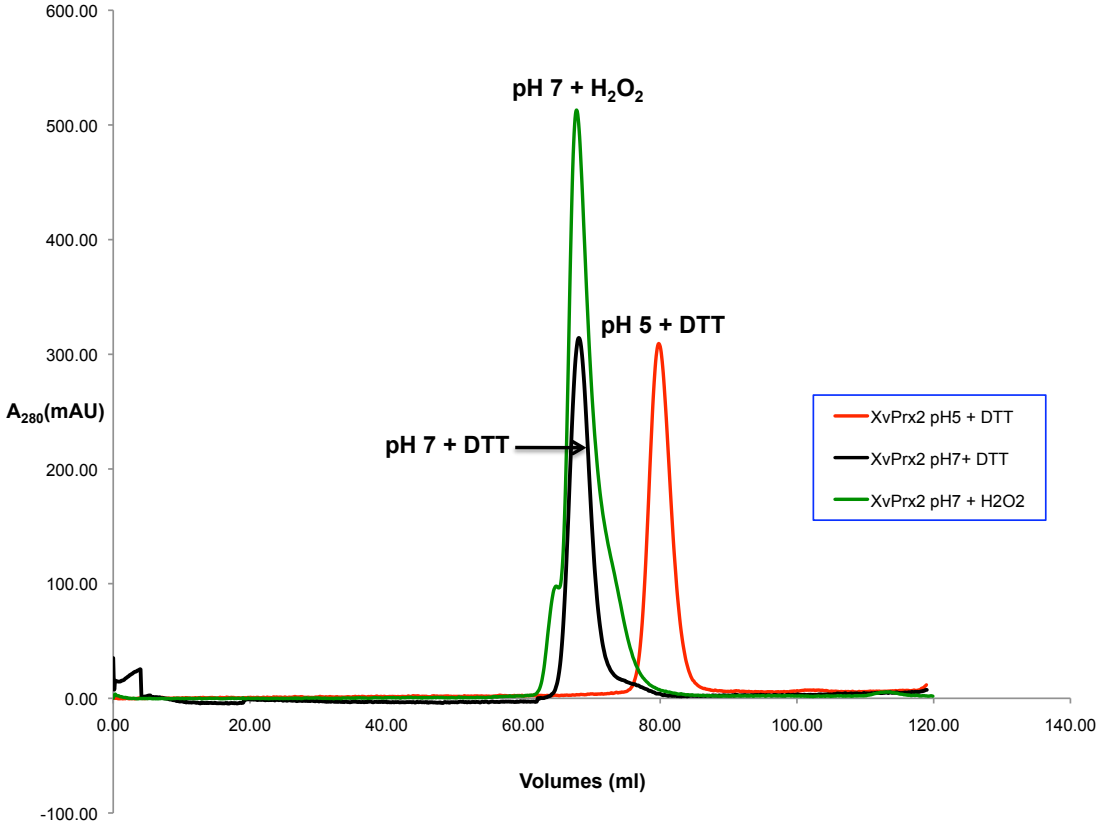

Fig 5.15: Overlay of *Xv*Prx2 SEC at pH 7 + DTT (non-oxidised, black), pH 7 + H_2O_2 (oxidised, green) and pH 5 + DTT (non-oxidised, red). The oxidised and non-oxidised pH 7 samples elute at the same volume demonstrating that oxidation does not affect the oligomeric state of *Xv*Prx2 at pH 7. The non-oxidised pH 7 sample had previously been shown to be a non-covalent homodimer (Fig 4.20, Table 4.3) implying that the oxidised sample is also non-covalent homodimeric. Although some monomeric peaks are visible in the ^{15}N-HSQC spectrum of the oxidised pH 7 sample (Fig 5.13 and 5.14) suggesting a change in local conformation of the protein, the overlay of the oxidised pH 7 and the non-oxidised pH 5 (monomeric) samples show that the oxidation does not induce the dissociation of the non-covalent homodimer into monomers. Our SEC data provides evidence that oxidation does not affect the oligomeric state of *Xv*Prx2.

formation of a disulphide bond with the thiol group of the tri-peptide glutathione. Glutathione is comprised of amino acids glutamic acid, cysteine and glycine, incorporating a non-standard peptide bond between the side chain carbonyl of glutamic acid and the backbone amino group of cysteine. When the thiol group is reduced the molecule is denoted "GSH"; under oxidizing conditions the thiol can form inter-molecular disulphide bonds, in which case the molecule is denoted "GSSG".

Proteins are reported to be glutathionylated under conditions of stress (Chock *et al*., 2010). Glutathionylation is reported to protect thiols from becoming irreversibly oxidised and a number of enzymes have been identified which de-glutathionylate thiols once stress levels have reduced (Chock *et al*., 2010).

5.3.1 The effect of glutathionylation on the oligomeric state of *Xv*Prx2

Noguera-Mazon and co-workers (Noguera-Mazon*, et al.*, 2006b) reported that PrxD from *Populus tremula*, which is a close homologue of *Xv*Prx2, became glutathionylated when incubated with 10 to 20-fold excess oxidised glutathione (GSSG), and that glutathionylation completely disrupted the non-covalent homodimer. The resulting monomers adopted a similar tertiary structure to that in the homodimer, although the α_2-helix incorporating the peroxidatic cysteine was shown to be unstructured.

Glutathionylation could be partially reduced by the addition of DTT, resulting in the reversal of the monomers back into dimers. However Noguera-Mazon and co-workers could not completely regenerate the homodimer, leading them to conclude that glutathionylation plays other roles apart from forming intermolecular disulphide bridges.

The regeneration mechanism for the Prx5 subfamily proposed by Noguera-Mazon and co-workers (Fig 1.25) suggests that the mixed disulphide (*Pt*PrxD-GS) is reduced by an electron donor, glutaredoxin, regenerating *Pt*PrxD back to its reduced (-SH) state. A similar mechanism for the reduction of 1-Cys Prx from Prx6 subfamily had previously been reported (Manevich*, et al.*, 2004), although GSH alone was not able regenerate the protein but required the presence of πGST. The suggestion is that GSH is not able to gain access to the C_P, but that a heterodimer between πGST and 1-CysPrx succeeds in opening up access to C_P, resulting in the glutathionylation of the oxidised C_P. The dissociation of the heterodimeric complex through a spontaneous reduction by GSH results in a glutathionylated protein with fully restored activity.

We therefore set out to determine whether *Xv*Prx2 could be directly glutathionylated by oxidised glutathione (GSSG). Glutathionylation was investigated by incubating *Xv*Prx2 with 10-fold excess GSSG (in the absence of DTT), following which ESI-MS was recorded, as shown in Fig 5.16B. When compared to the un-glutathionylated spectrum (Fig 5.16A), the raw glutathionylated spectrum contains many new species corresponding to 1, 3, 5 and 7 glutathione adducts. Species which become glutathionylated will increase in size by approximately 306 Da. For example, the 8^{th} ionisation of *Xv*Prx2 has shifted from m/z = 2238 to 2276, 2353 and 2430, corresponding to m = 18200, 18816 and 19432 Da respectively, which corresponds in turn to 17897 + 303, 17897 + 3 x 306.33 and 17897 + 5 x 307 Da respectively, as seen in the deconvoluted spectrum in Fig 5.17A. The resonance at m/z = 2754, which was

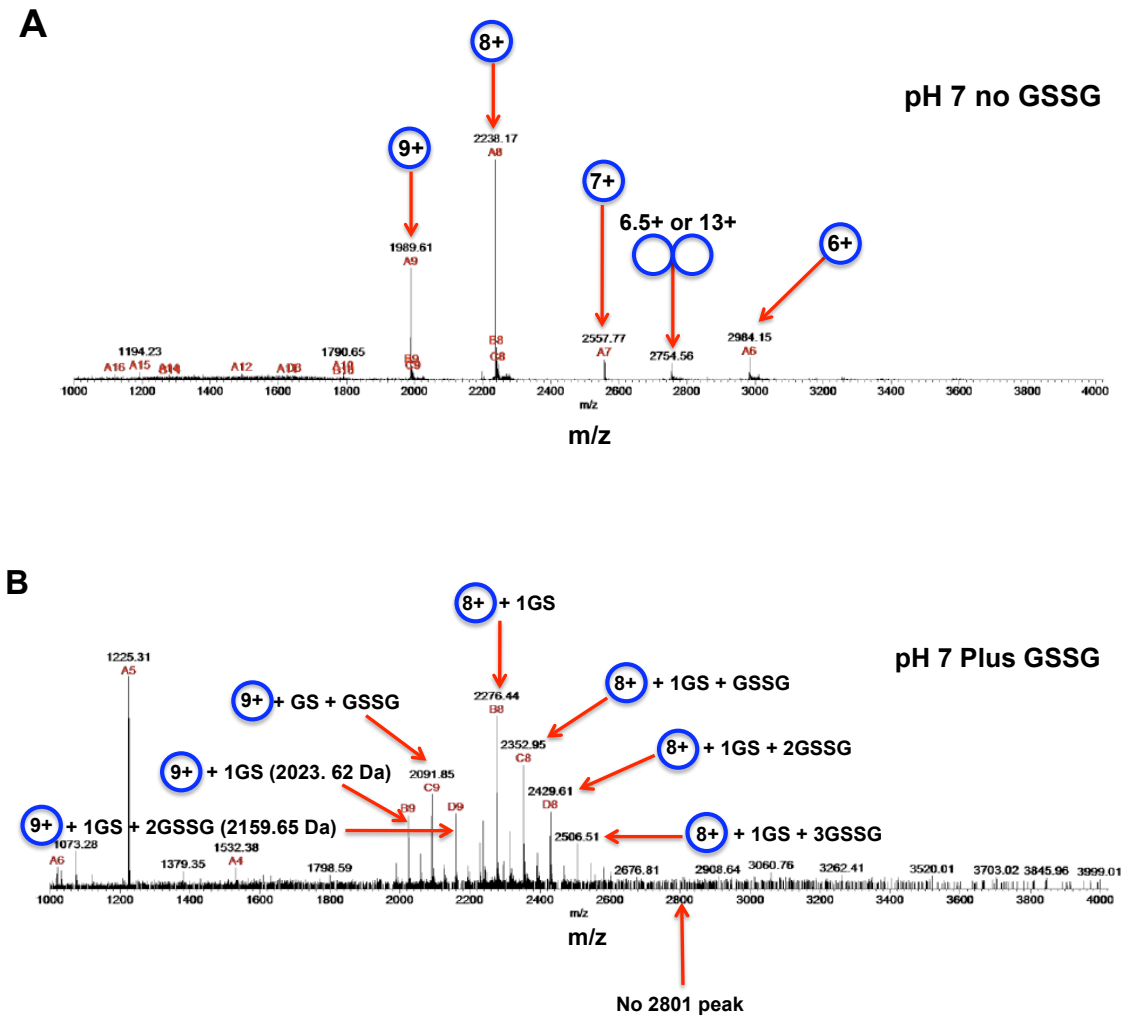

Fig 5.16: Non-denaturing electrospray mass spectrometry of annotated "raw" spectrum of glutathionylated and non-glutathionylated *Xv*Prx2 at pH 7. (A) Shows the mass spectrum of *Xv*Prx2 at pH 7 in the absence of GSSG while (B) shows the same mass spectrum in the presence of 10 fold excess GSSG. An increase in peaks size by 307 Da or a multiple thereof can be seen in the 8th and 9th ionisation states of the glutathionylated spectrum but not in the non-glutathionylated spectrum. For example the 8th ionisation state of the non-glutathionylated sample has m/z = 2238.17 (17897.36 Da) while same state for the glutathionylated sample has m/z = 2276.44, 2352.95, 2429.61 and 2506.51 corresponding to 18203, 18815.6, 19428.8 and 20044.08 Da, which corresponds to *Xv*Prx2 + 1GS, +1GS and GSSG + 1GS and 2GSSG and + 1GS and 3GSSG molecules respectively. A similar observation is made for the 9th ionisation state where the protein is attached to +1GS, +1GS and GSSG and + 1GS + 2GSSG molecules respectively. The peak at 2754 in the non-glutathionylated sample (previously shown to be evidence of the non-covalent homodimer) should have a value of approximately 2801 Da following glutathionylation. The absence of this peak in the glutathionylated spectrum suggests that the non-covalent homodimer has been abolished following glutathionylation. The 7th and 6th ionisation states present in the non-glutathionylated sample are absent in the glutathionylated sample suggesting that they represent the homodimeric state. Our data confirms that gluathionylation leads to the dissociation of the non-covalent homodimer of *Xv*Prx2 to monomers similar to results obtained by Noguera-Mazon and co-workers for Prx from *P. tremula* (*Pt*PrxD) (Noguera-Mazon, *et al.*, 2006b).

previously shown to arise entirely from the homodimeric form, should have a value of approximately 2801 Da following glutathionylation. The absence of this peak indicates that glutathionylation disrupts the homodimer.

GSSG has been previously reported to associate non-covalently with proteins, suggesting that the +3GS and +5GS aducts seen in Fig 5.17(A) may correspond to non-covalent association or 1 or 2 GSSG molecules with glutathionylated *Xv*Prx2. To test this hypothesis, the sample was subjected to denaturing mass spectrometry. As expected, only the +1GS resonance remained (Fig 5.17B).

1D proton spectra of *Xv*Prx2 at pH 7 in the presence and absence of GSSG are shown in Fig 5.18. With the exception of the sharp resonances in the vicinity of 8 ppm, which correspond to free glutathione, the GSSG sample is strikingly similar to the monomeric spectrum previously seen in the wild type at pH 5 (Fig 4.3A) and in the H55A mutant at pH 7 (Fig 5.5A). In particular the resonances at -0.5 ppm and at 11.1 ppm, which have been shown to be signatures of the dimeric form, are no longer observable in the presence of GSSG, suggesting that glutathionylated *Xv*Prx2 is monomeric.

A ^{15}N-labelled sample of *Xv*Prx2 was glutathionylated as above and used to record ^{15}N-HSQC spectra at pH 7. The overlaid spectra in Fig 5.19A reveal clear differences between the glutathionylated and non-glutathionylated samples at pH 7, whereas the glutathionylated spectrum is almost undistinguishable from the spectrum of *Xv*Prx2-H55A at pH7 (Fig 5.19B) and similar to the spectrum of *Xv*Prx2 at pH5, both of which have previously been shown to be monomeric.

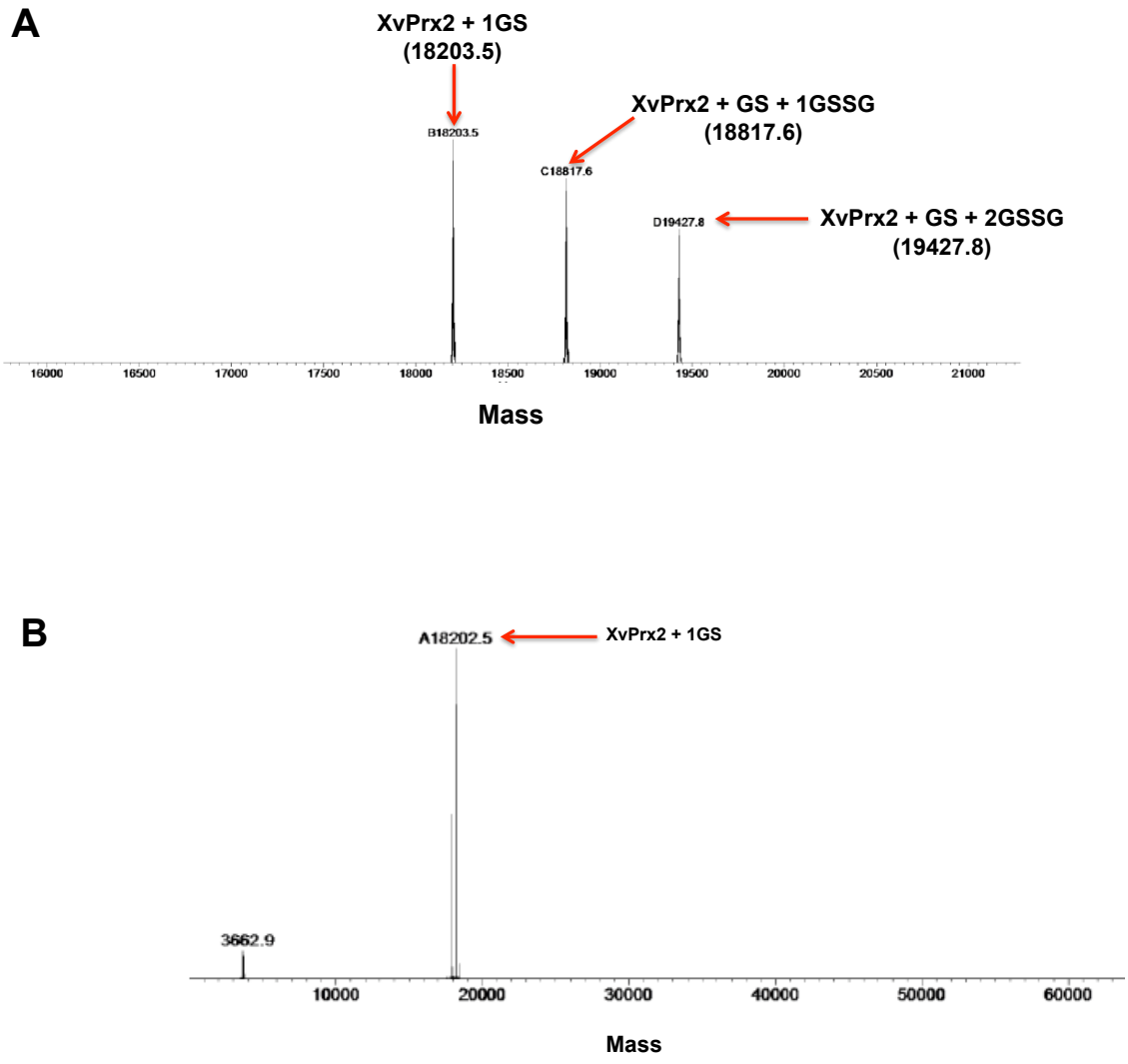

Fig 5.17: Deconvoluted ESI-MS spectra of glutathionylated *Xv*Prx2 at pH 7. (A) The MS spectrum of glutathionylated *Xv*Prx2 recorded under non-denaturing conditions displaying peaks corresponding to 1, 3 and 5 GS molecules attached to *Xv*Prx2 respectively. The spectrum in (B) was acquired in denaturing conditions; the disappearance of the +3GS and +5GS species shows that they correspond to non-covalent interactions.

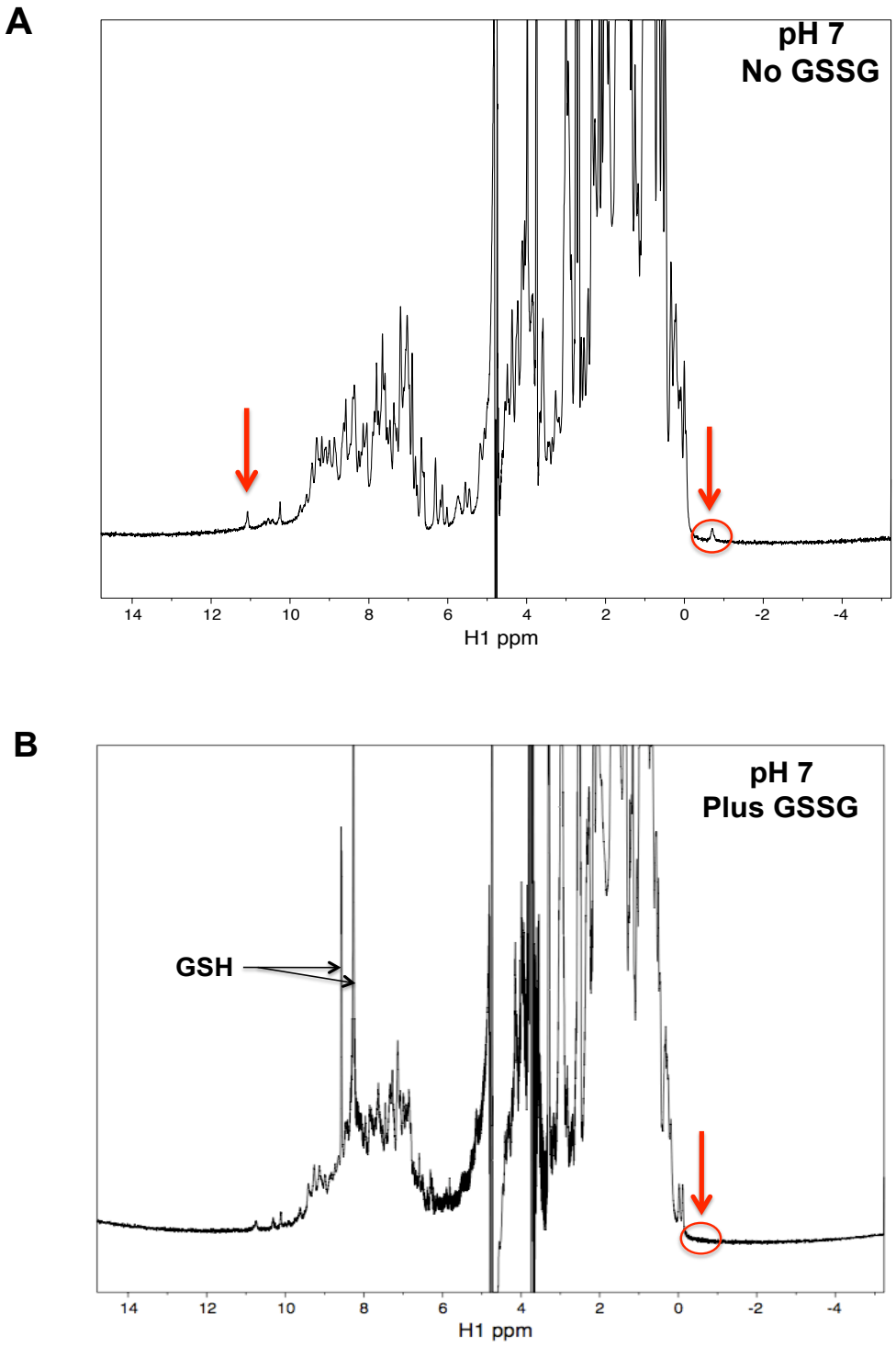

Fig 5.18: 1D ^{1}H spectrum of *Xv*Prx2 at pH 7, 25 ° C recorded at 600 MHz. (A) Shows the 1D proton spectrum of *Xv*Prx2 pH 7 in the absence of GSSG while (B) shows the same spectrum in the presence 10-fold excess GSSG. Both spectra are strikingly similar with the exception of sharp resonances found in the 8 ppm region, which correspond to GSH resonances. Of particular interest is the absence of the resonances at -0.5 ppm and 11.1 ppm, in the spectrum containing GSSG but not in the spectrum without GSSG. These resonances (-0.5 ppm and 11.1 ppm indicated with an arrow) have both previously been shown to be signatures of the dimeric form of the protein. The fact that the GSSG spectrum lacks the dimeric peak confirms that the non-covalent homodimeric configuration undergoes dissociation to monomers following glutathionylation.

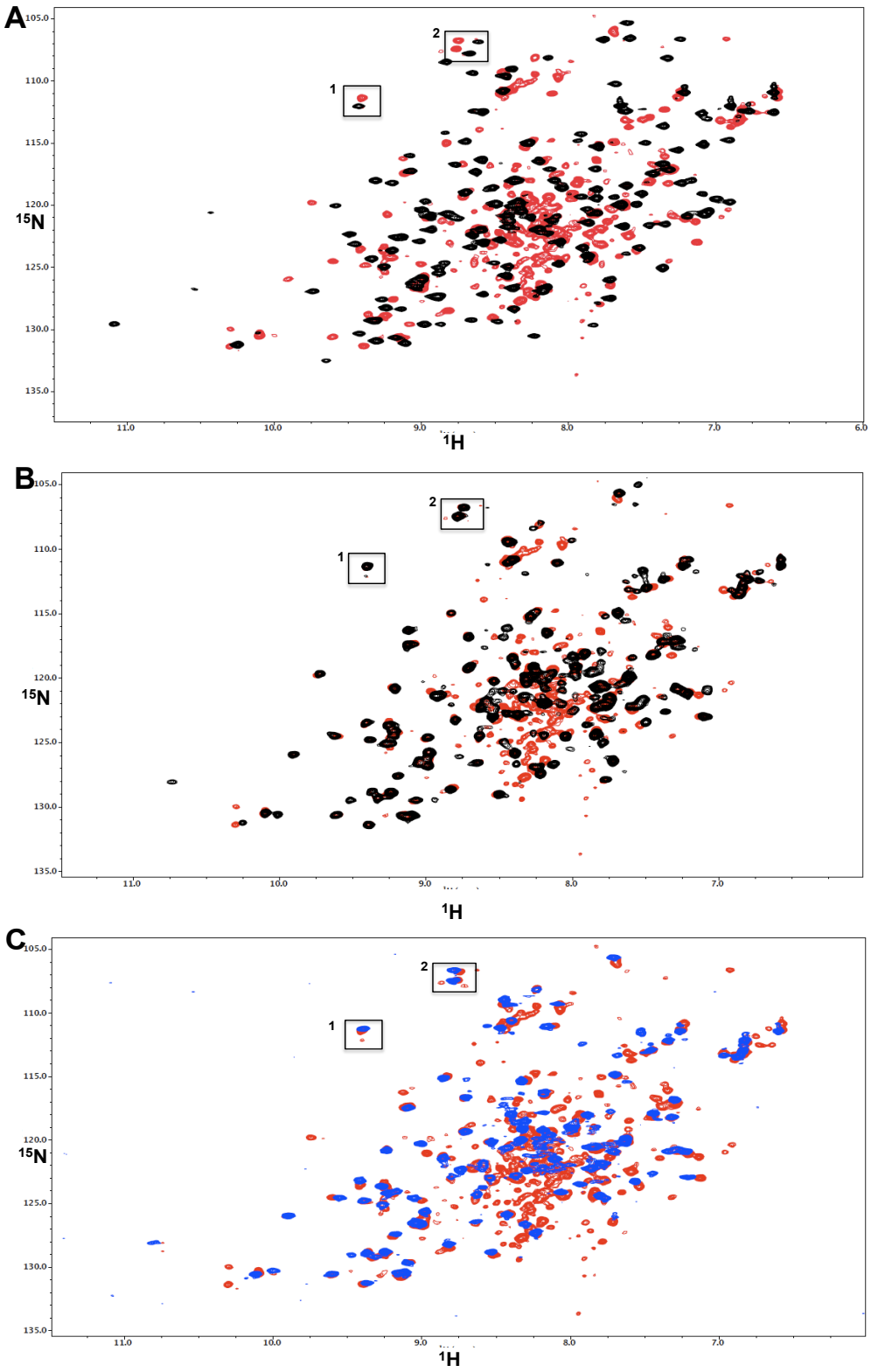

Fig 5.19: ^{15}N-HSQC spectra showing that glutathionylated *Xv*Prx2 is monomeric at pH 7. Glutathionylated *Xv*Prx2 at pH 7, shown in red in all panels, is overlaid with (A) un-glutathionylated XvPrxs at pH 7, shown in black, (B) *Xv*Prx2-H55A at pH7, shown in black and (C) *Xv*Prx2 pH5, shown in blue. Glutathionylated *Xv*Prx2 at pH7 is more similar to *Xv*Prx2-H55A at pH7 (panel B) and to *Xv*Prx2 at pH5 (panel C), both of which have been shown to be monomeric, than to homodimeric *Xv*Prx2 at pH 7. A large number of poorly-resolved resonances near the centre of the spectrum are evidence that the glutathionylated protein is partially unfolded. Both the glutathionylated and the pH 5 samples of *Xv*Prx2 used in this experiment precipitated overnight at 25 °C, whereas *Xv*Prx2-H55A was stable at pH 7 for more than 6 weeks at 25 °C, suggesting that the H55A mutant may be a useful proxy for either of the other conditions.

this is clear evidence that glutathionylated *Xv*Prx2 is monomeric at pH 7. Fig 5.19C similarly shows that the ^{15}N-HSQC of glutathionylated wild type *Xv*Prx2 is essentially identical to the H55A mutant, which was previously shown to be monomeric at pH 7. Note that the spectrum of H55A appears to be sharper and contain fewer poorly dispersed peaks than the spectrum of either the glutathionylated or wild type pH 5. This is consistent with our observation that while the H55A protein remained stable for more than six weeks at 25 °C, both the pH 5 and the glutathionylated samples precipitated within 24 hours at 25 °C. This suggests that the H55A sample may be more suitable for the structural investigation of the monomeric form than either the glutathionylated or the wild type pH 5 samples.

A consequence of the model shown in Fig 1.25 is that glutathionylation can occur by two different mechanisms: (I) by reacting oxidised glutathione (GSSG) with reduced peroxiredoxin (-SH), and (II) by reacting reduced glutathione (GSH) with oxidised peroxiredoxin (-SOH).

Pathway I has already been demonstrated above. To confirm that *Xv*Prx2 could be glutathionylated according to pathway (II), a sample of *Xv*Prx2 was first oxidised by addition of H_2O_2 and then incubated with reduced glutathione (GSH). MS was then performed, as shown in Fig 5.20. The sample used was ^{15}N-enriched, giving a molecular weight of 18102 (Fig 5.20A) corresponding to 99 % enrichment (204 of the 206 nitrogen atoms being ^{15}N isotopes. Addition of an equal molar quantity of H_2O_2 led to partial oxidation of the protein to sulphinic acid form (-SOOH), corresponding to the addition of 32 Da as seen in Fig 5.20B, and additon of twice the molar quantity resulted in complete oxidation of the protein to the sulphinic state (data not shown).

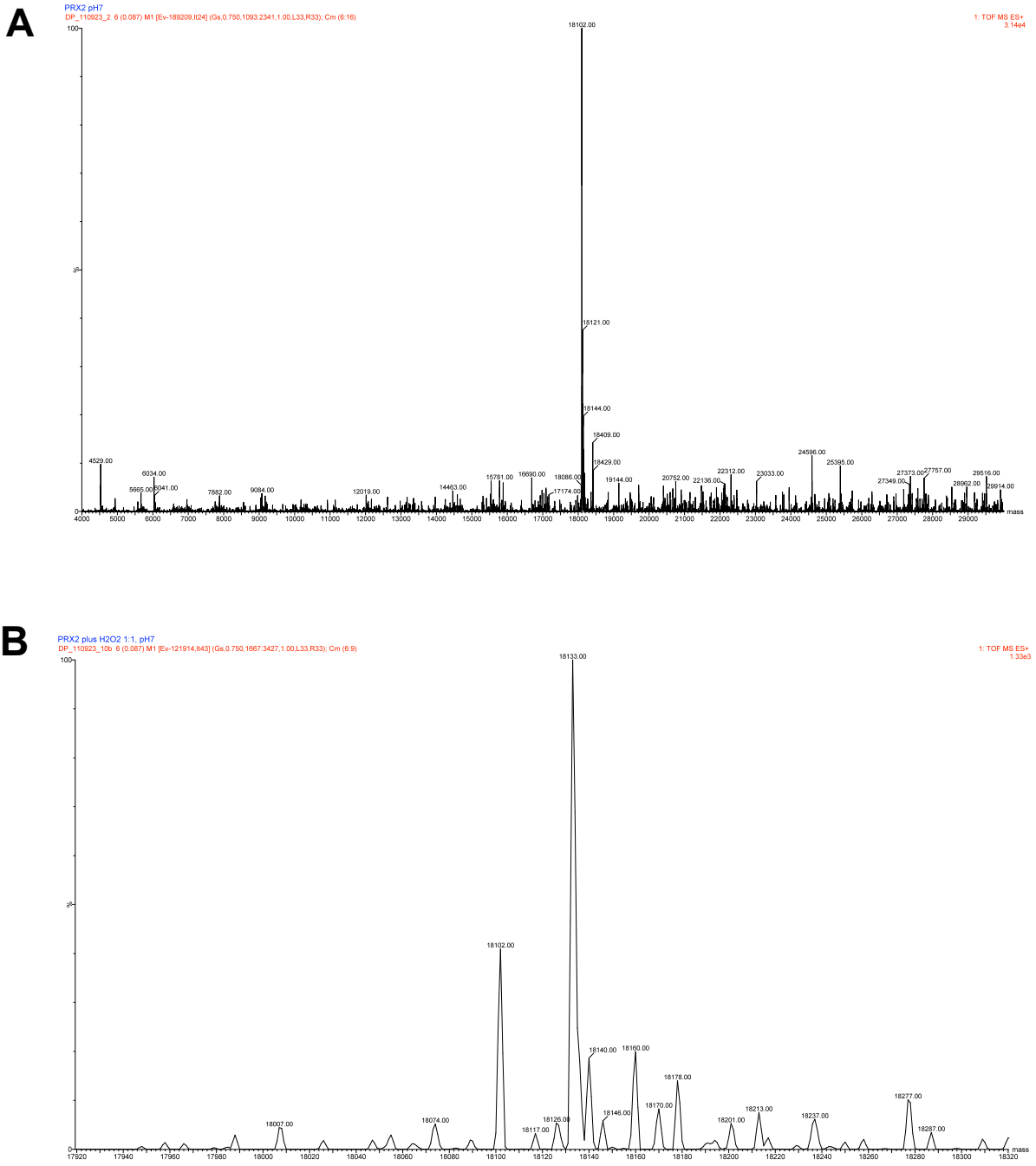

Fig 5.20: Deconvoluted MS spectra of non-oxidised and oxidised ^{15}N-labelled *Xv*Prx2. Spectrum of non-oxidised ^{15}N-labelled sample (+ DTT) (A) and partially oxidised (B) ^{15}N-labelled *Xv*Prx2. The spectrum in (B) contains peaks at 18102 and 18133 corresponding to the non-oxidised and oxidised forms respectively. The difference of the sizes of the non-oxidised and oxidised peaks is approximately 32 Da suggesting that the oxidised form is sulphinic (-SO_2H). The sulphenic (-SOH) acid form was not observed.

Again no evidence of the singly oxidised form was observed, as has been noted previously. Addition of 10-fold excess (GSH) to the oxidised sample led to complete glutathionylation of the protein, corresponding to the addition of 306 Da (Fig 5.21B). However addition of GSH without prior oxidation of the protein (Fig 5.21C) did not result in glutathionylation, suggesting that the protein needs to be oxidised for glutathionylation with GSH to occur.

A possible alternative explanation might be that glutathionylation by GSH is due to prior oxidation of GSH to GSSG by the excess H_2O_2 present in the sample, followed by glutathionylation by GSSG. The raw spectrum shown in Fig 5.21(A) discounts this possibility: although a peak corresponding to GSH is observed at 306 Da, no peak corresponding to GSSG is observed at around 612 Da. We conclude that glutathionylation of the oxidised *Xv*Prx2 is due to GSH alone.

When 10 mM DTT was added to the glutathionylated (^{15}N-labelled) *Xv*Prx2 shown in Fig 5.21B the mass reduced to 18104, showing that it had been completely de-glutathionylated (Fig 5.22). The ^{15}N-HSQC spectrum of de-glutathionylated *Xv*Prx2 is virtually identical to that of glutathionylated *Xv*Prx2 (Fig 5.23), showing that the addition of DTT resulted in complete regeneration of the protein from glutathionylated monomer to non-covalent homodimer. Similar experiments performed on PrxD from *P. tremula* suggested that DTT could only partially restore the dimeric configuration as some evidence of monomeric peaks were observed following addition of large quantities of DTT (Noguera-Mazon*, et al.*, 2006b). The reason for the discrepancy is not clear at this stage.

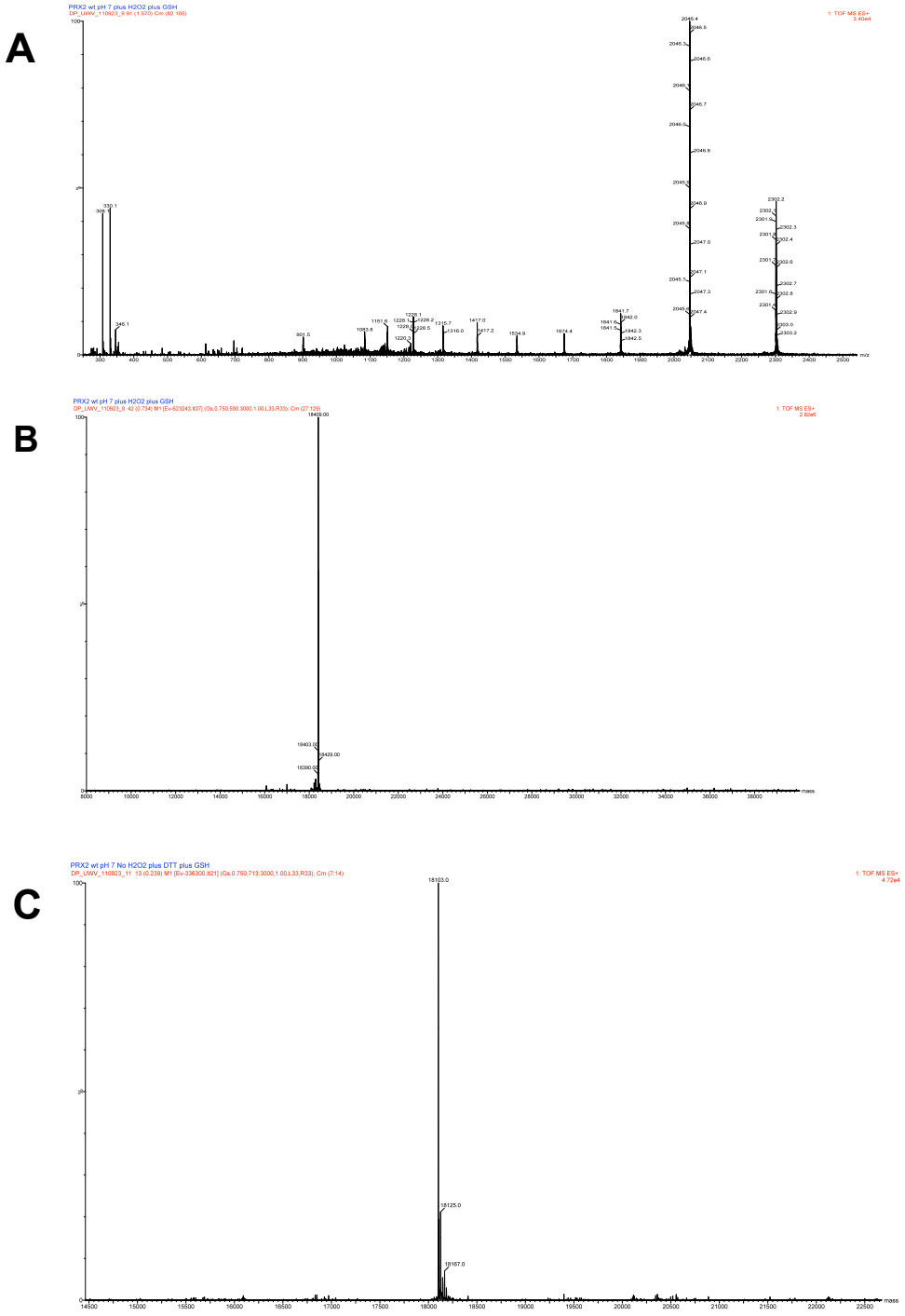

Fig 5.21: ESI-MS spectrum of glutathionylated ^{15}N-labelled *Xv*Prx2 pH 7. (A) Raw spectrum showing the 9th and 8th ionisation states (2046 and 2032 Da) of glutathionylated ^{15}N-labelled *Xv*Prx2, following addition of 10 mM DTT to oxidised *Xv*Prx2. Reduced glutathione (308 Da) is also visible. The absence of a peak at 616 Da corresponding to GSSG shows that glutathionylation of *Xv*Prx2 due to GSH and not due to prior oxidation of GSH by H_2O_2. (B) Deconvoluted spectrum of glutathionylated *Xv*Prx2 at 18407. (C) In the absence of H_2O_2 GSH was unable to glutathionylate *Xv*Prx2, resulting in a peak at 18103 Da, corresponding to the mass of reduced ^{15}N-labelled *Xv*Prx2.

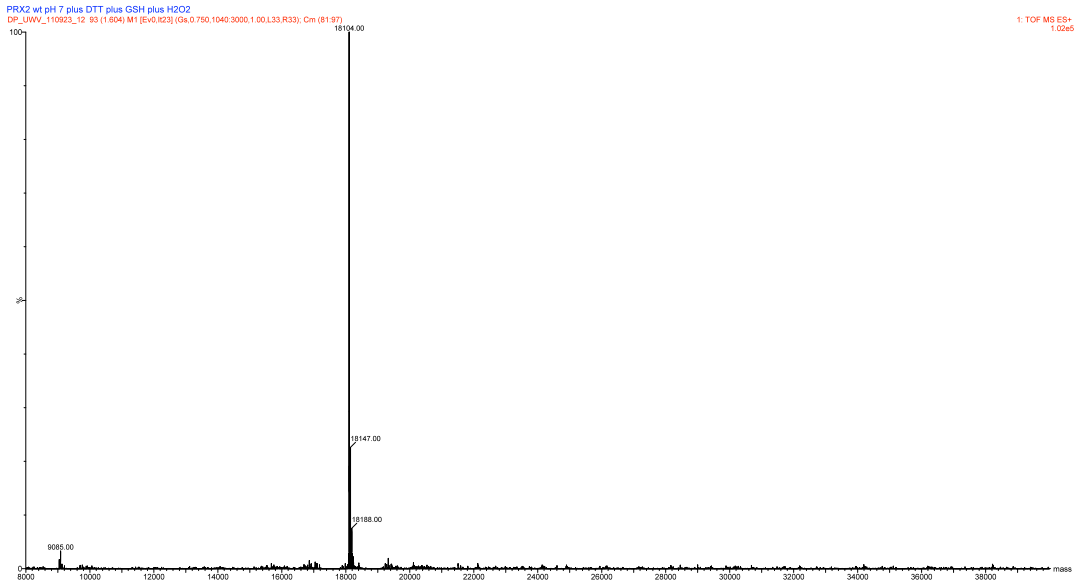

Fig 5.22: Addition of DTT effectively regenerates un-glutathionylated *Xv*Prx2. Deconvoluted MS spectrum of ^{15}N-labelled *Xv*Prx2 at pH 7 in the presence of 10 mM DTT. The peak at m = 18104 corresponds to the size of fully reduced *Xv*Prx2, showing that DTT breaks the mixed disulphide between *Xv*Prx2 and GS.

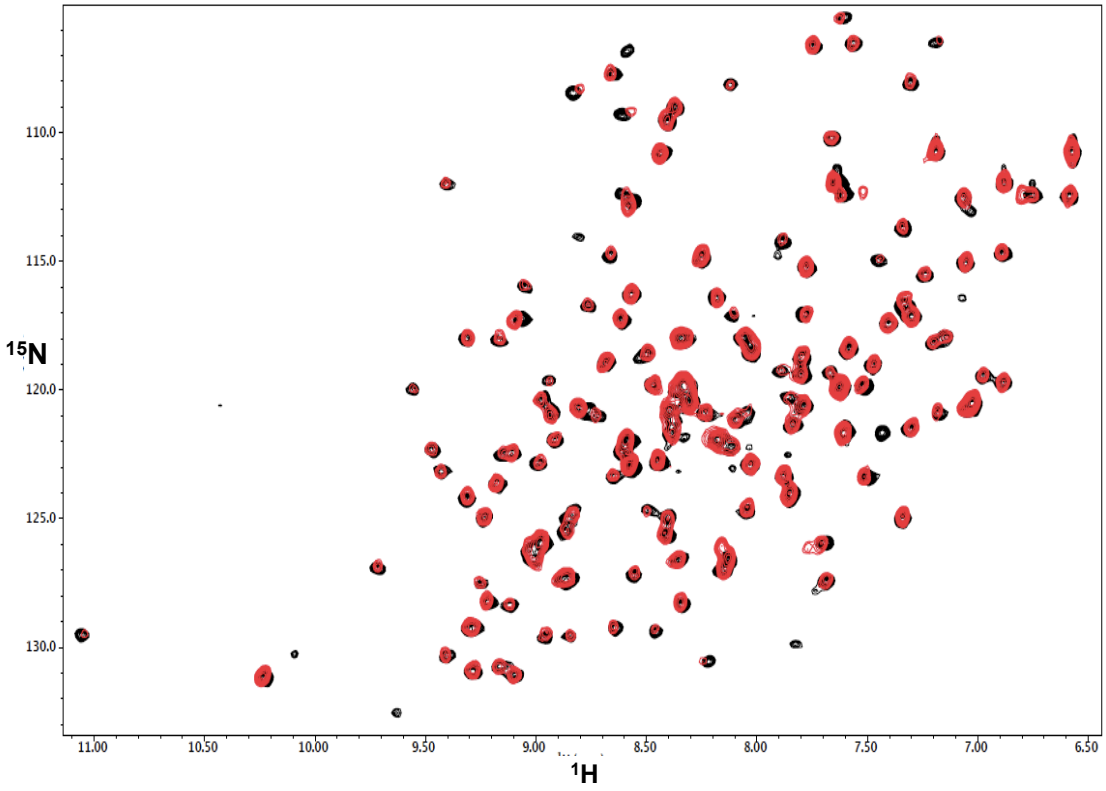

5.23: Addition of DTT effectively regenerates un-glutathionylated *Xv*Prx2. Following addition of 10 mM DTT the ^{15}N-HSQC spectra of glutathionylated *Xv*Prx2 (red) overlays perfectly with the spectrum of un-glutathionylated, reduced *Xv*Prx2 (black), showing that the tertiary configuration, as well as the homodimeric state, have been completely regenerated. Both spectra were recorded at pH 7.

Hence we can conclude that, as proposed by Noguera-Mazon and co-workers (Noguera-Mazon*, et al.*, 2006b), oxidised *Xv*Prx2 can be efficiently regenerated by addition of GSH and DTT. Provided a physiological replacement for DTT could be found, this mechanism would potentially provide a mechanism for regeneration of *Xv*Prx2 *in vivo*. Importantly, since the oxidised sample used for glutathionylation was predominantly in the sulphinic acid (-SOOH) form, this mechanism should would work for over-oxidised as well as single-oxidised *Xv*Prx2, without the need for sulphiredoxins.

Chapter 6: Conclusions and future work

6.1 Conclusions

*Xv*Prx2 is a member of the Prx5 subfamily of peroxiredoxins isolated from the resurrection plant *Xerophyta viscosa*. These plants are desiccation tolerant and can survive dehydration to 5% relative water content and yet reach full physiological activity within 3 days following rehydration (Sherwin & Farrant, 1998). *Xv*Prx2 was originally identified as one of the genes upregulated during periods of desiccation (Mowla*, et al.*, 2002) and subsequent work confirmed a role for *Xv*Prx2 in protecting nucleic acids and other cellular proteins from oxidative damage by reactive oxygen species (Govender, 2006).

A structure of *Xv*Prx2 is yet to be elucidated although the structure of the closely related PrxD from *Populus tremula* has been reported. The structure of *Pt*PrxD and associated studies revealed that it forms non-covalent homodimers across an A-type interface. Noguera-Mazon and co-workers showed that *Pt*PrxD could form disulphide bonds with glutathione (glutathionylation), and that this process resulted in the unfolding of the C_p-loop and α_2-helix and disruption of the homodimer. Noguera-Mazon and co-workers suggested furthermore that glutathionylation might play a physiological role in the regeneration of all members of the Prx5 subfamily.

The objectives we set out to achieve at the time of inception of this study included determination of the structure of *Xv*Prx2 using X-ray crystallography, investigation of the presence of a non-covalent homodimer, investigation of the effect of oxidation on

the oligomeric state of the protein and the validation of the proposed regeneration cycle for the Prx5 subfamily.

pH-dependent homodimerisation of XvPrx2

Despite repeated attempts with high quality samples of *Xv*Prx2 we were unable to get sufficiently well diffracting crystals for determination of the structure using X-ray diffraction. It is possible that the mixture of monomeric and dimeric isoforms identified in this work are responsible for the unwillingness of the protein to crystallise, something that possibly warrants further investigation. Our data suggests that future crystallization trials should be carried out at pH values either above 8 or below 5, where the protein is predominantly homodimeric or monomeric respectively. Mutant forms such as the H55A mutant reported in this thesis may prove more amenable to crystallization due to different oligomerization properties.

Attempts to determine the structure using nuclear magnetic resonance spectroscopy were also unsuccessful, due to poor sensitivity of the triple resonance data and broad line widths. With hindsight we conclude that this is due to the fact that wild type *Xv*Prx2 is either partially or completely homodimeric at pH ≥ 6; at ~ 36 kDa the dimer is beyond the capability of NMR without the use of a cryoprobe, which was not available, or partial deutration, which was not attempted. However we were able to almost completely assign the ^{15}N-HSQC spectrum of wild type *Xv*Prx2, and the spectrum proved to be a useful tool for investigating the oligomeric state of the protein and the effects of oxidation and glutathionylation. The assigned backbone chemical shifts will be useful for future endeavours aimed at completing the structure of the dimeric form of the protein using TROSY-based methods or deuterated samples.

Although assignment of the side chain resonances was not achieved due to the poor sensitivity of HC(C)H-TOCSY spectra, we were able to assign the highly downfield-shifted resonance at -0.5 ppm, which served as a useful marker for the homodimeric state (see below).

NMR studies suggested from an early stage that at pH 6 *Xv*Prx2 is a mixture of two different isoforms, which were slow exchange on the NMR timescale. At pH ≤ 5.5 one of the two predominated almost completely and at pH ≥ 7 the other predominated almost completely. Subsequent studies using non-denaturing mass spectrometry and analytical size exclusion chromatography showed that the high pH isoform corresponded to the homodimer and the low pH isoform to the monomer. Attempts to assign the ^{15}N-HSQC of the monomer at pH 5.0 were frustrated by the poor stability of the protein at this pH, which precipitated out of solution within a few hours at 25 °C as a result of which complete chemical shift perturbation analysis of the monomer/dimer switch was not possible.

Analysis of size exclusion data (Fig 4.23) suggested that it was consistent with ionisation of a single group with a pK_a in the vicinity of 6. Analysis of a homology model of *Xv*Prx2 based on the structure of PrxD from *Populus tremula* revealed the presence of His55 close to the peroxidatic cysteine (C_P). His55 is conserved in all members of the Prx5 subfamily and the same position is typically occupied by glutamic acid or glutamine in other Prx subfamilies. His55 had previously been identified as participating in the network of hydrogen bonds around Arg129 which is responsible for stabilising the α_2-helix and pulling it in towards the 5-stranded β-sheet at the core of the protein. Since the side-chain $N^{\delta 1}$ of His55 is only able to accept a

hydrogen bond when it is deprotonated (i.e. below its pKa, which is in the region of 6.5) our data implies that breaking of this hydrogen bond is responsible for the loss of structure in the α_2-helix at low pH and the resulting breaking of the homodimer.

In order to test the model we generated a mutant form of the protein by replacing His55 by alanine. As expected the H55A mutant remained monomeric at higher pH values than the wild type, as determined by size exclusion chromatography and NMR (Figs. 5.4 and 5.5A). To our surprise, however, the homodimer was reformed at pH values above 8. Since the only residue in the vicinity with the pK_a in this region is Cys51, the peroxidatic cysteine, we speculated that the proposed hydrogen bond accepted by the thiolate group of Cys51 from Arg129 may be responsible for re-formation of the α_2-helix at pH ≥ 8 when the thiol group of Cys51 is ionised. However when we replaced Cys51 by serine the dimeric form of the mutant was found to be stable at even lower pH values than the wild type. With hindsight it would possibly have been preferable to have generated the double mutant H55A-C51S or H55A-C51A in order to judge the effects of both H55 and C51 on the stability of the dimeric form of *Xv*Prx2.

Oxidation of XvPrx2 and its effect on the oligomeric state of the protein

We investigated oxidation of *Xv*Prx2 by H_2O_2 and its effect on the oligomeric state of the protein. The protein readily became oxidised into the sulphinic (*Xv*Prx2-SO_2H) acid form but we were unable to observe the singly oxidised form of the protein at various concentrations of H_2O_2 despite the co-existence of the non-oxidised and doubly oxidised forms of the protein (Figs. 5.11B and C). 1D NMR showed that the peaks at -0.5 ppm and 11.1 ppm, which had previously been identified as markers for the

homodimeric state, were absent from the oxidised sample, suggesting that it may be monomeric. However although the ^{15}N-HSQC spectrum of the oxidised sample was very different from that of the un-oxidised sample, it was qualitatively more similar to the spectrum seen at pH 8 than to that seen at pH 5, suggesting that the protein was still homodimeric. In SEC both oxidised and non-oxidised samples eluted at the same volume, consistent with the dimeric configuration.

We conclude from the above that oxidation does not affect the homodimeric state of *Xv*Prx2 at pH 7. However the widespread changes seen in the ^{15}N-HSQC do suggest significant structural re-arrangement. The NMR resonance at -0.5 ppm is diagnostic of the α_2-helix packing against to the central β-sheet of the protein; its absence suggests that the α_2-helix becomes unfolded when the protein is oxidised. However, unlike in the case of glutathionylation, oxidation does not appear to induce the dissociation of the non-covalent homodimer.

Previous reports on the effect of oxidation on two Prx5 subfamily members, human Prx5 and alkylhydroperoxide reductase from *Saccharomyces cerevisiae*, both of which are 2-Cys peroxiredoxins and form either intermolecular or intramolecular disulphide bonds during their reaction cycle, showed that oxidation did not affect the oligomeric state of these proteins. Our work provides the first report of a similar effect involving a 1-Cys member of the Prx5 subfamily.

Attempts to reduce the oxidised protein directly using DTT were only partially successful; small amounts of DTT partially reversed H_2O_2-induced changes to the ^{15}N-HSQC spectrum, but even larger amounts of DTT were unable to completely

regenerate the spectrum. It is possible that this is due to the fact that large amounts of H_2O_2 were used to oxidize the protein, which are likely to have over-oxidised it to the sulphinic acid form. However, in combination with reduced glutathione, DTT was able to completely regenerate even over-oxidised protein, completely restoring the ^{15}N-HSQC of the un-oxidised protein (see below).

Glutathionylation of XvPrx2 and its effect on the oligomeric state of the protein

We investigated the direct glutathionylation of *Xv*Prx2 through two independent routes. The first involved the incubation of reduced *Xv*Prx2 with oxidised glutathione (GSSG) and the second involved the incubation of oxidised *Xv*Prx2 with reduced glutathione (GSH).

Denaturing MS following incubation of *Xv*Prx2 with GSSG showed an increase in the size of the protein by 306 Da, indicative of covalent attachment of a single GS molecule; i.e glutathionylation. Interestingly, non-denaturing MS revealed additional species with +3GS and +5GS, corresponding to non-covalent attachment of one and two GSSG molecules respectively. 1D NMR showed the complete disappearance of the resonances at -0.5 ppm and 11.1 ppm (Fig 5.18B), which had previously been identified as markers of the dimeric state, indicating that the glutathionylated *Xv*Prx2 is monomeric. In support of this conclusion, at pH 7 the ^{15}N-HSQC spectrum of glutathionylated *Xv*Prx2 overlaid almost perfectly with the H55A mutant at pH 7 and reasonably well the non-glutathionylated spectrum at pH 5, both of which have been shown to be monomeric.

As predicted by Noguera-Mazon and co-workers, incubation of oxidised *Xv*Prx2 with

GSH yielded the same result as incubation of reduced *Xv*Prx2 with GSSG: glutathionylation of the peroxidatic cysteine. What was surprising was that GSH was able to glutathionylate over-oxidised *Xv*Prx2, which was the only oxidized state that we were able to observe using mass spectrometry.

Incubation of glutathionylated *Xv*Prx2 with DTT completely regenerated the protein, yielding a ^{15}N-HSQC spectrum undistinguishable from the original. The implication is that even over-oxidised *Xv*Prx2 may be regenerated by the combined action of reduced glutathione (GSH) and DTT. This is in contrast to other Prxs such as members of the Prx6 subfamily which require πGST to facilitate the access of GSH to the catalytic cysteine, or other Prxs reported to require sulferodoxins for the regeneration of over-oxidised C_PS.

Since DTT is not present under physiological condition, another agent must be responsible for reduction of the disulphide bond between glutathione and *Xv*Prx2. Glutaredoxin has been proposed as a likely candidate. Further investigations will be required to test this hypothesis.

Likely biological significance of this work

The biological significance of the pH-dependent change in the oligomeric state of *Xv*Prx2 remains unclear at this time. However, given that previous work revealed the presence of multiple homologues of *Xv*Prx2 in *X. viscosa* (Govender, 2006) which may be localized to different cellular compartments with varying pH requirements, it is possible that the protein may need to adopt different structures as a function of pH to access and remain functional within such compartments.

6.2 Future outlook

Investigation of the role of homodimerisation in the activity of XvPrx2

The Prx5 subfamily of peroxiredoxins are considered obligate homodimers that have only been reported to exist as monomers following the attachment of a glutathione molecule to the catalytic cysteine (Noguera-Mazon*, et al.*, 2006b). The importance of homodimerization for the activity of the protein has not been investigated up to now, presumably because monomeric forms of the protein with intact catalytic cysteine have not been available. Our own attempts to investigate the interface by chemical shift perturbation analysis were frustrated by the fact that the monomeric form at pH 5 was too unstable for assignment of the ^{15}N-HSQC to be completed. The H55A mutant reported in this thesis, which is monomeric and apparently stable at pH 7, may provide a useful opportunities for structural and functional studies, as discussed below.

Determination of the monomeric structure of XvPrx2

A recent review of peroxiredoxins has highlighted the fact that no monomeric structure of a 1-Cys member of the Prx5 is currently available, and the importance of such a structure for understanding the role of oligomerisation in the activity of the enzyme (Hall*, et al.*, 2011). The H55A mutant reported here should be ideal for structure determination by NMR as the ^{15}N-HSQC exhibits narrower bandwidths than the wild type and is stable for many weeks at 25 °C. Crystallization should also be attempted.

The first milestone would be backbone assignment of the H55A at both pH 6, at which it is monomeric and at pH 9, at which it is dimeric, from which the dimerisation interface could be mapped using chemical shift perturbation.

Investigation of the complete reaction cycle of XvPrx2

In this thesis we have shown that *Xv*Prx2 can reduce H_2O_2, becoming oxidized itself in the process, following which a combination of GSH and DTT is able to regenerate the enzyme. It should therefore be possible to set up a continuous reaction in which a large amount of H_2O_2 is reduced by a small amount of *Xv*Prx2. Kinetic studies could be carried out to determine kinetic parameters such as the V_{MAX} and K_M, monitoring the decrease in the amount of H_2O_2 using a colourimetric assay.

Since DTT is not a physiologically-relevant electron donor, attempts should be made to determine the physiological electron donor. Glutaredoxin, as proposed by Noguera-Mazon and co-workers (Noguera-Mazon*, et al.*, 2006b) is a promising candidate which reduces protein-glutathione disulphides by itself becoming oxidized, which involves the formation of an inter-molecular disulphide bond. Oxidised glutaredoxin is regenerated by GSH (reduced glutathione), yielding GSSG (oxidised glutathione). Finally, GSSG is reduced to GSH by glutathione reductase in conjunction with the oxidation of NADPH to $NADP^+$. Hence enzymatic assays to reduce H_2O_2 could be carried out in the presence of glutaredoxin, GSH, glutathione reductase and NADPH, monitoring the decrease in the absorbance of NADPH at 340 nm (Rouhier*, et al.*, 2002).

References

Andersen, J. F., Sanders, D. A., Gasdaska, J. R., Weichsel, A., Powis, G., & Montfort, W. R. (1997). Human thioredoxin homodimers: regulation by pH, role of aspartate 60, and crystal structure of the aspartate 60 --> asparagine mutant. *Biochemistry, 36*(46), 13979-13988.

Baier, M., & Dietz, K. J. (1997). The plant 2-Cys peroxiredoxin BAS1 is a nuclear-encoded chloroplast protein: its expressional regulation, phylogenetic origin, and implications for its specific physiological function in plants. *Plant J, 12*(1), 179-190.

Baker, L. M. S., & Poole, L. B. (2003). Catalytic Mechanism of Thiol Peroxidase from Escherichia coli. SULFENIC ACID FORMATION AND OVEROXIDATION OF ESSENTIAL CYS61. *J. Biol. Chem., 278*(11), 9203-9211.

Banmeyer, I., Marchand, C., Clippe, A., & Knoops, B. (2005). Human mitochondrial peroxiredoxin 5 protects from mitochondrial DNA damages induced by hydrogen peroxide. *FEBS Lett, 579*(11), 2327-2333.

Barranco-Medina, S., Lazaro, J. J., & Dietz, K. J. (2009). The oligomeric conformation of peroxiredoxins links redox state to function. *FEBS Lett, 583*(12), 1809-1816.

Bax, A., & Ikura, M. (1991). An efficient 3D NMR technique for correlating the proton and 15N backbone amide resonances with the alpha-carbon of the preceding residue in uniformly 15N/13C enriched proteins. *J Biomol NMR, 1*(1), 99-104.

Birnboim, H. C., & Doly, J. (1979). A rapid alkaline extraction procedure for screening recombinant plasmid DNA. *Nucleic Acids Res, 7*(6), 1513-1523.

Biteau, B., Labarre, J., & Toledano, M. B. (2003). ATP-dependent reduction of cysteine-sulphinic acid by S. cerevisiae sulphiredoxin. *Nature, 425*(6961), 980-984.

Bradford, M. M. (1976). A rapid and sensitive method for the quantitation of microgram quantities of protein utilizing the principle of protein-dye binding. *Anal Biochem, 72*, 248-254.

Bray, E. A. (1997). Plants response to water deficit. *Trends Plant Sci, 2*, 48-54.

Bystrova, M. F., Budanova, E. N., Novoselov, V. I., & Fesenko, E. E. (2007). [Study of the quaternary structure of rat 1-Cys peroxiredoxin]. *Biofizika, 52*(3), 436-442.

Cao, Z., Tavender, T. J., Roszak, A. W., Cogdell, R. J., & Bulleid, N. J. (2011). Crystal structure of reduced and of oxidized peroxiredoxin IV enzyme reveals a stable oxidized decamer and a non-disulfide-bonded intermediate in the catalytic cycle. *J Biol Chem, 286*(49), 42257-42266.

Cavanagh, J. (1996). 'Protein NMR spectroscopy: principles and practice.' (Academic Press: San Diego).

Chauhan, R., & Mande, S. C. (2001). Characterization of the Mycobacterium tuberculosis H37Rv alkyl hydroperoxidase AhpC points to the importance of ionic interactions in oligomerization and activity. *Biochem J, 354*(Pt 1), 209-215.

Choi, H. J., Kang, S. W., Yang, C. H., Rhee, S. G., & Ryu, S. E. (1998). Crystal structure of a novel human peroxidase enzyme at 2.0 A resolution. *Nat Struct Biol, 5*(5), 400-406.

Choi, J., Choi, S., Cha, M. K., Kim, I. H., & Shin, W. (2003). Crystal structure of Escherichia coli thiol peroxidase in the oxidized state: insights into intramolecular disulfide formation and substrate binding in atypical 2-Cys peroxiredoxins. *J Biol Chem, 278*(49), 49478-49486.

Clark, J. M. (1988). Novel non-templated nucleotide addition reactions catalyzed by procaryotic and eucaryotic DNA polymerases. *Nucleic Acids Research, 16*(20), 9677-9686.

Cole, S. T., & Barrell, B. G. (1998). Genetics and TuberculosisNovartis Foundation Symp. 217 (pp. 160-172).

D'Ambrosio, K., Limauro, D., Pedone, E., Galdi, I., Pedone, C., Bartolucci, S., & De Simone, G. (2009). Insights into the catalytic mechanism of the Bcp family: Functional and structural analysis of Bcp1 from Sulfolobus solfataricus. *Proteins: Structure, Function, and Bioinformatics, 76*(4), 995-1006.

Declercq, J.-P., Evrard, C., Clippe, A., Stricht, D. V., Bernard, A., & Knoops, B. (2001). Crystal structure of human peroxiredoxin 5, a novel type of mammalian peroxiredoxin at 1.5 Å resolution. *Journal of Molecular Biology, 311*(4), 751-759.

Dietz, K. J. (2003). Plant peroxiredoxins. *Annu Rev Plant Biol, 54*, 93-107.

Dietz, K. J. (2011). Peroxiredoxins in plant and Cyanobacteria. *Antioxid Redox Signal., 15*(4), 1129-1159.

Dietz, K. J., Horling, F., Konig, J., & Baier, M. (2002). The function of the chloroplast 2-cysteine peroxiredoxin in peroxide detoxification and its regulation. *J Exp Bot, 53*(372), 1321-1329.

Dietz, K. J., Jacob, S., Oelze, M. L., Laxa, M., Tognetti, V., de Miranda, S. M., Baier, M., & Finkemeier, I. (2006). The function of peroxiredoxins in plant organelle redox metabolism. *J Exp Bot, 57*(8), 1697-1709.

Echalier, A., Trivelli, X., Corbier, C., Rouhier, N., Walker, O., Tsan, P., Jacquot, J. P., Aubry, A., Krimm, I., & Lancelin, J. M. (2005). Crystal structure and solution NMR dynamics of a D (type II) peroxiredoxin glutaredoxin and thioredoxin

dependent: a new insight into the peroxiredoxin oligomerism. *Biochemistry, 44*(6), 1755-1767.

Edgar, R. C. (2004). MUSCLE: multiple sequence alignment with high accuracy and high throughput. *Nucleic Acids Research, 32*(5), 1792-1797.

Evrard, C., Capron, A., Marchand, C. c., Clippe, A., Wattiez, R., Soumillion, P., Knoops, B., & Declercq, J.-P. (2004). Crystal Structure of a Dimeric Oxidized form of Human Peroxiredoxin 5. *Journal of Molecular Biology, 337*(5), 1079-1090.

Farmer, B. T., 2nd, Venters, R. A., Spicer, L. D., Wittekind, M. G., & Muller, L. (1992). A refocused and optimized HNCA: increased sensitivity and resolution in large macromolecules. *J Biomol NMR, 2*(2), 195-202.

Finkel, T. (1998). Oxygen radicals and signaling. *Curr Opin Cell Biol, 10*(2), 248-253.

Gallogly, M. M., & Mieyal, J. J. (2007). Mechanisms of reversible protein glutathionylation in redox signaling and oxidative stress. *Current Opinion in Pharmacology, 7*(4), 381-391.

Goldmark, P. J., Curry, J., Morris, C. F., & Walker-Simmons, M. K. (1992). Cloning and expression of an embryo-specific mRNA up-regulated in hydrated dormant seeds. *Plant Mol Biol, 19*(3), 433-441.

Govender, K. (2006). Characterisation of XvPrx2, a type II peroxiredoxin isolated from the resurrection plant

Xerophyta viscosa (Baker). *Ph.D. thesis, University of Cape Town*.

Grzesiek, S., & Bax, A. (1992). Correlating backbone amide and side chain resonances in larger proteins by multiple relayed triple resonance NMR. *Journal of the American Chemical Society, 114*(16), 6291-6293.

Hall, A., Karplus, P. A., & Poole, L. B. (2009a). Typical 2-Cys peroxiredoxins--structures, mechanisms and functions. *FEBS J, 276*(9), 2469-2477.

Hall, A., Nelson, K., Poole, L. B., & Karplus, P. A. (2011). Structure-based insights into the catalytic power and conformational dexterity of peroxiredoxins. *Antioxid Redox Signal, 15*(3), 795-815.

Hall, A., Parsonage, D., Poole, L. B., & Karplus, P. A. (2010). Structural evidence that peroxiredoxin catalytic power is based on transition-state stabilization. *J Mol Biol, 402*(1), 194-209.

Hall, A., Sankaran, B., Poole, L. B., & Karplus, P. A. (2009b). Structural changes common to catalysis in the Tpx peroxiredoxin subfamily. *J Mol Biol, 393*(4), 867-881.

Hanefeld, U., Stranzl, G., Straathof, A. J., Heijnen, J. J., Bergmann, A., Mittelbach, R., Glatter, O., & Kratky, C. (2001). Electrospray ionization mass spectrometry,

circular dichroism and SAXS studies of the (S)-hydroxynitrile lyase from Hevea brasiliensis. *Biochim Biophys Acta, 1544*(1-2), 133-142.

Hofmann, B., Hecht, H. J., & Flohe, L. (2002). Peroxiredoxins. *Biol Chem, 383*(3-4), 347-364.

Holm, L., & Park, J. (2000). DaliLite workbench for protein structure comparison. *Bioinformatics, 16*(6), 566-567.

Jeong, W., Cha, M.-K., & Kim, I.-H. (2000). Thioredoxin-dependent Hydroperoxide Peroxidase Activity of Bacterioferritin Comigratory Protein (BCP) as a New Member of the Thiol-specific Antioxidant Protein (TSA)/Alkyl Hydroperoxide Peroxidase C (AhpC) Family. *Journal of Biological Chemistry, 275*(4), 2924-2930.

Johnson, B. A. (2004). Using NMRView to Visualize and Analyze the NMR Spectra of Macromolecules (Vol. 278, pp. 313-352).

Jonsson, T. J., & Lowther, W. T. (2007). The peroxiredoxin repair proteins. *Subcell Biochem, 44*, 115-141.

Kang, S. W., Chae, H. Z., Seo, M. S., Kim, K., Baines, I. C., & Rhee, S. G. (1998). Mammalian peroxiredoxin isoforms can reduce hydrogen peroxide generated in response to growth factors and tumor necrosis factor-alpha. *J Biol Chem, 273*(11), 6297-6302.

Kashiwagi, T., Yamada, N., Hirayama, K., Suzuki, C., Kashiwagi, Y., Tsuchiya, F., Arata, Y., Kunishima, N., & Morikawa, K. (2000). An electrospray-ionization mass spectrometry analysis of the pH-dependent dissociation and denaturation processes of a heterodimeric protein. *J Am Soc Mass Spectrom, 11*(1), 54-61.

Kay, L. E., Ikura, M., Tschudin, R., & Bax, A. (1990). Three-dimensional triple-resonance NMR Spectroscopy of isotopically enriched proteins. 1990. *J Magn Reson, 213*(2), 423-441.

Kim, K., Kim, I. H., Lee, K. Y., Rhee, S. G., & Stadtman, E. R. (1988). The isolation and purification of a specific "protector" protein which inhibits enzyme inactivation by a thiol/Fe(III)/O2 mixed-function oxidation system. *J Biol Chem, 263*(10), 4704-4711.

Kim, K., Rhee, S. G., & Stadtman, E. R. (1985). Nonenzymatic cleavage of proteins by reactive oxygen species generated by dithiothreitol and iron. *J Biol Chem, 260*(29), 15394-15397.

Kim, S. J., Woo, J. R., Hwang, Y. S., Jeong, D. G., Shin, D. H., Kim, K., & Ryu, S. E. (2003). The tetrameric structure of Haemophilus influenza hybrid Prx5 reveals interactions between electron donor and acceptor proteins. *J Biol Chem, 278*(12), 10790-10798.

Klomsiri, C., Karplus, P. A., & Poole, L. B. (2010). Cysteine-based redox switches in enzymes. *Antioxid Redox Signal, 14*(6), 1065-1077.

Knoops, B., Clippe, A., Bogard, C. d., Arsalane, K., Wattiez, R., Hermans, C. d., Duconseille, E., Falmagne, P., & Bernard, A. (1999). Cloning and Characterization of AOEB166, a Novel Mammalian Antioxidant Enzyme of the Peroxiredoxin Family. *Journal of Biological Chemistry, 274*(43), 30451-30458.

Kong, W., Shiota, S., Shi, Y., Nakayama, H., & Nakayama, K. (2000). A novel peroxiredoxin of the plant Sedum lineare is a homologue of Escherichia coli bacterioferritin co-migratory protein (Bcp). *Biochem J, 351*(Pt 1), 107-114.

Kristensen, P., Rasmussen, D. E., & Kristensen, B. I. (1999). Properties of thiol-specific anti-oxidant protein or calpromotin in solution. *Biochem Biophys Res Commun, 262*(1), 127-131.

Laemmli, U. K. (1970). Cleavage of Structural Proteins during the Assembly of the Head of Bacteriophage T4. *Nature, 227*(5259), 680-685.

Li, S., Peterson, N. A., Kim, M.-Y., Kim, C.-Y., Hung, L.-W., Yu, M., Lekin, T., Segelke, B. W., Lott, J. S., & Baker, E. N. (2005). Crystal Structure of AhpE from Mycobacterium tuberculosis, a 1-Cys Peroxiredoxin. *Journal of Molecular Biology, 346*(4), 1035-1046.

Lian, F.-M., Yu, J., Ma, X.-X., Yu, X.-J., Chen, Y., & Zhou, C.-Z. (2012). Structural Snapshots of Yeast Alkyl Hydroperoxide Reductase Ahp1 Peroxiredoxin Reveal a Novel Two-cysteine Mechanism of Electron Transfer to Eliminate Reactive Oxygen Species. *Journal of Biological Chemistry, 287*(21), 17077-17087.

Loo, J. A. (1997). Studying noncovalent protein complexes by electrospray ionization mass spectrometry. *Mass Spectrom Rev, 16*(1), 1-23.

Manevich, Y., Feinstein, S. I., & Fisher, A. B. (2004). Activation of the antioxidant enzyme 1-CYS peroxiredoxin requires glutathionylation mediated by heterodimerization with œÄGST. *Proceedings of the National Academy of Sciences of the United States of America, 101*(11), 3780-3785.

Mohan, P. M., Barve, M., Chatterjee, A., & Hosur, R. V. (2006). pH driven conformational dynamics and dimer-to-monomer transition in DLC8. *Protein Sci, 15*(2), 335-342.

Monteiro, G., Horta, B. B., Pimenta, D. C., Augusto, O., & Netto, L. E. S. (2007). Reduction of 1-Cys peroxiredoxins by ascorbate changes the thiol-specific antioxidant paradigm, revealing another function of vitamin C. *Proceedings of the National Academy of Sciences, 104*(12), 4886-4891.

Mowla, S. B., Thomson, J. A., Farrant, J. M., & Mundree, S. G. (2002). A novel stress-inducible antioxidant enzyme identified from the resurrection plant Xerophyta viscosa Baker. *Planta, 215*(5), 716-726.

Nelson, K. J., Knutson, S. T., Soito, L., Klomsiri, C., Poole, L. B., & Fetrow, J. S. (2011). Analysis of the peroxiredoxin family: Using active-site structure and sequence information for global classification and residue analysis. *Proteins: Structure, Function, and Bioinformatics, 79*(3), 947-964.

Nelson, K. J., Parsonage, D., Hall, A., Karplus, P. A., & Poole, L. B. (2008). Cysteine pK(a) values for the bacterial peroxiredoxin AhpC. *Biochemistry, 47*(48), 12860-12868.

Neumann, P. M. (1995). The role of cell wall adjustment in plant resistance to water deficits. *Crop Sci, 35*, 1255-1266.

Noguera-Mazon, V., Krimm, I., Walker, O., & Lancelin, J. M. (2006a). Protein-protein interactions within peroxiredoxin systems. *Photosynth Res, 89*(2-3), 277-290.

Noguera-Mazon, V., Lemoine, J., Walker, O., Rouhier, N., Salvador, A., Jacquot, J. P., Lancelin, J. M., & Krimm, I. (2006b). Glutathionylation induces the dissociation of 1-Cys D-peroxiredoxin non-covalent homodimer. *J Biol Chem, 281*(42), 31736-31742.

Ogusucu, R., Rettori, D., Munhoz, D. C., Netto, L. E., & Augusto, O. (2007). Reactions of yeast thioredoxin peroxidases I and II with hydrogen peroxide and peroxynitrite: rate constants by competitive kinetics. *Free Radic Biol Med, 42*(3), 326-334.

Page, R. D. M. (1996). TREEVIEW: An application to display phylogenetic trees on personal computers. *Computer Applications in the Biosciences, 12*, 357-358.

Parsonage, D., Youngblood, D. S., Sarma, G. N., Wood, Z. A., Karplus, P. A., & Poole, L. B. (2005). Analysis of the link between enzymatic activity and oligomeric state in AhpC, a bacterial peroxiredoxin. *Biochemistry, 44*(31), 10583-10592.

Pedrajas, J. R., Miranda-Vizuete, A., Javanmardy, N., Gustafsson, J.-Ö., & Spyrou, G. (2000). Mitochondria of Saccharomyces cerevisiae Contain One-conserved Cysteine Type Peroxiredoxin with Thioredoxin Peroxidase Activity. *Journal of Biological Chemistry, 275*(21), 16296-16301.

Plishker, G. A., Chevalier, D., Seinsoth, L., & Moore, R. B. (1992). Calcium-activated potassium transport and high molecular weight forms of calpromotin. *J Biol Chem, 267*(30), 21839-21843.

Ralat, L. A., Manevich, Y., Fisher, A. B., & Colman, R. F. (2005). Direct Evidence for the Formation of a Complex between 1-Cysteine Peroxiredoxin and Glutathione S-Transferase with Activity Changes in Both Enzymes,. *Biochemistry, 45*(2), 360-372.

Rehm, T., Huber, R., & Holak, T. A. (2002). Application of NMR in structural proteomics: screening for proteins amenable to structural analysis. *Structure, 10*(12), 1613-1618.

Rhee, S. G., Chae, H. Z., & Kim, K. (2005). Peroxiredoxins: a historical overview and speculative preview of novel mechanisms and emerging concepts in cell signaling. *Free Radic Biol Med, 38*(12), 1543-1552.

Rhee, S. G., Kang, S. W., Chang, T. S., Jeong, W., & Kim, K. (2001). Peroxiredoxin, a novel family of peroxidases. *IUBMB Life, 52*(1-2), 35-41.

Rhee, S. G., Kim, K. H., Chae, H. Z., Yim, M. B., Uchida, K., Netto, L. E., & Stadtman, E. R. (1994). Antioxidant defense mechanisms: a new thiol-specific antioxidant enzyme. *Ann N Y Acad Sci, 738*, 86-92.

Rochus, L. J. K. (2004). The Computer Aided Resonance Assignment Tutorial.

Rouhier, N., Gelhaye, E., Gualberto, J. M., Jordy, M. N., De Fay, E., Hirasawa, M., Duplessis, S., Lemaire, S. D., Frey, P., Martin, F., Manieri, W., Knaff, D. B., & Jacquot, J. P. (2004). Poplar peroxiredoxin Q. A thioredoxin-linked chloroplast antioxidant functional in pathogen defense. *Plant Physiol, 134*(3), 1027-1038.

Rouhier, N., Gelhaye, E., & Jacquot, J.-P. (2002). Exploring the active site of plant glutaredoxin by site-directed mutagenesis. *FEBS Letters, 511*(1,Äì3), 145-149.

Rouhier, N., Gelhaye, E., Sautiere, P. E., Brun, A., Laurent, P., Tagu, D., Gerard, J., de Fay, E., Meyer, Y., & Jacquot, J. P. (2001). Isolation and characterization of a new peroxiredoxin from poplar sieve tubes that uses either glutaredoxin or thioredoxin as a proton donor. *Plant Physiol, 127*(3), 1299-1309.

Rouhier, N., & Jacquot, J. P. (2005). The plant multigenic family of thiol peroxidases. *Free Radic Biol Med, 38*(11), 1413-1421.

Sarma, G. N., Nickel, C., Rahlfs, S., Fischer, M., Becker, K., & Karplus, P. A. (2005). Crystal structure of a novel Plasmodium falciparum 1-Cys peroxiredoxin. *J Mol Biol, 346*(4), 1021-1034.

Schröder, E., Littlechil*, J. A., Lebedev, A. A., Errington, N., Vagin, A. A., & Isupov, M. N. (2000). Crystal structure of decameric 2-Cys peroxiredoxin from human erythrocytes at 1.7 Å resolution. *Structure, 8*(6), 605-615.

Scott, P. (2000). Resurrection Plants and the Secrets of Eternal Leaf. *Annals of Botany, 85*(2), 159-166.

Seo, M. S., Kang, S. W., Kim, K., Baines, I. C., Lee, T. H., & Rhee, S. G. (2000). Identification of a New Type of Mammalian Peroxiredoxin That Forms an Intramolecular Disulfide as a Reaction Intermediate. *Journal of Biological Chemistry, 275*(27), 20346-20354.

Sherwin, H. W., & Farrant, J. M. (1998). Protection mechanisms against excess light in the resurrection plants Craterostigma wilmsii and *Xyrophyta viscosa*. Plant Growth Regul. 24: 203-210. *Plant Growth Regul., 24*, 203-210.

Smeets, A., Loumaye, E., Clippe, A., Rees, J.-F., Knoops, B., & Declercq, J.-P. (2008). The crystal structure of the C45S mutant of annelid Arenicola marina peroxiredoxin 6 supports its assignment to the mechanistically typical 2-Cys subfamily without any formation of toroid-shaped decamers. *Protein Science, 17*(4), 700-710.

Smirnoff, N. (1993). The role of active oxygen in the response of plants to water deficit and desiccation. *New Phytologist, 125*(1), 27-58.

Soito, L., Williamson, C., Knutson, S. T., Fetrow, J. S., Poole, L. B., & Nelson, K. J. (2010). PREX: PeroxiRedoxin classification indEX, a database of subfamily assignments across the diverse peroxiredoxin family. *Nucleic Acids Research*.

Stacy, R. A., Nordeng, T. W., Culianez-Macia, F. A., & Aalen, R. B. (1999). The dormancy-related peroxiredoxin anti-oxidant, PER1, is localized to the nucleus of barley embryo and aleurone cells. *Plant J, 19*(1), 1-8.

Sundaresan, M., Yu, Z. X., Ferrans, V. J., Irani, K., & Finkel, T. (1995). Requirement for generation of H2O2 for platelet-derived growth factor signal transduction. *Science, 270*(5234), 296-299.

Takahashi, M., & Asada, K. (1988). Superoxide production in aprotic interior of chloroplast thylakoids. *Arch Biochem Biophys, 267*(2), 714-722.

Tao, K. (2008). Subcellular localization and in vivo oxidation-reduction kinetics of thiol peroxidase in Escherichia coli. *FEMS Microbiol Lett, 289*(1), 41-45.

Tatusova, T. A., & Madden, T. L. (1999). BLAST 2 Sequences, a new tool for comparing protein and nucleotide sequences. *FEMS Microbiol Lett, 174*(2), 247-250.

Trivelli, X., Krimm, I., Ebel, C., Verdoucq, L., Prouzet-Mauleon, V., Chartier, Y., Tsan, P., Lauquin, G., Meyer, Y., & Lancelin, J. M. (2003b). Characterization of the yeast peroxiredoxin Ahp1 in its reduced active and overoxidized inactive forms using NMR. *Biochemistry, 42*(48), 14139-14149.

Wakita, M., Masuda, S., Motohashi, K., Hisabori, T., Ohta, H., & Takamiya, K.-i. (2007). The Significance of Type II and PrxQ Peroxiredoxins for Antioxidative Stress Response in the Purple Bacterium Rhodobacter sphaeroides. *Journal of Biological Chemistry, 282*(38), 27792-27801.

Wood, Z. A., Poole, L. B., Hantgan, R. R., & Karplus, P. A. (2002). Dimers to doughnuts: redox-sensitive oligomerization of 2-cysteine peroxiredoxins. *Biochemistry, 41*(17), 5493-5504.

Wood, Z. A., Poole, L. B., & Karplus, P. A. (2003a). Peroxiredoxin evolution and the regulation of hydrogen peroxide signaling. *Science, 300*(5619), 650-653.

Wood, Z. A., Schroder, E., Robin Harris, J., & Poole, L. B. (2003b). Structure, mechanism and regulation of peroxiredoxins. *Trends Biochem Sci, 28*(1), 32-40.

Zhang, O., & Forman-Kay, J. D. (1995). Structural characterization of folded and unfolded states of an SH3 domain in equilibrium in aqueous buffer. *Biochemistry, 34*(20), 6784-6794.

Zhou, Y., Wan, X. Y., Wang, H. L., Yan, Z. Y., Hou, Y. D., & Jin, D. Y. (1997). Bacterial scavengase p20 is structurally and functionally related to peroxiredoxins. *Biochem Biophys Res Commun, 233*(3), 848-852.

APPENDICES

APPENDIX I: Alignment of Peroxiredoxin from *Xerophyta viscosa* (Insilco) and sequenced *Xerophyta viscosa* sequence

Identities = 513/513 (100%), Gaps = 0/513 (0%)

Strand = Plus/Minus

```
Query 1    GATGCTGGATCCATGGCTCCGATCGCAGTCGGTGAAACGATCCCAGACGGAACGCTCGGA 60
           ||||||||||||||||||||||||||||||||||||||||||||||||||||||||||||
Sbjct 609  GATGCTGGATCCATGGCTCCGATCGCAGTCGGTGAAACGATCCCAGACGGAACGCTCGGA 550

Query 61   TGGTTCGACGAGAAGGACGAGTTGAAGCAGATCTCGATCCACTCGCTCGCCGCCGGAAAG 120
           ||||||||||||||||||||||||||||||||||||||||||||||||||||||||||||
Sbjct 549  TGGTTCGACGAGAAGGACGAGTTGAAGCAGATCTCGATCCACTCGCTCGCCGCCGGAAAG 490

Query 121  AAGATCGTGCTCATCGGTGTCCCCGGCGCATTCACTCCTACTTGCAGTATGCAACACGTT 180
           ||||||||||||||||||||||||||||||||||||||||||||||||||||||||||||
Sbjct 489  AAGATCGTGCTCATCGGTGTCCCCGGCGCATTCACTCCTACTTGCAGTATGCAACACGTT 430

Query 181  CCAAGTTTCATTGAGAAAGCAGAGGAGCTGAAAGCTAAGGGCGTTGATGAGTTCCTTGTT 240
           ||||||||||||||||||||||||||||||||||||||||||||||||||||||||||||
Sbjct 429  CCAAGTTTCATTGAGAAAGCAGAGGAGCTGAAAGCTAAGGGCGTTGATGAGTTCCTTGTT 370

Query 241  ATTAGTGTTAATGATCCCTTCGTGATGAAGGCTTGGTCGAAAACATATCCTGAGAACAAG 300
           ||||||||||||||||||||||||||||||||||||||||||||||||||||||||||||
Sbjct 369  ATTAGTGTTAATGATCCCTTCGTGATGAAGGCTTGGTCGAAAACATATCCTGAGAACAAG 310

Query 301  CATGTGAAGTTCCTAGCCGATGGATCGGGGAAGTACACCCAAGCTCTTGGCGTGGAACTC 360
           ||||||||||||||||||||||||||||||||||||||||||||||||||||||||||||
Sbjct 309  CATGTGAAGTTCCTAGCCGATGGATCGGGGAAGTACACCCAAGCTCTTGGCGTGGAACTC 250

Query 361  GATCTGTCCGAGAAGGGGCTCGGGCTCCGTTCACGGAGGTTTGCTATCCTTGTAGACGAC 420
           ||||||||||||||||||||||||||||||||||||||||||||||||||||||||||||
Sbjct 249  GATCTGTCCGAGAAGGGGCTCGGGCTCCGTTCACGGAGGTTTGCTATCCTTGTAGACGAC 190

Query 421  TTGAAGGTTAAGGTTGCAAATGTCGAGGAGGGCGGAGCATTTACCATTTCAGGTGCCGAT 480
           ||||||||||||||||||||||||||||||||||||||||||||||||||||||||||||
Sbjct 189  TTGAAGGTTAAGGTTGCAAATGTCGAGGAGGGCGGAGCATTTACCATTTCAGGTGCCGAT 130

Query 481  GAGATCTTGAAGGCAGTCTAGCTCGAGGTCTTC 513
           |||||||||||||||||||||||||||||||||
Sbjct 129  GAGATCTTGAAGGCAGTCTAGCTCGAGGTCTTC 97
```

Identities = 513/513 (100%), Gaps = 0/513 (0%)

Strand=Plus/Plus

```
Query 1    GATGCTGGATCCATGGCTCCGATCGCAGTCGGTGAAACGATCCCAGACGGAACGCTCGGA 60
           ||||||||||||||||||||||||||||||||||||||||||||||||||||||||||||
Sbjct 119  GATGCTGGATCCATGGCTCCGATCGCAGTCGGTGAAACGATCCCAGACGGAACGCTCGGA 178

Query 61   TGGTTCGACGAGAAGGACGAGTTGAAGCAGATCTCGATCCACTCGCTCGCCGCCGGAAAG 120
           ||||||||||||||||||||||||||||||||||||||||||||||||||||||||||||
Sbjct 179  TGGTTCGACGAGAAGGACGAGTTGAAGCAGATCTCGATCCACTCGCTCGCCGCCGGAAAG 238

Query 121  AAGATCGTGCTCATCGGTGTCCCCGGCGCATTCACTCCTACTTGCAGTATGCAACACGTT 180
           ||||||||||||||||||||||||||||||||||||||||||||||||||||||||||||
Sbjct 239  AAGATCGTGCTCATCGGTGTCCCCGGCGCATTCACTCCTACTTGCAGTATGCAACACGTT 298
```

```
Query 181  CCAAGTTTCATTGAGAAAGCAGAGGAGCTGAAAGCTAAGGGCGTTGATGAGTTCCTTGTT  240
           ||||||||||||||||||||||||||||||||||||||||||||||||||||||||||||
Sbjct 299  CCAAGTTTCATTGAGAAAGCAGAGGAGCTGAAAGCTAAGGGCGTTGATGAGTTCCTTGTT  358

Query 241  ATTAGTGTTAATGATCCCTTCGTGATGAAGGCTTGGTCGAAAACATATCCTGAGAACAAG  300
           ||||||||||||||||||||||||||||||||||||||||||||||||||||||||||||
Sbjct 359  ATTAGTGTTAATGATCCCTTCGTGATGAAGGCTTGGTCGAAAACATATCCTGAGAACAAG  418

Query 301  CATGTGAAGTTCCTAGCCGATGGATCGGGGAAGTACACCCAAGCTCTTGGCGTGGAACTC  360
           ||||||||||||||||||||||||||||||||||||||||||||||||||||||||||||
Sbjct 419  CATGTGAAGTTCCTAGCCGATGGATCGGGGAAGTACACCCAAGCTCTTGGCGTGGAACTC  478

Query  361 GATCTGTCCGAGAAGGGGCTCGGGCTCCGTTCACGGAGGTTTGCTATCCTTGTAGACGAC  420
           ||||||||||||||||||||||||||||||||||||||||||||||||||||||||||||
Sbjct  479 GATCTGTCCGAGAAGGGGCTCGGGCTCCGTTCACGGAGGTTTGCTATCCTTGTAGACGAC  538

Query  421 TTGAAGGTTAAGGTTGCAAATGTCGAGGAGGGCGGAGCATTTACCATTTCAGGTGCCGAT  480
           ||||||||||||||||||||||||||||||||||||||||||||||||||||||||||||
Sbjct  539 TTGAAGGTTAAGGTTGCAAATGTCGAGGAGGGCGGAGCATTTACCATTTCAGGTGCCGAT  598

Query  481 GAGATCTTGAAGGCAGTCTAGCTCGAGGTCTTC  513
           |||||||||||||||||||||||||||||||||
Sbjct  599 GAGATCTTGAAGGCAGTCTAGCTCGAGGTCTTC  631
```

Restriction sites are highlighted in red, GGATCC- BamHI and CTCGAG- XhoI. “Query” denotes the expected sequence, and “Sbjct” denotes the experimental sequence determined by sequencing. A comparison of the expected sequence against the Plus and Minus strands of the experimental sequence showed that the experimental sequence matched a 100 percent to the expected sequence.

APPENDIX II: Analysis of effect of pH on size exclusion volume

1. We assume that a purely monomeric sample of the protein elutes at volume Ve^m, and a purely homodimeric sample elutes at Ve^d. A mixture of monomeric and homodimeric molecules will elute at an intermediate volume Ve.
2. We assume that an individual protein molecule interchanges rapidly between the monomeric and homodimeric forms, spending a fraction α of its time in the monomeric state and $1-\alpha$ in the homodimeric state $0 \le \alpha \le 1$, then Ve should be given by the expression:

$$Ve = \alpha Ve^m + (1-\alpha)Ve^d$$

3. The above expression can be re-written as

$$Ve = Ve^d + \alpha\left(Ve^m - Ve^d\right) \qquad 0 \le \alpha \le 1$$

which states that the fractional shift in the peak is given by the monomeric fraction α.

4. We assume that there is a single ionisable group in the interface and that the dimer can only form when the group is ionized. This is equivalent to saying that α, the monomeric fraction, also corresponds to the fraction of molecules that are protonated.
5. If we represent the protonated state as HA and the ionized state as A^-, then

$$HA \leftrightarrow H^+ + A^-$$

from which the Henderson Hasselbach equations follows:

$$pH = pKa + \log_{10}\frac{\left[A^-\right]}{\left[HA\right]}$$

Re-arranging gives:

$$\frac{[A^-]}{[HA]} = 10^{pH-pka}$$

6. Since α corresponds to the protonated fraction,

$$\alpha = \frac{[HA]}{[HA]+[A^-]} = \frac{1}{1+[A^-]/[HA]} = \frac{1}{1+10^{pH-pKa}}$$

and we finally have that:

$$Ve = Ve^d + \frac{Ve^m - Ve^d}{1+10^{pH-pKa}} \quad .$$

7. This expresses the elution volume Ve as a function of pH, with unknown parameters Ve^d, Ve^m and pKa. Fitting the expression to an experimentally-determined graph of Ve as a function of pH will allow the values of Ve^d, Ve^m and pKa to be extracted.

APPENDIX III: Prediction of protein parameters

Parameters for *Xv*Prx2

Protparam user-provided sequence:

```
        10         20         30         40         50         60
GPLGSMAPIA VGETIPDGTL GWFDEKDELK QISIHSLAAG KKIVLIGVPG AFTPTCSMQH

        70         80         90        100        110        120
VPSFIEKAEE LKAKGVDEFL VISVNDPFVM KAWSKTYPEN KHVKFLADGS GKYTQALGVE

       130        140        150        160
LDLSEKGLGL RSRRFAILVD DLKVKVANVE EGGAFTISGA DEILKAV
```

Number of amino acids: 167

Molecular weight: 17898.6

Theoretical pI: 5.43

Amino acid composition:

```
Ala(A)15    9.0%  Arg(R)3     1.8%  Asn(N)3     1.8%  Asp(D)10    6.0%
Cys(C)1     0.6%  Gln(Q)3     1.8%  Glu(E)13    7.8%  Gly(G)17   10.2%
His(H)3     1.8%  Ile(I)11    6.6%  Leu(L)16    9.6%  Lys(K)16    9.6%
Met(M)3     1.8%  Phe(F)8     4.8%  Pro(P)8     4.8%  Ser(S)11    6.6%
Thr(T)7     4.2%  Trp(W)2     1.2%  Tyr(Y)2     1.2%  Val(V)15    9.0%
Pyl(O)0     0.0%  Sec(U)0     0.0%  (B)0  0.0% (Z)0   0.0% (X)0  0.0%
```

Total number of negatively charged residues (Asp + Glu): 23
Total number of positively charged residues (Arg + Lys): 19

Atomic composition:

Carbon	C	811
Hydrogen	H	1294
Nitrogen	N	206
Oxygen	O	240
Sulfur	S	4

Formula: $C_{811}H_{1294}N_{206}O_{240}S_4$
Total number of atoms: 2555

Extinction coefficients:

Extinction coefficients are in units of M^{-1} cm^{-1}, at 280 nm measured in water.

Ext. coefficient13980
Abs 0.1% (=1 g/l) 0.781, assuming all pairs of Cys residues form cystines

Ext. coefficient13980
Abs 0.1% (=1 g/l) 0.781, assuming all Cys residues are reduced

Estimated half-life:

The N-terminal of the sequence considered is G (Gly).

The estimated half-life is: 30 hours (mammalian reticulocytes, in vitro).
>20 hours (yeast, in vivo).
>10 hours (Escherichia coli, in vivo).

Instability index:

The instability index (II) is computed to be 29.24
This classifies the protein as stable.

Aliphatic index: 98.08

Grand average of hydropathicity (GRAVY): 0.037

APPENDIX IV: *Xv*Prx2 Chemical shifts

Residue number	Residue name	Atom name	Chemical shift
1	M	CA	55.90
1	M	CB	33.46
2	A	N	126.62
2	A	HN	31.95
2	A	CA	50.96
2	A	CB	19.39
3	P	CA	63.45
3	P	CB	32.74
4	I	N	121.04
4	I	HN	7.51
4	I	CA	61.13
4	I	CB	38.99
5	A	N	127.80
5	A	HN	47.82
5	A	CA	50.51
5	A	CB	22.50
6	V	N	118.92
6	V	HN	8.13
6	V	CA	65.32
6	V	CB	32.06
7	G	N	111.14
7	G	HN	9.21
7	G	CA	45.22
8	E	N	120.90
8	E	HN	7.92
8	E	CA	56.45
8	E	CB	30.99
9	T	N	119.02
9	T	HN	8.76
9	T	CA	62.23
9	T	CB	70.21
10	I	N	124.77
10	I	HN	8.94
10	I	CA	59.23
10	I	CB	38.62
11	P	CA	63.00
11	P	CB	31.85
12	D	N	122.19
12	D	HN	8.65
12	D	CA	52.78
12	D	CB	41.15
13	G	N	109.72
13	G	HN	8.55
13	G	CA	45.91
14	T	N	115.08
14	T	HN	8.37
14	T	CA	60.11
14	T	CB	70.74
15	L	N	128.89
15	L	HN	9.24
15	L	CA	54.216
15	L	CB	46.093

Residue number	Residue name	Atom name	Chemical shift
16	G	N	107.95
16	G	HN	8.84
16	G	CA	45.67
17	W	N	126.63
17	W	HN	9.13
17	W	CA	58.11
17	W	CB	32.77
18	F	N	128.16
18	F	HN	8.42
18	F	CA	58.68
18	F	CB	40.83
19	D	N	124.93
19	D	HN	8.20
19	D	CA	52.35
19	D	CB	42.69
20	E	N	117.49
20	E	HN	9.18
20	E	CA	59.37
20	E	CB	28.78
21	K	N	122.05
21	K	HN	8.34
21	K	CA	55.83
21	K	CB	32.01
22	D	N	118.19
22	D	HN	8.48
22	D	CA	56.51
22	D	CB	40.05
23	E	N	120.06
23	E	HN	8.49
23	E	CA	55.89
23	E	CB	31.49
24	L	N	126.87
24	L	HN	8.49
24	L	CA	55.71
24	L	CB	40.75
25	K	N	130.76
25	K	HN	9.31
25	K	CA	53.94
25	K	CB	35.26
26	Q	N	120.72
26	Q	HN	8.40
26	Q	CA	54.59
26	Q	CB	29.14
27	I	N	124.95
27	I	HN	9.36
27	I	CA	59.17
27	I	CB	41.40
28	S	N	121.09
28	S	HN	8.49
28	S	CA	55.98
28	S	CB	64.08
29	I	N	129.54
29	I	HN	8.59
29	I	CA	63.28

Residue number	Residue name	Atom name	Chemical shift
29	I	CB	37.32
30	H	N	120.85
30	H	HN	9.15
30	H	CA	60.45
30	H	CB	31.40
31	S	N	115.30
31	S	HN	7.91
31	S	CA	61.88
31	S	CB	63.22
32	L	N	121.82
32	L	HN	7.50
32	L	CA	56.87
32	L	CB	43.91
33	A	N	118.21
33	A	HN	8.24
33	A	CA	53.25
33	A	CB	21.47
34	A	N	124.37
34	A	HN	7.95
34	A	CA	55.08
34	A	CB	18.17
35	G	N	112.22
35	G	HN	9.54
35	G	CA	46.51
36	K	N	118.68
36	K	HN	7.75
36	K	CA	55.19
36	K	CB	38.09
37	K	N	124.52
37	K	HN	9.46
37	K	CA	56.12
37	K	CB	33.73
38	I	N	118.57
38	I	HN	9.32
38	I	CA	58.38
38	I	CB	42.80
39	V	N	121.58
39	V	HN	8.24
39	V	CA	60.09
39	V	CB	35.10
40	L	N	128.14
40	L	HN	9.39
40	L	CA	53.83
40	L	CB	44.64
41	I	N	129.45
41	I	HN	9.47
41	I	CA	60.79
41	I	CB	39.47
42	G	N	119.30
42	G	HN	8.04
42	G	CA	44.74
43	V	N	114.34
43	V	HN	8.02
43	V	CA	56.962

Residue number	Residue name	Atom name	Chemical shift
43	V	CB	33.46
44	P	CA	64.57
44	P	CB	33.27
45	G	N	108.25
45	G	HN	8.88
45	G	CA	48.88
46	A	N	129.32
46	A	HN	7.92
46	A	CA	52.16
46	A	CB	19.92
47	F	N	129.47
47	F	CA	63.22
47	F	CB	36.04
48	T	N	113.73
48	T	HN	7.49
48	T	CA	62.23
48	T	CB	66.98
49	P	CA	65.10
49	P	CB	32.79
50	T	N	111.27
50	T	HN	8.30
50	T	CA	61.15
50	T	CB	64.79
51	C	N	116.91
51	C	HN	8.91
51	C	CA	56.86
51	C	CB	33.99
57	P	CA	66.84
57	P	CB	31.58
58	S	N	112.96
58	S	HN	7.25
58	S	CA	62.39
58	S	CB	63.60
59	F	N	118.27
59	F	HN	7.39
59	F	CA	63.16
59	F	CB	40.70
60	I	N	119.83
60	I	HN	7.80
60	I	CA	66.26
60	I	CB	38.08
61	E	N	118.27
61	E	HN	8.51
61	E	CA	59.46
61	E	CB	30.21
62	K	N	115.12
62	K	HN	7.06
62	K	CA	55.05
62	K	CB	32.97
63	A	N	125.30
63	A	HN	7.51
63	A	CA	56.89
63	A	CB	18.40
64	E	N	116.46

Residue number	Residue name	Atom name	Chemical shift
64	E	HN	8.68
64	E	CA	60.61
64	E	CB	29.17
65	E	N	122.96
65	E	HN	8.13
65	E	CA	60.04
66	L	N	120.15
66	L	HN	8.42
66	L	CA	59.09
66	L	CB	43.03
67	K	N	123.78
67	K	HN	9.29
67	K	CA	45.89
68	A	N	123.63
68	A	HN	8.02
68	A	CA	54.88
68	A	CB	18.30
69	K	N	117.37
69	K	HN	7.47
69	K	CA	56.20
69	K	CB	33.19
70	G	N	106.85
70	G	HN	7.90
70	G	CA	45.92
71	V	N	121.63
71	V	HN	7.97
71	V	CA	47.59
72	D	N	125.30
72	D	HN	8.99
72	D	CA	57.52
72	D	CB	45.66
73	E	N	112.86
73	E	HN	6.77
73	E	CA	54.40
73	E	CB	33.86
74	F	N	122.43
74	F	HN	9.51
74	F	CA	56.29
74	F	CB	41.99
75	L	N	123.81
75	L	HN	8.81
75	L	CA	53.10
76	V	N	127.50
76	V	HN	9.00
76	V	CA	61.50
76	V	CB	32.23
77	I	N	128.33
77	I	HN	9.29
77	I	CA	60.59
77	I	CB	41.34
78	S	N	115.82
78	S	HN	7.41
78	S	CA	56.24
78	S	CB	66.03

Residue number	Residue name	Atom name	Chemical shift
79	V	N	132.70
79	V	HN	9.73
79	V	CA	61.31
79	V	CB	29.30
80	N	N	122.32
80	N	HN	8.26
80	N	CA	53.99
81	D	N	115.01
81	D	HN	8.12
82	P	CA	65.78
82	P	CB	32.72
83	F	N	121.03
83	F	HN	8.97
83	F	CA	62.23
83	F	CB	37.15
84	V	N	124.90
84	V	HN	8.68
84	V	CA	67.12
84	V	CB	32.76
85	M	N	117.39
85	M	HN	8.24
85	M	CA	57.88
85	M	CB	31.70
86	K	N	121.95
86	K	HN	8.51
86	K	CA	59.75
86	K	CB	32.08
87	A	N	123.74
87	A	HN	7.71
87	A	CA	55.79
87	A	CB	17.61
88	W	N	120.84
88	W	HN	8.94
88	W	CA	57.94
88	W	CB	28.72
89	S	N	118.72
89	S	HN	8.61
89	S	CA	61.79
89	S	CB	62.86
90	K	N	121.00
90	K	HN	7.23
90	K	CA	57.85
90	K	CB	32.41
91	T	N	110.49
91	T	HN	7.82
91	T	CA	63.19
91	T	CB	69.44
92	Y	N	120.02
92	Y	HN	7.05
93	P	CA	65.20
93	P	CB	32.30
94	E	N	118.22
94	E	HN	9.38
94	E	CA	57.22

Residue number	Residue name	Atom name	Chemical shift
94	E	CB	29.30
95	N	N	119.73
95	N	HN	7.96
95	N	CA	54.77
95	N	CB	40.07
96	K	CA	58.38
96	K	CB	32.24
97	H	N	121.39
97	H	HN	8.22
97	H	CA	58.24
97	H	CB	35.34
98	V	N	122.19
98	V	HN	9.05
98	V	CA	63.81
98	V	CB	31.88
99	K	N	129.37
99	K	HN	8.77
99	K	CA	56.35
99	K	CB	36.65
100	F	N	122.91
100	F	HN	9.25
100	F	CA	58.28
100	F	CB	40.09
101	L	N	127.10
101	L	HN	9.85
101	L	CA	55.00
101	L	CB	45.07
102	A	N	123.13
102	A	HN	9.15
102	A	CA	52.86
102	A	CB	22.84
103	D	N	127.66
103	D	HN	9.06
103	D	CA	52.83
103	D	CB	43.29
104	G	N	109.27
104	G	HN	8.63
104	G	CA	49.29
105	S	CA	57.99
105	S	CB	64.54
106	G	N	112.50
106	G	HN	8.69
106	G	CA	46.82
107	K	N	120.22
107	K	HN	7.68
107	K	CA	59.90
107	K	CB	33.60
108	Y	N	129.61
108	Y	HN	11.15
108	Y	CA	63.02
108	Y	CB	38.65
109	T	N	120.42
109	T	HN	9.74
109	T	CA	67.830

Residue number	Residue name	Atom name	Chemical shift
109	T	CB	68.84
110	Q	N	118.96
110	Q	HN	7.93
110	Q	CA	59.66
110	Q	CB	29.36
111	A	N	126.30
111	A	HN	7.87
111	A	CA	55.54
111	A	CB	17.98
112	L	N	117.24
112	L	HN	7.95
112	L	CA	55.80
112	L	CB	44.80
113	V	N	106.64
113	V	HN	7.73
113	V	CA	46.87
114	V	N	108.44
114	V	HN	7.45
114	V	CA	59.63
114	V	CB	31.58
115	E	N	122.92
115	E	HN	8.81
115	E	CA	58.25
115	E	CB	31.20
116	L	N	126.04
116	L	HN	9.13
117	D	CA	54.87
117	D	CB	40.47
118	L	N	130.73
118	L	HN	8.41
118	L	CA	54.16
118	L	CB	42.83
119	S	N	121.35
119	S	HN	9.09
119	G	CA	46.54
123	L	N	118.30
123	L	HN	7.36
123	L	CA	56.08
123	L	CB	44.76
124	G	N	106.70
124	G	HN	7.27
124	G	CA	46.09
125	L	N	125.41
125	L	HN	8.50
125	L	CA	56.33
125	L	CB	42.58
126	R	N	126.09
126	R	HN	9.00
126	R	CA	52.74
126	R	CB	35.27
127	S	N	116.57
127	S	HN	8.54
127	S	CA	58.15
127	S	CB	65.23

Residue number	Residue name	Atom name	Chemical shift
128	R	N	120.92
128	R	HN	8.51
128	R	CA	57.22
128	R	CB	33.13
129	R	N	120.57
129	R	HN	7.99
129	R	CA	56.67
129	R	CB	29.95
130	F	CA	57.39
130	F	CB	43.66
130	A	N	121.31
130	A	HN	8.88
131	A	CA	53.45
131	A	CB	22.83
132	I	N	123.34
132	I	HN	9.59
132	I	CA	59.68
132	I	CB	43.39
133	L	N	129.80
133	L	HN	9.01
133	L	CA	54.27
133	L	CB	46.10
134	V	N	130.71
134	V	HN	9.56
134	V	CA	61.32
134	V	CB	33.62
135	D	N	129.50
135	D	HN	9.43
135	D	CA	53.36
135	D	CB	43.87
136	D	N	131.05
136	D	HN	9.40
136	D	CA	56.09
136	D	CB	39.43
137	L	N	107.19
137	L	HN	8.72
137	L	CA	58.67
137	L	CB	40.70
138	K	N	120.25
138	K	HN	7.79
138	K	CA	55.08
138	K	CB	33.66
139	V	N	126.32
139	V	HN	9.12
139	V	CA	195.47
139	V	CB	31.92
140	K	N	131.06
140	K	HN	9.42
140	K	CA	45.63
141	V	N	117.56
141	V	HN	7.57
141	V	CA	62.20
141	V	CB	37.21
142	A	N	131.211

Residue number	Residue name	Atom name	Chemical shift
142	A	HN	9.20
142	A	CA	51.88
142	A	CB	20.33
143	N	N	127.60
143	N	HN	8.70
143	N	CA	52.42
143	N	CB	38.56
144	V	N	125.81
144	V	HN	8.50
144	V	CA	61.94
144	V	CB	33.57
145	E	N	127.70
145	E	HN	9.00
146	E	CA	58.19
146	E	CB	29.95
147	G	N	112.42
147	G	HN	8.60
147	G	CA	48.16
148	G	CA	42.65
149	A	N	126.76
149	A	HN	8.24
149	A	CA	53.51
149	A	CB	19.91
150	F	N	120.08
150	F	HN	8.56
150	F	CA	56.05
150	F	CB	40.82
151	T	N	121.09
151	T	HN	10.60
151	T	CA	63.07
151	T	CB	71.73
152	I	N	119.10
152	I	HN	8.71
152	I	CA	61.94
152	I	CB	41.79
153	S	N	113.38
153	S	HN	7.23
153	S	CA	58.41
153	S	CB	63.02
154	G	N	109.20
154	G	HN	8.46
154	G	CA	45.27
155	A	N	121.13
155	A	HN	7.32
155	A	CA	55.31
155	A	CB	19.52
156	D	N	117.31
156	D	HN	8.73
156	D	CA	57.75
156	D	CB	39.88
157	E	N	119.18
157	E	HN	7.59
157	E	CA	59.15
157	E	CB	29.64

Residue number	Residue name	Atom name	Chemical shift
158	I	N	119.64
158	I	HN	7.16
158	I	CA	61.63
158	I	CB	35.82
159	L	N	121.13
159	L	HN	8.36
159	L	CA	58.47
159	L	CB	42.70
160	K	N	115.37
160	K	HN	7.22
160	K	CA	58.42
160	K	CB	33.37
161	A	N	122.06
161	A	HN	7.77
161	A	CA	52.50
161	A	CB	21.83
162	V	N	120.76
162	V	HN	7.18